DOCTOR OF PHILOSOPHY

Investigation of control problems of the PEM fuel cell for variable power demand

Abul Hawa, Ali

Award date:
2010

Awarding institution:
Coventry University

Investigation of Control Problems of the PEM Fuel Cell for Variable Power Demand

By

Ali A. Abul-Hawa

A thesis submitted in partial fulfilment of the requirements
of Coventry University for the degree of
Doctor of Philosophy

May 2010

ABSTRACT

Most of our energy supply nowadays relies on converting thermal energy to mechanical energy. Mechanical energy is then either used directly to drive vehicles or electric generators that supply the global needs of electricity. The main source of thermal energy is combustion of fossil fuels, which are limited, and have many detrimental effects on polluting the environment and adding to the greenhouse effect. Fuel cells offer the best alternative to replace existing energy conversion processes, as they convert the chemical energy of hydrogen fuel directly into electricity, bypassing fuel combustion. In addition, the only by-products in fuel cells are water and low temperature heat, and both are benign to the environment. Being a single step energy converting devices, fuel cells have high efficiencies. However, the fuel cell outputs unregulated voltage that depends on the operating conditions of the fuel cell and the load connected across its terminals.

A dynamic fuel cell model was developed in Simulink and integrated with the load in what is believed to be a new approach to reproduce and analyse the actual fuel cell-load interactions. Upon this, a control strategy was developed to match the power demand and regulate the output voltage for varying power demand. The strategy is based on using DC-to-DC converters and regulating the flow of the reactants. The control strategies are believed to be the first to deal with system's nonlinearities and covering the entire operational range. A novel solution was proposed to deal with the problem of irrecoverable control observed when the fuel cell was overdriven to the concentration losses region, which if untreated, would short-circuit the fuel cell and permanently damage it.

The overall fuel cell power generation system was simulated under varying load conditions observed in automotive driving schedules and domestic applications. Results showed promising performance of power regulation that meets the requirements of modern electrical voltage standards. An energy storage device could be used to improve the efficiency and performance of the system by absorbing the excess energy generated and using it during sudden increases in demand.

ACKNOWLEDGEMENT

I would like to extend my sincere gratitude and recognition to His Eminence Sheikh Ahmad Al-Hadi Al-Yashruti, for his concern, encouragement, and support that enabled me to pursue this study.

Special thanks and appreciation to my supervisor Professor Fateh Bhinder for his continuous support, guidance, and motivation during my study, and for his philosophical and professional influence that exceed the limits of my study. I would like also to express my gratitude and appreciation to my co-supervisor Dr William Hall for his guidance and support. I acknowledge and express my gratitude to Professor Paul Ivey and Professor Erik Holdø (now vice-chancellor at Narvik University College). This work would not have been possible without their support and guidance. Further thanks to Dr Raj Calay, who was my supervisor at University of Hertfordshire.

Of course, my greatest gratitude goes to my family for their infinite support; my parents; Ahmad and Fatima, and my sisters; Sa'eda, Bahia and Nadeen. Finally and most importantly, my greatest thanks to my dearest wife, Aminah, for her support, caring, and patience that she gave me during my studies.

TABLE OF CONTENTS

LIST OF FIGURES

LIST OF TABLES

NOMENCLATURE

Symbol	:	Description	Units
A	:	Fuel cell area	cm^2
A_F	:	Vehicle frontal area	m^2
C_D	:	Vehicle drag coefficient	–
C_{dl}	:	Double layer capacitance	$F.m^{-2}$
C_{RR}	:	Vehicle rolling resistance coefficient	–
C_w	:	Vehicle curb weight	kg
D	:	Duty ratio of the switching device of the converter	–
D_{jk}	:	Mutual diffusivity coefficient	$atm.cm^2.s^{-1}$
E	:	The ideal voltage of the fuel cell	V
$E°$	:	The ideal voltage of the fuel cell at standard conditions	V
E_a	:	The activation energy of a reaction	$Joule.mol^{-1}$
F	:	Faraday's constant (96485)	$C.mol^{-1}$
GDL	:	Gas Diffusion Layer	
G_f	:	Gibbs free energy of formation	J
Δg_f	:	Molar form of G_f	$J.mol^{-1}$
H_{excess}	:	Hydrogen excess ratio (>1)	–
i	:	The fuel cell external current density	$A.cm^{-2}$
I	:	The fuel cell current	A
i_c	:	The crossover current density	$A.cm^{-2}$
i_o	:	The exchange current density	$A.cm^{-2}$
i_r	:	Fuel cell reaction current	$A.cm^{-2}$
K_{io}	:	Reaction rate tuning coefficient	–
K_{dif}	:	Diffusion tuning coefficient	–
K_p	:	Gain constant of PI controller	–
K_I	:	Integral constant of PI controller	–
k	:	Reaction rate coefficient	s^{-1}
k_D	:	Equivalent thickness of diffusion layer	mm
L_D	:	Thickness of GDL	mm

M_i	:	Molar mass of species *i*	$g.mol^{-1}$
MEA	:	Membrane Electrode Assembly	
$\dot{m}_i$	:	Mass flow rate of species *i*	$g.s^{-1}$
n	:	Number of electrons released from the fuel	–
N	:	Number of cells	–
N_i	:	Molar flux of species *i*	$mol.cm^{-2}.s^{-1}$
P	:	Pressure	atm - Pa
P_i	:	Partial pressure of species *i*	atm
$P_{i,ch}$	:	Partial pressure of species *i* in flow channels	atm
$P_{i,r}$	:	Partial pressure of species *i* at reaction sites	atm
P_{ci}	:	Critical pressure of species *i*	atm
P_T	:	Total pressure	atm
R	:	Universal gas constant (8.314)	$J.K^{-1}.mol^{-1}$
R_d	:	Universal gas constant (82.057)	$atm.cm^3.mol^{-1}.K^{-1}$
R_i	:	Universal gas constant for species *i*	$J.K^{-1}.mol^{-1}$
R_{mem}	:	Protonic resistivity of the membrane	$\Omega.m^2$
T	:	Absolute temperature	K
T_{ci}	:	Critical temperature of species *i*	K
V	:	Volume	m^3
V_{act}	:	Activation overvoltage	V
V_{fc}	:	Fuel cell voltage	V
V_{ohm}	:	Ohmic overvoltage	V
α	:	Charge transfer coefficient, equals 0.43	–
α_T	:	Membrane resistance-temperature coefficient	$\Omega.m^2.K^{-1}$
η_{drv}	:	Drive train efficiency	–
Λ	:	The pre-exponential frequency factor	s^{-1}
ϵ	:	Porosity of GDL	–
v	:	The number of exchanged electron at the electrode, 1	–
ρ_a	:	Air density	$kg.m^{-3}$
ζ	:	Tortuosity of GDL	–

Chapter 1

INTRODUCTION

1.1 Energy Crisis

Energy is a key to national economy and maintaining our current standard of living. We are very dependent on a continuous and abundant supply of energy to provide us with heat and electricity. Energy is also needed in industry, transport, and for all public utilities.

Many energy sources exist naturally in different forms (Fig. 1.1), such as kinetic energy of wind and of moving water in rivers, potential energy of water at the top of waterfalls, chemical energy of some materials such as coal, oil and gas, nuclear energy, geothermal energy, solar energy, etc.

Most of these forms of energy cannot be used unless they are converted first into a more useful form of energy such as heat or electricity. Heat can be used to drive combustion engines. For example, in internal combustion engines, air and fuel are mixed and compressed in a cylinder-piston arrangement. Then, this mixture is ignited, releasing heat to produce hot combustion products, which expand rapidly forcing the piston to move in a linear motion. The linear motion of the piston is converted to a rotational motion by means of a connecting rod and a crankshaft. The crankshaft is connected to gears that eventually turn the wheels of a car or the propellers of an aircraft or of a ship. Similarly, coal can be burnt to boil pressurised water in order to raise high-pressure steam that drives a steam turbine. The steam turbine in turn can be connected to a generator, which produces electricity.

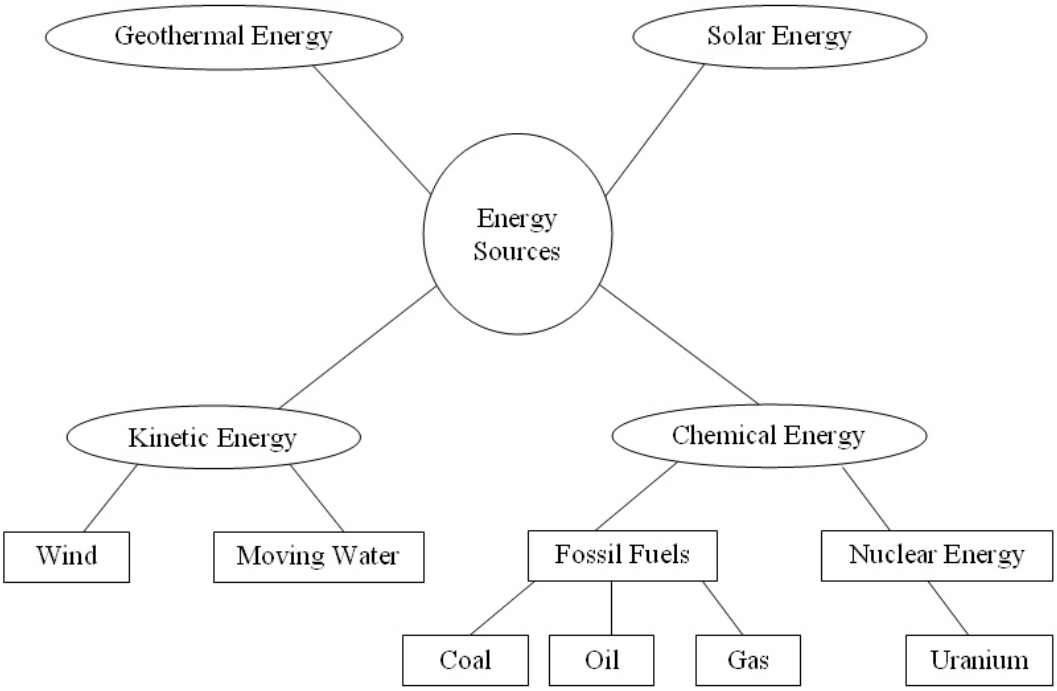

Fig. 1.1. Energy sources.

Every energy conversion process suffers from losses that reduce the overall efficiency of energy utilization. An energy conversion system with less energy conversion steps would have a greater efficiency than a system with more energy conversion steps. Fig. 1.2 shows two different systems for converting the chemical energy of a fuel into electrical energy.

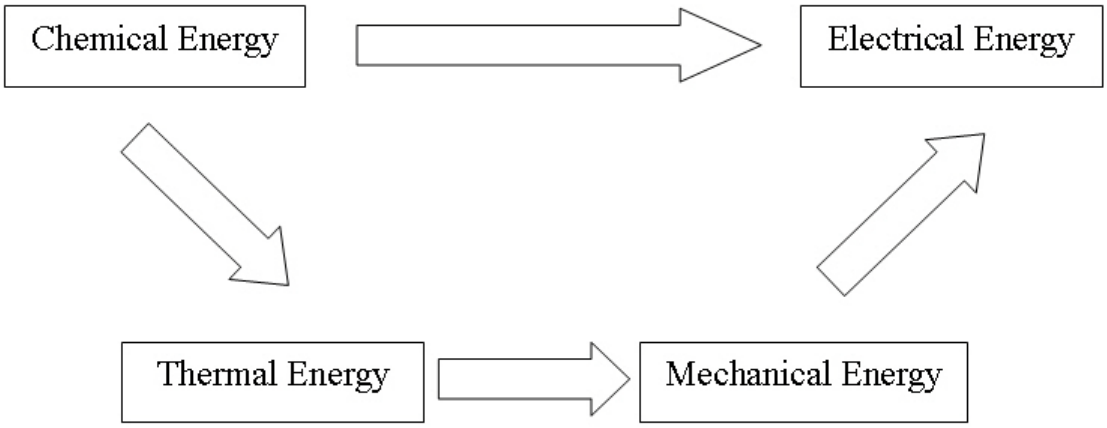

Fig. 1.2. Chemical energy conversion to electrical energy.

The first system converts the chemical energy directly into electrical energy, while the second system first converts the chemical energy to thermal energy. Then, thermal energy is converted to mechanical energy. And finally, the mechanical energy is converted to electrical energy. The overall efficiency of the first system would be inevitably higher than that of the second system because of the less number of stages in the overall conversion process.

Our primary source for producing thermal energy is fossil fuel, known as hydro-carbon fuels, i.e. coal, oil, and gas. The global reserves of these fuels are finite; they are depleting at an alarming rate because of escalating worldwide consumption to meet the growing demand for energy.

The demand for energy would continue to increase due to growing world population, rising living standards and general economic growth globally. Consequently, the prices of fossil fuels will continue to rise. Fig. 1.3 shows the predicted growth in world population and energy demand up to 2030 [1]. The predicted world population in 2030 is nearly 8.3 billion, based on about 1 % annual increase. The corresponding energy consumption increases by about 1.5 % annually.

In view of the aforementioned energy scenario, the scientific community globally is faced with two problems; the first is that the main source of energy, fossil fuels, is rapidly running out. There may be some disagreement on how long the fossil fuel would last, but there is no doubt that the reserves of fossil fuels are finite; eventually they must run out. Long before that time, the recovery of fossil fuels for use in energy devices will become very expensive; hence, they will not be economically viable. Therefore, to find alternative sources of energy to replace fossil fuels is a matter of utmost urgency.

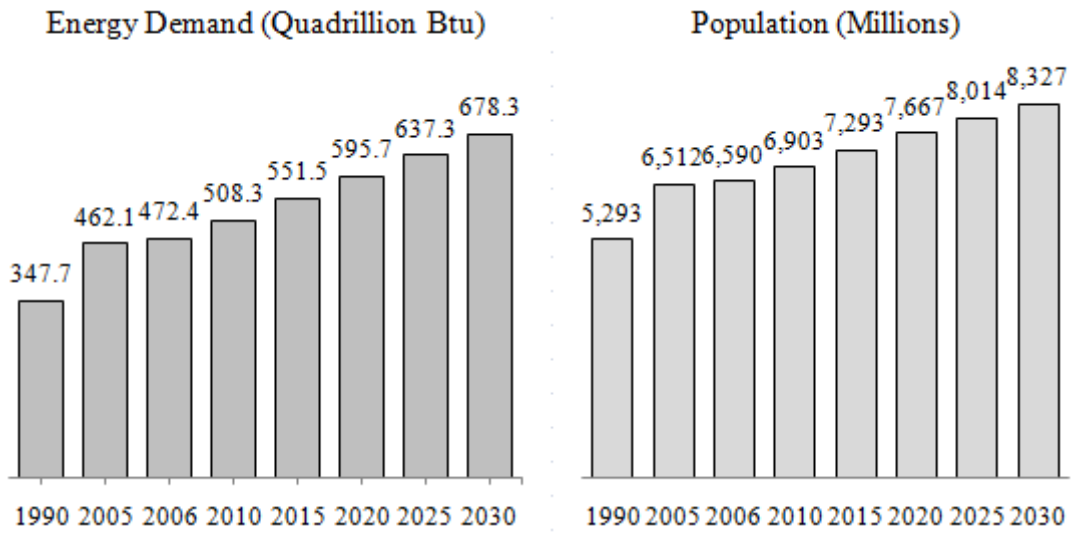

Fig. 1.3. Population and energy demand growth [1].

The second problem concerns the environment as energy conversion processes that involve combustion of hydrocarbon fuels have two ill effects on the environment. One is that the by-products of combustion; obnoxious gases such as oxides of nitrogen, carbon dioxides, carbon monoxide and sulphur dioxide, pollute the atmosphere and affect the health of all air breathing life forms on Earth. The pollutants also cause the green house effect on earth, raising the temperatures and damaging the ozone layer. As energy demand grows, combustion devices will increase, therefore, the pollution effect will become unbearable. Furthermore, all combustion engines, by Carnot's law, can only work if they eject certain amount of heat into the environment. This ejection of heat raises the temperature of the atmosphere and adds to the green house effect as already mentioned.

In view of the seriousness of the energy and the environment crises, there is an urgent need to find alternatives for energy conversion devices that do not rely on combustion. The fuel cell offers the ideal solution as it does not require combustion of fuel. Therefore, it does not discharge hazardous combustion products. Furthermore, the fuel cell has high energy conversion efficiency; therefore, per unit mass of fuel used the amount of useful work produced is more and the quantity of heat rejected to the environment is far less than that by combustion engines.

In a vehicle running on a fuel cell, the electrical energy would drive an electrical motor, a part of the power train. Electrical motors have very high efficiencies in converting electricity to work that drives the wheels of the vehicle. Figure 1.4 shows schematically the power trains for the fuel cell and the IC engine. The former would not only be more efficient than the latter because of less number of steps in the energy conversion process but it would also be simpler from the point of view of power train.

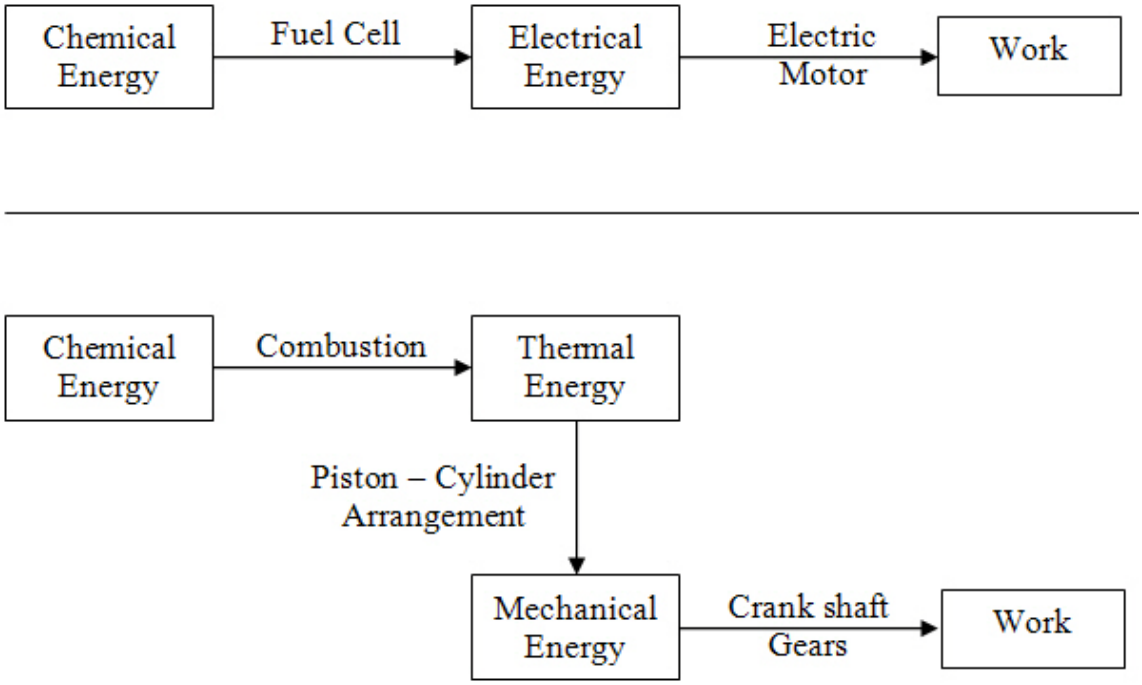

Fig. 1.4. Energy conversion in Fuel Cell vehicle and IC engine vehicle.

1.2 Fuel Cells

An electric cell, also known as the Daniell cell [2], produced electricity by eroding one electrode in a solution and depositing it on the other electrode. In order to have a cell which could operate without consuming the electrodes, it was necessary to supply the fuel along the electrode. The concept of such a device, called a fuel cell, is simply described as a mechanism by which a reaction occurring in a single reaction zone, such as the reaction in Eq.1.1, is split into two sub-reactions occurring apart in two separate reaction zones; sub-reactions given in equation 1.2 and 1.3.

$$2H_2 + O_2 \rightarrow 2H_2O \qquad (1.1)$$

The first sub-reaction consists of oxidizing hydrogen molecules, in other words, releasing the electrons from hydrogen gas molecules and leaving the positive protons.

$$H_2 \rightarrow 2H^+ + 2e^- \tag{1.2}$$

In the second reaction zone, where the other sub-reaction is taking place, oxygen is reduced. Oxygen molecules break into negatively charged ions, and eventually oxygen ions react with hydrogen ions (protons) to form water:

$$½O_2 + 2e^- \rightarrow O^{2-} \xrightarrow{H^+} OH^- \xrightarrow{H^+} H_2O \tag{1.3}$$

If these two reactions occurred in the same reaction zone as in Eq.1.1, electrons will remain attached to their atoms throughout the reaction. However, in a fuel cell, electrons are detached from hydrogen and are forced to go through an external circuit. The movement of electrons through the external circuit provides that circuit with electricity.

The implementation of the fuel cell concept was first demonstrated by Sir William Grove in 1839. Fig. 1.5 shows Grove's sketch of his fuel cell in the "Philosophical Magazine and Journal of Science, 1842" [3]. It consisted of two electrodes immersed in two tanks of reactants, representing the two reaction zones. The tanks were connected by an electrolytic bridge. The electrolytic bridge allowed only positive hydrogen ions to pass through from one tank to the other. Negatively charged electrons, which accumulated at the hydrogen electrode, were permitted to pass from one electrode to the other through an electrically conducting circuit (such as a lamp or a resistor). This setup represented the basic principles of fuel cells.

Fig. 1.5. A sketch of Grove's cell [3].

However, the fuel cell remained only a laboratory curiosity until 1932 when Francis Thomas Bacon started experimenting on fuel cells. He developed the first practical 5 kW stationary fuel cell in 1959.

The start of space exploration created a need for an electricity-generating device, which had high power density, energy efficiency and reliability as well as noise and pollution free operation. The fuel cell met all of these requirements; therefore, NASA selected the fuel cell as an electrical auxiliary device for use in the Apollo space programme in the late 1950s. Later on, NASA started funding hundreds of research contracts for developing the fuel cell technology even further.

The fuel cell being a pollution free and highly efficient energy conversion device is ideally suited to many civilian applications, such as a prime mover for road transport vehicles and many stationary devices. However, in order to use the fuel cell for civilian applications, it must be able to compete with the existing energy conversion devices in terms of price, performance, and durability. In addition, certain applications impose further restrictions on the use of fuel cells, such as the problem of water and heat produced and the storage of the hydrogen fuel in personal mobile applications (e.g. laptops, mobile phones...etc).

There are different types of fuel cells to satisfy the needs of different applications; they are named after the electrolyte they require. Table 1.1 shows the main fuel cell types and important differences between them.

Table 1.1 : Fuel cell types [4-6]

Type	Electrolyte	Catalyst	Operating Temp. (°C)	Efficiency	Use
Alkaline Fuel Cell	KOH	Platinum	80-120	40-50 %	Military, aerospace, automotive
Polymer Electrolyte Membrane Fuel cell	Solid polymer	Platinum	50-100	35-50 %	Transport, small/medium stationary, portable
Phosphoric Acid Fuel Cell	H_3PO_4	Platinum	150-220	35-45 %	Medium stationary
Molten Carbonate Fuel Cell	Molten carbonate salt	Nickel	650	50-60 %	Large utility
Solid Oxide Fuel Cell	Ceramic	Perovskites	800-1000	45-55 %	Large utility, small APU residential

*APU: Auxiliary Power Unit

The development of fuel cells for civilian use was held up because of two main reasons: 1) the intricate manufacturing technology that the fuel cell needed was not available; 2) the use of platinum, a very expensive material, as a catalyst was a serious limitation for the economic viability of the fuel cell. Therefore, in order to reduce the cost of manufacturing fuel cells, advances in manufacturing technology were needed. These included low cost production of bipolar, gas flow plates and application of nanotechnology to minimise the amount of platinum needed per square centimetre area of the membrane. The need for mobility and practicality led to the invention of modern fuel cells, which used advanced material design to build the heart of a fuel cell; the polymer electrolyte membrane (PEM), also known as Proton Exchange Membrane.

A PEM fuel cell in its simplest form resembles Grove's fuel cell, but it uses the PEM instead of an electrolytic bridge. The PEM, or for short membrane, is manufactured in a way to posses the main features of an electrolytic bridge, which are high proton conductivity and high electrons resistivity. In other words, only protons can pass through the membrane, and hence the name "Proton Exchange Membrane". PEM fuel cells use hydrogen at the anode and oxygen at the cathode in their gaseous forms. Hydrogen is usually supplied from a pressurized tank through pressure and/or flow

regulation valves to gas flow channels. Fig. 1.6 shows the basic components of a PEM fuel cell.

A practical PEM fuel cell is composed of the following components:

1) A Membrane Electrode Assembly (MEA): consists of a membrane sandwiched between two catalyst layers.
2) Gas Diffusion Layers (GDL) sandwiching the MEA: are made of electrically conducting, porous material to allow gases to diffuse to the MEA to improve gas distribution, and to allow electrons to pass to the external circuit.
3) Gas-channels plate, also called bipolar plate if it was between two fuel cells or an end plate if no other cell is connected to it: this plate ensures delivery of reactant gases to the fuel cell and conducts electrical current, or electrons to the adjacent cell (bipolar plate) or to the external circuit (end plate).

Fig. 1.6. Basic components of a PEM fuel cell. (Image taken from [7])

Hydrogen and oxygen go through the gas flow channels and diffuse through the gas diffusion layers until each gas (H_2 and O_2) reaches its reaction zone. The main

purpose of introducing the gas diffusion layer is to increase the active area of the reaction zone, which would have been reduced due to the solid edges of the flow channels. Platinum, a very expensive metal, is used as catalyst to reduce loss of energy (known as the activation energy) needed for the two sub-reactions to occur. Without a fuel cell, hydrogen gas ignites in the presence of oxygen to form water vapour and emit heat. The activation energy barrier for this reaction is reached by a heat source in the form of a spark or a flame source. In the fuel cell arrangement, hydrogen breaks into electrons and protons at the reaction zone in the presence of platinum catalyst. If the produced protons and electrons are not removed from the reaction zone, when the external circuit is open, they will react again to form hydrogen gas. However, when an external circuit connects the two reaction zones, electrons are removed from the hydrogen side and transported to the oxygen side, and at the same time, hydrogen protons are transported to the oxygen zone through the membrane. When all the elements meet at the cathode; oxygen, electrons, and hydrogen protons, they react in the presence of platinum catalyst to produce water. Both reactions release energy in the form of heat. In the fuel cell, the produced water is considered as a by-product, as it is not the aim of the reaction. The aim of the reaction is to generate electrical output in the form of direct current *DC*. This is achieved when electrons flow from the anode side to the cathode side.

At each electrode, the oxidation or reduction reactions generate an absolute electrode potential. The potential difference between the electrodes is the driving force for electrons' flow, and that is the fuel cell voltage. A fuel cell operating point is defined by its voltage and current. The cell voltage depends on many variables known as the operating conditions. The main operating conditions include the temperature of the reaction, pressures of the reactants, and the water content of the membrane. Fuel cell characteristics are usually defined by polarization curves that give the operating current and voltage of the fuel cell. As the current output increases, losses in the fuel cell cause the voltage to drop. These losses include reaction kinetics, and ohmic voltage drops across the membrane. They are described in more detail in the methodology chapter.

Most electrical devices and machines nowadays require a constant voltage at their input terminals, with a certain degree of tolerance. Fuel cells have a varying output

voltage that decreases as the current or power output increases. Each load connected across the fuel cell terminals defines a fixed operating point. This operating point would not meet the standard voltage required by most devices. Hence, a *power conditioning unit* (PCU) is needed between the load and the fuel cell. The PCU includes DC-to-DC converters and/or DC-to-AC inverters. The PCU needs to be controlled in order to have a constant output voltage from the fuel cell system. This study aims to regulate the output voltage to a constant DC voltage at a selected reference value. If the load requires an AC power supply, a DC-to-AC inverter may be added between the fuel cell system and the load.

The operating conditions of the fuel cell tend to change as the power demand or the operating point changes. Control over these operating conditions is needed to maintain optimum conditions for the desired load. For PEM fuel cells, the optimum operating conditions are 60 °C to 80 °C, a constant pressure of the reactants with sufficient flow to meet the demand, and a fully humidified membrane.

For fuel cells to replace combustion engines, i.e. spark ignition and compression ignition engines or gas turbines, they would be expected to have at least the same response to power demand. The performance of the fuel cell depends on its operating conditions, which are defined by the flow properties of the reactants, the temperature, and the moisture in the membrane. These operating conditions vary with the rate of electrical energy absorbed from the fuel cell. Therefore, additional components are required to regulate the operating conditions of the fuel cell on one hand, and to regulate the output power on the other hand. The operating conditions of the fuel cell have different response times to changes in the set points or changes in the fuel cell operating point (defined by its output voltage and current). Temperature and moisture in the membrane have slow response times, and once the desired set point is reached, variations in these conditions can be very well regulated and controlled. However, the concentration of the reactants, which is directly related to their flow rates, has a faster response time than the temperature and the moisture in the membrane. Hence, reactant flow regulation, which is directly proportional to the electrical power, has more demanding as well as complex control requirements.

The fuel cell output constitutes electrical power, which is the product of voltage and current. Since the process of converting the chemical energy of fuel into electricity is not assumed to be reversible, the internal losses within the fuel cell cause a drop in the voltage as the output current increases. With modern electricity regulations and standardized electrical devices, the output voltage at the load's terminals must be kept constant within a certain tolerance. Therefore, a power-conditioning unit is needed to match the output power of the fuel cell with the demand and to regulate the voltage.

1.3 The Aim of this Research

The aim of the research reported in this thesis was to study all aspects of the fuel cell system as a prime mover for stationary as well as automotive applications. A comprehensive study was needed in order to formulate control strategies as an aid to the design of efficient controllers to control the output power of PEM fuel cells that would match the requirements of varying power demands such as those encountered in automotive and domestic applications.

Chapter 2

LITERATURE REVIEW

2.1 Introduction

A fuel cell energy conversion system is a multidisciplinary subject of study; it includes electrochemistry, chemistry, and electrical engineering (electronics and control). Research papers on fuel cells published in the open literature tend to cover subject specific and narrow areas. A comprehensive study that includes all these branches of science is difficult to find because of its highly confidential nature. However, the control of a fuel cell system depends on understanding all the disciplines involved in the fuel cell.

In this chapter, a literature review is carried out. In order to use fuel cells safely and efficiently, it is important to understand how fuel cells can be controlled, and how they respond to changes in load and operating conditions. Therefore, the first step in control design is to understand the theory behind fuel cells and their interactions with auxiliary components and control devices. In the open literature, a lot of work has been done to describe fuel cells and their characteristics. With control as the objective in this study, it would be necessary to use a simple yet comprehensive dynamic model that describes most of the major characteristics affecting the performance of the fuel cell.

2.2 Literature Review

In the review given below a certain number of papers are of serious relevance to this study. Two areas are of interest in this study, and each area attracted attention from investigators from different backgrounds. Therefore, the literature review is divided into two parts:

1) review of the fuel cell mathematical models reflecting its behaviour;
2) review of fuel cell control strategies.

2.2.1 Fuel Cell Behaviour and Modelling

Hou et al. [8] presented a model to predict the fuel cell voltage for given values of currents. The model is built using simple steady state semi-empirical equations. The steady state model is compared with experimental results obtained from a fuel cell. A purely mathematical term is derived by curve fitting experimental data to match with the steady state model. The resultant final model predicts the transient response of the fuel cell voltage at fixed operating conditions (temperature, pressure, etc). This model would not be suitable for simulating varying power applications, as it does not allow variations of the fuel cell operating conditions. It also limits any future study to only the modelled fuel cell.

A more detailed model is presented by Wang and Wang [9]. They describe a three dimensional model of the transient response of the fuel cell, including the effects of membrane hydration, reactant gas flow and electrochemical reaction kinetics. Step changes in the relative humidity of the cathode gas were simulated, while maintaining a fully humidified anode gas. The study concluded that membrane hydration has the largest time constant, of the order of 10 seconds, and the transport of gases through the gas diffusion layers has a time constant between 0.01 and 0.1 seconds. It was also shown that for fully humidified reactants a small step change in the fuel cell voltage (from 0.6 V to 0.7 V) results in a settling time of about 1 second in the current. An undershoot in the current was noticed and it was attributed to the concentration losses of oxygen. However, for relative humidities of 100 % and 0 % for the anode and cathode, respectively, an additional overshoot, following the undershoot in the current was noticed and the settling time increases to about 6 seconds. This overshoot was related to the membrane hydration time constant, which was slower than oxygen transport. When the voltage is increased, the current drops, and therefore, the amount of water produced at the cathode decreases, as well as the amount of water molecules being dragged through the membrane. Since the actual flow velocity is low and not very turbulent, it is a complicated mathematical model to describe the fuel cell. It is impractical to use such model for developing a control strategy for an entire fuel cell system, as it requires high processing powers and long simulation times. This type of three-dimensional modelling, similarly found in [7, 9-12], or two-dimensional modelling such as [13-15], may be

useful where fuel cell geometrical design is concerned. However, some of these papers were useful for this study in studying and determining some of the parameters such as in modelling the gas diffusion layer, such as [12, 13].

Weydahl et al. [16] studied the transient response of a proton exchange membrane fuel cell experimentally. Excess amounts of reactants were supplied to avoid concentration losses during transients. It was reported that the fuel cell response time to load changes depends on the initial and final values of the steady state operating points. During step changes, the instantaneous operating points of the fuel cell follow two transitions. The first transition starts from the initial steady state point and continues on a straight line with a slope equal to the internal resistance of the membrane and ends at an operating point that lies on the second load curve. This transition takes place almost instantly, however, due to measurements sampling limitations; the transition was equal to the fastest sampling rate used. The second transition lies on the load curve, with a much slower response time than the first transition and ends on the steady state curve of the fuel cell. It was reported by the authors that the response times ranged from 1.6 ms to 380 ms. Furthermore a second transient occurs after about 0.1 s of the step change, and settles down in about 2 seconds. This was attributed to diffusion transients.

Zenith et al. [17] investigated the behaviour of high-temperature Polybenzimidazole (PBI) PEM fuel cells. The basic principles of operation for all types of fuel cell are the same. The more recent PBI membrane fuel cells differ from Nafion® based fuel cells in the functionality of proton transport from the anode to the cathode. PBI fuel cells do not depend on water content of the membrane to transport hydrogen ions. Thus, water management is of less importance. Zenith et al. reported experimental results on PBI fuel cells to verify a dynamic model of fuel cells suitable for control analysis. The experiments were performed using constant flow rates of the reactants that ensured enough supply to avoid starvation or concentration losses of the fuel cell. Obviously, these experiments would result in loss of excess hydrogen and reducing the fuel cell efficiency; however, for research purposes and for studying certain phenomena, this might be necessary to identify the importance of each phenomenon more accurately. It is important to keep in mind that the sampling rate of the data acquisition device was reported to be 10 Hz (i.e. 1 measurement every 100 ms). The steady state

polarization curve achieved hysteresis behaviour. When the fuel cell operating condition changed from open circuit to maximum current, it differed from the curve plotted in the opposite direction of change. The full cycle (sweep) was performed once, and the hysteresis was attributed to “changes in the access of oxygen on the reaction site” or “changes in the catalyst during the cycle”. A more plausible conclusion could be drawn if the change was run for another cycle immediately following the first cycle. This would have confirmed the type of changes on the catalyst whether it was due to aging or poisoning. The authors realised the limitation due to the maximum sampling rate of the data acquisition device. The sampling rate was probably smaller than the frequencies of some important phenomena in the fuel cell, which could have been either missed or led to wrong conclusions. In the proposed model, a few assumptions were stated; most of them would be justified. However, it was assumed that diffusion transients settle immediately, although it was reported from Wang and Wang [9] that the diffusion transients range from 0.01 to 0.1 seconds. Clearly, such transients would require a data acquisition device with a sampling rate of at least twice the frequency of the measured property, according to the Nyquist-Shannon sampling theorem. Therefore, diffusion transients would not have been detected with a sampling frequency of 10 Hz. The model included concentration losses in the term of the activation voltage, where the exchange current density was defined as a function of the partial pressures of the reactants at the reaction sites (Butler-Volmer equations). This representation is believed to be better than using a separate empirical term for concentration losses where the limiting current is assumed constant for all operating conditions, and this was adopted in this thesis for the fuel cell model. It was reported that the time constants were larger when switching the load to a larger resistance than when switching to smaller resistance loads. No explanation was given in the paper although it might be attributed to the fact that for any RC (resistance-capacitor) circuit, the time constant is equal to ‘R times C’. Hence, the time constant increases for a larger resistance. Zenith noted two transients in the response of the fuel cell to step changes in the load, similar to the observations by Weydhal et al. [16]. The first transient takes about one second followed by another slower transient with smaller amplitude. The second transient was attributed to the dynamics of proton concentration in the membrane. The slower transients were ignored on the basis that they can be controlled by a simple PI controller. The proposed model

ignores diffusion transients and does not realize the overshoots/undershoots. Zenith et al. reported perfect control of the fuel cell output power as long as the current was less than the maximum current before falling into concentration losses, and assuming no diffusion transients.

Benziger et al. [18] presented what they called the power performance curve which was claimed to be a useful metric that describes the power delivered by the fuel cell in relation to the impedance of the load connected to the fuel cell electrodes. However, this metric was only suitable for steady state analysis. It was concluded that the maximum fuel cell power output and the maximum efficiency do not occur simultaneously, which could be found out from the polarization and power density curves. At maximum power, the efficiency was only 50 %, which occurred when the load's impedance matched the internal resistance of the fuel cell. This was based on a simple fuel cell circuit model comprised of a voltage source with an internal resistance, where the "maximum power theorem" applies. When the external resistance equals the internal resistance, half the generated power is dissipated at the internal resistance, and the other half constitutes useful energy. As a consequence, for external resistances larger than the internal resistance, the efficiency is greater than 50 % while the output power is less than the maximum power. It was confirmed that the operating point of a fuel cell was determined by the external circuit connected to it.

Ceraolo et al. [19] proposed a dynamic semi-empirical model of a PEM fuel cell, based on the knowledge of different phenomena that occur within the fuel cell. The model, implemented in Simulink, was compared with experimental results and was found to be in agreement. It was noted that the membrane resistance was inversely proportional to temperature as a main factor and varied as the fuel cell current changed depending on the operating temperature. The resistance decreased with current within temperatures from 20 °C to 45 °C, and increased with current between 45 °C to 80 °C. However, at each temperature the cell resistance was chosen as the average of all values at the different currents. The average values of the resistance at various currents were used to model the resistance of the membrane, and this model was adopted in this thesis as shown later in Eq.3.12. Ceraolo et al. reported that the anodic activation losses were negligible compared to the other losses of the fuel cell. It was also noted that cathode

flooding, due to poor removal of product water, degraded the performance at high currents that could only be reached using pure oxygen. Since air was used, flooding would not occur. It was reported that proton (H^+) concentration in the cathode catalyst layer increased with current, due to an increase in product water at the cathode, which increased the water content of the membrane and the number of mobile protons. This explains the overshoot of the fuel cell voltage that was noticed when the current was stepped down. The transient behaviour of the fuel cell voltage was explained by two phenomena: from the initial point to the peak of the overshoot was attributed to the gas diffusion and the double layer capacitance, while the remaining part of the transient starting from the peak of the overshoot to steady state was attributed to proton concentration variations.

Correa et al. [20] presented a dynamic fuel cell model composed of a steady state voltage term integrated with an exponential term with a time constant to represent the transient response of the fuel cell. The steady state model was reported to be in agreement with actual data obtained experimentally from different fuel cells. However, no comparison was made to verify the transient behaviour of the fuel cell model. The transient response of the proposed model partially agreed with findings reported in other studies. It was not shown how the transient term was integrated with the model; however, it was clear from the simulation results that the fuel cell model was not implemented properly with the load. It was assumed that the fuel cell current was an independent control variable and the voltage was a dependent variable. Therefore, the current was simulated as a clean square wave with no transients, contrary to the actual behaviour of the fuel cell. In addition, the reported simulation results for power output versus time showed no deficiency at all during transients. The concentration losses term assumed a fixed limiting current value irrespective of the actual pressures and flow rates of the reactants. This phenomenon has been reported in many other publications, but it can only be used for steady state analysis. Therefore, concentration losses in the fuel cell would not be modelled properly for a system where the flow rates and pressures of the reactants change with varying load demands.

Uzunoglu and Alam [21] simulated a fuel cell-ultra capacitor hybrid system for vehicle power demand profile using Simulink. The model did not reflect the diffusion

behaviour of gases through the gas diffusion layer, thus concentration losses were ignored. The dynamic behaviour of the charge double layer capacitance, which is an important phenomenon in the fuel cell, was also not modelled. The dynamic behaviour was limited to time delays introduced to the flow of the reactants only. The ultra capacitors were connected in parallel with the fuel cell through two power switches and two diodes. A buck-boost converter was used and modelled for average values of the input/output voltages related only by the duty ratio. The duty ratio was controlled with a PI controller with a reference voltage. The simulation results were plotted on a time scale of 1400 seconds, and not much information on the transient operation could be easily obtained. The work was considered useful for reference of MATLAB/Simulink® modelling.

Meiler et al. [22] proposed a fuel cell dynamic model based on experimental data. The model was composed of two parts; (i) a steady-state part that found the operating point of the fuel cell from a look-up table; and (ii) the second part comprised the transient behaviour of the fuel cell, which was added to the steady-state part to make the complete fuel cell dynamic model. The model was designed for real-time simulations; therefore, the steady state, nonlinear, behaviour of the fuel cell was saved in a look-up table to minimize processing time. The transient behaviour of the fuel cell was reported to be linear, and was modelled by the summation of two transfer functions that represented both: the fast transient response of the double layer capacitance; and the slower over/under shoots during a step change in the current. The proposed modelling process depended on system identification through experimentation on carefully selected conditions. The number of experiments to be performed varied exponentially with the number of variables included in the model, as well as the range and step size of the variations of the variables. Although the advantage of this method was that it did not require any knowledge of geometrical, physical, electrochemical, and other properties of the fuel cell, nonetheless it would pose a major disadvantage if any of those properties or components of the fuel cell were modified. Hence, this model could not predict the behaviour of the fuel cell under conditions that had not been tested and verified already by experiments. Consequently, this model was not applicable for testing

any changes in the control strategies or DC/DC converters, before building the actual system. Hence modelling in this case would be limited to educational purposes.

The papers reviewed above, and many others, have different approaches and degrees of detail for describing the fuel cell behaviour. Steady state models are useful for optimizing operating conditions, efficiency, and geometrical designs. However, for process control, a flexible and dynamic model is required to study the interactions between the unsteady output of the fuel cell and varying power demands. This is achieved in this thesis by modelling relevant time dependent properties, such as the double layer capacitance, and by using semi-empirical modelling which relies on theoretical and experimental equations. Thus, variations in the fuel cell stack can be matched by changing the relevant variables of the model.

2.2.2 Fuel Cell System Control

In a fuel cell system, there are two main control problems; the control of the operating conditions of the fuel cell, and the control of the output power to match the load demand. Some studies try to regulate the output power by changing the operating conditions. Other strategies consider the two control problems independent from each other. In this thesis, the latter approach is recognised as the optimum approach, where the operating conditions of the fuel cell are maintained at their optimum values that ensure highest efficiencies of the fuel cell. The output power is regulated by DC-to-DC converters to match the time-variant demand. Nonetheless, both approaches have been reviewed below.

Woo and Benziger [23] proposed a strategy to control the fuel cell current by regulating the mass flow rates of the reactants. Their design used water reservoirs at the outlets of the anode and cathode gas streams, to maintain a constant pressure (Fig. 2.1).

Fig. 2.1. [23]).

The inlet flow was regulated to control the output power. When the pressure inside the anode or cathode flow channels dropped, water flowed from the reservoirs to the channels, blocking the reactant gases from reaching part of the membrane and reducing the active area. Thus, the internal resistance of the membrane was increased. It was reported that the response time to change the output by varying the mass flow rate of hydrogen was about 10 seconds, and a response time ranging from 20 to 50 seconds for step changes in oxygen flow rate. As this strategy was aimed at fixed resistance loads, it was not suitable for changes in the load. The pressures of the reactants inside the flow channels usually decrease when the consumption of reactants increases due to sudden increase in the power demand. According to proposed strategy, when this situation occurs water would block part of the active area of the membrane consequently that would reduce the output power.

Thounthong et al. [24] presented a fuel cell system model and experimental data claimed to be suitable for automotive applications. Their solution to deal with the transient problem of the fuel cell was by using super-capacitors acting as auxiliary power source, while the fuel cell operated nearly at steady state to keep the super-capacitors' voltage at the reference value. During a sudden increase in power demand, the super-capacitors would supply the extra power needed for a certain period to ensure that the rate of change of the fuel cell current did not exceed 4 A/s. This value was chosen to ensure that enough time was available to allow the supplies of the reactant gases to cope with the sudden increase in consumption rates. The sluggishness of the fuel cell was attributed to the slow response of the flow control valves and/or air compressors. However, the fuel cell had a fast response to load changes when adequate

amounts of reactants were supplied. The same observation was presented by many authors such as [19, 25, 26]. Excess reactants' flow would degrade the efficiency of the fuel cell system, unless the excess reactants, and especially hydrogen, which is not free, are utilized and reused efficiently. The proposed use of six 3500 F super-capacitors as auxiliary power source with a 500 W fuel cell indicates that the fuel cell is being used to recharge the super-capacitors, while they act as the main energy source.

Pischinger et al. [27] described a practical fuel cell system for vehicle applications composed of air compressors/blowers, fuel processing reformers (gasoline to hydrogen), converters, super-capacitors, controllers, general vehicle dynamics and power requirements for a cold start-up and transients during acceleration and braking. Their study shows the difficulties in controlling the fuel cell system and suggests general solutions. They described some practical parameters representing time constants for the different phenomena related to fuel cells. For instance, it is estimated that the amount of thermal energy needed to raise the temperature of a fuel cell weighing 100 kg (steel and carbon mass) from 20 °C to 80 °C requires about 4000 kJ based on an average heat capacity of 0.667 J/(g.K) for steel and carbon. The time needed to change the cathode air pressure from 1 bar to 2 bar is about 0.15 s, which negates the claims that the fuel cell response is slow due to gas supply system. It was reported that using an energy storage device for transients, such as super-capacitors, would save about 8 % of fuel consumption when braking energy is used to recharge the super-capacitors. The general overview presented in this paper gives a good starting point in planning the control system of the fuel cell and the DC-to-DC converter, giving estimates of the various time constants for the operating conditions of the fuel cell.

Jiang and Dougal [28] investigated a hybrid power source combining a fuel cell and a lithium-ion battery controlled digitally. They implemented a control strategy to share the power needed by an electrical load from a fuel cell and a battery to achieve a higher peak power than the power that could be delivered by any one of the sources alone. Their analysis was for steady state conditions; therefore their simulated results did not show any transient behaviour of the fuel cells. Jiang and Dougal used a buck DC/DC converter to step down and control the fuel cell voltage and power delivery; the battery was connected directly to the load, i.e. without a converter. Their control

strategy imposed three constraints to the mode of operation to ensure proper operation of the fuel cell and the battery; the fuel cell current limit (fixed at design stage) and battery voltage and current limits. However, their study was focused on manipulating the power sharing between the fuel cell and the battery, and did not involve control of the fuel cell operating conditions. Nonetheless, their study was considered useful as it reflected the control strategies that could be implemented in the design of a complete fuel cell system. It is believed that their model would suffer a large discrepancy in the case of real fuel cells when the system is scaled up to a practical application. Their experimental work was based on a 35 W fuel cell stack of 25 cells, which indicated that a relatively small area of a fuel cell was used. A larger scale fuel cell would impose limitations and additional requirements on the control system. The fuel cell current limit was an important parameter in their controller operation; an improper setting would make the system vulnerable to damage. The transient behaviour of the fuel cell involves an overshoot of the fuel cell current to a considerably large value for a short period, which would certainly be greater than the fuel cell current limit proposed. This is another limitation on the use of this strategy, where changes in load should be slow.

Drolia et al. [29] proposed a strategy to connect an ultra-capacitor in parallel with a fuel cell through a power converter. The parallel configuration was then connected to a second DC-to-DC converter, as shown in Fig. 2.2. An inductor passed the ultra-capacitor current to the second converter; it was claimed that step changes occurred for this current.

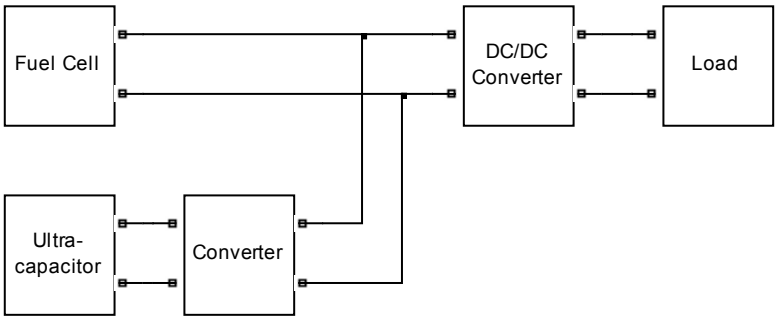

Fig. 2.2. Block diagram of the fuel cell system proposed by [29].

The fuel cell model seemed to give erroneous simulation results during sudden changes in the load, compared to most of the published experimental results on fuel cells, where the rate of change of voltage during sudden changes in the load was slower than the model and the physical fuel cell emulator developed in this study. The use of an inductance between the ultra-capacitor and the DC converter limited transients in the current to flow in/out of ultra-capacitors. Hence, this degraded the dynamic performance, which ultra-capacitors were supposed to enhance. The study was based on a fuel cell model that did not resemble most published experimental results of the dynamic response of the fuel cell directly, and lacked modelling various phenomena. Therefore, the validity of their strategy for modelling was not successful.

Rodatz et al. [30] reported experimental results on a fuel cell/super-capacitor powered electric vehicle. The tests included in-lab and on the road vehicle experiments. The anode was a closed system, where the inflow of hydrogen depended on the amount of hydrogen consumed by the fuel cell reaction. One of the reported problems in this design was the accumulation of water at the anode. This prevented hydrogen from reaching the reaction sites and consequently degrading the fuel cell performance and damaging the membranes of most affected cells. A purge valve was introduced to remove the accumulated water. A significant improvement in the fuel cell performance was noticed when hydrogen was purged; however, this process must have resulted in wasting some hydrogen. The fuel cell supplied the power demand calculated by the controller, and the super-capacitors maintained a stable voltage of the output to meet the remaining power demand especially during transients. In order to avoid depleting the reactants during sudden increases in power demand, which causes excessive concentration losses and a drop of the fuel cell voltage that might damage it, the power drawn from the fuel cell was limited to a rate of 2.5 kW/s. However, it was reported that the fuel cell stack suffered from irreversible damage to some of its cells due to concentration losses. The reason for this might be attributed to the closed supply system of the anode, where sudden increases in demand would not be met by an instant supply of the reactants.

In another study, Rodatz et al. [31] reported experimental and simulation results on a strategy to manage power sharing between a fuel cell and a super-capacitor for

optimising hydrogen fuel consumption in vehicular applications. The proposed strategy did not require previous knowledge of the load profile. It was noted that using an energy storage device could reduce the size of the fuel cell to the average power needed by the application, while fluctuations and transient peak power demand might be met by the energy storage device. The control strategy to reduce fuel consumption was based on evaluating a probability term that depended on the energy availability from the fuel cell at maximum output power and a given amount of energy required by the application over a certain time interval. The authors reported insignificant improvement in fuel efficiency using their strategy due to the fixed design of the fuel cell used.

Zenith and Skogestad [25] proposed a control strategy to deal with the fuel cell power output. A theorem was established to conclude that the output power of the fuel cell could be controlled perfectly to match the power demand as long as the demand was less than the maximum steady-steady power output of the fuel cell. On the basis of this theorem, a dynamic model was developed, and a control strategy of DC/DC converters was proposed based on logical switching rules. The disadvantage of this control strategy was the number of variables that needed to be measured at all times of operation. In addition, some of these variables were within the DC/DC converter, which made this strategy more vulnerable to sensor tolerances, failures, and difficult to implement. The settling time for the converter output was reported to be 5 ms to 10 ms. The proposed strategy was tested numerically on an electric DC motor. The output voltage was varied to enable variable motor loads. The results reported 50 ms for voltage rise time and less than 0.2 s for settling time.

Caux et al. [32] proposed a control strategy for a fuel cell system including an air compressor, control valves and a power converter unit. The fuel cell model used was for steady state operation, and the only dynamic behaviour described in the model was for the reactant flow properties and the air compressor. The pressure of the cathode was kept constant at 1.5 bar, while the flow rate of air was regulated to meet the power demand and reactant consumption by controlling the compressor speed and the pressure control valve at the outlet of the cathode. Super-capacitors were used to absorb braking energy. The fuel cell was connected to a boost converter, while the super-capacitors were connected to a bidirectional converter that allows transfer of energy from the

super-capacitors to the electric motor during sudden increases in power demand, and it allows regenerative braking energy to be transferred from the motors (acting as generators) to the super-capacitors during reductions in motor velocity. Both converters were connected in parallel with the load. The fuel cell converter was controlled to regulate the voltage, while the super-capacitor converter was controlled to regulate the current for charging or discharging the super-capacitors. The reported simulation results show perfect voltage regulation and power management. It is impossible to obtain such results for any practical system and one may conclude that the proposed model does not reflect the actual behaviours of the phenomena involved in a fuel cell system. However, the study is useful for steady state controller design.

Choe et al. [33] described a fuel cell system composed of a fuel cell, an air blower and humidifier, an energy storage device and a converter. Every component was modelled in Simulink. The dynamics of the fuel cell system were limited to reactants mass transport, heat balance in the fuel cell, and water balance in the membrane. A DC/DC converter was controlled by PWM signals under a PI feed forward controller with the output voltage as a reference signal. The output of the fuel cell converter was connected in parallel with a battery and its converter, to supply the load. The model uses the fuel cell current as an input (control) variable for the converter. This might be viable for modelling and simulation only, but it is not practical in a real fuel cell system, because the fuel cell current is a state variable that depends on other variables and conditions. In addition, the dynamic behaviour of an actual fuel cell current, exhibits large overshoots during changes in load conditions and cannot be limited to a square wave. Many phenomena were ignored without justification, such as the effect of the double layer capacitance of the fuel cell. The reported simulation results on transients showed large undershoots in the output voltage by nearly 160 Volts away from the reference 500 V. Hence, the use of super-capacitors to overcome transients would not be justified.

Williams et al. [34] presented experimental results on a commercial fuel cell (Nexa – Ballard®) rated 1.2 kW. The results reported that the fuel cell might be used without additional energy storage devices in load-following applications with high frequency transients of 1 kHz. Dynamic load following was controlled using a PI

controller based on the power demand as a reference. The reported results indicated an overshoot in the output power during transients that reached 200 % of the rated steady-state power for the fastest load transient of 1 kHz. The fuel cell was tested under a scaled down Federal Urban Driving Schedule (FUDS) matching the 1.2 kW Nexa and assuming a 50 Hz rate of change as the maximum frequency of the transients. The overall response of the system reported a settling time of 0.1 seconds and reached 90 % of steady-state within 10 ms. It was reported that the cell output was unable to follow power demands greater than 700 W due to losses in the converter used. The controller suffered from integrator wind-up and over-drove the load when the demand dropped.

Fontes et al. [35] is one of few published studies that describe the behaviour of fuel cells connected to power converters. They presented an acceptable level of modelling the dynamic behaviour of fuel cells for the objective of their study. A sinusoidal signal imposed on a DC value of current was used to find the influence of current variations on the fuel cell operating point. At low frequencies (less than 1 Hz), the fuel cell operating points laid on the steady state polarization curve of the fuel cell, no transient effects were reported. For mid-range frequency (100 Hz) the operating points laid on an elliptical curve with its major axis almost parallel to the steady state curve. At high frequencies (10 kHz) the operating points laid on an almost straight line parallel to the slope of the membrane internal resistance characteristic line. Hysteresis appear when the time constant of the fuel cell, represented by the double layer capacitance and activation resistance (activation overvoltage divided by current), was close to the period of the sinusoidal current. Therefore, the hysteresis depended on the average (DC) value of the fuel cell current. The authors reported simulation and experimental results of a fuel cell connected to a simple buck converter and to a boost converter, both at about 20 kHz switching frequency. For both converters, the operating pressures were 2 bar for hydrogen and pure oxygen. It was not reported how the mass flow rates were controlled. Most of the reported results were for less than 10 μs except for one figure on the boost converter that was a window of 200 μs at timestamp 0.5 s. It was reported that at 20 kHz, fuel cell current harmonics have negligible influence on the chemical reaction of the fuel cell as they would be filtered out by the double layer capacitance. In other words, fast changes in current go through the capacitor without

causing a significant change in its voltage, i.e. it remains constant. This is because the double layer capacitance does not have enough time to charge and discharge. As a consequence, all the over voltages were affected and calculated based on the average current, except for the ohmic overvoltage which was related to the instantaneous value of the current. The experimental results reported a 6 % and 1.2 % ripple on the fuel cell voltage for buck and boost converters, respectively. However, they did not study the effect of varying the load while maintaining a fixed output voltage by controlling the converter.

Liu et al. [36] proposed a DC-to-DC converter designed and tested experimentally on a Nexa 1.2 kW fuel cell. An output LC filter was used to regulate the electrical output. The switches were controlled with a PID controller with phase modulation. The transient response of the fuel cell was measured experimentally and reported to be 5 μs. The fuel cell was tested with the converter for a load change from 160 W to 800 W, and the results showed a well regulated output voltage. However, the tested dynamic change in power demand was within the linear region of the fuel cell, and did not deal with the non-linearities in fuel cells, which appear near the low and maximum power outputs regions.

Chiu and Lin [37] described the operation of a DC-to-DC converter for a fuel cell/battery system. The fuel cell was connected directly to the load, while the battery was connected to the load through a bidirectional converter. The converter boosted the voltage and drew power from the battery when the fuel cell voltage dropped below a set point. If the fuel cell voltage was high enough, the converter would operate in buck mode and deliver energy to the battery. The proposed converter offered electrical isolation using transformers between the load and the battery. However, the design did not offer this advantage to the fuel cell. It was not clear whether a fuel cell was included in the simulations and experimental work. As in many publications, the study was limited to a specific area in a fuel cell system. Only the main field of interest was studied in detail while other important phenomena relevant to fuel cells were simplified and were not sufficient for a complete fuel cell system design. It appeared that the focus here was on the battery and converter part rather than on the complete fuel cell system.

Similarly, Marshall and Kazerani [38] proposed a novel boost converter for fuel cell applications, but their main focus was on energy management with an energy storage device. Their simulations and experimental work used a 12 V battery to replace the fuel cell.

2.3 Summary

Most of the published work on the fuel cell focuses on a certain aspect and neglects some important phenomena required for an overall control of the fuel cell power regulation. It is important to build the control strategy on a model that reflects the effect of the main variables such as the double layer capacitance, and the diffusion properties in the fuel cell. Most published work on converter design and its control neglected one or more of these important characteristics of the fuel cells. On the other hand, published work describing the fuel cell, neglected to properly implement the interactions between the fuel cell and the load. For example, it was assumed that the fuel cell current is an independent variable that can be controlled regardless of the load connected across the fuel cell terminals. In addition, published studies on fuel cell control used model linearization, then developed and tested the control strategy on a limited operational region. Therefore, fuel cell nonlinearities were not observed, or treated.

2.4 Thesis Objectives

Different models of the fuel cell are available in the literature; each seems to be suitable to deal with certain phenomena of fuel cells relevant to particular applications. These variations in fuel cell models have created several more variations in the proposed control strategies of the fuel cell and the power conditioning techniques. The objectives of this research were:

1) to obtain a new fuel cell model that is comprehensive and represents the main phenomena within the fuel cell which could have an influence on its dynamic behaviour during changes in power demand;

2) to find a new approach to properly integrate the model with the remaining components of a complete fuel cell system indicating the interactions between them,
3) to propose a control strategy for the fuel cell operating conditions found in objective (1),
4) to obtain a reasonably suitable DC-to-DC converter for realising the fuel cell electrical output and its effect on the fuel cell operating variables;
5) to apply a novel control strategy on the DC-to-DC converter that would satisfy the general requirements of an electrical load or application over the entire operational region, without using an energy storage device.

Chapter 3

METHODOLOGY

3.1 Introduction

A fuel cell system is modelled in this study including the fuel cell stack, power conditioning unit and the control necessary to achieve the required operation. A block diagram shown in Fig. 3.1 gives the main components of the fuel cell system analysed in this study. A fuel cell model is developed to represent the dynamic behaviour of fuel cells. The influential fuel cell variables are further modelled and a control strategy is proposed and tested. As mentioned earlier, a power conditioning unit is the best method to match the fuel cell output with load requirements. A control strategy is developed to maintain a constant load voltage.

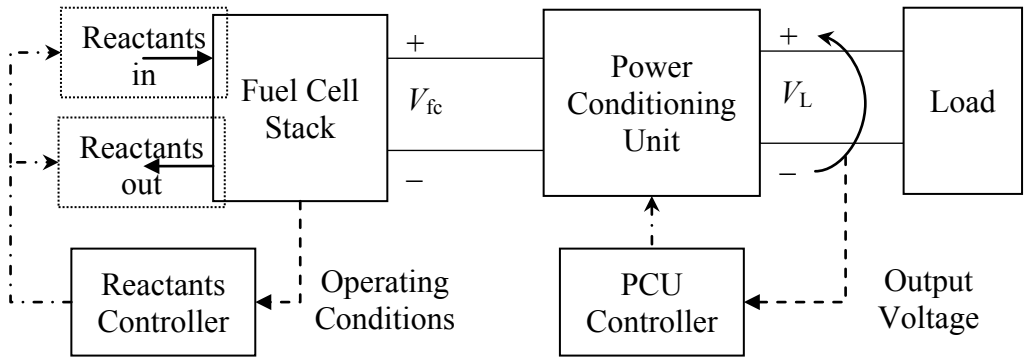

Fig. 3.1. Block diagram of a Fuel Cell System Control

A powerful tool for developing control systems is modelling and simulation. "Modelling and simulation" reduces the time and cost of "building and testing" the actual system. A comprehensive model that takes into consideration all the phenomena involved in or related to the subject under investigation reduces the development process. A well-designed model can satisfy being right from the first time when it comes to building the actual physical system.

The process of developing the control strategy is shown in Fig. 3.2. It begins with the main objective to have a fuel cell control system that results in a controllable output power in terms of quantity and quality. The quality of the output power is usually defined by a constant voltage, and fast response times to changes in power demand, as agreed by standardisation institutions. The first task in the development process is to study the theoretical background needed to recognise the fuel cell behaviour and its operating requirements. This study is translated into a mathematical model built into an interactive environment and validated with available experimental data from the literature. If the model does not produce acceptable results, the theoretical background needed for the model is improved until an acceptable model is obtained. For instance, the initial design of the fuel cell model incorporated only the steady state behaviour of the fuel cell, however, this model was found to be unacceptable for the design of DC-to-DC converters and the controllers. Hence, further improvements on the model were done by studying the dynamic behaviour of the fuel cell, forming the theory and equations behind this behaviour, and then re-simulating the model. The next step in the process is motivated with the need to have a DC-to-DC converter design that is developed in a similar process to that of the fuel cell model. After satisfactorily models of the fuel cell and all auxiliary components are obtained, a control strategy is studied and developed for the fuel cell and the DC-to-DC converter.

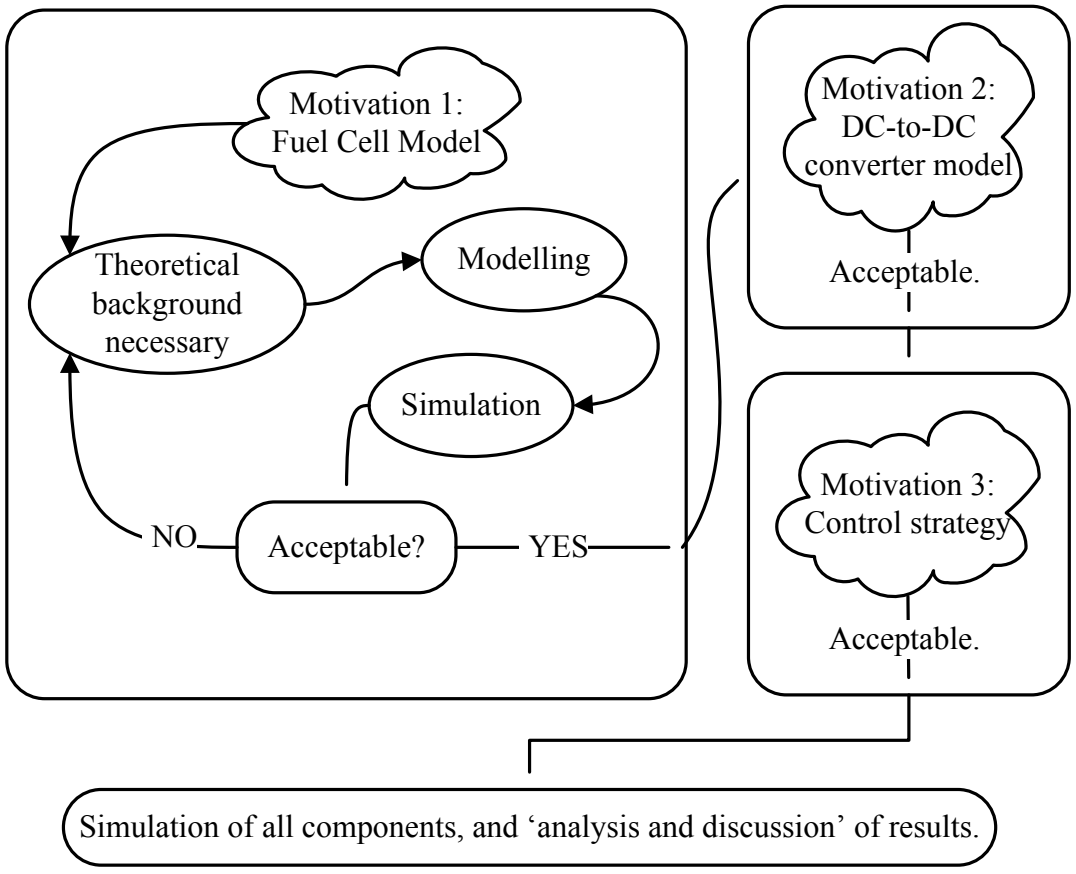

Fig. 3.2. Flow of modelling process needed for control strategy development.

The equations that describe the fuel cell system are implemented and solved using a computer-programming package developed by The MathWorks, Inc. called Simulink®, which installs as an additional product within MATLAB®. Simulink® is an advanced tool for modelling, simulating and analysing dynamic systems [39]. It is capable of modelling linear and nonlinear systems, in continuous time, sampled time or a mixture of both. A single model in Simulink can be used to simulate various phenomena, such as electrical circuits, electrochemistry, and the interactions between them.

3.2 The Fuel Cell

The fuel cell is an electrochemical device that converts the chemical energy stored in the reactants into electrical energy. The rate of the reaction is an important factor in improving the energy conversion efficiency, mainly by reducing the activation energy, discussed later in this chapter. However, the rate of energy output, in other

words the output power, depends on other factors besides the rate of the reaction. The fuel cell is described in sufficient details in the following sections. A parametric study (presented in Chapter 4) is carried out to determine the key variables in the fuel cell performance in terms of controlling the electrical output power to match the demand of the load.

3.2.1 Fuel Cell Electrochemistry

In a fuel cell where energy is converted from one form to another, the input and output energies are of utmost interest. In a fuel cell energy conversion process, the input energy is the chemical energy of the reaction's reactants (Hydrogen and Oxygen), while the output energy is the chemical energy of the reaction's products (water and heat) and the requested electrical energy. In other words, for an ideal process, the output electrical energy equals the difference between the energies of the reactants and the products of the reaction. The change in Gibbs free energy of formation (G_f) is used to define the energy change for the fuel cell reaction as follows:

$$\Delta G_f = \Sigma G_f \text{ (products)} - \Sigma G_f \text{ (reactants)} \tag{3.1}$$

This can be written in molar form (g_f) for the fuel cell reaction as:

$$\Delta g_f = \left(g_f\right)_{H_2O} - \left(g_f\right)_{H_2} - \frac{1}{2}\left(g_f\right)_{O_2} \tag{3.2}$$

Hence, for an ideal process, the output electrical energy is:

$$\text{Electrical Energy} = n.F.E = -\Delta g_f \tag{3.3}$$

Where n is the number of electrons transferred in the external electrical circuit per one molecule of fuel, and is equal to 2 for hydrogen, F is Faraday's constant, and E is the open circuit voltage of the fuel cell. Hence, the open circuit voltage is:

$$E = -\frac{\Delta g_f}{2F} \tag{3.4}$$

The open circuit voltage of the fuel cell (E) is dependent on the temperature and pressure of the reactants and is usually calculated with reference to the open circuit voltage ($E°$) at standard conditions of 1 atmospheric pressure and 25 °C. This can be derived using Gibb's free energy and entropy as given by Larminie and Dicks in [5]. However, Nernst's equation defines the relationship between the open circuit voltage of the fuel cell (E_{Nernst}) and the activities of the reactants and products. The activity of species x (a_x) is defined as the partial pressure of species x at the reaction site ($P_{x,r}$) divided by the standard pressure (1 atm). Hence, when 'atm' units are used, $a_x = P_{x,r}$. The Nernst equation for hydrogen fuel cells is defined by Eq.3.5 [40].

$$E_{Nernst} = E^o + \frac{RT}{2F}\ln\left(\frac{P_{H_2,r}.P_{O_2,r}^{1/2}}{P_{H_2O,r}}\right) \tag{3.5}$$

Where T is the temperature in Kelvin, R is the universal gas constant. The partial pressure of species x at the reaction site is denoted as $P_{x,r}$, compared to $P_{x,ch}$ denoting the partial pressure of x at the flow channels before it diffuses through the GDL, described in Section 3.2.4. However, $E°$ is temperature dependent and the Nernst equation is modified [40, 41] as shown in Eq.3.6 to take into account the temperature effect with reference to standard temperature (25 °C). The open circuit voltage (E) is implemented in Simulink as shown in Fig. 3.3.

$$E = E^o + 8.5\times10^{-4}(T - 298.15) + \frac{RT}{2F}\ln\left(\frac{P_{H_2,r}.P_{O_2,r}^{1/2}}{P_{H_2O,r}}\right) \tag{3.6}$$

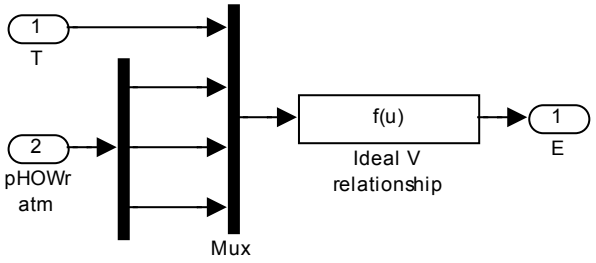

Fig. 3.3. Block diagram of the ideal voltage in Simulink.

3.2.2 Fuel Cell Losses

The fuel cell ideal output voltage is equal to 1.18 V for any output current. However, actual operation suffers from activation, ohmic and concentration losses. These losses depend on a number of variables and conditions. For purposes of systems control analysis, it is necessary to have a fuel cell model that depicts the dynamic operation of the main variables, including control, operational, and geometrical variables. A dynamic fuel cell model is built using Simulink to relate the operating points of the fuel cell with its operating conditions and geometric variables according to the load connected across the fuel cell terminals. In order to have a model that dynamically interacts with any load connected to its terminals, it is necessary to ensure that neither the current nor the voltage is chosen independently of the load across the fuel cell. Since the fuel cell voltage and current are the same as that of the load, they must satisfy the load and the fuel cell electrical characteristics.

In addition to the aforementioned losses, imperfections in the membrane's resistivity allow some electrons to pass through it, as well as some reactants in their gaseous form. The membrane's internally crossing over electrons do not pass through the external circuit, and their contribution to do useful electrical work is wasted. Similarly, gases passing through from one side of the membrane to the other may take part in the reaction but on one side only, bypassing the external circuit. Both electrons and gases going through the membrane are given the name crossover currents. Crossover currents are assumed constant in most research studies and in this study, their value is given as 30 A/m^2. The crossover current, i_c, exists even when the fuel cell is not connected to any external circuit, thus, consuming very small amounts of hydrogen.

In electrochemistry, the activation, ohmic and concentration losses are defined to represent an equivalent voltage drop caused by each of these losses, known as overvoltages. For a PEM fuel cell, where pure hydrogen is used as the fuel, the activation energy of the reaction at the anode is much smaller than that required for the reaction at the cathode [19]. Therefore, only the losses at the cathode are considered from this point, unless otherwise stated. For control purposes, this would not have a significant effect on the overall controller design, which should be immune, to a certain

degree, to external disturbances as well as some acceptable modelling inaccuracies. In other types of fuel cells where other fuels may be used, the losses at the anode may be significant.

3.2.2.1 Activation and Concentration Overvoltages

The activation overvoltage is due to the minimum amount of energy (activation energy) that the reactants need to have in order to get a noticeable reaction rate. The activation energy is different from one reaction to another and it is usually found experimentally. Arrhenius formulated a simple empirical equation in 1889 that defines the reaction rate coefficient with respect to temperature [42, 43]:

$$k = \Lambda e^{-E_a/RT} \tag{3.7}$$

Where k is the reaction rate coefficient, Λ is called a pre-exponential or frequency factor and E_a is the activation energy of a reaction. This equation is implemented in Simulink as shown in Fig. 3.4.

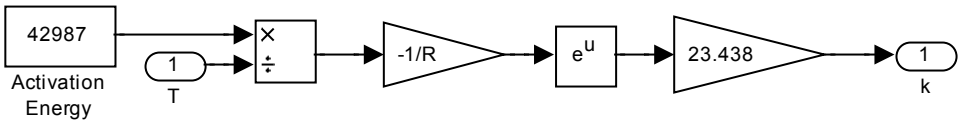

Fig. 3.4. Block diagram of Arrhenius' relationship in Simulink.

In case of a fuel cell, the reaction represents transfer of electrons and protons between the reactants and products at each electrode. For example, at the anode, the reactants are only hydrogen molecules, and the products are electrons and protons. For an open circuit fuel cell, where no electrons are moving externally, the reaction at the anode is taking place but in equilibrium, where the products, are reacting in the reverse direction to produce hydrogen molecules, H_2. In other words, at each electrode and under open circuit condition, the forward reaction is occurring as well as the reverse, or opposite, reaction and at the same rate. This rate is known as the exchange current density (i_o) and is defined in the following equation:

$$i_o = \nu F k \left(\frac{P_{O_2,r}}{P^o} \right)^{\alpha} \left(\frac{P_{H_2O,r}}{P^o} \right)^{(1+\alpha)/2} \tag{3.8}$$

Where ν is the number of electrons exchanged at the electrode, α is the charge transfer coefficient. P^o is used to denote reference to standard atmospheric pressure, which equals to 1 atm when 'atm' units are used in the equation. The implementation of Eq.3.8 in Simulink is shown in Fig. 3.5. The exchange current density is a function of the activation energy embodied in the reaction rate coefficient, and the concentration of reactants at the reaction sites represented as the partials pressures of the reactants.

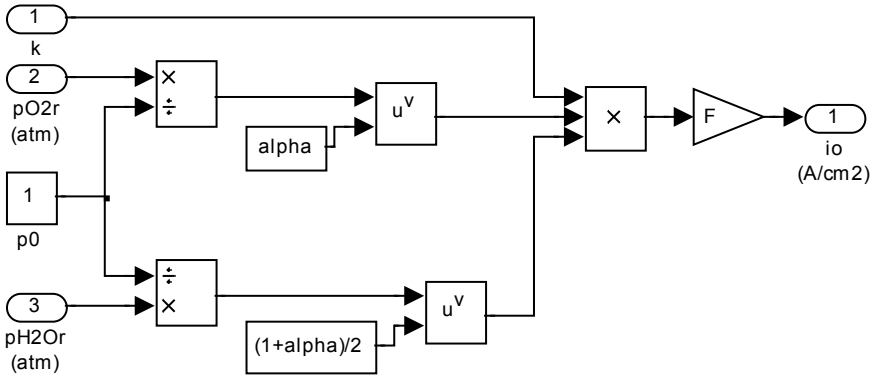

Fig. 3.5. Block diagram of the exchange current density in Simulink.

Concentration overvoltages are equivalent to the drop in voltage due to depletion of the reactants at the reaction zones, which is either due to the physical limitation of the gas flow zones and GDL or due to the insufficient supply of the reactants at the supply manifolds. Concentration losses are dominant at high current densities, while activation losses are more significant at low current densities.

A relationship between the activation overvoltage (V_{act}) and the reaction current (i_r) is defined as the *Butler−Volmer* equation at the cathode as follows:

$$i_r = i_o \left(e^{(nF/RT)\alpha . V_{act}} - e^{(nF/RT)(\alpha-1)V_{act}} \right) \tag{3.9}$$

Where i_r is the reaction current density (A.cm^{-2}), which indicates the consumption rate of the reactants, n here equals 1, and V_{act} is in Volt. This equation is

implemented in Simulink as shown in Fig. 3.6, while Fig. 3.7 shows all sub-block diagrams used to build the total *Butler−Volmer* equation. The tuning coefficient K_{io} shown in Fig. 3.7 is discussed later in Section 3.2.5.

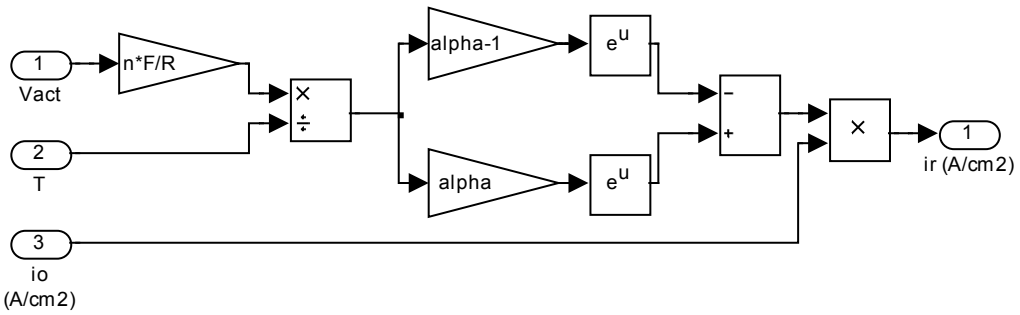

Fig. 3.6. Block diagram of the reaction current relationship in Simulink.

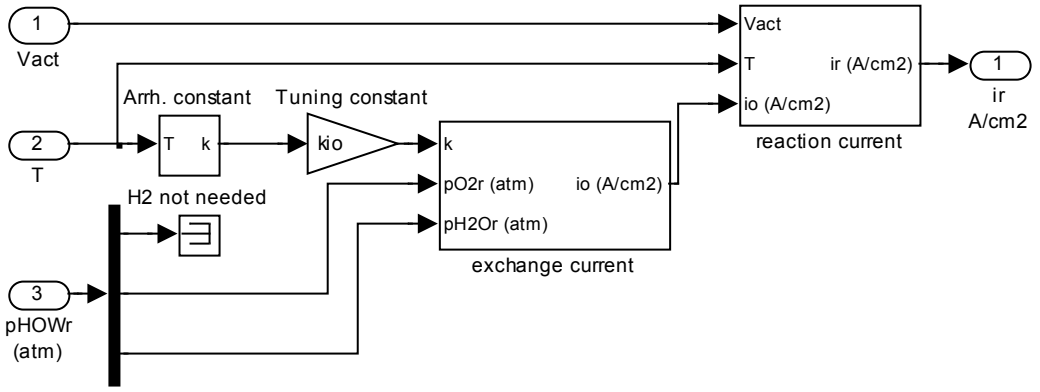

Fig. 3.7. Block diagram of Butler-Volmer (i_r) relationship in Simulink.

The dynamic behaviour of the fuel cell voltage is described by the double layer capacitance (C_{dl}) which is formed at the interfacing boundaries between the fuel cell components/layers. Under steady state operation, the reaction current equals the summation of the crossover current and the current through the external circuit, $i_r = i_c + i$. The voltage acting on C_{dl} is the activation overvoltage, V_{act} and the following relationship applies:

$$\dot{V}_{act} = \frac{i + i_c - i_r}{C_{dl}} \tag{3.10}$$

Details of the dynamic behaviour of the fuel cell are studied in section 3.2.3. Both i_r and V_{act} are dependant variables and the relevant equations are solved iteratively in Simulink. Implementation of Eq.3.10 in Simulink is shown in Fig. 3.8.

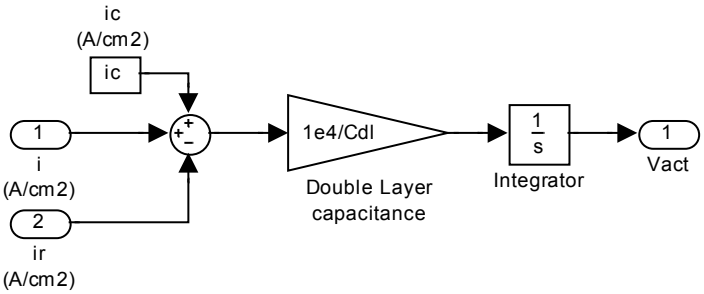

Fig. 3.8. Block diagram of the activation overvoltage in Simulink.

3.2.2.2 Ohmic Overvoltage

In electrical engineering, a voltage drop due to electrons passing through a resistance is called ohmic voltage drop, and is defined by Ohm's law. In electrochemistry, this term is slightly modified to represent the voltage drop due to proton movement through the membrane's 'protonic resistance', and is called ohmic overvoltage. The ohmic overvoltage would also include the voltage drop due to electrons' movement from the point where they are produced at the reaction site, going through the catalyst layer, the GDL, bipolar plates, and any other interconnections between the cells and/or the fuel cell terminals. However, the amount of resistivity to electrons' movement is relatively small compared to the protonic resistance, hence it will be ignored. The ohmic protonic overvoltage is found by Ohm's law:

$$V_{ohm} = i.R_{mem} \tag{3.11}$$

Where i is the current density in A/m^2 and R_{mem} is the membrane protonic resistivity in $\Omega.\mathrm{m}^2$. In this equation, the value of the external current is used since the number of electrons equals the number of protons for each atom of fuel.

The crossover current passes through the membrane in the same direction as the protons, hence, it does not contribute to the ohmic overvoltage, and consequently is not included in the ohmic overvoltage.

The protonic conductivity of the membrane is greatly dependent on the water content of the membrane. When protons move from the anode to the cathode, some water molecules inside the membrane are dragged to the cathode side, causing low water content at the anode side of the membrane. Usually, humidified hydrogen is supplied at the anode to balance the water content distribution within the membrane. This problem is of major importance on the performance of fuel cells. However, transients in the water content of the membrane have time constants between 10-30 seconds, hence; this control problem is not within the scope of this study. The membrane is assumed fully humidified with uniformly distributed water content. This phenomenon of membrane water content transients are not examined any further in this study, and only the effect of temperature on the membrane's resistivity is taken into account in the ohmic overvoltage model. The value of the protonic resistivity of the membrane is found empirically by [19] as follows:

$$R_{mem} = R_{ref} - \alpha_T (T - T_{ref}) \tag{3.12}$$

This equation is valid only for temperatures in the range of 40 to 80° C, which is the range of normal operation of the fuel cell. R_{ref} is a reference resistivity of the membrane at the reference temperature, T_{ref} = 343.15 K. α_T is found empirically, and the value used here is 2.02 x 10^{-7} Ω.m^2/K [19]. The Simulink block diagram of the ohmic overvoltage is shown in Fig. 3.9.

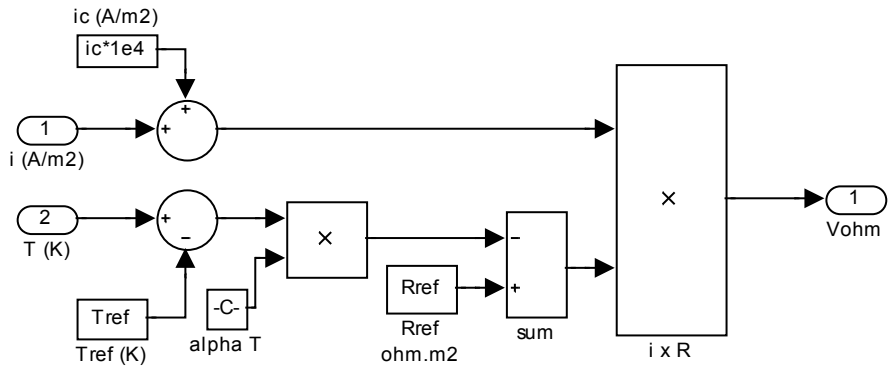

Fig. 3.9. Block diagram of the ohmic overvoltage in Simulink.

3.2.2.3 The Fuel Cell Polarization Curve

The actual output voltage of the fuel cell (V_{fc}) drops as the current output increases, as noted by the overvoltages discussed earlier. The total voltage (V_{fc}) is found by subtracting the activation and ohmic overvoltages from the open circuit voltage:

$$V_{fc} = E - V_{act} - i.R_{mem} \tag{3.13}$$

The total fuel cell voltage implementation in Simulink is shown in Fig. 3.10. It is assumed that a fuel cell stack consists of N cells with an active area A, and all cells have identical performance. The diffusion block diagram is discussed in detail in Section 3.2.4.

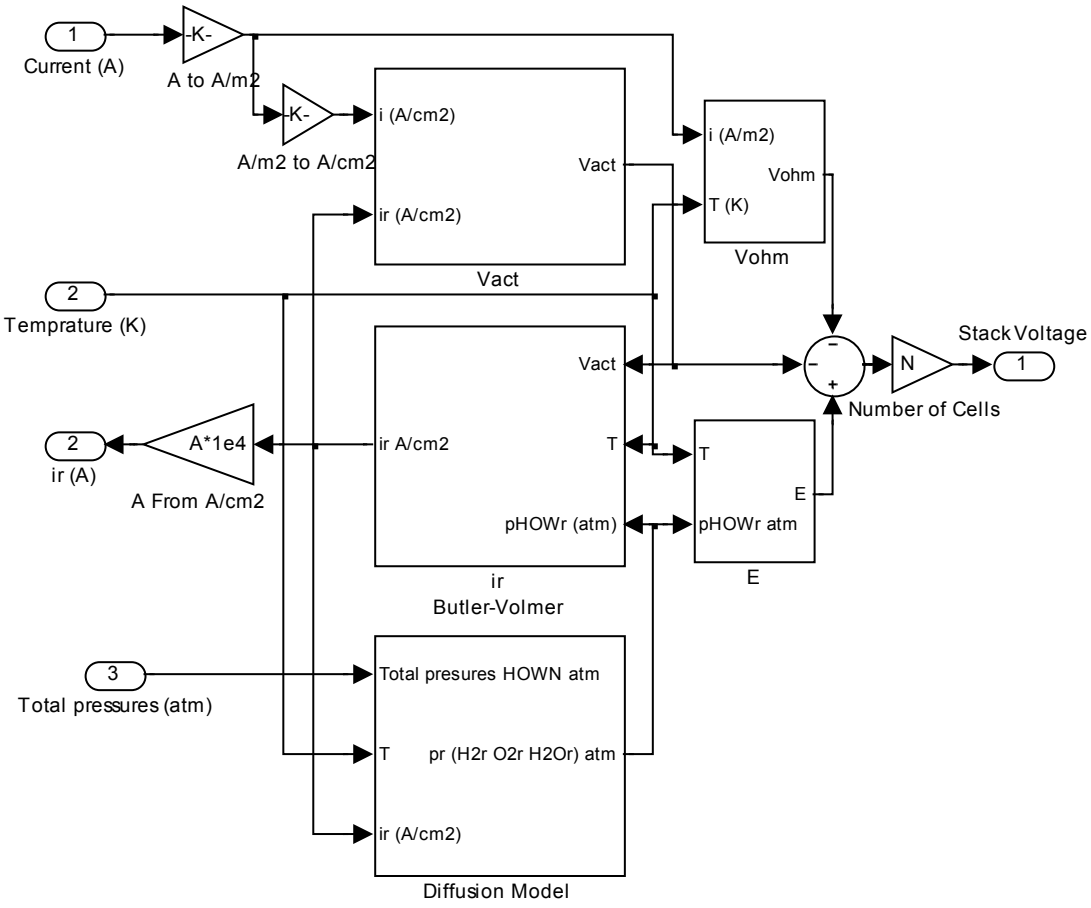

Fig. 3.10. Fuel cell voltage model in Simulink.

3.2.3 Dynamic Response of Fuel Cell

The dynamic response of the fuel cell is important for the design of DC-to-DC converters and important to give the overall system model a more realistic behaviour. There has been a lot of opposing arguments in the literature on the dynamic response of the fuel cell. This is mainly because of the different points of view taken, the phenomenon being studied, and the concerned time scale of dynamics. For instance, the temperature transients are reported to have time constants in the range 10-60 seconds, membrane water content transients have a time constant in the range 10-30 seconds, gas flow/pressure/diffusion has a time constant in the range of 0.01-0.1 seconds, while the electrochemical reaction response is reported in the range of nano- to micro-seconds [9, 16, 17, 19].

The fuel cell is connected to a DC-to-DC converter, which has switching frequencies that can be designed in the range of 1-10 kHz. This is equivalent to 0.1-1 ms. From this point of view, and at this range of time scale, the phenomena that are 10 times or more slower than the switching frequency are seen constant. Only the electrochemical reaction response can react to changes in that range of operation. However, this does not mean that the slow varying phenomena may be ignored; it just means that they would have less influence on the design of the DC-to-DC converter's control.

The dynamic response of the fuel cell is realized by the double layer capacitance, C_{dl}, as noted earlier in Eq.3.10. Some researchers claim that it exists between the gas diffusion layer and the catalyst layer, others claim that it exists between the catalyst layer and the PEM membrane. In any case, the exact location of the double layer capacitance is insignificant in this study.

A simple electrical circuit model of the fuel cell voltage is shown in Fig. 3.11. The location of the internal resistance of the membrane is chosen different from most models available in the literature; to avoid the crossover current passing through it, as explained in Section 3.2.2.2.

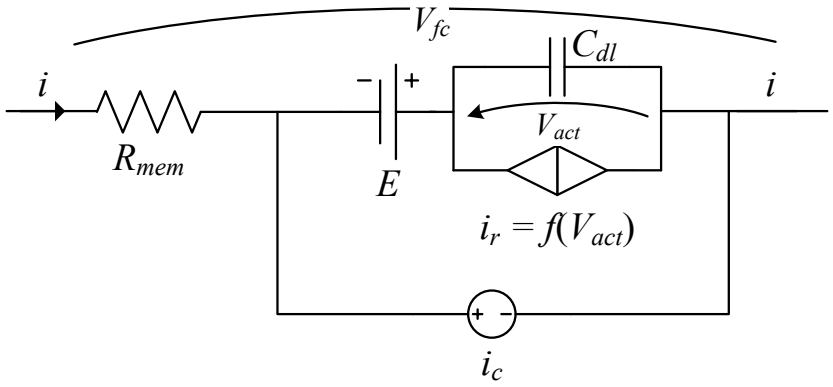

Fig. 3.11. Fuel cell voltage circuit model.

It should be noted that a value of the double layer capacitance could only be obtained experimentally. Taking into consideration variations in experimental setup, fuel cell design and materials of the components used, and the pressure used to tighten the fuel cell components; all these would result in a wide range of reported values of C_{dl}. Hence reported values of C_{dl} were 13.70 mF/cm^2 [44], 41 mF/cm^2 [19], 100 mF/cm^2, and 480 mF/cm^2. In this study, C_{dl} is assumed constant (150 mF/cm^2) as reported in [17], although high temperature PEM fuel cell was tested, but because they recognised a lumped capacitance value, and reported details of their experimental work, which used a sampling rate of 1μs/sample. Fig. 3.12 shows a typical polarization curve (solid line) of a single 1 cm^2 fuel cell obtained by running the fuel cell model as detailed later in Section 3.6.1. The polarization curve, also known as the characteristic curve, of a fuel cell gives all possible operating points (output voltage and current) of the fuel cell at steady state operation, when the load does not vary with time. For any load connected across the fuel cell terminals, there is only one possible operating point, which is the intersection point of the polarization curve and the load characteristic curve. The dynamic behaviour, verified experimentally by Weydahl et al. [16], of the fuel cell during a sudden change in the load is shown by the dotted line in Fig. 3.12.

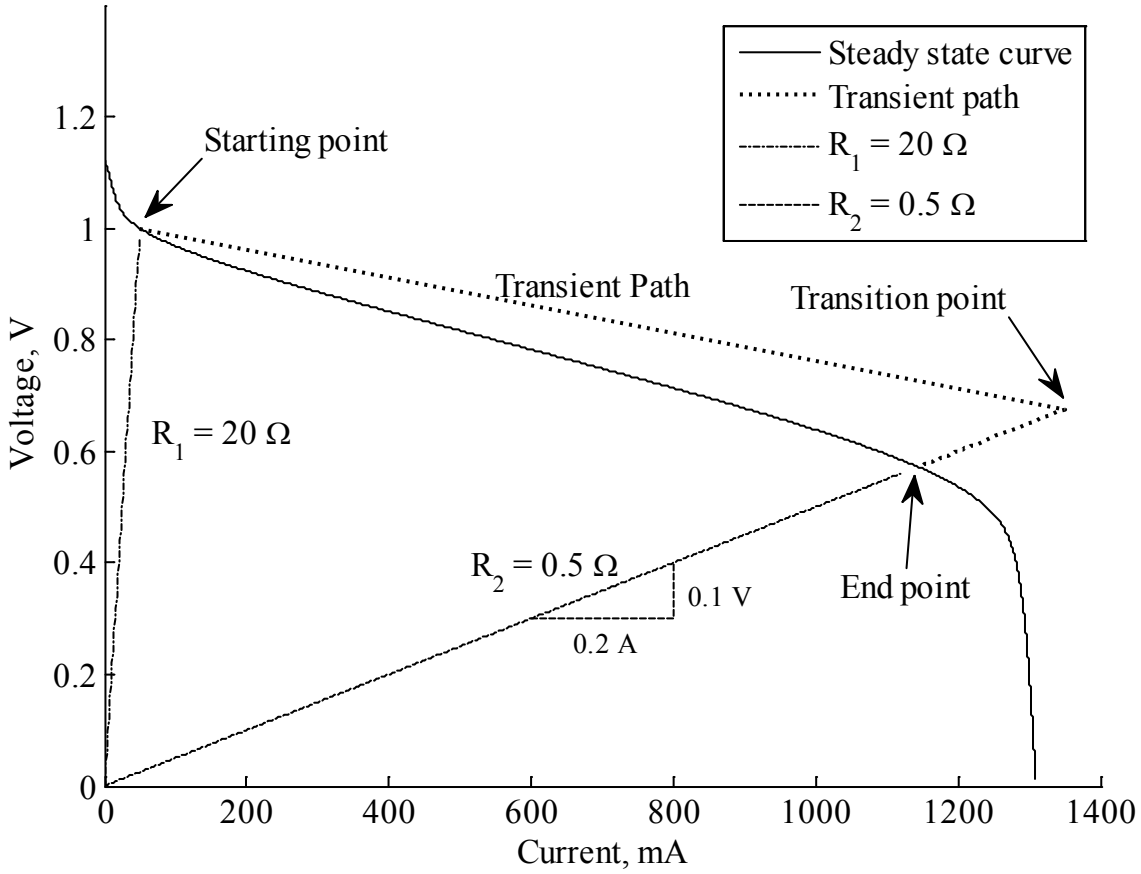

Fig. 3.12. Transient operating points of the fuel cell to load changes from 20 Ω to 0.5 Ω.

Initially the fuel cell is connected to a 20 Ω load resistance, operating at the operating point denoted on Fig. 3.12 as the starting point. Changing the load instantly to 0.5 Ω forces the fuel cell operating point to follow the transient path shown as a dotted line. The slope of the straight-line transient path between the starting point and the transition point is equal to the negative of the internal resistance of the membrane. The transition point (shown on figure) is the intersection point between the transient path and the external resistance line. The reported exact duration of time between the starting point and the transition point could not be experimentally measured due to limitations of the sampling rate of measuring devices. The reported value by Zenith et al [7] is 1 μs. The response between the 'transition point' and the 'end point' follows an exponential decay response with a time constant that depends on the internal resistance of the membrane, C_{dl} and its initial charge, and the external resistance of the load.

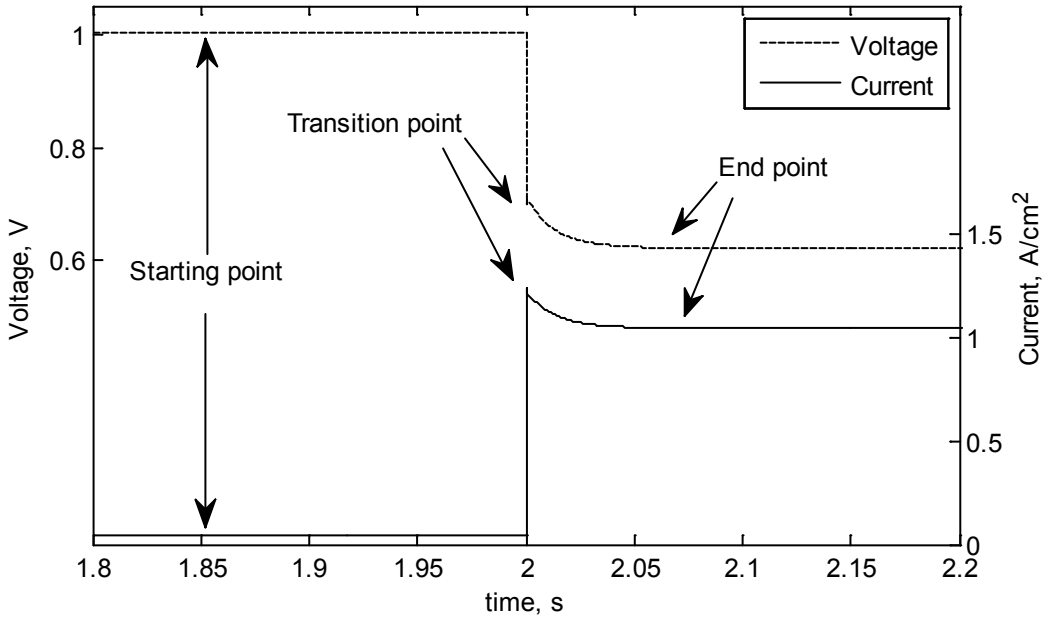

Fig. 3.13. Fuel cell voltage and current time response to a load change from 20 to 0.5 Ω at timestamp 2 s.

An explanation of the dynamic response shown in Fig. 3.12 is detailed by analysing the components of the fuel cell voltage. The ideal voltage, E depends on the partial pressures of the reactants and the temperature of the reaction. Both the pressure and the temperature are continuous in time, and do not change stepwise. Consequently, E is continuous in time and does not change instantly as the change in the load. The activation voltage, V_{act}, across C_{dl} changes continuously with time, however, the capacitance current can change instantly. Initially the capacitor is charged with electrostatic charges that can charge/discharge abruptly when the load changes. The charging current through the double layer capacitance is $i+i_c-i_r$, which is zero at steady state. The reaction current (i_r) is a function of the activation voltage and hence it is continuous in time. Since i_c is constant, only the external current (i) changes instantly, as well as the ohmic overvoltage and the voltage across the load. The response of the fuel cell voltage and current in the time domain due to the step change in load from 20 Ω to 5 Ω is shown in Fig. 3.13.

3.2.4 Diffusion

Fuel cells breathe hydrogen and oxygen (taken from air) to produce electricity. The partial pressures of the reactants at the reaction sites have a great influence on the performance. Reactant gases diffuse from the gas flow channels, through the gas diffusion layer (GDL) to reach the reaction site. For the fuel cell consumption rates, diffusion transients are insignificant, and therefore they are ignored [17]. Hence, at the anode where pure hydrogen is fed, the pressure of hydrogen at the reaction site would be the same as that at the flow channels. Consequently, hydrogen diffusion is ignored. At the cathode side, the produced water vapour diffuses in the opposite direction of oxygen diffusion to reach the flow channels. The partial pressures of the reactants depend on geometrical parameters of the GDL, the partial pressure of gases at the gas flow channels and the rate of consumption of the reactants. Stefan-Maxwell equations are used to describe the multicomponent diffusion in an ideal gas mixture, more details in Bird et al. [45]. A modified form of Stefan-Maxwell equation [19] (Eq.3.14) is used to describe the diffusion through a porous material such as the gas diffusion layer. The coefficient ε/ξ^2 accounts for the diffusion through porous materials. This equation determines the partial pressures of the reactants after they diffuse through the GDL, given their partial pressures at the flow channels and their flow flux, which is determined by the consumption/production rates of the reaction, as shown in Eqs. 3.15 and 3.16.

$$\frac{\varepsilon}{\xi^2}\frac{\partial P_j}{\partial x} = \sum_k \frac{R_d T}{P_T D_{jk}}(P_j N_k - P_k N_j) \tag{3.14}$$

Where ε is the porosity of the GDL (values of 0.3-0.5 are found in the literature and from manufacturers), a value of $\varepsilon = 0.4$ is used in this study. ξ is the tortuosity of the GDL and a value of 7 is common [17] for commercial GDL, whereas x is defined as the distance from the reaction site towards the gas channel. The universal gas constant in this equation is denoted as R_d (82.057 atm.cm^3.mol^{-1}.K^{-1}) because the units used in this equation are different from those used in other equations in this thesis. P_T is the total pressure of air (atm), D_{jk} (atm.cm^2/s) is the mutual diffusivity coefficient of species j and k, where $j, k = O_2, N_2, H_2O$. The molar flux of species j (N_j) is the number of moles

of species *j* that passes through a unit area per unit time (mol.cm^{-2}.s^{-1}). This is equal to the molar consumption and production of oxygen and water, respectively, and is determined in Eqs. 3.15 and 3.16. Diffusion transients are negligible and neglected, and it is assumed that the diffusion flux is uniform in the plane perpendicular to *x*.

$$N_{O_2} = -\frac{i_r}{4F} \tag{3.15}$$

$$N_{H_2O} = \frac{i_r}{2F} \tag{3.16}$$

Nitrogen is not consumed in the reaction, therefore, $N_{N_2} = 0$. Assuming linear pressure variation across the GDL thickness (L_D), i.e. $P(x) = P(0) + x\partial p / \partial x$, and substituting Eqs.3.15 and 3.16 in Eq.3.14 gives the partial pressures of oxygen and water vapour at the reaction zone, $P_{O_2,r}$ and $P_{H_2O,r}$:

$$P_{O_2,r} = P_{O_2,ch} - i_r \frac{L_D \xi^2}{\varepsilon} \frac{R_d T}{4F} \left(\frac{2P_{O_2,ch} + P_{H_2O,ch}}{P_T D_{O_2,H_2O}} + \frac{P_{N_2,ch}}{P_T D_{O_2,N_2}} \right) \tag{3.17}$$

$$P_{H_2O,r} = P_{H_2O,ch} + i_r \frac{L_D \xi^2}{\varepsilon} \frac{R_d T}{4F} \left(\frac{2P_{O_2,ch} + P_{H_2O,ch}}{P_T D_{O_2,H_2O}} + 2\frac{P_{N_2,ch}}{P_T D_{H_2O,N_2}} \right) \tag{3.18}$$

Where $P_{O_2,ch}$ and $P_{H_2O,ch}$ are the partial pressures of oxygen and water vapour before the GDL, at the gas channels, respectively.

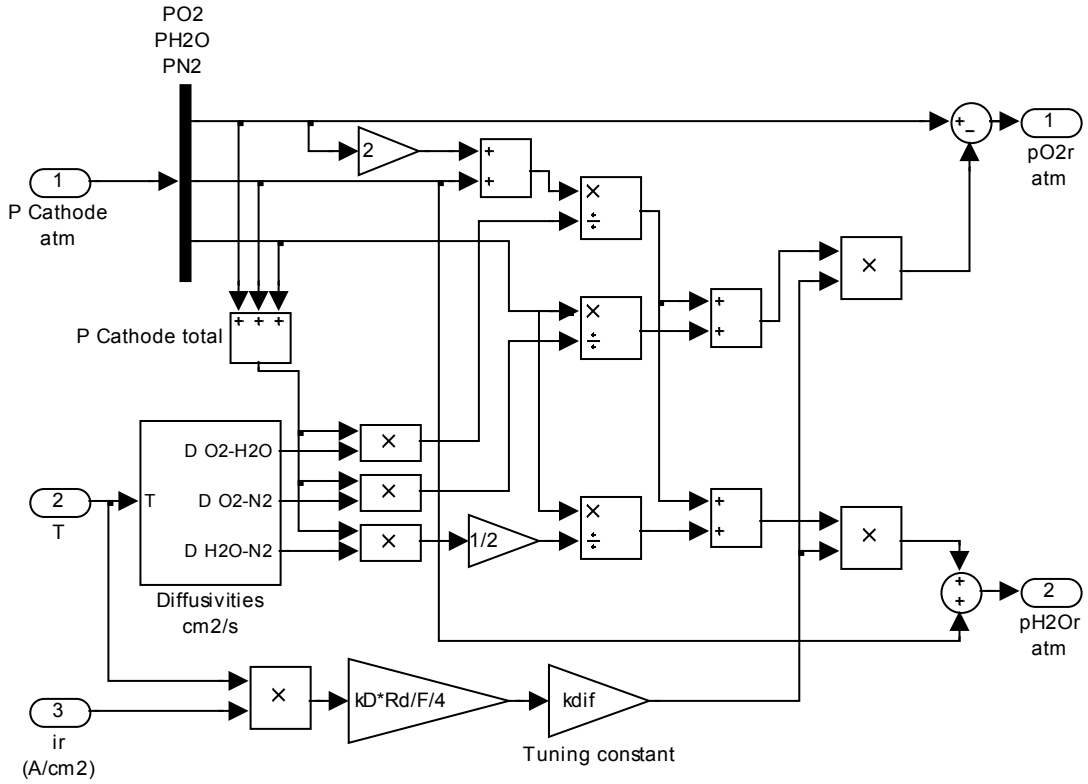

Fig. 3.14. Sub-block diagram of the diffusion calculations in Simulink.

Equations 3.17 and 3.18 are implemented in Simulink as shown in Fig. 3.14. The effective diffusion through porous materials (related to nonporous media) is modified by different authors in a number of ways, for example Um et al. [13] uses the correction factor $\varepsilon^{1.5}$ x D_{ij}. The one adopted in this study is ε/ξ^2 x D_{ij} as in [17, 19] because it incorporates the tortuosity (ξ) in evaluating the effective diffusion making the model flexible to further changes in the GDL. The term $\varepsilon / L_D \xi^2$ is evaluated and substituted with $1/K_D$. A block diagram is created containing that in Fig. 3.14, named 'Cathode Diffusion' as shown in Fig. 3.15. The tuning coefficient K_{dif} shown in Fig. 3.14 is discussed later in Section 3.2.5.

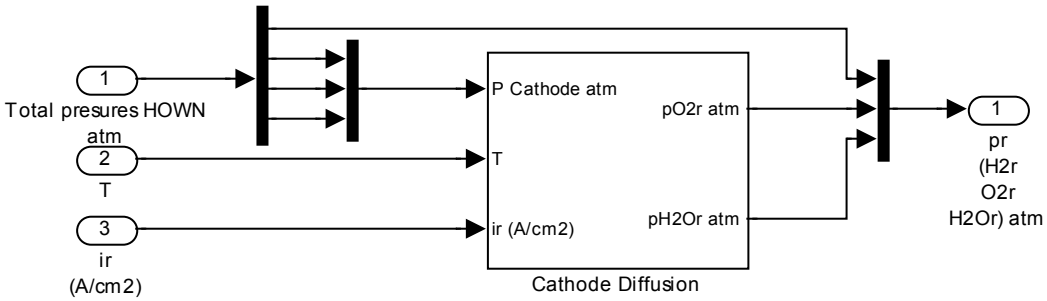

Fig. 3.15. Main block diagram of the diffusion calculations in Simulink.

The binary diffusion coefficients, D_{jk}, can be calculated using the following estimation by Bird et al. [45]. The estimation is used for gas mixtures at low pressures:

$$P_T D_{jk} = a\left(\frac{T}{\sqrt{T_{cj}T_{ck}}}\right)^b .\left(P_{cj}P_{ck}\right)^{1/3} .\left(T_{cj}T_{ck}\right)^{5/12}\sqrt{\frac{1}{M_j}+\frac{1}{M_k}} \qquad (3.19)$$

Where D_{jk} is in cm^2/s, P_{cj} is the critical pressure of gas j in atm, T_{cj} is the critical temperature of gas j in Kelvin, and M_j is the molar mass in g/mol. The parameters a and b have been experimentally formulated by Bird et al. as shown in Table 3.1.

Table 3.1: Parameters a and b used in diffusion equations

	For nonpolar gas pairs (e.g. N_2, O_2)	For H_2O with a nonpolar gas
a	2.745×10^{-4}	3.640×10^{-4}
b	1.823	2.334

Table 3.2 summarises the values of the parameters used in Eq.3.19.

Table 3.2: Parameters used in Eq.3.19

i	M_i (g/mol)	P_{ci} (atm)	T_{ci} (K)
O_2	32	49.8	154.6
H_2O	18	217.7	647.1
N_2	28	33.5	126.2

Source: en.wikipedia.org/wiki/Critical_temperature :: (Emsley, John (1991). *The Elements*) ((2002) *Thermodynamics: An Engineering Approach*)

The constants in Eq.3.19 are evaluated and substituted with k_{jk} to yield:

$$P_T D_{jk} = k_{jk}.T^b \qquad (3.20)$$

Table 3.3 summarises the fuel cell parameters, properties and other coefficients used in the model.

Table 3.3: The parameters used in the fuel cell model in Simulink

Parameter	Value	Unit
Fuel cell stack design parameters (50 kW output power)		
Number of cells in the stack, N	350	–
Area, A	15 × 15	cm^2
Anode & cathode manifold thickness, l	1.5	mm
Anode & cathode volume per cell	3.375 x 10^{-5}	m^3
Hydrogen excess ratio, H_{ex}	1.2	–
Fuel cell parameters		
Membrane thickness (Nafion® 115), L	127.5	μm
Cross over current, i_c	3	mA/cm^2
Double layer capacitance, C_{dl}	1500	F/m^2
Transfer coefficient, α	0.43	–
Electron exchange, n	1	–
Reaction rate tuning coefficient, K_{io}	0.5	–
E^o (for vapour H_2O product)	1.18	V
Activation Energy, E_a	42987	J/mol
Frequency Factor, A	23.438	s^{-1}
Number of electron exchanged at electrode, v	1	–
Gas diffusion layer (GDL)		
Porosity of GDL, ε	0.4	–
Tortuosity of GDL, ξ	7	–
Thickness of GDL, L_D	0.15	mm
Diffusion tuning coefficient, K_{dif}	0.3	–
Equivalent thickness of diffusion layer, K_D	1.8375	mm
k_{O_2,N_2}	6.347×10^{-6}	$atm.cm^2.s^{-1}.K^{-1.823}$
k_{O_2,H_2O}	4.203×10^{-7}	$atm.cm^2.s^{-1}.K^{-2.334}$
k_{N_2,H_2O}	4.398×10^{-7}	$atm.cm^2.s^{-1}.K^{-2.334}$
Membrane Resistivity		
Reference resistivity, R_{ref}	26.9 x 10^{-6}	$\Omega.m^2$
Reference temperature, T_{ref}	343.15	K
Resistivity coefficient, α_T	0.202 x 10^{-6}	$\Omega.m^2/K$
Constants		
Universal gas constant, R	8.314	J/(K.mol)
Universal gas constant, R_d	82.057	$atm.cm^3/(K.mol)$

Application specific geometrical design parameters should be taken into account in the fuel cell stack model. Geometric design parameters affect the area of the fuel cell, the method of interconnecting the cells, the available space where the stack is to be placed and its effect on heat management, and fuel cell exhaust, etc. These parameters

may have an influence on the controllers; however, the control strategy is believed to be valid under any changes, since these geometrical design changes have an influence on parameters with slower dynamics than the most influential dynamics of the fuel cell electrical characteristics.

The fuel cell design parameters are calculated based on a rated output power of 50 kW, which is the minimum recommended power for vehicular applications. At a later stage, the fuel cell stack is simulated under household load profile with a stack rated power of 8 kW, and the changes on the design parameters are discussed. All cells are assumed to have the same voltage and performance properties.

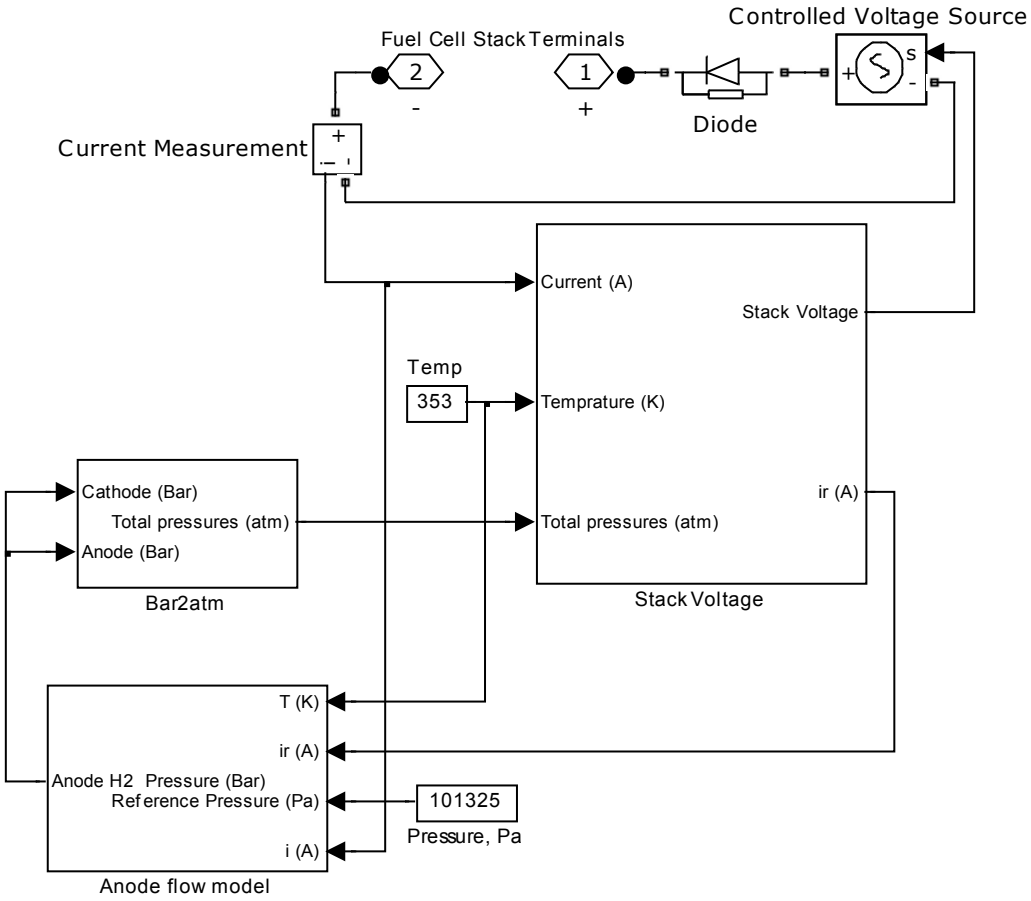

Fig. 3.16. Block diagram of the fuel cell stack and its operating conditions.

The fuel cell model provides a maximum power density of 0.656 W/cm^2. The geometrical size of the active area of membrane is set to 15 cm by 15 cm, which is a reasonable size that should fit smoothly under the hood of a vehicle. Other sizes can

easily be designed, for example if the fuel cell stack is to be placed under the passenger compartment similar to Honda's fuel cell vehicle prototype. The exact geometrical design of the fuel cell stack has no influence on the outcome of this study, since it is based on non-dimensional calculations, except for the diffusion phenomenon, which is modelled uniformly in 1-dimensional space.

The fuel cell stack model in Simulink is shown in Fig. 3.16. The key elements integrating the fuel cell to an external load in Simulink are the 'Voltage Controlled Source' and the 'Current Measurement' blocks. The "Stack Voltage" block contains the subsystem shown earlier in Fig. 3.10, and the "Anode flow model" block contains the subsystem shown later in Fig. 3.21. The "Bar2atm" block simply converts the units of pressures from Bar to atm. Neither the fuel cell current nor voltage act as a control variable in determining the operating point of the fuel cell and both depend on the load connected across the fuel cell stack terminals. This way, the fuel cell model is closer to realistic load interactions than most other model integrations, where the operating point is resolved numerically according to the load. However, it should be noted that the fuel cell current is used as a control variable in the control of the reactants mass flow rates, discussed later in Section 3.3. The block diagram shown in Fig. 3.16 is grouped and masked under the block named "Fuel Cell Stack" as shown in the complete fuel cell system diagram in Fig. 3.18.

3.2.5 Tuning the Fuel Cell Voltage Model

Two tuning coefficients are introduced in the fuel cell voltage model to allow flexibility to variations in fuel cell designs and characteristics. In this study, these tuning coefficients are chosen and fixed, as shown in Table 3.3, to create a general behaviour of the fuel cell steady state voltage. The introduced tuning coefficients, K_{io} and K_{dif}, are placed as shown in Fig. 3.7 and Fig. 3.14. The exchange current density tuning coefficient, K_{io}, affects the rate of the reaction and i_o to allow for variations in catalyst loading, and reaction kinetics that are unaccounted for in the model. Hence, this has an influence on the activation overvoltage; as K_{io} increases, the activation overvoltage decreases. On the other hand, K_{dif} affects the diffusion phenomenon by increasing/decreasing the pressure drop across the GDL. As K_{dif} increases, the pressure

drop increases. Hence, this affects the concentration overvoltage and limits the maximum current density that the fuel cell can produce. Different polarization curves are obtained in Fig. 3.17 to show the effect of varying the tuning coefficients compared to the reference curve, where $K_{dif} = 0.3$ and $K_{io} = 0.5$. Only one tuning variable is changed for each plotted curve. It can be seen from Fig. 3.17 that K_{dif} is inversely proportional to the concentration losses, while K_{io} is directly proportional to the activation losses. These tuning variables add more flexibility to the steady state fuel cell model to meet the differences between various fuel cells, as shown in Section 4.2.

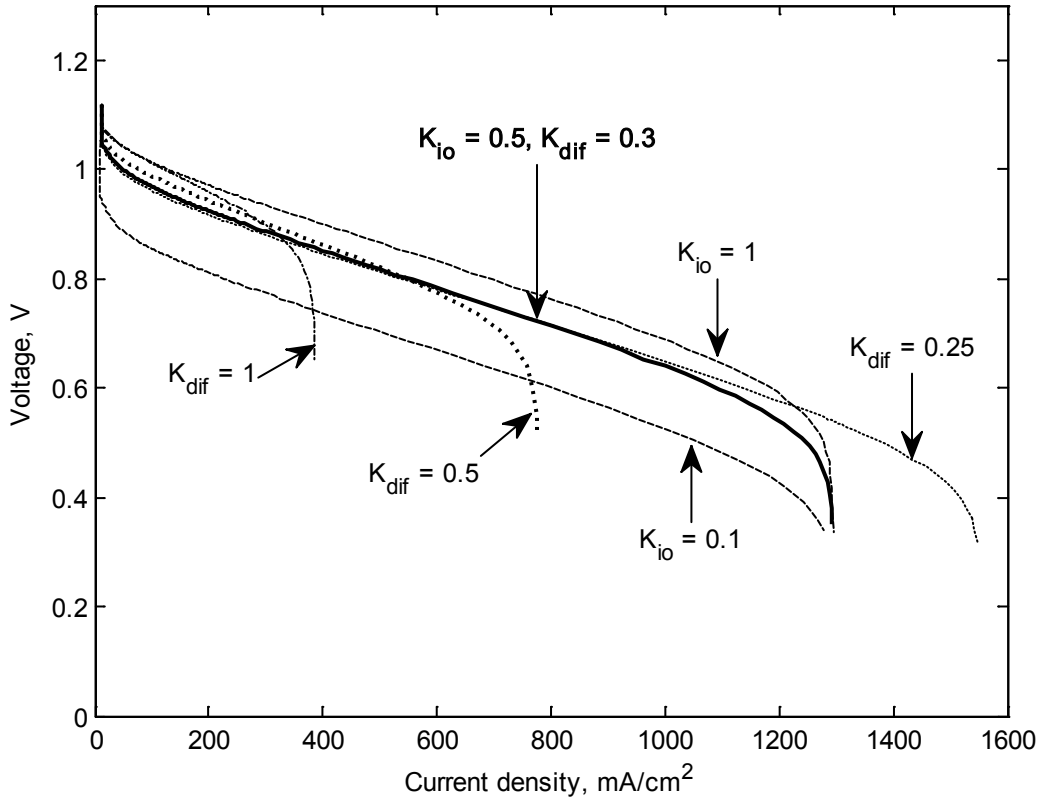

Fig. 3.17. Polarization curves with different tuning coefficients. The thick solid line represents the reference polarization curve used in this study. One tuning coefficient is varied in each curve.

3.3 Fuel Cell Control

Most electrical devices and machines nowadays require a constant voltage at their input terminals, with a certain degree of tolerance. For a specific load connected

across the fuel cell terminals, only one operating point defined by a fixed voltage, current, and power can be obtained from the fuel cell. A DC-to-DC power converter is used to achieve the desired control objectives.

As discussed earlier, the operating conditions may be used to vary the fuel cell output, on the expense of reducing the efficiency and having less control over the dynamic response to changes in load conditions. Hence, the control objective for operating conditions is to maintain maximum efficiency by fixing the operating conditions to their optimum values. The temperature and water content of the membrane have relatively long time constants in the order of 100 seconds and 10 seconds, respectively [9]. Consequently, they have insignificant effect on the control of DC-to-DC converters and they will be assumed constant. The pressures and reactants mass flow rates of the reactants have the smallest time constants that are comparable to the fuel cell voltage. Hence, a control strategy is proposed aimed for achieving constant pressure of the reactants and minimizing concentration losses during sudden increases in power demand.

In this study, two control problems are investigated for a complete fuel cell system; the control of the reactants' pressures and flow rates to achieve maximum efficiency of the fuel cell output, and the control of the power output using DC-to-DC converters.

The complete fuel cell system model implemented in Simulink is shown in Fig. 3.18. It includes the fuel cell stack, the DC-to-DC converter and its controller, and a variable resistance as the electrical load. The fuel cell stack model includes the fuel cell voltage model discussed earlier in this chapter, and the reactants' mass flow and pressure controller.

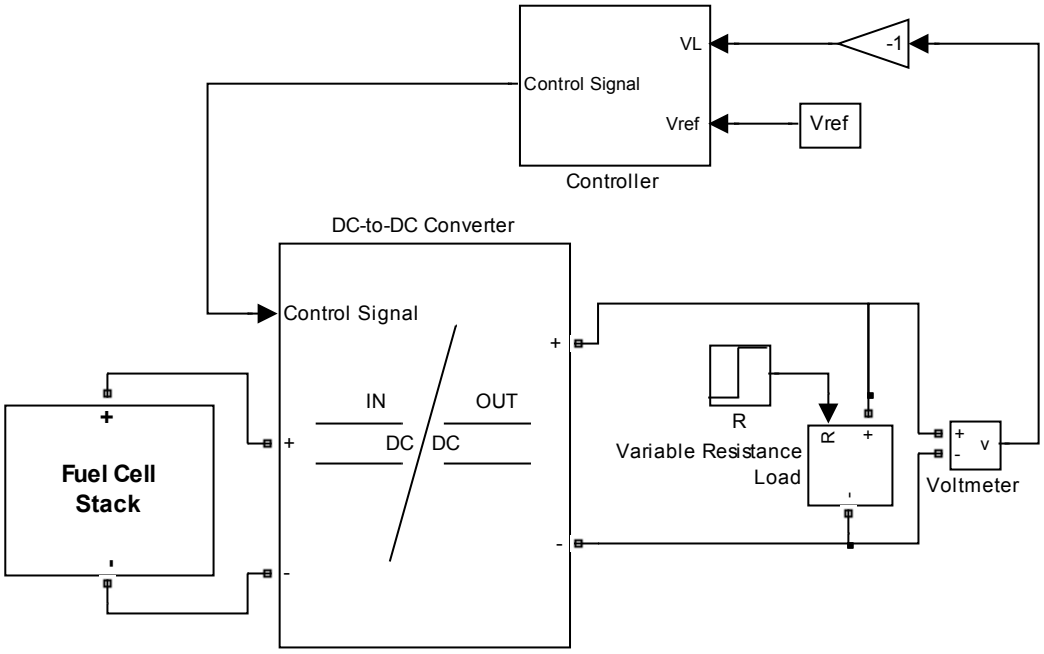

Fig. 3.18. Fuel cell system diagram in Simulink.

Reactants Flow Control

A control strategy is proposed for the basic design of flow channels; an open-end flow channel configuration. This configuration is needed especially for the cathode side where air is supplied. Nitrogen, the produced water, and other gases not taking part in the reaction are taken out with the outlet flow. On the anode side, this configuration is needed to remove any water that may accumulate due to over humidifying the hydrogen stream, or due to the back-diffusion of water through the membrane, as reported in [30]. In addition, the open-end configuration will allow the use of impure hydrogen, such as that generated from reformers, where impurities need to be removed. The dynamics of hydrogen flow in the anode are modelled in this study with time constants of 100 ms. While the dynamics of the air supply system including control valves, compressors, and manifold filling have a time constant in the range of 0.01-10 seconds [26]. Therefore, the same control strategy is assumed applicable for both the anode and cathode reactants supply in terms of pressure requirements and the time constants of flow rate changes. The multi-component gas (air and product water vapour) flowing through the cathode makes the modelling problem more complicated,

and solving it has no effect on the control strategy which is found for the anode flow. Therefore, cathode flow is not modelled and it is assumed that the pressure in the cathode equals that at the anode. This would not affect the diffusion phenomenon on the cathode side since it depends on the pressure inside the flow channels.

Reactants flow control has two objectives:

(i) To prevent reaction starvation that leads to excessive concentration losses under steady and varying load conditions.
(ii) To regulate the pressure inside the flow channels to a set point. A value of 1 atm is assumed for the set point of the operating pressure.

The first objective necessitates supplying excess reactants to meet the sudden unpredictable increase in consumption rates as the power demand increases. This dictates the use of the open-end flow channel configuration. Common values of excess hydrogen in the literature are set to more than 20 % of the consumption rate [30, 46]. Excess hydrogen is usually recirculated to the supply stream. The first objective is mainly important for the cathode supply system, as oxygen constitutes only 21 % of the supplied air; hence, reduction in its concentration losses is more noticeable than hydrogen. Simulation results given in chapters 5 and 6 show how oxygen's partial pressure changes during transients. Therefore, oxygen is usually supplied in excess of more than 100 % of that consumed in the reaction.

The second objective is necessary in order to obtain a stable output voltage and current delivered to the DC-to-DC converter. In addition, a fixed operating pressure would ensure minimum differential pressure between the cathode and the anode across the membrane. Under normal operation, the differential pressure is minimised to extend the lifetime of the membranes and to reduce the permeation of gases from one side of the membrane to the other.

Hydrogen is usually supplied to the fuel cell from highly pressurised tanks through pressure reducers and flow control valves. The hydrogen flow control

objectives are realised using two control valves; one at the inlet and one at the outlet of the anode manifold, as shown in Fig. 3.19.

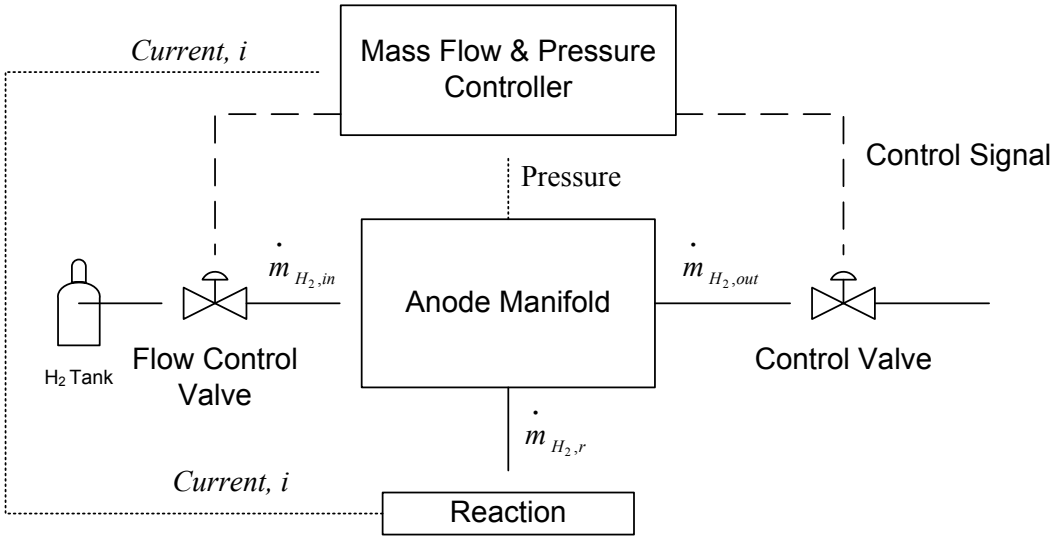

Fig. 3.19. Anode mass flow and pressure control diagram.

The inlet valve controls the mass flow rate of hydrogen using a feed-forward control approach by supplying an excess ratio of the consumption rate of hydrogen. The excess ratio of hydrogen (H_{excess}) is defined as the ratio of the mass flow rate of the hydrogen inlet to the reacted hydrogen mass consumption rate. H_{excess} should be greater than 1, and in this thesis, it is set to 1.2. The amount of consumption rate of hydrogen is calculated as follows:

$$\dot{m}_{H_2,r} = \frac{M_{H_2} i_r N}{2F} \tag{3.21}$$

From the definition of the excess ratio, the mass flow rate of hydrogen input should be calculated using the reaction current (i_r). However, in order to make the control strategy more realistic, the external fuel cell output current (i) is used in the controller as shown in Eq.3.22.

$$\dot{m}_{H_2,in} = H_{excess} \frac{M_{H_2} \left(i + i_c\right) N}{2F} \tag{3.22}$$

The reason for using the output current is that the reaction current cannot be measured physically, and can only be estimated theoretically with a precision limited by the quality of the fuel cell model. Any modelling errors would propagate to affect the performance of controller. In addition, using i instead of i_r as the control variable reduces the processing cost and time of calculating i_r. In terms of operational objectives, the dynamic response of hydrogen supply is expected to improve by using the external current as a control variable. The external current overshoots when the demand increases, hence the dynamic response of hydrogen supply system would react to a greater and faster transient than that by the reaction current. The crossover current, i_c, is summed to the external current as it consumes hydrogen as well, and should be accounted for during an open circuit when no load is connected across the fuel cell terminals.

The outlet control valve is a one-way valve allowing excess hydrogen to flow out of the anode, while aiming to maintain constant pressure in the anode. This is controlled by a proportional and integral (PI) feedback control loop with the required pressure of the anode as a reference set point as shown in Fig. 3.20.

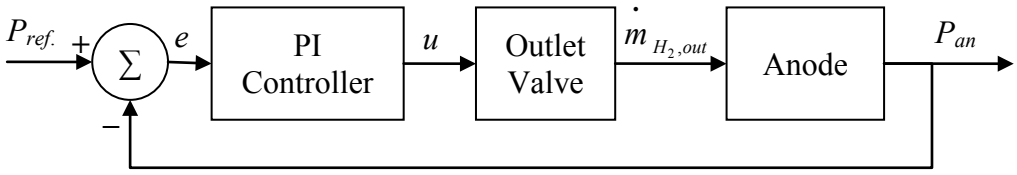

e: error
u: valve control signal

Fig. 3.20. Block diagram of the outlet valve control.

The PI controller of the outlet valve is tuned manually to get a stable and controllable range of operation. The parameters of the controller for a 50 kW fuel cell were found to be 5×10^{-7} for the proportional coefficient (K_p) and 1×10^{-6} for the integral coefficient (K_I). The outlet valve model includes a lower saturation limit of zero flow when it is completely closed, and an upper saturation limit, as well. The upper

saturation limit is equal to the maximum flow rate expected to flow through the input valve at maximum power operation. This limit is needed for sudden change in demand from maximum power to zero power, to prevent excessive hydrogen pressure build-up in the fuel cell. Integral anti windup mechanism is also implemented to take into account the saturation limits of the outlet valve. A detailed description of the anti-windup mechanism implemented is presented in Section 3.4.6.

A block diagram of the overall anode flow model and controls implemented in Simulink is shown in Fig. 3.21. The anode mass flow continuity equation is used with the ideal gas law to model the change of anode pressure as follows:

$$\frac{V_{An}}{R_{H_2}T}\frac{dP_{An}}{dt} = \dot{m}_{H_2,in} - \dot{m}_{H_2,out} - \dot{m}_{H_2,r} \tag{3.23}$$

Where V_{An} is the total volume of the anode flow channels, R_{H_2} is the hydrogen gas constant, T is the operating temperature, P_{An} is the pressure of hydrogen in the anode, and $\dot{m}_{H_2,out}$ is the outlet mass flow rate of hydrogen.

At steady-state conditions ($i_r = i+i_c$), $\dot{m}_{H_2,out} = (H_{excess} - 1)\dot{m}_{H_2,r}$. Hence, the change in pressure inside the anode manifold (dP_{AN}) is zero. Under unsteady state conditions, when the flow rates of hydrogen entering and leaving the anode manifold are not equal, the pressure of hydrogen inside the manifold would change according to Eq.3.23, governed by the performance of the outlet valve controller.

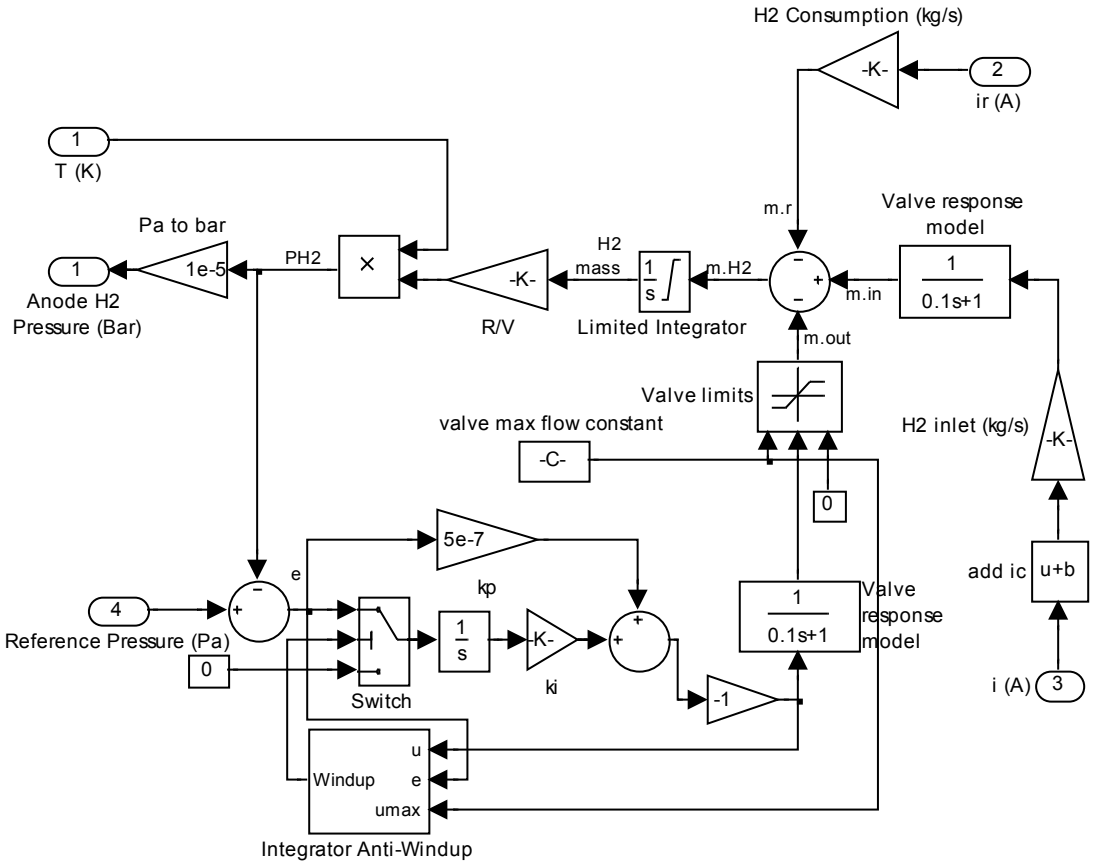

Fig. 3.21. Anode flow model and control in Simulink.

The inlet and outlet control valves are modelled as linear control valves with a fixed time constant of 100 ms, which may be found commercially. In addition, the outlet valve is restricted by a maximum output flow rate based on the ratings of the fuel cell system that is the maximum outlet flow rate at maximum output current, which is 1.1 A/cm^2.

The overall anode flow model in Simulink is grouped into a single block as shown in Fig. 3.22. It accepts 4 inputs; temperature T, currents i and i_r, and the reference pressure, P_{Ref}, and outputs the total pressure of hydrogen in the anode.

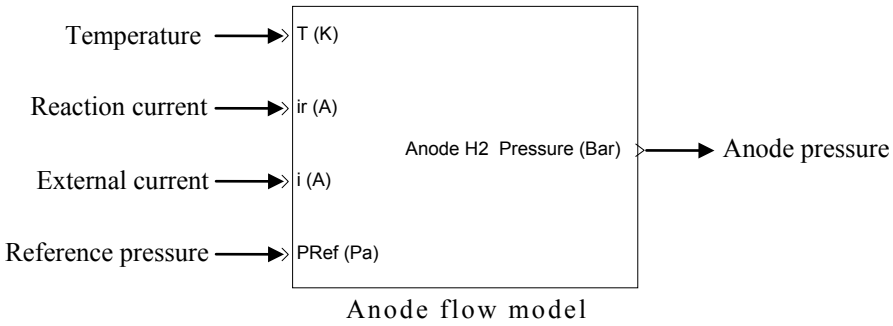

Fig. 3.22. Anode flow model input/output diagram.

Validation of the control strategy and performance of the model are presented in Chapters 4, 5 and 6.

3.4 DC-to-DC Power Converters

Most electrical devices operate from a regulated voltage supply, such as 220 VAC or 24 VDC. In low power (<10 kW) residential photovoltaic power systems, DC-to-AC inverters are developed to accept a wide range of DC voltages from 25 to 900 V to generate AC voltage at the standard residential voltages [47]. Commercially available residential inverters from '*Kaco New Energy*' have an input DC voltage range from 125 V to 550 V with a maximum of 600 V. In vehicular application, Toyota developed a hybrid vehicle (Priuse Model NHW20) with an operating voltage of 500 V and 50 kW power. In this thesis, the fuel cell system investigated for the vehicular applications resembles the Priuse, that is 500 V output voltage from the converter as electric motors require high voltages to produce the required high speeds with a maximum power of 50 kW, which is a typical minimum power requirement for saloon electric vehicles. Since this study is mainly concerned with the control aspects rather than the design of the converter, the control strategy developed for the 500 V output would be applicable to other voltages, with minor modifications on the controller. In terms of electrical components availability, there are many research and commercially available DC-to-DC converters at this voltage and power levels. For high power levels such as 50 kW, a balance between the voltage and current levels should be carefully chosen to ensure the safety and efficiency of the electrical components used in

the electrical system. A higher voltage level results in lower current and less heat dissipation. In this study, a regulated DC voltage is obtained, which can afterwards be converted to specific application requirements. For example, residential applications require AC voltage, while DC motors have power converters to control the motor's speed and/or torque by varying the motor's voltage or current.

3.4.1 Principles of DC-to-DC Converters

DC-to-DC power converter is a term used in electrical engineering to refer to a circuit that transfers electrical energy at a certain voltage level from a power source to a circuit at a different voltage level. DC-to-DC power converters are widely used in electronic devices, which contain one power source and several circuits operating at different voltage levels.

In DC-to-DC converters, supplied energy is stored for a short period then released to the external circuit at the desired voltage level. According to the law of energy conservation, the energy at the output of an ideal converter must be equal to the energy input, hence, the voltage and current products at the input and output must be equal. Consequently, a step-up converter that increases the voltage by a certain ratio, steps-down the current by the same ratio, and vice versa. Fig. 3.23 shows a typical voltage step-up converter, also known as a boost converter as it boosts the voltage of the source. The principles of operation of the DC converter are usually explained using circuit analysis during the different states of the switches. In the simple converter shown in Fig. 3.23 there is only one switch and therefore two modes of operation. Consider the circuit in Fig. 3.23 with a purely resistive load and ideal components. When the switch is ON, i.e. closed, for a time t_{ON}, the DC voltage source, V_s, is applied to the inductor, L. The inductor's current, i_L, increases linearly with time (since t_{ON} is small) according to the following relationship:

$$\Delta i_{L,ON} = \frac{V_s}{L} t_{ON} \tag{3.24}$$

The amount of magnetic energy stored in the inductor is proportional to the square of the current in the inductor. During the ON state, the resistive load, R, is short

circuited with zero voltage. Since the current through an inductor cannot be discontinuous, when the switch is turned OFF for a duration t_{OFF}, the current passing through the inductor and the switch during the ON state, would continue to pass through the diode and the resistive load. The output voltage, V_o, across the resistance would equal the product of the current and the resistance. The current through the inductor starts to drop at a rate proportional to the voltage across it, until the switch is turned back ON at the end of the switching period, T. If the current does not drop to zero, this mode of operation is called continuous mode, however, if the switch was kept in the OFF state long enough, the current would drop to zero; this is called discontinuous mode. This discontinuity in converter's operation is described in greater detail in [48, 49] and [50]. Here only the continuous mode of operation is considered. Since the voltage across the load is not constant, and would be similar to a saw-tooth waveform, a capacitor is usually added across the output voltage to filter out the fluctuations across the load to obtain a smooth constant voltage V_o.

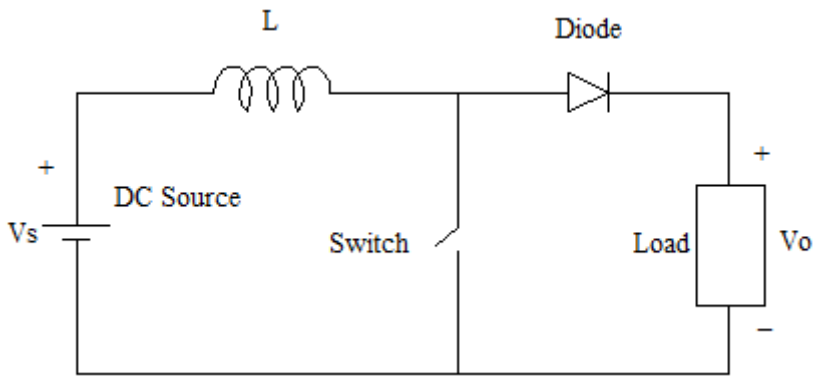

Fig. 3.23. Basic circuit diagram of a boost converter.

At the end of the OFF state, the change in the inductor's current is found by the following relationship:

$$\Delta i_{L,OFF} = \frac{(V_s - V_o)}{L} t_{OFF} \tag{3.25}$$

At steady state operation, the current would have the same value at the end of the OFF state as that at the beginning of the ON state; hence, the increase in current during the ON state equals the drop in current during the OFF state:

$$\Delta i_{L,ON} + \Delta i_{L,OFF} = 0 \tag{3.26}$$

Substituting Eqs. 3.24 and 3.25 in 3.26 and rearranging, gives:

$$\frac{V_o}{V_s} = \frac{t_{ON} + t_{OFF}}{t_{OFF}} = \frac{T}{T(1-D)} = \frac{1}{1-D} \tag{3.27}$$

Where D is the duty ratio of the switch, defined as the percentage of time the switch is ON during one period of time. Hence, $t_{ON} = DT$, and $t_{OFF} = T(1-D)$. The output voltage is always greater than the source voltage, and ideally can go up to infinity when D is 1. In reality, the internal resistance of the voltage source and losses in the converter would limit the maximum current drawn from the source and the output voltage would be limited.

3.4.2 DC-to-DC Converter Model

Fuel cells are characterised by low voltage levels, and high currents. Therefore, boost conversion is usually needed. Instead of using the traditional boost converter, a converter design proposed by Marshall & Kazerani [38] for a 65 kW load is adopted in this study. The adopted converter is a series connected 'buck-boost' converter ('buck' for step-down converters); however, due to its circuit connections, shown in Fig. 3.24, it would only boost the voltage. The traditional buck-boost converter, without capacitor C_3 and inductor L_3, has the following output/input voltage ratio:

$$\frac{V_o}{V_i} = -\frac{D}{1-D} \tag{3.28}$$

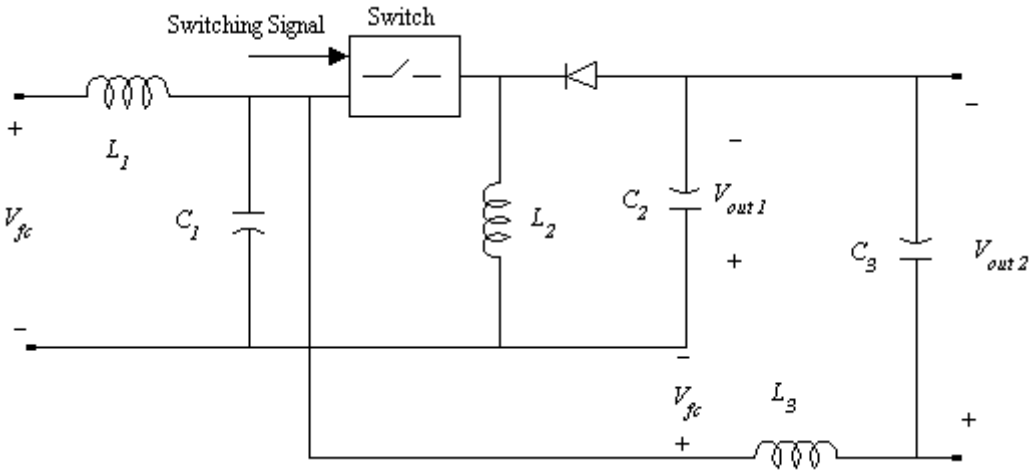

Fig. 3.24. Circuit diagram of series connected buck-boost converter.

The addition of C_3 and L_3 connected as shown in Fig. 3.24, makes the output voltage equal to $V_{out\ 1} + V_{fc}$, or in other words, the output voltage of the buck-boost converter is boosted up by an amount equal to the input voltage. This might be easier to understand by looking at the circuit when the switch is always ON; the output voltage is $V_{out\ 1} + V_{fc}$. when the switch is always OFF, the output voltage is V_{fc}. The overall output/input voltage ratio becomes similar to that of the traditional boost converter:

$$\frac{V_{out2}}{V_{fc}} = -\left(\frac{D}{1-D}+1\right) = -\frac{1}{1-D} \tag{3.29}$$

The advantage of this series-connected buck-boost converter is that it has higher efficiency, specific power, and voltage boost ratio compared to the traditional boost or buck-boost converters [38].

The converter is implemented in Simulink, as shown in Fig. 3.25, taking into consideration the non-ideal behaviours of electrical components by adding resistive elements to those components. The switching device used in the Simulink® model is a generic design incorporating switching losses, which are one of the main losses contributing to the inefficiencies of DC-to-DC converters.

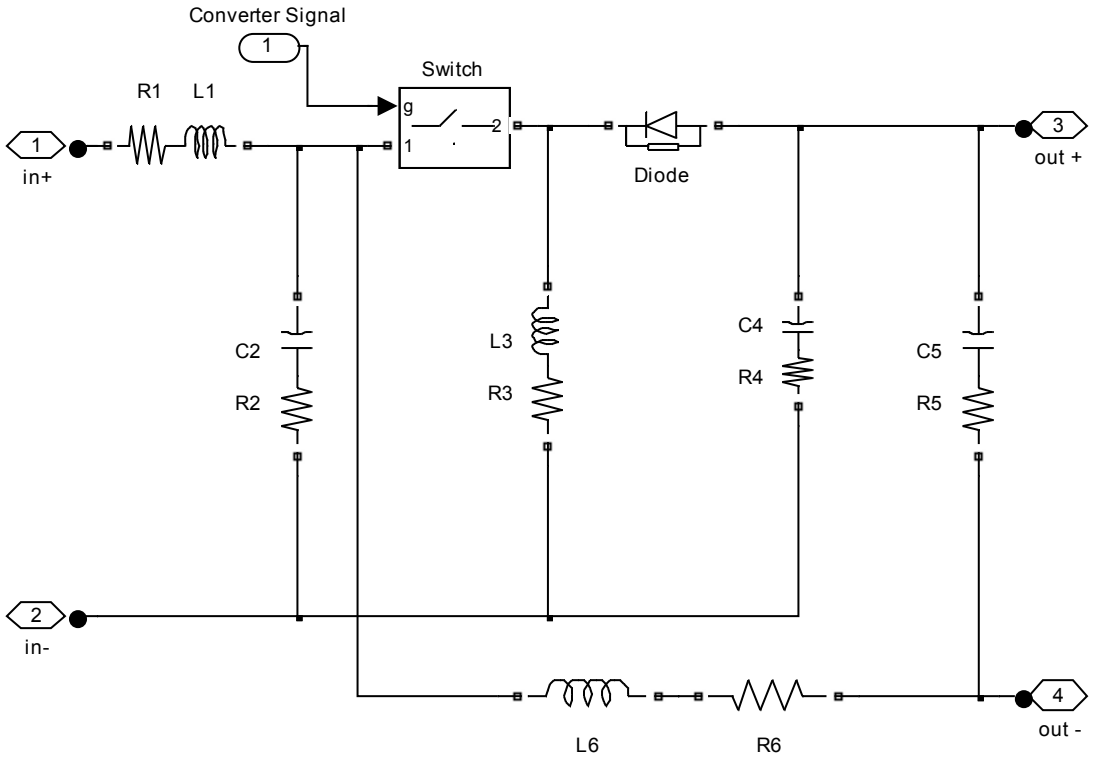

Fig. 3.25. DC-to-DC converter model in Simulink.

Table 3.4 lists the values of components used in the DC-to-DC converter model. The values of the component were chosen by trial and error and fine-tuning the output of converter. Components sizes were checked against those available commercially and with reference to a 400 kW fuel cell system model by Caux et al. [32].

Table 3.4: DC-to-DC converter components

Parameter	Value	Parameter	Value
L_1, R_1	1 mH, 1 mΩ	Switch's internal resistance	1 mΩ
C_2, R_2	3.3 mF, 1 mΩ	Diode's internal resistance	0.01 Ω
L_3, R_3	1 mH, 1 mΩ	Diode's forward voltage	0.7 V
C_4, R_4	3.3 mF, 0.01 Ω	Diode's snubber (parallel) resistance	500 Ω
C_5, R_5	3.3 mF, 0.2 Ω	Diode's snubber capacitance	250 nF
L_6, R_6	1 mH, 1 mΩ		

3.4.3 Control of DC-to-DC Converters

The output to input voltage ratio of the converter is regulated by the duty ratio of the switching device, as shown earlier. One of the commonly used methods for changing the duty ratio of the switch is by Pulse Width Modulation (PWM) signal to

trigger the switch. The switch is turned on when the switching signal is one and switched off when the signal is zero. The PWM signal generator outputs pulses at a certain frequency, such as 1 kHz, of rectangular shape waveforms with values of either one or zero. The input of the PWM generator accepts values between −1 and 1, and outputs pulses with duty ratios ranging between 1 and 0, respectively. The PWM generator has the following relationship between its input (control) signal (u) and the output duty ratio (D) of the generated pulse waveform:

$$D = \frac{1-u}{2} \tag{3.30}$$

A Proportional Integral (PI) feedback controller is proposed to control the converter for the ultimate objective of achieving a constant load voltage (V_{ref}) as shown in Fig. 3.26. The controller calculates a weighted sum of the error value (e) and the integral of e. the error signal (e) is the difference between the measured output voltage (V_L) and the set point, or reference, voltage (V_{ref}). The output of the controller is the control signal (u) of the PWM. For a positive error ($V_{ref} > V_L$), the duty ratio should increase. However, the duty ratio is inversely proportional to the control signal. Hence, the PI controller must have a negative gain value.

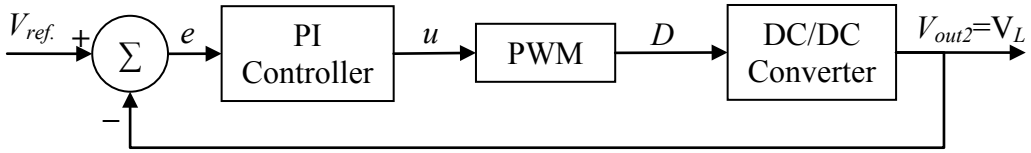

e: error
u: PWM control signal

Fig. 3.26. Block diagram of the DC-to-DC converter control.

A Simulink block diagram of the controller of the DC-to-DC converter is shown in Fig. 3.27. An anti-windup mechanism is shown and it will be discuss later in this chapter. The PWM generator in Simulink (Fig. 3.27) outputs an additional stream of pulses complementary to the other stream (i.e. when stream 1 is high “1”, then steam 2

is low “0” and vice versa), which is not needed. The block diagram of the PI controller is grouped under one subsystem block, called controller, as shown in Fig. 3.18.

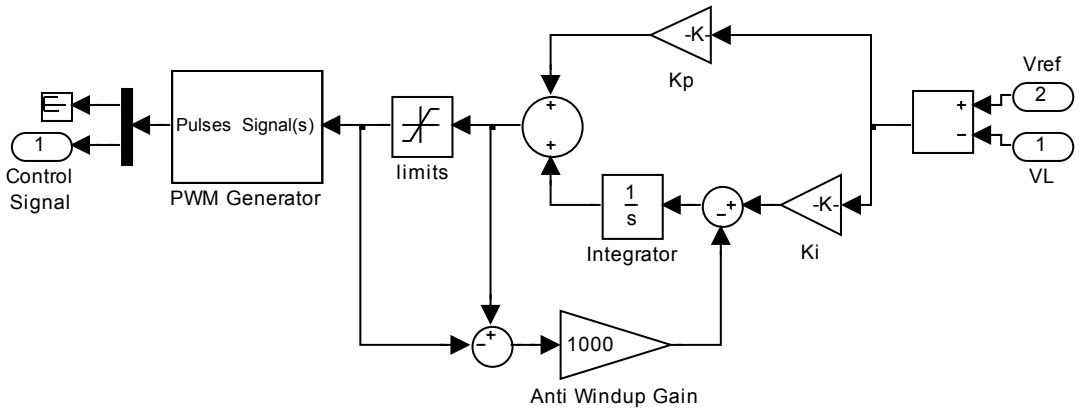

Fig. 3.27. Block diagram of the PI controller of the DC to DC converter in Simulink.

3.4.4 Setting the Parameters of the Controller

Unlike the PI controller of the outlet flow valve of the anode, the parameters of the converter’s controller were not easily found. Therefore, a well established method called Ziegler–Nichols tuning method is used to obtain an optimum performance of the PI controller. In the Ziegler–Nichols tuning method, the integral and derivative gains are first set to zero. The proportional gain is increased gradually until the output of the controlled system starts to oscillate. At this point, the proportional gain is defined as the critical gain, K_u, and the period of the oscillations is defined as the critical period, P_u. For the fuel cell and converter model in this study, $K_u = -0.0049$, and $P_u = 0.0207$ s. Next, the proportional and integral coefficients are defined as follow:

$$\begin{aligned} &\text{Proportioanl Coefficient } K_p = K_u / 2.2 \\ &\text{Integral Coefficient } K_I = 1.2K_p / P_u \end{aligned} \tag{3.31}$$

Substituting the values of K_u and P_u in Eq.3.31 results in $K_p = -0.00223$, and $K_I = -0.1293$.

A PID controller was also tested in this study, where the following parameters are obtained using the Ziegler-Nichols method:

$$\begin{aligned} &\text{Proportioanl Coefficient } K_p = K_u / 1.7 \\ &\text{Integral Coefficient } K_I = 2K_p / P_u \\ &\text{Derivative Coefficient } K_D = K_p P_u / 8 \end{aligned} \tag{3.32}$$

This gives K_p = −0.00288, K_I = −0.2785, and K_D = −7.458 x 10^{-6}. However, there was not a considerable improvement in performance compared to the PI controller. Therefore, only the proportional and integral actions were implemented in this study.

3.4.5 Limitations on the Controller

In addition to the natural saturation limits of the switching device, limitations are imposed to prevent uncontrollability of the system. In the initial stages of simulating the PI controller with the fuel cell, a problem was noticed during a fast and large power demand increase where the load voltage decreases below the set point. The error signal (e), in this case, becomes more positive ($e > 0$) pushing the controller to increase the output/input voltage ratio by increasing the duty ratio of the converter. However, because the fuel cell output voltage (and power) is non-linear, as the duty ratio continues to increase, the fuel cell operating point falls in the excessive concentration losses region. This causes a further shortage in power, and consequently, a further demand to increase the duty ratio. Once the controller enters this region of operation, and even if the load demand drops to zero, the controller becomes unable to regain control of the system by pulling the operating point of the fuel cell from the concentration losses region. This problem is also noticed when the load demand is greater than the maximum rated power of the fuel cell system for a certain period. One strategy to deal with this problem is by interconnecting feedback signals from the fuel cell to the converter's controller. For instance, the strategy may be implemented by setting a minimum operating voltage of the fuel cell, beyond which the power drawn from the fuel cell should not be increased. The reason the fuel cell voltage may be chosen and not its current or power is due to the natural transient behaviour of the fuel cell, which allows the current (and power) to overshoot for a very short period of time beyond steady state limits. However, the fuel cell voltage does not overshoot or undershoot during transients. Another strategy that could be considered as a different

way for implementing the first proposed strategy is by setting a smaller upper limit on the duty ratio, found at maximum steady state output power. This strategy is adopted in this study because of the simplicity of its implementation without the need to interconnect feedback signals from the fuel cell. In order to find the maximum duty ratio, the model is simulated with a maximum-power-consumption load. The duty ratio of the converter is increased gradually until maximum power is reached, and the duty ratio value is noted. As it will be shown later in Section 4.5, the maximum voltage ratio of the converter modelled in this thesis occurs at a duty ratio of nearly 0.96. Hence, from Eq.3.30, the input signal of the PWM (u) is limited between −0.92 and 1.

The maximum duty ratio for a 50 kW load is found to be 0.6012. This was implemented in the control strategy of the converter by changing the lower limit of the input of the PWM to −0.2024, while the upper limit remains unchanged at 1. Fig. 3.28 shows the response of the output voltage of an unbound controller compared to that bound to a duty ratio of 0.6012. The scenario is presented for a load power demand that changes at timestamp 1 s from 5 kW (50 Ω) to 62.5 kW (4 Ω) and then at timestamp 2 s to 50 kW (5 Ω). For an unbound duty ratio, when the load changes to 4 Ω the output voltage drops to 46 V, and the fuel cell is nearly short circuited; in this situation the stack voltage is 2.6 V and the total current is 288 A. In addition, due to the transient behaviour of the fuel cell, at timestamp 1.152 s the fuel cell voltage reverses in polarity for nearly 30 ms, acting as an electrolyser, which damages the fuel cell.

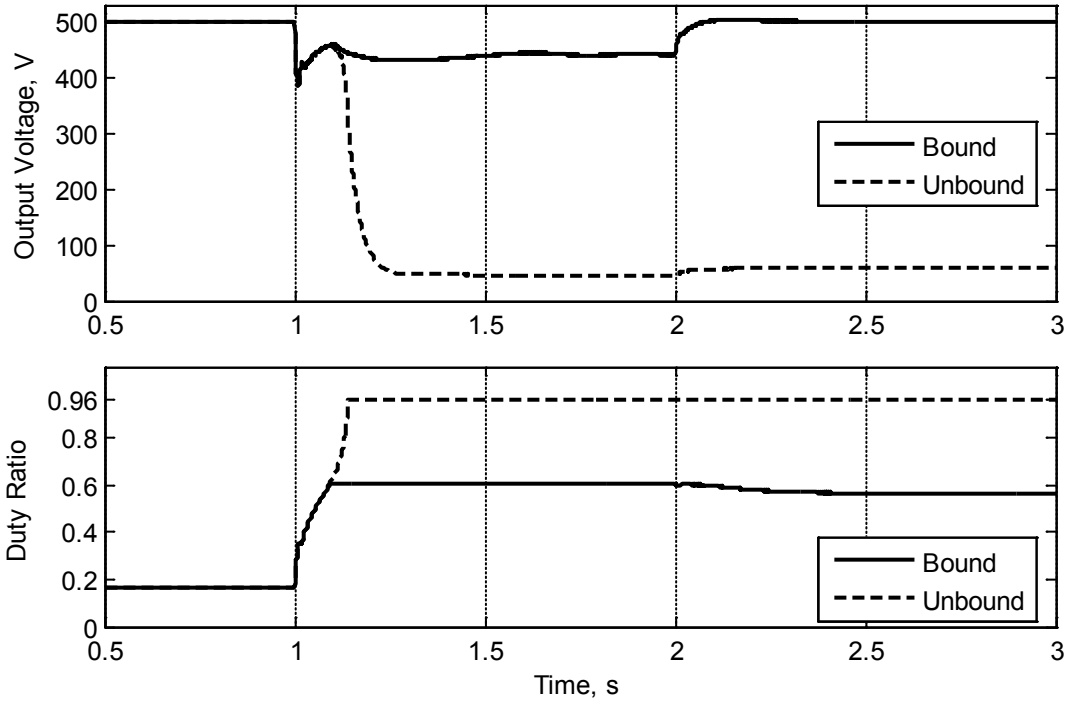

Fig. 3.28. The output voltage and duty ratio response when the duty ratio is Bound (to a maximum value of 0.6012) compared to that of an Unbound duty ratio (maximum 0.96) for a load change from 50 Ω to 4 Ω to 5 Ω at timestamps 1 s and 2 s.

3.4.6 Controller Windup Problem

In almost all control applications, actuators have saturation limits. In the anode flow model, a valve cannot be opened more than its maximum opening, and cannot be closed beyond the fully closed state. Similarly, electronic power converters have limits for the duty ratio as discussed earlier. Taking the case where the actuator reaches its upper saturation limit and the error $e < 0$, any further increase in the value of the control signal (u) would not influence the saturated actuator, nor the controlled variable. Until the controlled variable reaches its set point, where $e = 0$, the integral part of the PI controller would continue to build up. Due to the large integral value that accumulated during saturation of the actuator, the controlled variable would need to deviate from the set point to cause a positive error $e > 0$ to diminish the value of the integral part for a period causing the controller to be in a wind-up state. Controller windup is noticed during sudden large increases or decreases in the load. This problem is well known in the control systems community and has been addressed and resolved by several

strategies. One of the studied and implemented anti-windup strategies that appears to be effective with the best performance [51] is called “integrator clamping”.

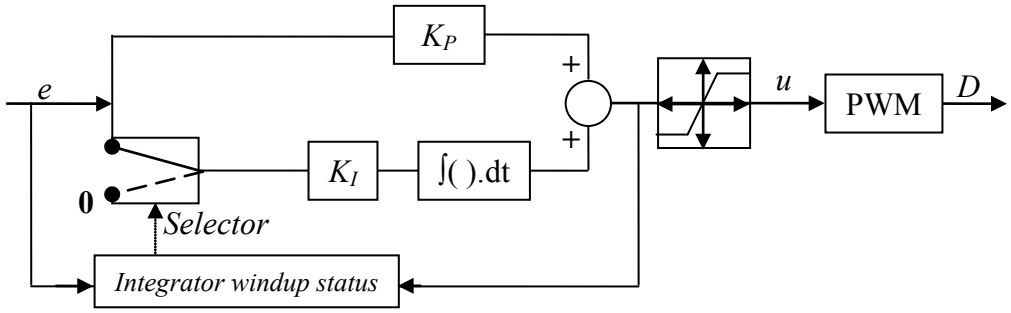

e: error
u: PWM control signal

Fig. 3.29. Integral clamping anti-windup strategy.

Fig. 3.29 shows a block diagram of a PI controller with the integral clamping anti-windup mechanism. When integrator windup conditions are satisfied, the integrator term is ‘frozen’ by switching its input to zero until the windup conditions are cleared. The anti-windup strategy is triggered under any of the following two conditions:

1) The control signal, *u*, is larger than the maximum limit of the actuator ***AND*** the error signal, *e*, is negative.
2) The control signal, *u*, is smaller than the minimum limit of the actuator ***AND*** the error signal, *e*, is positive.

In programming language format, this translates to the following expression:

$$\left(u > u_{max} \,\&\, e < 0\right) \text{ OR } \left(u < u_{min} \,\&\, e > 0\right) \tag{3.33}$$

This anti-windup mechanism is used and implemented for the outlet valve of the anode flow control. The Simulink implementation of expression 3.33 is shown in Fig. 3.30.

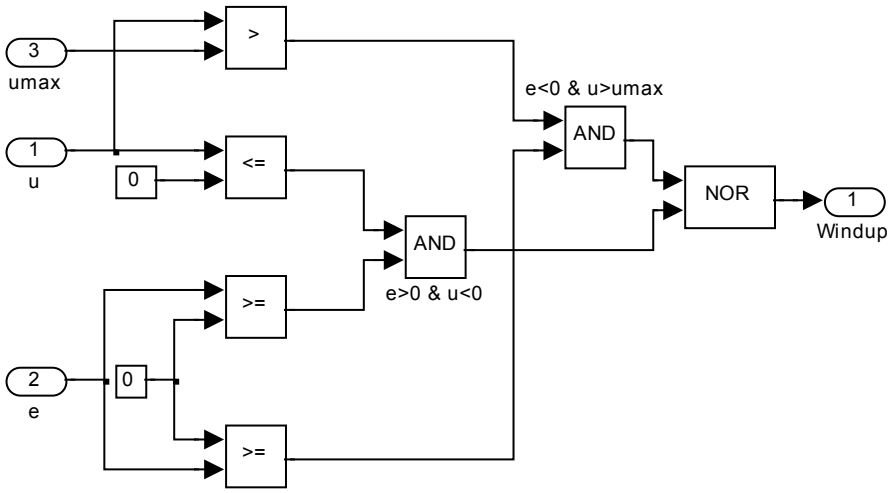

Fig. 3.30. Outlet valve anti-windup mechanism.

However, for the controller of the DC-to-DC converter, this design of anti-windup mechanism caused a problem of high oscillations around the saturation limits of the actuator during windup conditions. These oscillations caused a severe slow down in the simulations time. In a real physical system, this would increase the processing cost of the controller. To avoid this problem, a different strategy was implemented, which is called 'Tracking anti-windup, back-calculation' [51], described in a block diagram shown in Fig. 3.31.

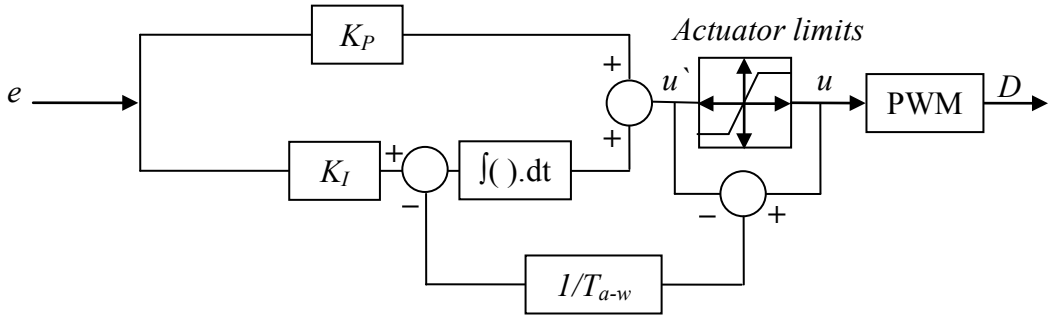

e: error
u: PWM control signal

Fig. 3.31. Tracking anti-windup, back calculation strategy.

The newly modified anti-windup mechanism does not use comparison of the control signal with the limits, but takes the difference between the control signal and its value after imposing the saturation limits. The difference is subtracted from the integrator input. The difference between u and $u`$ has a value other than zero during windup conditions. This is multiplied by an anti-windup reset constant, $1/T_{a\text{-}w}$, and fed to the integrator action of the controller as shown in Fig. 3.31. $1/T_{a\text{-}w}$ represents the rate at which the integrator value is reset, and in [51] the value of $1/T_{a\text{-}w}$ was suggested to be equal to the integrator's coefficient K_I/K_P. However, in this study, it was found by simulation runs that $1/T_{a\text{-}w}$ gives better performance when its value is much higher than K_I/K_P, and closer to the frequency of the PWM pulses. This reduces the build-up of the integral part during windup.

3.5 Variable Resistance Load Model

A variable resistance Simulink model was developed (Fig. 3.32) to simulate varying electrical loads.

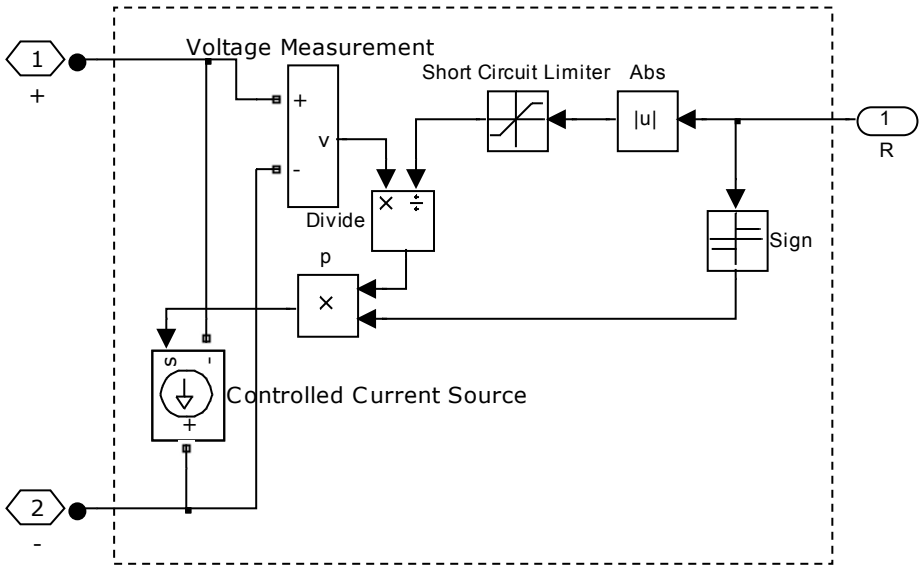

Fig. 3.32. Variable resistance model has one numerical input port to specify the resistance value, and two electrical ports to connect to the electrical circuit.

The required power demand profile is calculated using Ohm's law to find a resistance equivalent to the power demand for a constant voltage across the resistance, as shown in Eq.3.34:

$$R(t) = \frac{V_L^{\,2}}{Power(t)} \tag{3.34}$$

Where *R(t)* is the load resistance as a function of time and V_L is the load voltage.

3.6 Simulation and Data Processing

The simulation environment is described as well as the necessary sampling times in each set of results obtained in the following chapters.

3.6.1 Model Validation

The polarizations curves represent the steady state characteristics of the fuel cell. They are obtained from the fuel cell voltage model developed in this study by recording the voltage that results from applying a defined current signal. The current signals starts with 0 A for 100 seconds to avoid simulation start-up errors and to give the transients enough time to settle down. Then the current is gradually increased at a rate of 1×10^{-7} A/s.

3.6.2 Automotive Application

The performance of the fuel cell system was tested under automotive driving cycles obtained from the US Environmental Protection Agency (EPA) [52]. Two driving cycles were studied; the Urban Dynamometer Driving Schedule (UDDS) which represents the velocity of a vehicle in a city, and the Highway Fuel Economy Driving Schedule (HWFET) which has less variations of velocity of a vehicle on a motorway. Driving schedules are usually given as the velocity of a vehicle for a specific period, for example, UDDS has a length of 1369 seconds, while the HWFET has a length of 765 seconds.

From the velocity profile, the amount of power needed by the vehicle is estimated based on the vehicle specifications [53] as shown in Table 3.5.

Table 3.5: Vehicle specifications used for UDDS and HWFET power estimation

Parameter	Symbol	value
Curb Weight (including payload)	C_w	1680 kg
Drag Coefficient	C_D	0.32
Rolling resistance coefficient	C_{RR}	0.009
Vehicle frontal area	A_F	2.31 m^2
Vehicle drivetrain efficiency	η_{drv}	0.90
Air density	ρ_a	1.2 kg/m^3
Earth's standard gravity	g	9.81 m/s^2

The power is estimated as follows, assuming horizontal vehicle movement:

$$\begin{aligned}
&\text{Intertial force, } F_I = C_w.acceleration \\
&\text{Aerodynamic drag force, } F_{AD} = 0.5\rho_a.A_F.C_D.velocity^2 \\
&\text{Rolling resistance force, } F_{RR} = g.C_w.C_{RR} \\
&\text{Total force, } F_T = F_I + F_{AD} + F_{RR} \\
&\text{Power required at wheels, } P_{wheels} = F_T.velocity \\
&\text{Load Power, } P_L = P_{wheels} \Big/ \eta_{drv}
\end{aligned} \tag{3.35}$$

The electrical system of modern vehicles requires power in the range of 1 kW to 3 kW [54]. A constant 1 kW power consumption for the electrical system is assumed in this study and is added to the power needed by drive train for each driving schedule.

3.6.3 Data Processing

The simulations run on variable-step-size time increments, with a maximum allowed step size of 50 microseconds. The size of the time step decreases to obtain a converging answer especially when one of the variables in the model changes. The time step could decrease to 1 x 10^{-14} second. Large amounts of data points are generated; for example, 90,000 to 200,000 data points were generated for a 7-second duration of the load profile. Running the simulation over a period of 1369 seconds would take a lot of

time, and requires a very powerful computer with extremely large memory (RAM) to accommodate the generated data. Initially, the model was simulated where data points are saved to variables in the MATLAB environment. These variables occupy the RAM of the computer, which nowadays are limited to 3 GB to 4 GB for a regular use computer. Therefore, to overcome this problem, the simulation was split into 7-second periods of simulation. The first 2 seconds of every simulation run were removed at a later stage to avoid simulation starting-up errors needed for the system to reach the steady state value, since the initial conditions of the model were not modified at each simulation run. Hence, for each simulation run, only 5 seconds of the total simulation run were used. After obtaining all the data points for the whole duration of 1369 s, data processing and plotting were not being handled easily, and large computer delays were caused because of the large amount of data points. Therefore, reduction in the number of data points was needed to enable handling of plots, and mathematical operations on the data.

The raw data was reduced by removing sample points at timestamp i that satisfy the following rule:

$$\left\{t_i - t_{i-1} < 10\ \mu\text{s}\right\}\ \text{AND}\ \left\{V_i - V_{i-1} < 2\ \text{mV}\right\} \tag{3.36}$$

Where t_i is the i$^{\text{th}}$ time sample and V_i is the i$^{\text{th}}$ load voltage sample. After the first attempt to reduce the data points according to relationship 3.36, the size of data points for each of the 18 recorded variables was nearly 18.7 million samples each occupying memory between 90 MB to 150 MB.

To manipulate the data and use it smoothly for analysis, further reduction of the data points (or down sampling) was still needed. However, reduction of sample points should be carefully performed to avoid losing any useful information in the results. This reduction of sample points could not have been performed at the simulation stage because it was necessary for reaching a converging solution. Down sampling the data points for larger time intervals using expression 3.36 required a large amount of computing power and another method is used. Linear interpolation of the down sampled data (expression 3.36) is performed at the required sampling time points using a built-in

function in MATLAB called *'interp1q'*, which is used for non-uniformly spaced data points. Fig. 3.33 shows a sample of the data points that are down sampled to uniformly spaced data points with intervals of 0.1 s, 3 ms, 2 ms and 1 ms compared to the raw data processed by expression 3.36.

Clearly, down sampling the data every 0.1 s or 3 ms is not sufficient to reconstruct the original behaviour of the observed variable. However, among the data down sampled to 1 ms and 2 ms, it was found that the mean and standard deviation in output power was indifferent. Hence, 2 ms down sampling was used. This resulted in 228 MB of data points of all the variables recorded for UDDS, and 188 MB for HWFET.

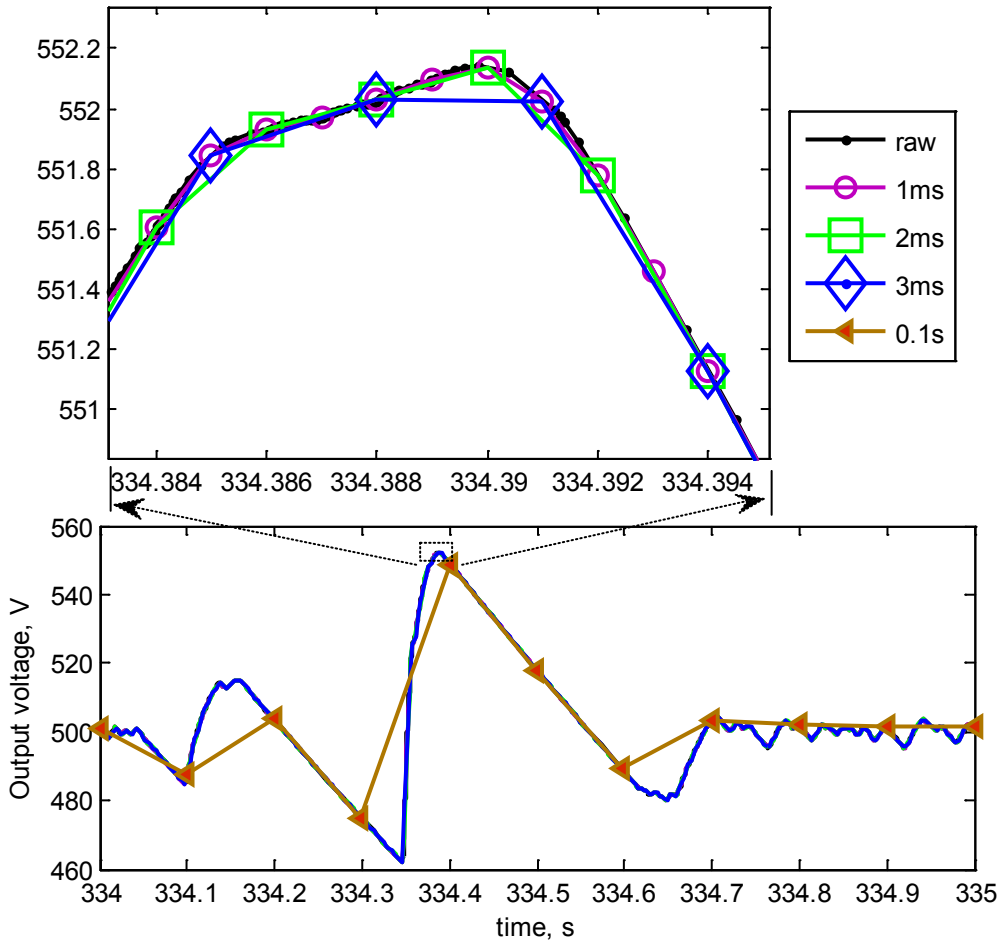

Fig. 3.33. A portion of the output voltage from UDDS showing downsampled lines compared to the raw data line.

At a later stage, data points were saved directly to a file on the hard drive instead of the RAM, which enabled continuous simulation for longer periods of time, without saturating the available memory of the computer.

3.6.4 Error Analysis

Linearly interpolated data of the output voltage have been analysed using Simulink. The data after the initial down sampling (expression 3.36) and the interpolated data are imported to a simple model (Fig. 3.34) where they are subtracted using different simulation time steps summarised in Table 3.6. The model is simulated at fixed time steps of 1 ms and 2 ms and the simulation time for processing the data over the entire 1369 seconds of the UDDS profile is shown. As data processing is performed at certain time steps, each data set must have a value at that time step. For the interpolated data, the availability of a data point at a certain time step depends on the interpolation used. However, the probability of having a data point of the raw data at a certain time step is very unlikely, since they were obtained using variable time steps with a maximum of 50 microseconds. The block diagram that imports data from MATLAB's workspace has two options: to use data interpolation, where any missing data at the sampling time of the simulation is linearly interpolated or to use the most recent values at the desired simulation time steps.

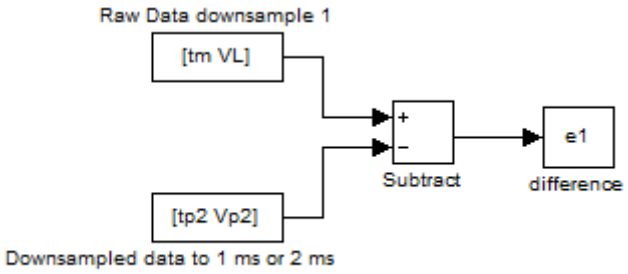

Fig. 3.34. Down sampling error analysis using Simulink

Using non-interpolation option in Simulink import block shows that the mean of the difference between the raw data and the down sampled data for the 1 and 2 ms are nearly equal, while the standard deviation of the difference is about 0.05 better for the 1 ms down sampled data. Simulation run times are doubled using a sampling rate of

1 ms instead of 2 ms. Minimal increase in accuracy is achieved by using 1 ms sampling rate instead of 2 ms. However, the amount of data halves, from 1.37 million to 0.685 million data points. This reduction in data points is a compromise between the computational time and the accuracy of the results. Hence, 2 ms is used for data analysis of UDDS and HWFET driving schedules. However, with this error analysis, a different approach was used for the domestic load simulations, where the recorded variables were sampled at 2 ms intervals at the simulation and data saving stage.

Table 3.6: Summary of standard deviation and mean of raw and sampled data.

Raw data interpolation	Down sampled data interpolation	Down sampled data	Standard deviation of difference	Mean of difference	Simulation run time, s
Yes	No	2 ms	0.1553	-1.4×10^{-4}	1.43
No	No	2 ms	0.1687	0.0277	1.44
No	No	1 ms	0.1125	0.0278	2.80
Yes	No	1 ms	0.0798	-3×10^{-5}	2.70

It is worth to mention another issue faced during simulating the driving schedules. The available data on driving schedules is at 1 second intervals. Hence the calculated power required by the vehicle is found every 1 s. Since the variable load (resistance) block diagram accepts ohmic values of the load, the resistance equivalent to the power profile is found by dividing the square of the output voltage (500 V) by the power of the vehicle:

$$R_{L(Vehicle)} = \frac{500^2}{P_{Vehicle}} \tag{3.37}$$

Pre-calculating the resistance according to Eq.3.37, results in data point values for the resistance spaced every 1 second. Using the Simulink import block that performs linear interpolation at the simulation step times is not the correct approach to follow. Because between every 2 data points of the power profile spaced by one second, the power profile is linear with time. Hence, linearly interpolating the original power profile is not equal to that obtained from the linearly interpolating the values of the resistance calculated every one second. For example, assume the power profile given is 1 kW at timestamp 1 s then 2 kW at timestamp 2 s. The correct power demand at timestamp 1.5 s should be 1.5 kW, however, the resistance at 1 s is 250 Ω and at 2 s is 125 Ω.

Interpolating the resistance at time 1.5 s gives a value of 187.5 Ω, which results in a power demand of 1.34 kW instead of 1.5 kW. Instead, the power profile is imported to the Simulink model, and the resistance value is calculated during each simulation time step.The power profile obtained using interpolated resistance values compared to the original power profile between timestamps 179 s and 182 s from the UDDS driving schedule is shown in Fig. 3.35. The power profile data is spaced every one second, but Simulink simulates the model under variable time steps less than 50 microseconds. Hence, it performs linear interpolation between the given data points to find the data at the simulation step times.

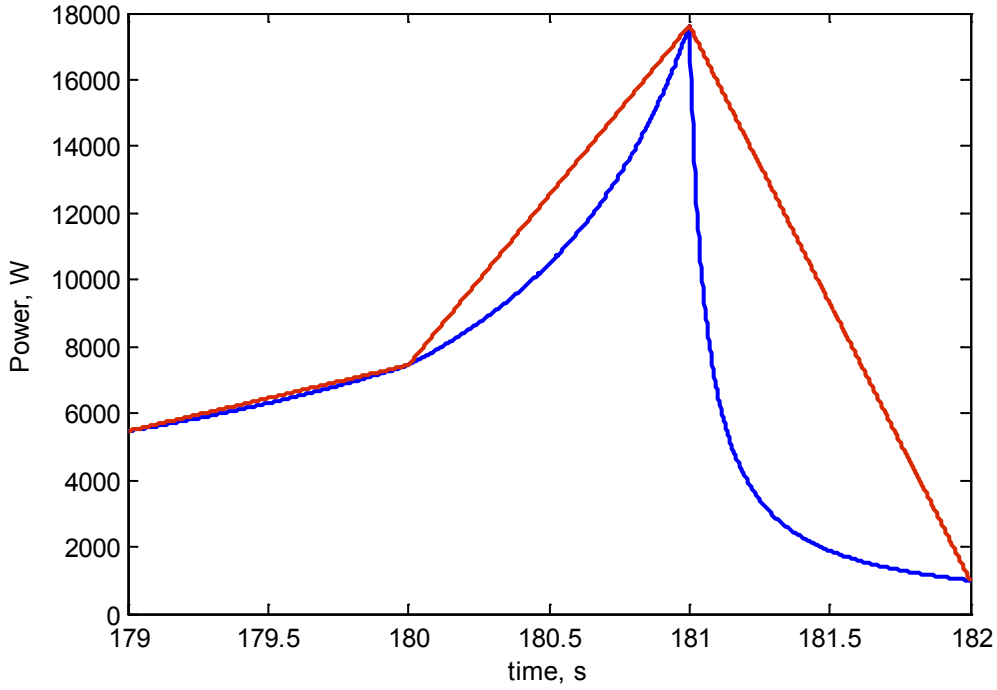

Fig. 3.35. Original power profile (red), compared to that obtained by interpolating the equivalent resistance (blue).

Simulations run times for UDDS and HWFET driving schedules on an Intel Quad Core Q8200 CPU, 4 GB RAM computer are as follows. UDDS simulation run time took nearly 9430 seconds (2 hours and 37 minutes) and HWYFET simulation run time took 5250 seconds (1 hour and 28 minutes).

3.6.5 Domestic Application

In domestic applications, the maximum power demand for the studied power profile is much less than that required in automotive applications. Therefore, the maximum power of the fuel cell stack is reduced to 8.25 kW. The reduction in output power can be done by changing the active area of the membrane or by reducing the number of cells in the stack or a combination of both. Although the typical DC voltage for DC-to-AC inverters for residential applications is less than 400 V [47, 55], 500 V is used in this study to enable comparison with the automotive application simulations. Changing the voltage level requires changing the controller's parameters. Hence, the number of cells is not changed, and only the area of the membrane is reduced to 36 cm^2. The only modification made on the controller of the DC-to-DC converter model is changing the maximum duty ratio to 0.45 instead of 0.6 by setting the lower limit of signal to the PWM to +0.1. This is found by connecting a 31 Ω (from $500^2/8250$) at the load terminals. Due to converter losses, the actual output power is 8.07 kW, which is still higher than the maximum power demand (7.2 kW).

As it will be shown later in the results chapters, the output voltage tolerances depend on the rate of change of power demand. In order to comply with acceptable voltage tolerances for the domestic sector, the rate of power demand is limited using different techniques such as a current rate limiter device, or signal rate limiter in the controller. An additional energy storage system may be used to supply the difference in power demand. In this study, the mechanism of power limitation is not covered, and only the maximum/minimum limits on the rate of change in power demand are investigated. These limits are used in estimating the durations of the step changes in domestic power profile, which are only available graphically.

According to British standards [56], the acceptable tolerances of AC voltage variations are +10 % and −6 %. Obtaining an AC voltage using DC-to-AC inverters is roughly equivalent to scaling the tolerance range to a 500 V DC voltage. This equates to a voltage range of the fuel cell system between 470 V and 550 V.

In order to determine the maximum transient that a fuel cell system can cope with resulting in an acceptable voltage level for a domestic 8 kW power supply, a

transient analysis on the power demand is investigated. For the domestic power profile studied, the maximum increase in power demand is nearly 7 kW and the maximum drop in power demand is about 5.5 kW. Therefore, worst-case scenarios are studied for different power changes and at several rates of change in power demand, summarised in Table 3.7. The first column gives the initial and final power demand values, and the second column shows the rate at which the power changed from the initial power demand to the final power demand value (ΔPower/Δt). The change in power demand from 0.5 kW to 7.5 kW is tested for different transition periods (Δt), whereas the remaining changes are tested for a change taking place within $\Delta t = 200$ ms. The change in power demand is tested for both a drop and an increase in the power demand to find the voltage overshoots and undershoots, as shown in Table 3.7 in the third and fourth columns, respectively. Voltage transients for a change in power demand between 0.5 kW and 7.5 kW at different rates are shown in Fig. 3.36. A drop in power demand occurs at timestamp 2 s, resulting in an overshoot of the load voltage, while an increase in power demand occurs at timestamp 4 s and results in an undershoot in the voltage.

Table 3.7: Voltage transients for different load changes.

Power demand change	Rate of change ± Δpower/Δt	Voltage overshoot (Demand decrease)	Voltage undershoot (Demand increase)
0.5 kW – 7.5 kW	700 MW/s	598 V	438 V
	7 kW/s	510 V	492 V
	35 kW/s	542 V	472 V
1 kW – 7.5 kW	32.5 kW/s	540 V	474 V
1 kW – 8 kW	35 kW/s	550 V	473 V
0.5 kW – 8 kW	37.5 kW/s	554 V	470 V

From Table 3.7, the maximum voltage tolerance (550 V) occurs at a rate of 35 kW/s, while the minimum voltage tolerance (470 V) occurs at a rate of 37.5 kW/s. Therefore, ±35 kW/s will be considered as the maximum/minimum limit imposed on the overall fuel cell system.

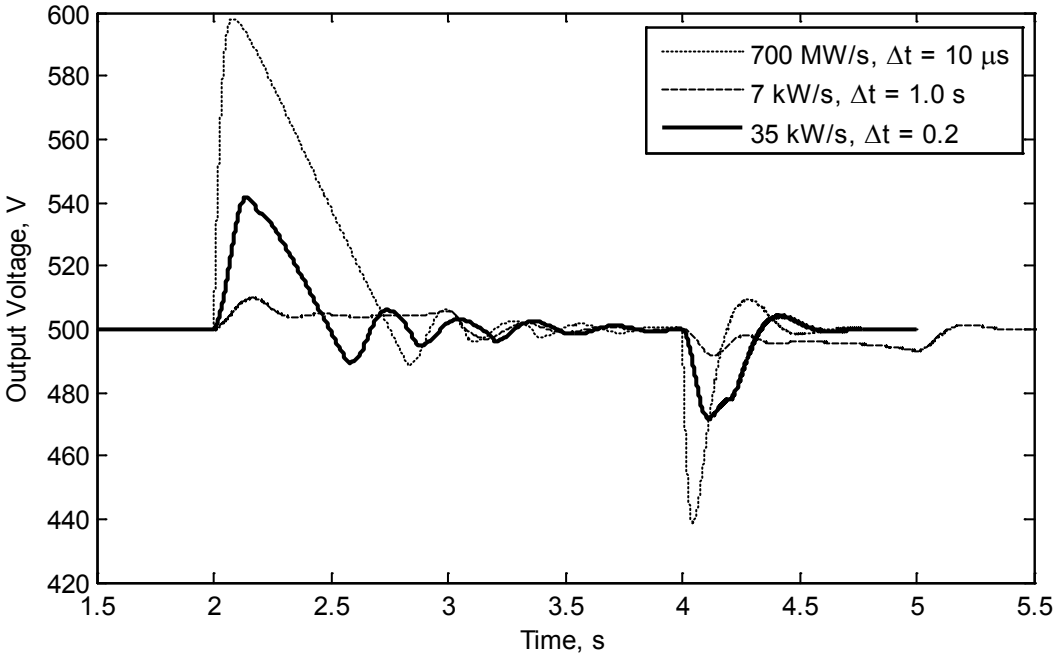

Fig. 3.36. Voltage transients at different rates of change in power demand. Changes occurring at timestamp 2 s and 4 s.

The limitation imposed on the power demand would have a different influence on the electrical devices and appliances used in a typical household. However, for a household power profile with a maximum load of nearly 7 kW, a limited rate of 35 kW/s, would have a negligible, if any noticeable, effect of up to 200 ms delay on the user of the electrical load.

Simulation was run in 'Accelerated Mode' to reduce simulation runtimes. On average, one second of the domestic load profile, required 8.5 seconds of simulation. Hence, due to the long simulation runtimes, two main durations of interest were simulated, as indicated in Chapter 6. The first duration covered an 83-minute portion of the load profile, and took nearly 11 hours and 36 minutes to complete. While the second duration covered a 75-minute portion of the load profile and took 10 hours and 48 minutes to complete.

Chapter 4

MODEL VALIDATION & SENSITIVITY ANALYSIS

4.1 Introduction

The fuel cell model developed in this thesis is a semi-empirical model, constructed from theoretical and empirical mathematical equations obtained from well-known research studies. However, the various phenomena in the fuel cell necessary for control system aspects are not available from one source in the literature. Therefore, the model developed in this study combines and adapts the necessary equations needed to simulate a practical fuel cell system. Hence, before going forward with obtaining the results and designing a control strategy, it is necessary to validate the developed model with actual experimental data obtained from one or more sources. In the following sections, the fuel cell model is validated against steady state and dynamic response data. For control-oriented objectives, an exact match to actual characteristic data is not always required, but the overall trend in fuel cell response is sufficient to design a control strategy that is flexible and robust to changes in the system being controlled [17].

As mentioned earlier in the methodology chapter, the fuel cell model is tuneable. By changing a few newly inserted parameters (K_{dif} and K_{io}) along with R_{ref}, the fuel cell steady state characteristics are matched to the different fuel cell geometrical designs.

Fuel cell system variables can be divided into three categories:

1. Geometrical variables;
2. Operating conditions or operational variables; and
3. Performance variables.

Usually, where the design of a fuel cell is concerned, operating conditions variables are fixed and the geometrical variables are chosen to optimize the performance

variables. On the other hand, when a control system for the fuel cell is considered, the geometrical variables of the fuel cell are fixed, and the operating conditions variables are chosen to optimise its performance. A limited design of a control strategy would only be applicable to the specific geometrical variables of the fuel cell used to develop this control strategy. Some fuel cell control strategies are based on certain operating points, e.g. maximum power output point. In this thesis, although the developed model delves deeply into the theory and technical details of the fuel cell components, the control strategy is flexible and immune to changes in the model including geometrical and operational variables. Such conclusions are not possible to verify without a detailed model of the fuel cell system. Of course, the flexibility of the control strategy is not a 'plug-n-play' strategy for considerable variations in the system's variables, but is achieved easily by resetting the main parameters of the controller. In the next section, an example is presented showing the controller's flexibility using two sets of steady state fuel cell responses.

4.2 Steady State Response Validation

Fuel cell characteristics data, or polarization curves, are obtained from research studies that involve experimental and sometimes modelling work. Some research studies concentrate on designing flow channels of the reactants, while others investigate the possibility of improving the current membrane characteristics by synthesizing new materials or new manufacturing techniques. The fuel cell steady state model developed in this thesis is compared against fuel cells from the major manufacturers of PEM fuel cells in addition to one PEM fuel cell developed in-house by a research group.

The polarization curve of the fuel cell model is compared against experimental data obtained from various sources. The first set of data were obtained by Song et al. [57] who developed a single 4.4 cm^2 PEM fuel cell based on 'Nafion® 112' membranes. The experimental data were obtained for a range of operating temperatures and pressures. The model is compared against the experimental data obtained at a temperature of 80 °C, and an operating pressure of 3 atm. All the experiments were performed under 100 % relative humidity of the reactants with hydrogen and air supplied at a fixed flow rate of 0.1 L/min and 1 L/min, respectively, which are sufficient

to meet the requirements of the maximum consumption rate. Song et al.'s fuel cell output achieved 0.68 V at 1 A/cm^2.

Song et al. presented experimental data for operating pressures of 3 atm only. However, experiments were carried out at ambient pressure, and it was reported that the voltage drop over the whole current density range at ambient pressure was only 30 − 60 mV compared to voltages obtained by operating at 3 atm.

The fuel cell model developed in this study was simulated under operating temperature and pressure similar to that of the experimental data. The steady state response of the model was adjusted to match the experimental data found by Song et al. This was done by adjusting the tuning parameters that influence the activation, concentration, and ohmic overvoltages. The values of the adjusted parameters are: $K_{io} = 0.025$ which affects the activation overvoltage, $K_{dif} = 0.75$ which affects the diffusion and the concentration overvoltages, and $R_{ref} = 1.6 \times 10^{-5}$ ohm.m^2, which affects the ohmic overvoltage. The model is compared against experimental data obtained by Song et al. as shown in Fig. 4.1. The figure shows agreement with the experimental data up to a current density of 1500 mA/cm^2, which is beyond the maximum power density output point. Fuel cell operation is normally avoided for currents greater than that resulting in maximum output power.

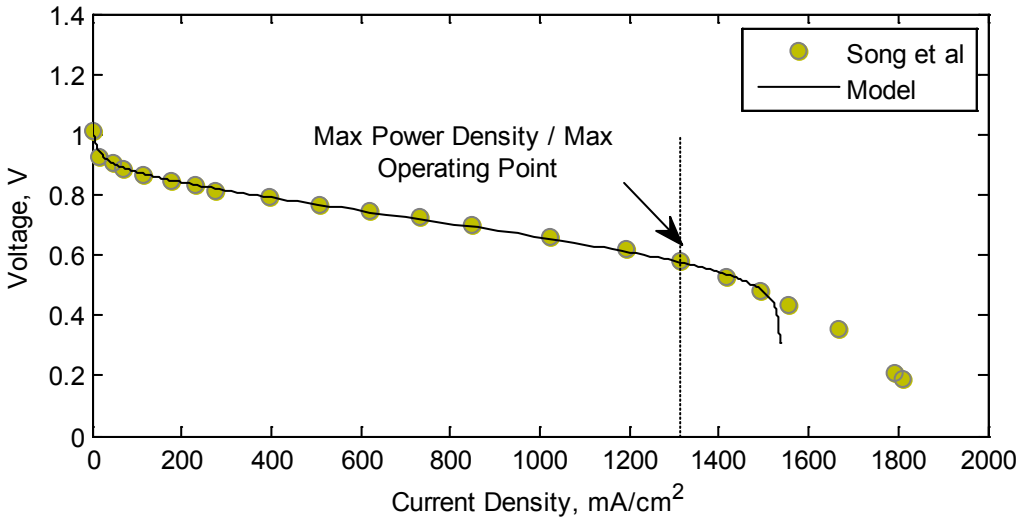

Fig. 4.1. Song et al. [57] experimental results, and the fuel cell model at matching operating conditions.

Xue et al. [58] presented data sets for three fuel cells, whose characteristics were obtained either from the fuel cell manufacturer or by experimentation by other researchers. Only the 'Ballard Mark V' fuel cell was a single cell with an area of 50.6 cm^2, while the other two were a stack of 12 and 48 cells with different active areas. Table 4.1 summarises the main properties of each fuel cell tested, and the conditions under which the experiments were carried out.

Table 4.1 : Fuel cell properties and the operating conditions of the experiments [57]

	Ballard Mark V	BCS 500W	Avista SR12 PEM
Number of cells	1	32	48
Active area (cm^2)	50.6	64	62.5
Pressure (atm)	1.0/1.0 (H_2/O_2)	1.0/1.0 (H_2/Air)	1.48/1.0 (H_2/Air)
Temperature (K)	343	333	323

The fuel cell steady state response data were presented as polarization curves plotted using a scale equivalent to the measuring devices. In order to enable comparison between the different data sets and the model, it is necessary to scale down the plots to a unified scale with the voltage of a single cell on the y-axis, and the current density in the units of mA/cm^2 on the x-axis.

For the Ballard Mark V fuel cell experimental data, the model was simulated under conditions similar to the operating conditions of the experiment. In addition, the fuel cell model was adjusted by changing the tuning parameters as follows: $K_{io} = 0.06$, $K_{dif} = 0.23$, $R_{ref} = 2.2 \times 10^{-5}$ ohm.m^2. The model and the experimental data are plotted in Fig. 4.2, where it can be seen that there is a good agreement between the model and the experimental data over the entire experimental data range. The maximum operating point, defined as the point of maximum output power is at a current density 1258 mA/cm^2.

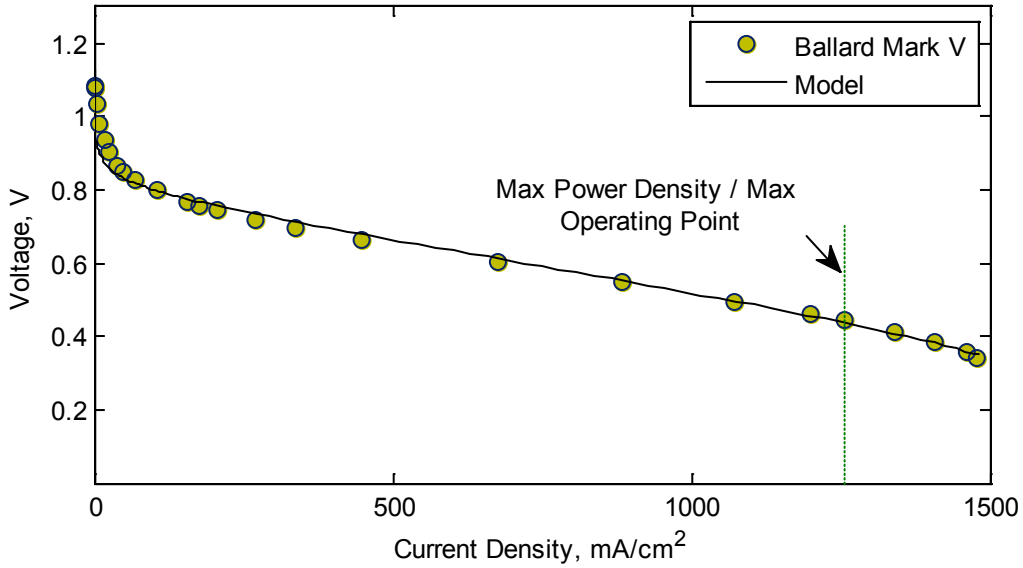

Fig. 4.2. Ballard Mark V experimental data and the tuned fuel cell model.

In order to show the claimed flexibility of the controller to changes in the model, the complete fuel cell system is simulated using the model tuned to match Ballard's fuel cell. However, Ballard's fuel cell has a maximum power density output less than that of the model developed in this thesis. Therefore, the number of cells in the tuned model matching Ballard's fuel cell was increased by the ratio of the fuel cell maximum power of the un-tuned model to that of the model tuned to match Ballard's fuel cell, which is 17 % or 412 cells instead of 350 cells. The active area was kept the same for both the model of this thesis and that tuned to match Ballard's fuel cell. A step change in the load resistance from 5 Ω to 500 Ω is applied at timestamp 1 s, and another step change from 500 Ω to 5 Ω at timestamp 4 s, shown in Fig. 4.3. It can be seen that without changing the controller of the DC/DC converter or any of its parameters, the dynamic behaviour is similar for both the original model of this study and the one tuned to match Ballard's cell.

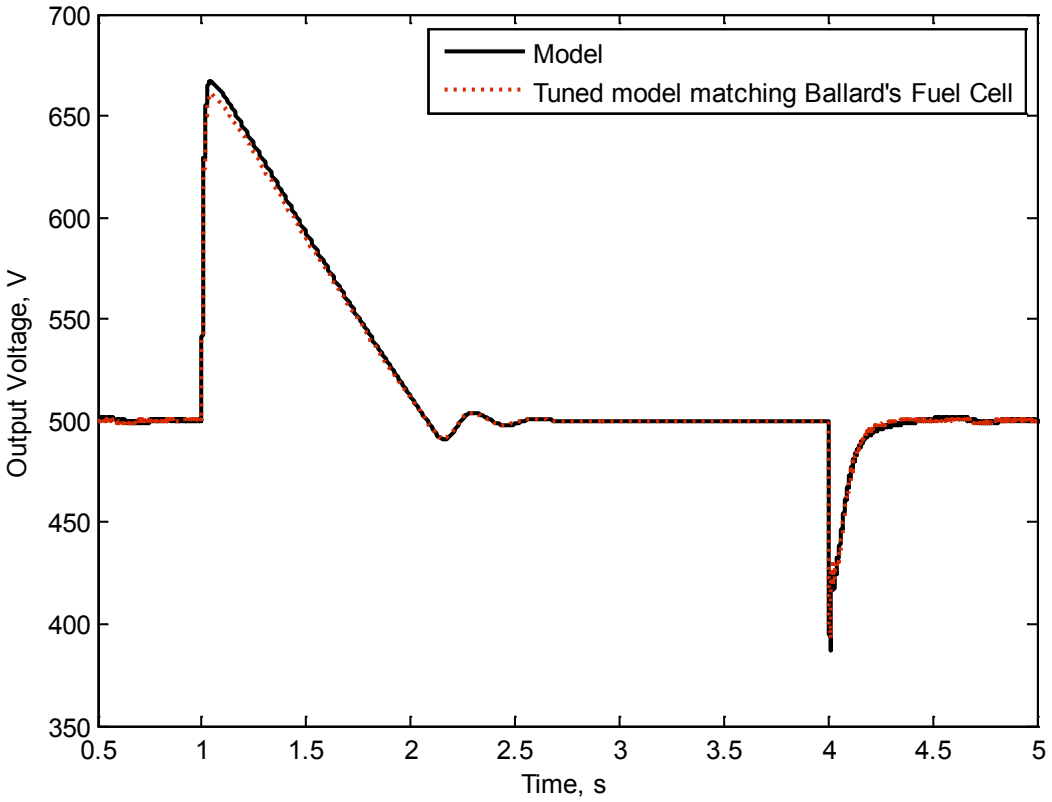

Fig. 4.3. Response of the model tuned to match Ballard's fuel cell and the model used in the rest of this thesis. A step change in the load resistance from 5 Ω to 500 Ω at timestamp 1 s then a step back to 5 Ω at timestamp 4 s.

It is worth mentioning, however, that the steady state characteristics of a fuel cell stack composed of N cells cannot be obtained by multiplying the characteristics of a single cell by N, and the same is applicable to the area. Because of this fact, it is necessary to have a control strategy designed to be flexible to changes in the characteristics of the fuel cell.

The original model developed in this thesis, which is used in analysing and developing the control strategy, is plotted in Fig. 4.4 along side the experimental data discussed earlier. It is clear that the fuel cell steady state behaviours, or the polarization curves, vary significantly from one manufacturer or research study to another. There are various reasons for this inconsistency between results, such as:

1. the process of building the membrane electrode assembly,

2. the quantities of catalyst densities on the anode and cathode,
3. the different materials and pore sizes used in the gas diffusion layers,
4. the bipolar plates material and design affecting the reactant's flow behaviour, and the electrical resistance interconnecting the cells, and
5. the operating conditions.

The experimental data plotted in Fig. 4.4 are not based on a single fuel cell with an area of 1 cm^2, therefore, the additional losses resulting from stacking fuel cells are incorporated in the plot of the single cell polarization curves. The polarization curve of the model is obtained for an operating temperature of 353 K and atmospheric pressures of hydrogen and air at the anode and cathode, respectively. While the operating conditions and actual sizes of each experimental fuel cell data were given in Table 4.1 The polarization curve of the fuel cell model lies in-between actual experimental data taking into account some of the losses that occur due to stacking losses. The results shown in Fig. 4.4 for Song et al. and the model are more comparable because they are dimensionally similar. The voltage variation between the model and Song's cell lies within ± 10 % over the operating range of the model, that is up to 1100 mA/cm^2.

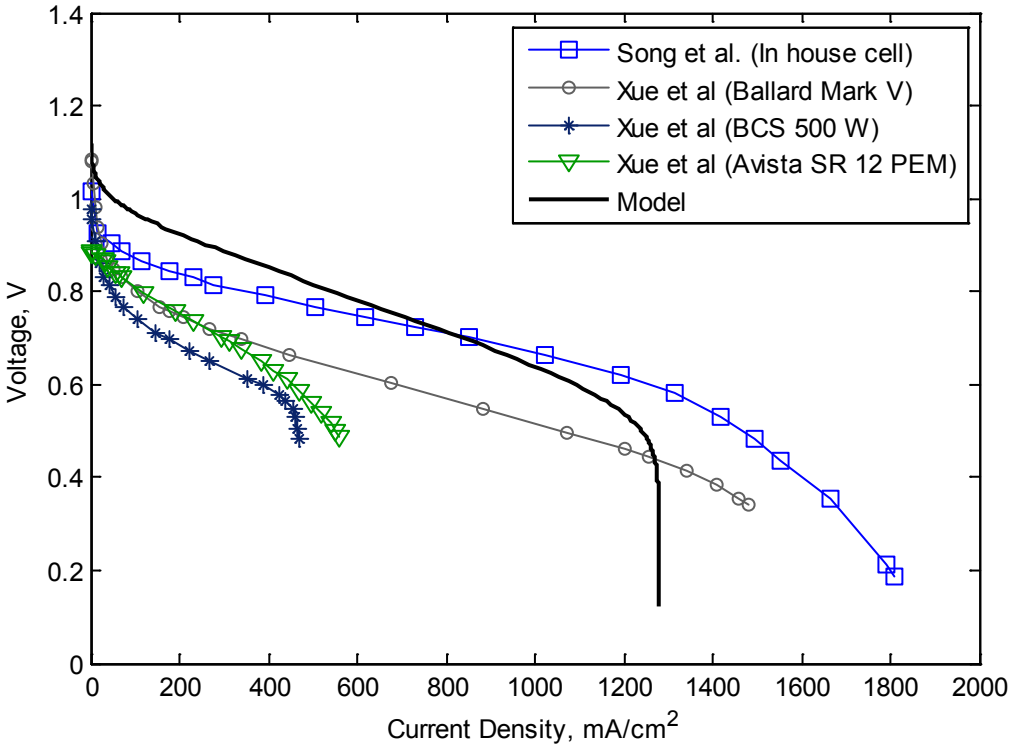

Fig. 4.4. Experimental results for various fuel cells, and the model developed in this study.

4.3 Validating the Dynamic Behaviour of Fuel Cells

The dynamic behaviour of the fuel cell is an important factor affecting the design and performance of control processes. Validating the dynamics in the fuel cell model, is as important as validating the steady state response of fuel cells before proceeding with the design and development of control strategies. The relevant dynamic behaviour of fuel cells is the response of the output current and voltage to changes in the operating point. In order to reduce the validation process, a maximum change in the operating point is considered, where the load resistance changes from one point to another in a near step change manner. This is represented as the time domain response, shown in Fig. 4.5, of the voltage and current of a single cell to a change in the load resistance. The resistive load, which defines the operating point of the fuel cell, changes at timestamp 0.5 s from 0.6 Ω to 1.2 Ω and back to 0.6 Ω at timestamp 1 s.

The general dynamic behaviour of the fuel cell when the load resistance increases is described as a rapid drop in the current to a value less than the steady state

value, followed by a slower increase in current as shown in Fig. 4.5. The voltage increases rapidly to a value lower than the steady state value at timestamp 0.5 s, then increases gradually to the steady state value at a time constant equal to that of the current. A similar behaviour but in reverse occurs when the load resistance drops.

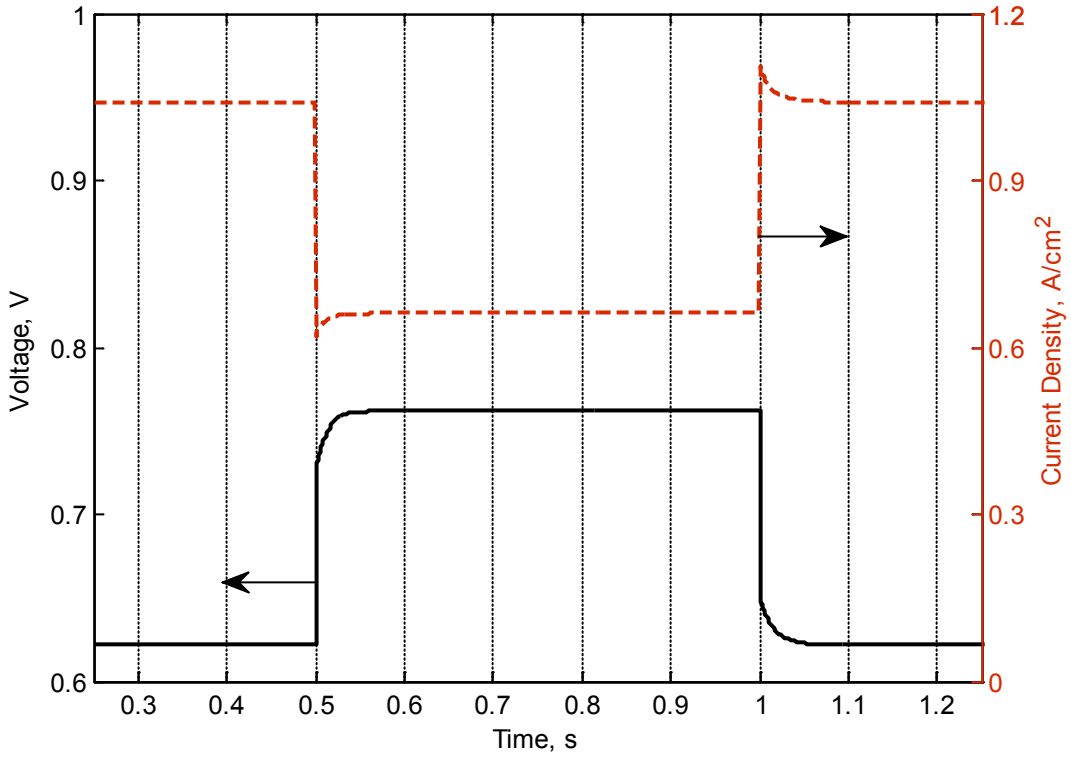

Fig. 4.5. Dynamic response of the output current and voltage of the fuel cell model.

The dynamic response of the model is compared against experimentally obtained data, although there could not be found many experimental data on the dynamic response of the fuel cell, which could mainly be due to the fast response times of the fuel cell in the microsecond scale. Such response time detection requires sensing devices of fast sampling rates, which add to the cost of the testing devices. Therefore, the dynamic behaviour modelled in this thesis is observed experimentally by a few research studies. It should be noted that the size of the undershoots or overshoots in the output current during changes in the operating points varies with the initial and final values of the load connected across the fuel cell terminals. In addition, the time constant also depends on the initial and final values of the resistance.

Andrea et al. [59] presented results of experimental work performed to test the dynamic response needed for building a simplified electrical model of the fuel cell. The experiment was carried out for a transient in the load resistance from infinity (open circuit) to 3 Ω. The voltage and current responses are shown in Fig. 4.6. The fuel cell used in the experimental work is a 'StaXX2' by 'H-Tek', and has an active area of 4×16 cm^2. The measured voltage and current during a transient from open circuit to 3 Ω then to open circuit.

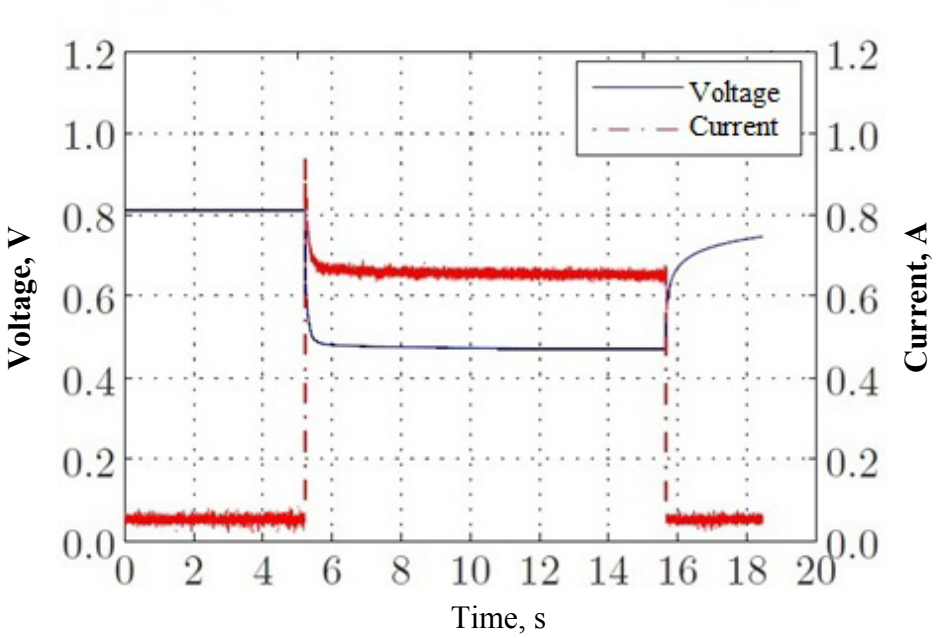

Fig. 4.6. Experimental results from Andrea et al. [59] showing the response of the fuel cell voltage and current during a transient from an open circuit to 3 Ω to an open circuit.

The response of the measured current and voltage is similar to that of the model shown in Fig. 4.5 for a step down in the resistance. However, for the step increase in the resistance, the measured current seems to be dissimilar to that of the model. The reason is that because the final value of the resistive load in the experiment is infinity (open circuit) and the fuel cell current is not expected to drop below the minimum open circuit current, which is equal to the cross over current. Usually a protective measure is implemented to avoid reversal of current by using a one-way charge flow device, such as a diode. Hence, the measured current in this case does not conflict with that of the

model. The response of the measured voltage, on the other hand, shows agreement with the model.

Weydahl et al. [16] presented more detailed experimental results on the dynamic behaviour of PEM fuel cells. In Fig. 4.7, the load is stepped down from 200 Ω to several load values showing the influence of the final load value on the time constant of the response. A smaller final value of the load, results in a faster response of the voltage reaching its steady state value. In addition, a larger step change causes a larger overshoot (Fig. 4.7) or undershoot (not shown) in the output current.

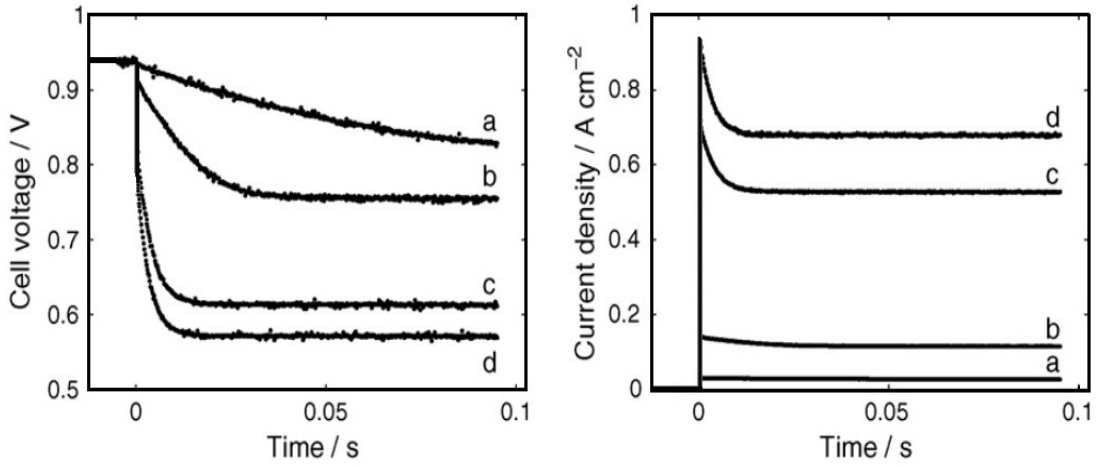

Fig. 4.7. Experimental results of the fuel cell voltage to a load transition from 200 Ω to (a) 5 Ω (b) 1 Ω (c) 0.15 Ω and (d) 0.10 Ω [16]

Weydahl et al. also presented measured results of the output voltage for a change in the load from several load values to 200 Ω, as shown in Fig. 4.8. It was reported that steady state values were reached in 5 seconds. Weydahl et al. reported that the output current followed a response similar to that of the model shown in Fig. 4.5. It was noted that a second transient in the output voltage and current occurs after reaching the steady state values causing a slight drop in voltage. These transients have a slower response time and these are attributed to the formation of oxides on the surface of the electrode on the cathode. Since the second transient has a slower response time (on a scale of 100 s), it has a negligible effect on the design and performance of the controller, and therefore, these are not included in the model. It should be noted that the response times of the voltage shown in Fig. 4.8 are larger than that of the transient case of the model

shown in Fig. 4.5 because the final value of the load resistance in the experimental setup is much larger than that of the model.

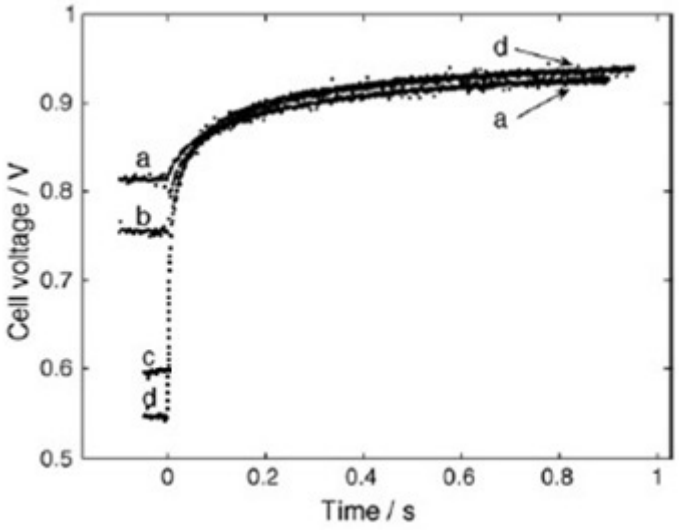

Fig. 4.8. Experimental results of the fuel cell voltage to a load transition from (a) 5 Ω (b) 1 Ω (c) 0.15 Ω and (d) 0.10 Ω to 200 Ω [16]

4.3.1 The Hysteresis Behaviour of Fuel Cells

In a complete energy conversion system, the fuel cell is connected to a DC-to-DC converter. The main operating principle of converters relies on a switching circuit at a certain frequency and/or duty ratio. The switching circuit emulates a change between two operating points on the polarization curve. The speed or frequency of the change affects the dynamic path of the operating points of the fuel cell. Hysteresis behaviour occurs due to the double layer capacitance of the fuel cell and causes harmonics in the current. These harmonics affect the performance of the DC-to-DC converter and its control and should be avoided in the design of the converter. A small signal analysis is performed to find the limiting switching frequencies, which may be filtered by the double layer capacitance. A sinusoidal change in current is applied to the fuel cell model around an operating point of 0.6 A/cm^2 with a peak-to-peak magnitude of 0.6 A/cm^2. The fuel cell response is plotted at frequencies of 1 Hz, 10 Hz, 100 Hz, and 1 kHz as shown in Fig. 4.9. A considerable hysteresis behaviour is noticed for frequencies around 10 Hz because of the double layer capacitance. The hysteresis effect

diminishes at a low frequency of 1 Hz because the double layer capacitance has enough time to charge and discharge. Similarly, it is found that at frequencies greater than 1 kHz hysteresis behaviour diminishes. Therefore, an optimum switching frequency of 1 kHz is used for the converter to avoid hysteresis and minimize switching losses, which are directly proportional to the switching frequency. Operating at frequencies below 1 Hz is not recommended, as this would make the operation of the converter sensitive to the other slower phenomena taking place in the fuel cell. These slower phenomena include the temperature and water content of the membrane, as well as the reactants' flow response.

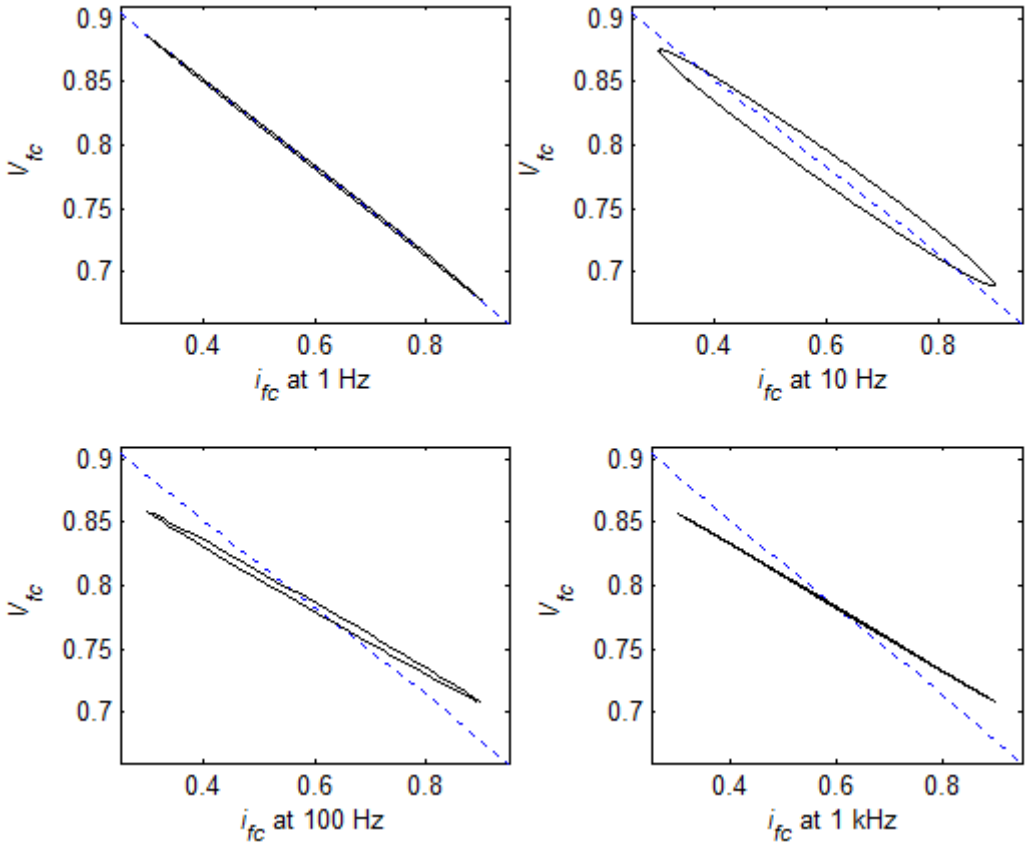

Fig. 4.9. Sinusoidal change in current of 0.6 A/cm^2 around an operating point of 0.6 A/cm^2. The dotted line shows the steady state portion of the polarization curve.

4.4 Sensitivity Analysis

Any system under investigation involves many variables, and the fuel cell is of no exception. Including all the variables in the model does not necessarily result in a noticeable improvement on the overall objective of the study. Therefore, for the objective of studying the control problem of the fuel cell for varying power demands, it is necessary, as a first step, to recognise the main influential variables on the fuel cell performance, and further to filter out those variables that do not contribute to the dynamic behaviour of the fuel cell system in the relevant response time.

Sensitivity analysis is used to find the significant operating variables that would change the performance variables in the desired manner. In addition, sensitivity analysis is used to draw the specifications of measuring devices, such as the resolution, the error range, and the response time of the device. The performance of the fuel cell at an operating point is defined by its efficiency, which is the ratio of output power to input power. The output power at an operating point is directly proportional to the operating voltage and current, while the input power is directly proportional to the consumption rate of hydrogen. At steady state, the consumption rate of hydrogen is directly proportional to the output current. Hence, the efficiency of the fuel cell is directly proportional to its output voltage at a certain operating current. In addition, the output power may be used to indicate the performance of the fuel cell at an operating current.

The effect of changing the operating conditions on the fuel cell performance is discussed earlier in this thesis and the model is validated here by studying the polarization and power density curves.

4.4.1 Temperature Effect

As discussed previously in Chapter 3, a relatively quick change in temperature is unlikely to occur in fuel cells due to the high specific heats of its components. Hence, the control of temperature is not considered in this study, and model validation is restricted to confirming that the fuel cell model takes into account the effect of temperature on performance. Therefore, the effect of a temperature change on the fuel cell performance is only observed under steady-state conditions using the fuel cell stack

model shown in Fig. 3.16 with the same parameters in Table 3.3 but for 1 cell with an area of 1 cm^2 connected to a variable resistance load without the diode, and the DC-to-DC converter. The pressure input is set to a fixed value of 1 atm and the change in current is limited to a maximum of 1 x 10^{-7} A/s to obtain steady state operation. Two simulation results are obtained to observe the effect of temperature on the performance of the fuel cell; first, the polarization curves of the fuel cell are obtained at 80 °C and 60 °C along with the power density curves, as shown in Fig. 4.10.

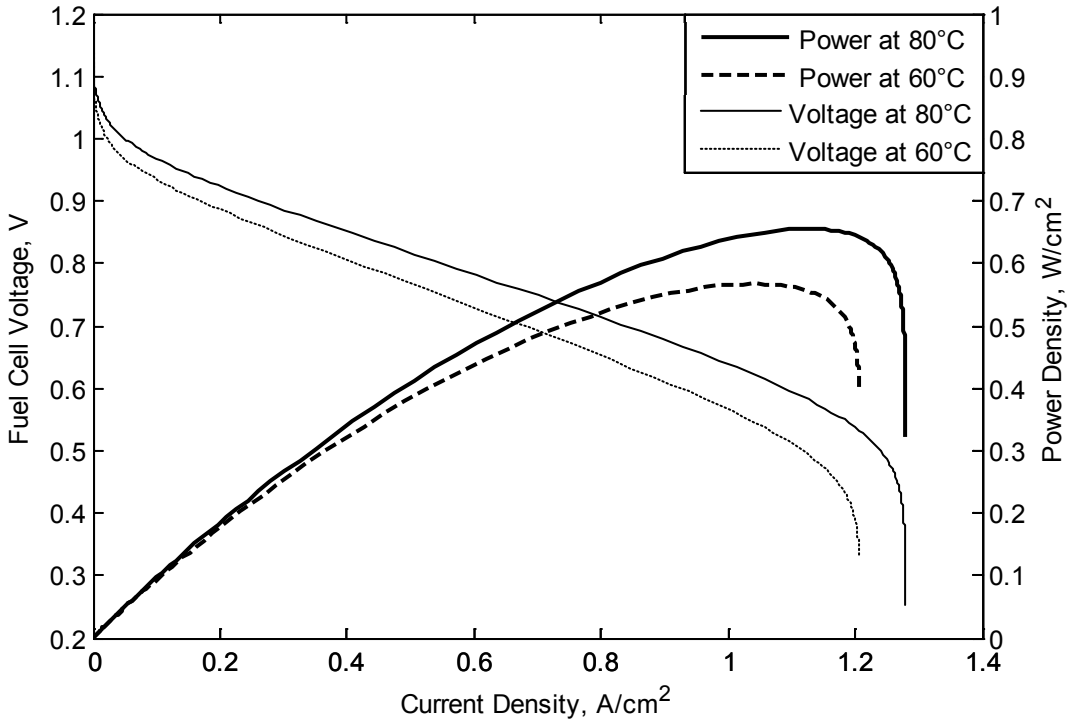

Fig. 4.10. Polarization and power density curves of a single fuel cell at 60 and 80 °C

These plots are graphical representations of the fuel cell model simulated under sufficient reactant flow rates, constant atmospheric pressure, and perfect humidity of the membrane. Only the temperature is varied to observe its effect on the polarization and power density curves. As the temperature of the reactant increases, the molecules gain higher thermal and vibrational energies; hence, more collisions occur, increasing the reaction rate. The activation losses drop as the temperature increases, and this can be seen more obviously at low current densities less than 75 mA/cm^2. At current densities higher than 75 mA/cm^2 the voltage exhibits a linear drop with current defining the

ohmic region, which has a smaller slope at the higher temperature. Near the end of the linear ohmic region, the voltage starts to drop sharply due to concentration losses, which under sufficient flow rate depend on the maximum reaction rates. These reaction rates are directly proportional to temperature, according to Arrhenius' equation discussed in Chapter 3.

In the second simulation result, both at 80 °C and 60 °C, the voltage and power density of the fuel cell are found at several resistances ranging from 1000 Ω to 0.1 Ω connected to the fuel cell without a power conditioning unit. The ratio of the fuel cell voltage at 80 °C to that at 60 °C for each resistance is calculated, as well as the ratio of the power density. These results are not plotted, but the findings are reported as follows.

It is found that for an increase in temperature from 60 °C to 80 °C, the maximum increase in voltage and power occurs at maximum power demand, which is at 0.5 Ω for a 1 cm^2 single fuel cell. Temperature has a significant effect on the performance of the fuel cell. A 20-degree increase in temperature from 60 °C to 80 °C increases the maximum output power of the fuel cell across a 0.5 Ω load by about 15 %. This is a large value that should not be neglected under normal conditions, however, a 20-degree temperature change is for demonstrating the effect of temperature on performance, and is unlikely to occur in a short period. A reasonably well controlled heat management system should be able to react to changes in temperatures smoothly without reaching such excessive values of error. It is expected that the error range of temperature will be within ± 5 °C. Therefore, this piece of the model is suitable for determining the optimum steady-state operating point of temperature.

There is a limited number of ways to change the operating temperature of the fuel cell, and that is by changing the temperature of the reactants or by having a separate heating and cooling system added to the components of the fuel cell stack. At low power outputs, the amount of heat generated is small, and heat is needed to raise the operating temperature to 80 °C. On the other hand, when the power demand is high, the generated heat needs to be removed to avoid reaching high temperatures, which would dehydrate the membrane, and reduce performance. In addition, high temperatures would damage the membrane itself permanently.

Changing the operating temperature also has an effect on the mass flow rates of the reactants. Since the inlet mass flow is a direct feed-forward loop proportional to the output current, the outlet mass flow rate is adjusted to maintain the required operating pressure. As an increase in temperature reduces the density of the reactant gases and increases the pressures of the anode and the cathode; consequently, the outlet flow rate has to be increased by the pressure controller, hence reducing the total mass of the reactants available in the anode and the cathode.

4.4.2 Pressure Effect

The density (or in chemical terms 'concentration') of the reactants, affects the number of collisions between the molecules of the reactants. For a larger concentration, the number of reactants' collisions increases, hence increasing the reaction rate, as explained by the collision theory of chemical reactions. At constant temperature and constant volume, the concentration of a gas is directly proportional to its pressure.

The effect of the reactants' pressure on the fuel cell performance is investigated by obtaining the polarization (Fig. 4.11), and power density (not shown) curves as the pressure varies. The simulation results are obtained by fixing the other operating conditions, such as temperature of 80 °C, perfect water content of the membrane and sufficient flow rates of reactants that meet the maximum demand.

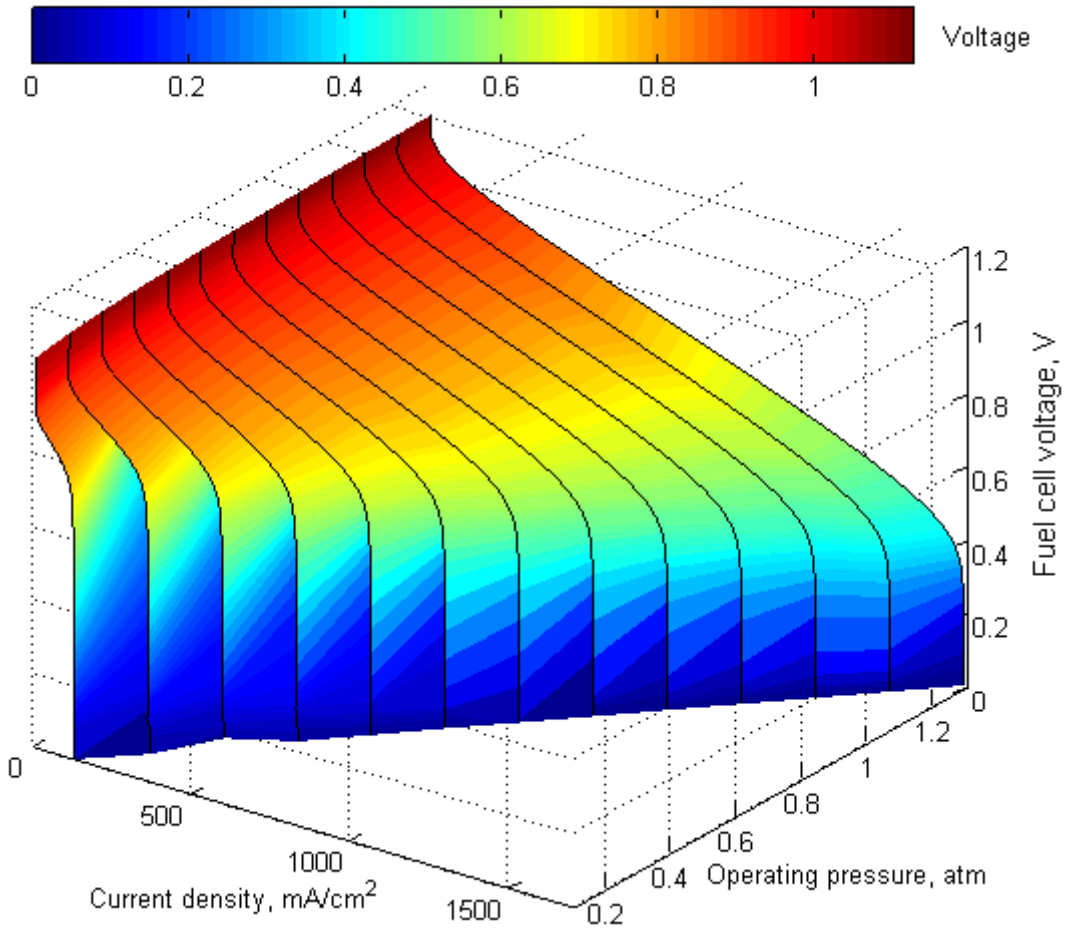

Fig. 4.11. Polarization curves as a function of operating pressure

The ratio of voltage and power at 1.0 atm to that at 0.8 atm operating pressures are observed at various load resistances. It is found that an insignificant increase in voltage (< 2 %) and power (< 4 %) are observed for operating points up to 70 % of maximum power demand. However, a significant increase in voltage (14 %) and power (30 %) is observed near maximum power output. This is attributed to the higher consumption rate of the reactants, which becomes near the reaction rate limits at that pressure.

It is found that as the pressure increases, the improvement in performance decreases. For pressures above 1.0 atm, an increase of 10 % in pressure increases the output power by 5 %. However, as the operating pressure is increased, more power is consumed by compressors, and a careful study is needed to find out the exact figures of the overall power balance using compressors.

Although the pressure of the reactants may have less influence on the performance of the fuel cell than the operating temperature, its dynamics and fast response times, make it more important to control it. Hence, reactants flow is modelled in this study and a control strategy is proposed and analysed.

4.4.3 Mass Flow Rate Effect

Hydrogen supply constitutes a major factor in a fuel cell system since it is the energy carrier and is the only running expense on the user. From the point of view of this study, hydrogen supply rate is considered for optimising operation and performance under all conditions. In order to observe the importance of hydrogen supply, polarization curves are obtained at various but constant hydrogen flow rates, as shown in Fig. 4.12.

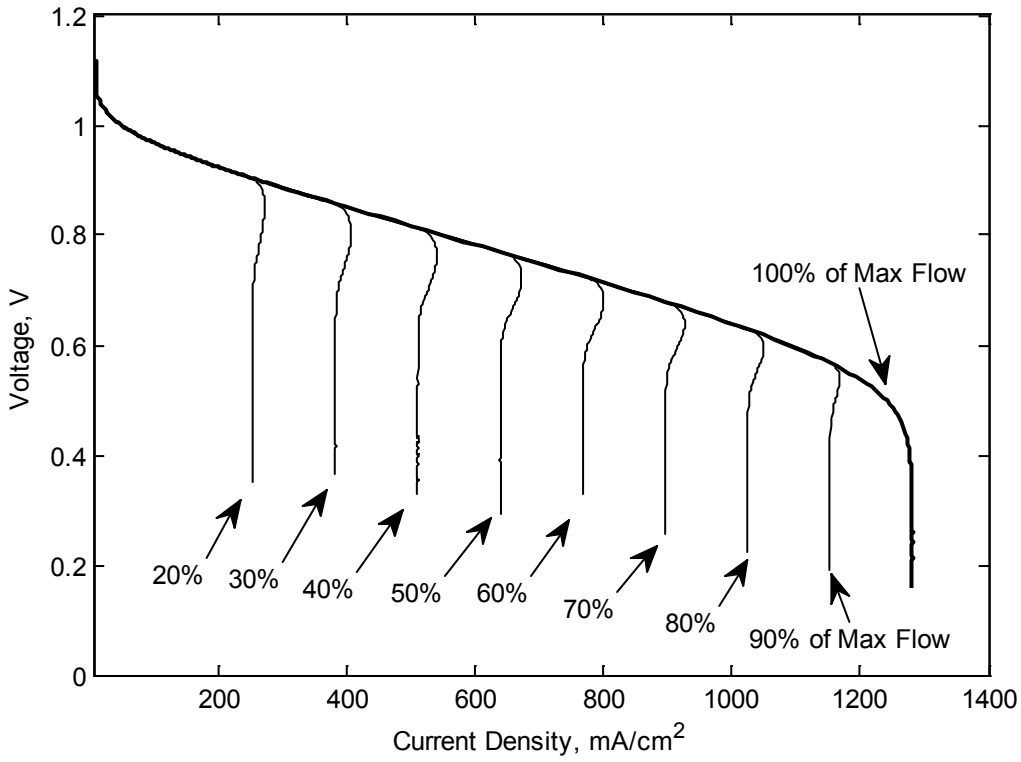

Fig. 4.12. Polarization curves at various fixed flow rates

The normal polarization curve of a fuel cell is obtained with sufficient flow rates of the reactants to meet the consumption demands. Under these circumstances,

concentration losses are only due to the limitations of the fuel cell reaction rates and/or the maximum diffusion rate of hydrogen flow. At steady state operation, hydrogen consumption is directly proportional to the output current. The maximum current in the polarization curve, also known as the limiting current, is associated with a maximum flow rate of hydrogen needed for the reaction. It can be observed from Fig. 4.12 that for the polarization curve with sufficient flow rates, the maximum current is 1282 mA/cm^2, which consumes the maximum rate of hydrogen of 13.4×10^{-6} g/s. This rate of hydrogen mass flow rate is labelled in Fig. 4.12 as '100 % of Max flow'. For any hydrogen mass flow rate less than that, the operating points follow the polarization curve until they deviate due to concentration losses caused by insufficient flow. The deviation in the operating points occurs at a current smaller than the maximum current. The polarization curves at flow rates less than 100 % have a slight increase in current at the point where the curve deviates from the 100 % polarization curve. The reason for this is attributed to the outlet valve of the flow controller, which boosts the initial fall in pressure by fully closing the outlet valve. However, as the consumption continues to exceed the inlet flow, the pressure eventually drops and concentration losses increase.

For dynamic, varying power demands, a conclusion may be drawn that as long as the supplied mass flow rates are greater than consumption rates, any changes in the external resistance or current have negligible, if any, effect on the voltage performance. However, if the supplied hydrogen mass flow rate equals the consumption rate, any increase in the current cannot be instantly met by an increase in the flow rate. This causes reaction starvation and degradation in the performance of the fuel cell. In other words, the fuel cell voltage would suffer from concentration losses at lower current values than that occurring at sufficient flow rates. This justifies supplying excess hydrogen to avoid degradation in performance due to sudden increases in the demand.

The results from this study can help in determining the design of an energy storage system, such as super capacitors, taking into account the amount of sudden change in power demand, and the amount of excess hydrogen supplied. In addition, the excess value can be chosen to be dynamic, instead of being fixed at 20 %. For example, the excess ratio can be designed to decrease as the output power increases.

4.5 DC-to-DC Converter

The operation of DC-to-DC converter is validated by connecting a 200 V ideal voltage source to its input terminals, and a 5 Ω load to its output. The duty ratio is manually increased and the output voltage is measured. The output to input voltage ratio is compared to an ideal converter with an output to input ratio of 1/(1–D), as shown in Fig. 4.13. The maximum voltage ratio is 12.72 at a duty ratio of 0.9625. This value defines the allowed upper limit of the duty ratio of the converter. The upper limit for the fuel cell system is adjusted to 0.6 to prevent the fuel cell from operating in the concentration region and ensure controllability, as discussed in Chapter 3.

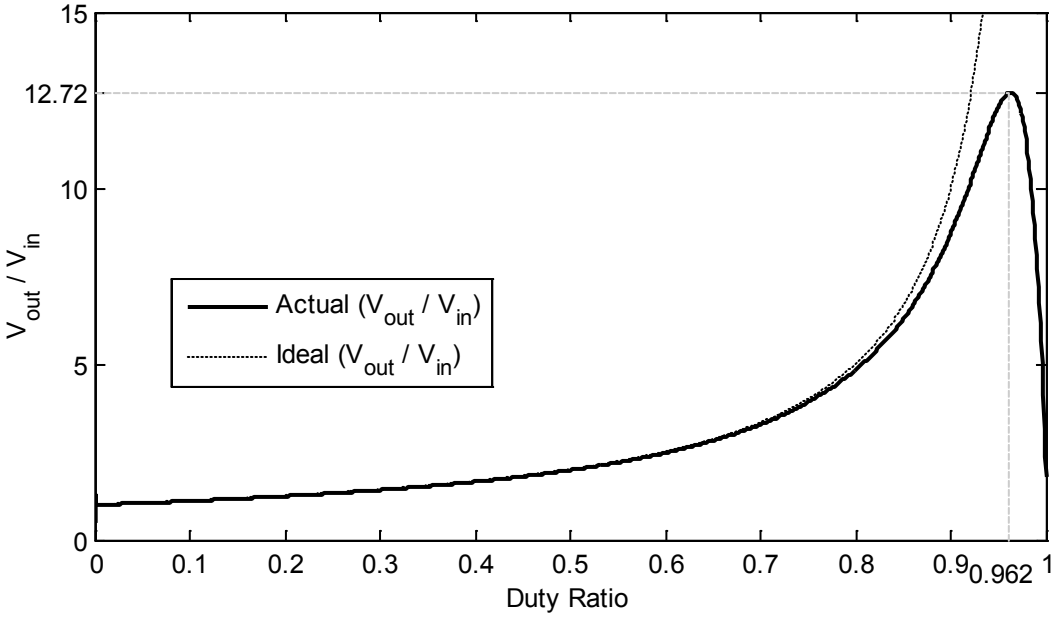

Fig. 4.13. The output to input voltage ratio of ideal and actual converters.

4.6 Summary

The overall fuel cell model showed comparable behaviour to data obtained experimentally by different researchers and/or manufacturer's data sheets. The model showed flexibility to match wide variations of fuel cell designs and conditions. The fuel cell model responds to variations in temperature, pressure, and flow rates. Finally, the output to input voltage ratio of the DC-to-DC converter was tested using an ideal voltage source to prove its principle of operation when the duty ratio is varied.

Chapter 5

AUTOMOTIVE APPLICATION

In this chapter, the fuel cell system is investigated for use in automotive applications. The deliverability of power demand by the fuel cell, its power conditioning, and control systems are all studied. A fuel cell vehicle could contain one main electric motor, and a mechanical power transmission system, or electric motors at each wheel (front-wheel-drive, rear-wheel-drive or 4-wheel-drive) without mechanical power transmission. In case of the former vehicle, no electric power transmission is needed as opposed to the latter vehicle, which requires electric power transmission. In either case, an electric motor requires a controller to regulate its torque and/or speed according to the driver's requirements. However, the details of motor controllers are out of the scope of this thesis, and in order to test the performance of the fuel cell system, it is assumed that the load consists of both the electric motor and its controller. Hence, from the fuel cell system point of view, the load is a constant-voltage power profile, which means a variable resistance represents the load requirements.

Two driving cycles were simulated to study the performance of a fuel cell vehicle under city and motorway driving conditions. The available data on driving conditions only provides the velocity profile. As described in Chapter 3, the power demand profile is estimated based on typical light duty vehicle characteristics, from which the resistance profile is calculated and used in the simulations. The results obtained from the simulations are presented and a few case studies of interest are investigated in detail.

5.1 Urban Dynamometer Driving Schedule

The Urban Dynamometer Driving Schedule (UDDS) is used to represent city driving scenarios for light duty vehicles. From the power demand calculated in Chapter 3, the rate of change of power demand and the difference between the demand and the actual power output by the fuel cell system are shown in Fig. 5.1, along with the velocity and acceleration profiles of the UDDS driving schedule. The difference

between the requested power and the delivered power ranges between a maximum value of +240 W and a minimum value of about –250 W. The positive sign indicates shortage in the power supplied to the load, and the negative sign indicates excess power supplied to the load. Simulation results (Fig. 5.1) show that the output voltage deviates within ±8 V, which is nearly 2 % of the reference 500 V voltage. This is well within acceptable voltage tolerances (about ±10 %) of commercially available electric motors. Table 5.1 summarises the analysis of the entire driving schedule.

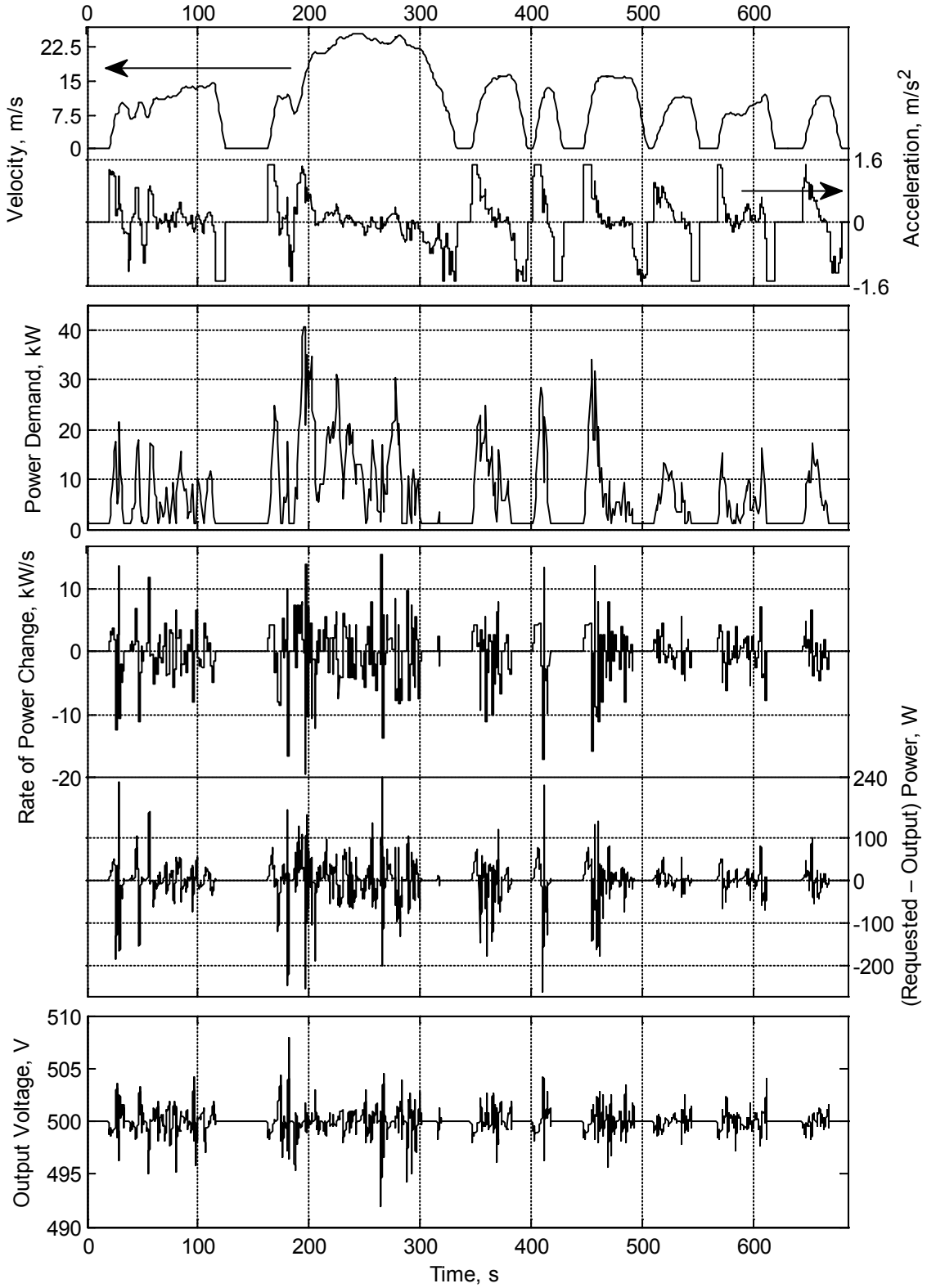

Fig. 5.1.(A) UDDS velocity, acceleration, rate of change of power demand, difference in power, and the output voltage for duration 0 s to 685 s.

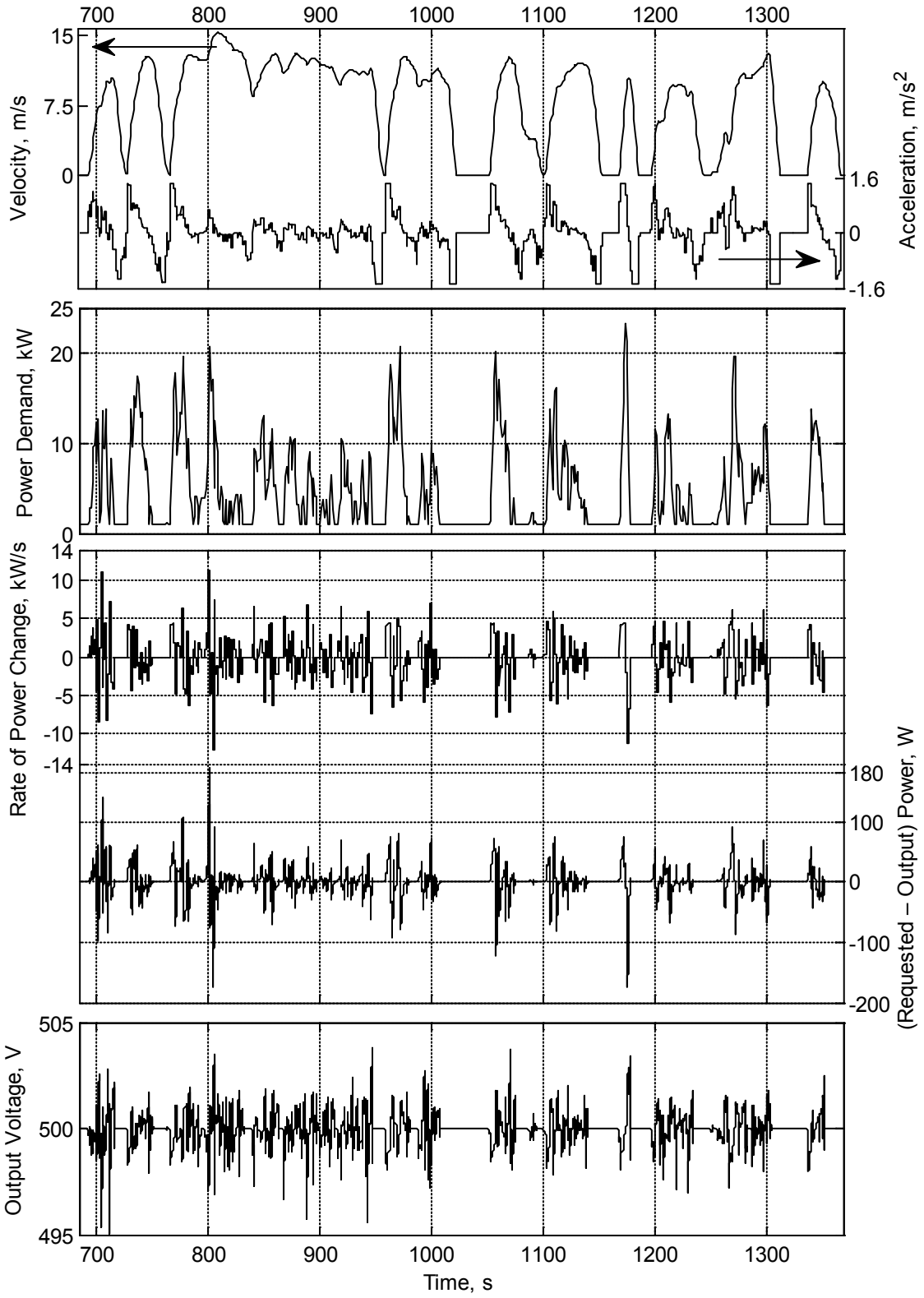

Fig. 5.1.(B) UDDS velocity, acceleration, power demand, rate of change of power demand, difference in power, and the output voltage for the duration 685 s to 1369 s.

Table 5.1 : UDDS analysis

Maximum velocity	25.4 m/s (91.3 km/hr)
Maximum acceleration	1.48 m/s^2 (1.92 x 10^4 km/hr^2)
Maximum deceleration	1.48 m/s^2 (1.92 x 10^4 km/hr^2)
Maximum power demand	40.6 kW
Minimum power demand	1 kW
Maximum power shortage	240 W
Maximum excess power	250 W
Maximum rate of change of power demand	15.6 kW/s
Minimum rate of change of power demand	–19.6 kW/s

5.1.1 Case Study 1: Maximum Acceleration and Maximum Power Demand

The first case study is between timestamps 162 s to 200 s, shown in Fig. 5.2 to Fig. 5.7. Several interesting events occur in this period such as a maximum acceleration of 1.475 m/s^2 attained between timestamps 163 s to 169 s increasing the velocity from zero to 8.85 m/s or 32 km/hr. Although this is a maximum acceleration point, it does not result in maximum power demand, but only 24.9 kW, because power depends on other factors such as velocity, as mentioned in Chapter 3.

Another near maximum acceleration point at timestamp 194 s results in the maximum power demand (40.6 kW) over the entire UDDS cycle, with a shortage of power of 110 W. However, this shortage in power is relatively smaller than shortages occurring at lower velocities or lower power demands, such as between timestamps 180 s to 181 s and 197 s to 198 s, which result in power shortages of 165 W and 152 W, respectively, as shown in Fig. 5.2. This may be explained because the rate at which power demand increases at timestamp 194 s is 8 kW/s, which is smaller compared to 10 kW/s and 14 kW/s at 180 s and 197 s, respectively. In addition, although the rate of change of power demand at time 180 s is smaller than that at 197 s, the power shortage at 180 s is greater than that at 197 s.

This is explained by noticing that prior to the event leading to the “high” rate of change of power demand is different in each situation. For the 197 s timestamp, the system had excess power output because the demand was sharply decreasing prior to the

change and the capacitors and inductors of the DC-to-DC converters were transferring more power than necessary, whereas at timestamp 180 s, the system already had a shortage of power. Had the duration of operating conditions at the higher rate of change of power demand been persistent for more than one second, the system would have eventually had a greater shortage of power compared to that occurring at a smaller rate of change of power demand.

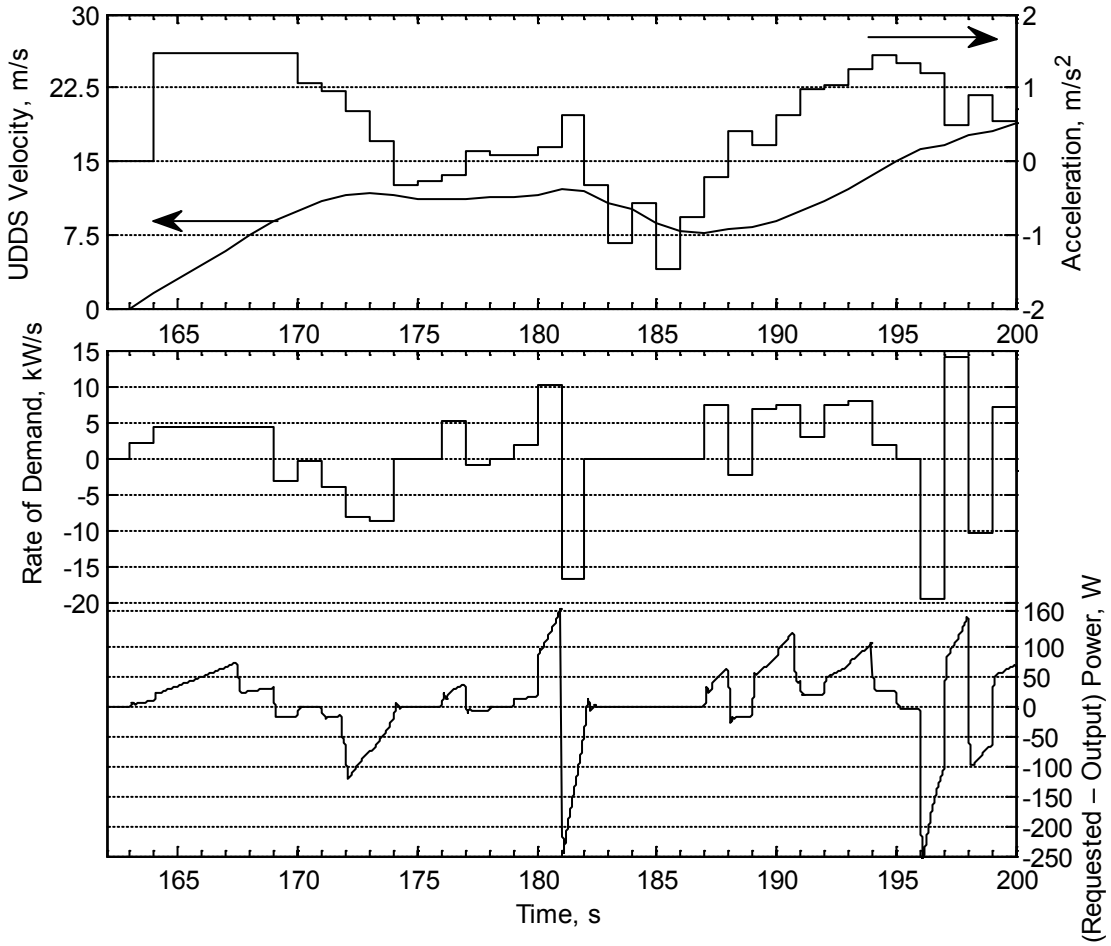

Fig. 5.2. Velocity, acceleration, rate of change of power demand and the difference of output power for case study 1.

For a drop in power demand at a negative rate of change, the initial value of excess power is proportional to the negative rate of change of power demand and depends on the difference in power (excess or shortage) prior to the change, as shown in Fig. 5.2. The excess power gradually diminishes to zero at a rate inversely proportional to the rate of change of power demand. For example, comparing the changes taking

place at timestamps 181 s and 196 s, the greater negative rate of demand occurring at 196 s results in more excess power, and the rate at which the difference is decreasing is greater for the smaller rate of demand occurring at 181 s.

A point of interest occurs near timestamp 167.5 s, where the difference in power drops from 75 W to 25 W in 200 ms although the power demand is increasing a constant rate. The fuel cell and converter operating conditions and the controller are also not changing at this timestamp, as shown in Fig. 5.3 to Fig. 5.6, in a way that would cause such behaviour. However, a further investigation in converter operations reveals the cause pointing to the nonlinearity in the discontinuous current mode of operation in the converter, discussed briefly in Chapter 3. At timestamp 167.5 s, the converter crosses the boundary from the discontinuous to continuous current modes. Further details on the discontinuous mode of converter operation is discussed in UDDS case study 3, Section 5.1.3, where the converter crosses the boundary between continuous and discontinuous modes more frequently than this case study.

The maximum overshoot in output voltage for the whole UDDS cycle reaches 508 V and occurs at timestamp 182 s. This large overshoot occurs because of a fast drop in power demand from 17.5 kW to a low level of 1 kW. Prior to the drop in power demand, the power output was increasing and therefore, the current through the output inductance of the converter was increasing. When the power demand drops, the current through the inductance reverses its rate of change and starts to decrease. Because the inductance tends to resist changes in the rate of its current by an induced voltage proportional to the rate of change in its current, a reversal of current rate causes a large voltage induced at the inductance terminals, which adds up at the output voltage as a fast voltage overshoot. In addition, with voltage being regulated, the time required for the energy stored in the inductance to be transferred to the load is directly proportional to the resistance of the load, or in other words, inversely proportional to the power being consumed by the load. As the resistance increases to reflect a drop in power demand, the voltage becomes proportional to the increase in resistance because of the slowly varying current due to the inductance's behaviour to resist the change in its current. All these combined factors add together to create a maximum voltage overshoot at this timestamp. On the other hand, a larger negative rate of change of power demand

occurring at 196 s does not cause a larger voltage overshoot, because prior to the change the power demand was 40.6 kW, then it drops to 21 kW which is much larger than 1 kW seen at timestamp 182 s.

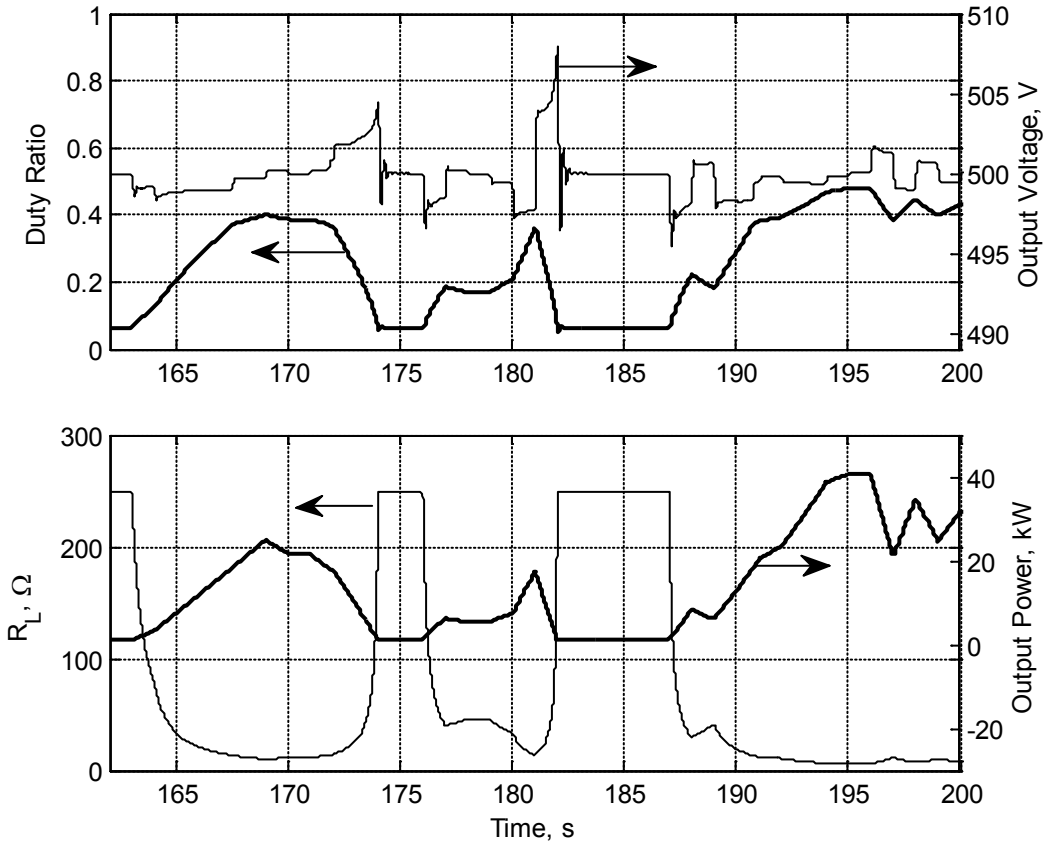

Fig. 5.3. Duty ratio of the converter, output voltage & power, and load resistance for case study 1.

From Fig. 5.3 and Fig. 5.4, it can be seen that the DC converter and its controller are able to maintain an acceptable level of regulation on the output voltage within 495 V and 508 V (less than 2 %) for a wide range of output power and a large variation of the fuel cell voltage. For this case study, the fuel cell voltage varies from 368 V down to 262 V.

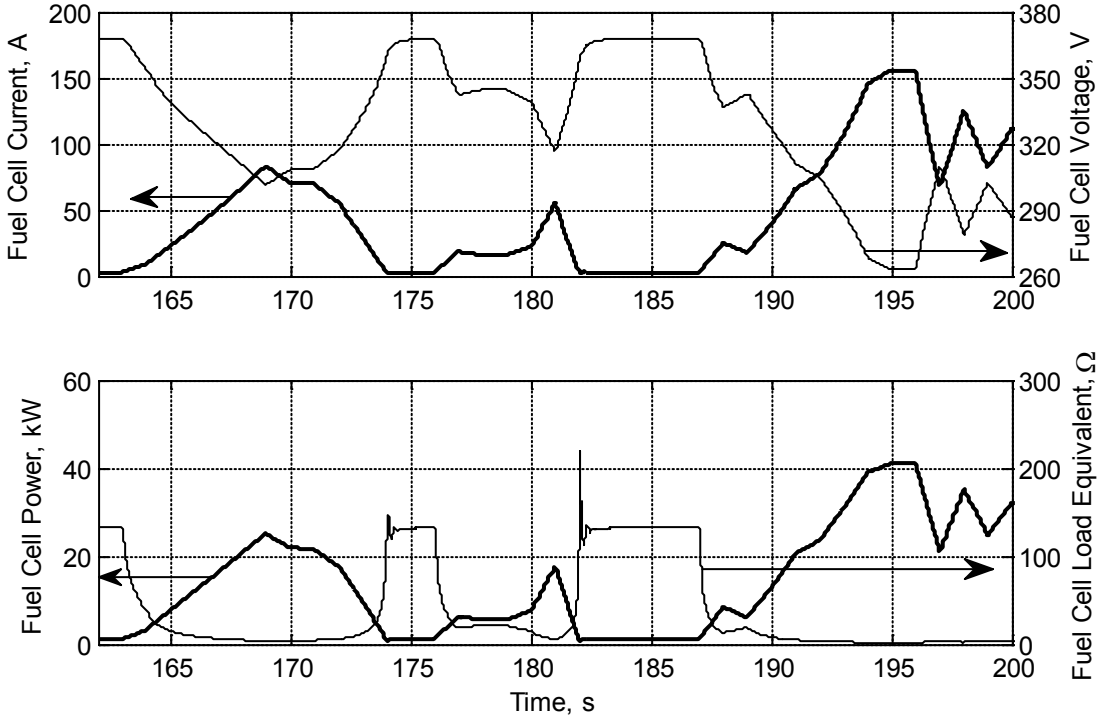

Fig. 5.4. Current, voltage, power & equivalent resistance of the FC for case study 1.

The partial pressure of oxygen at the fuel cell cathode is more sensitive to variations in power demand than hydrogen, because at the cathode, air is supplied and water is produced. However, it should be noted that this arrangement is because, as discussed in Chapter 3, the total pressure of the cathode has a higher priority in control than the pressure of oxygen, in order to ensure minimum differential pressure across the membrane, which has a deteriorating effect on its lifetime. As membrane manufacturing technologies advance, membranes become tolerable to high differential pressures. In this case, the pressure of cathode should be increased to overcome the drop in the partial pressure of oxygen when the load increases.

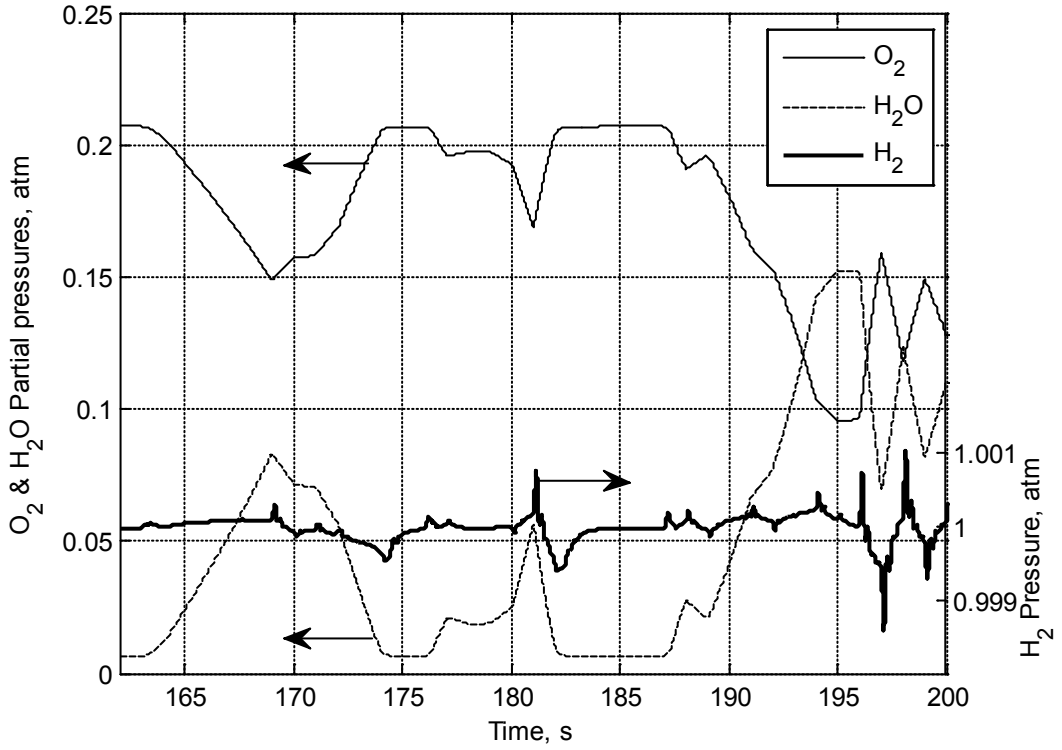

Fig. 5.5. Hydrogen, oxygen, and water partial pressures for case study 1.

Hydrogen mass flow rate regulation by the input valve and the pressure of hydrogen regulation by the output valve is shown in Fig. 5.6. Since the control of the reactants is dependent only on the fuel cell operating conditions, it is appropriate to refer only to the relevant figures affecting the performance of the reactants control.

At timestamp 171 s, the fuel cell current starts to drop and as a result hydrogen input flow rate drops in proportion according to the feedforward control algorithm. It might be expected that when the consumption rate drops, the pressure of hydrogen would increase. However, due to the delay in response of the output valve, the pressure of hydrogen continues to drop until timestamp 174.25 s, which is 200 ms after the current has reached a steady state value. This corresponds to the summation of the response times of the inlet and outlet valves, which describes the overall behaviour of hydrogen flow regulation.

The lowest drop in pressure occurs at timestamp 197.1 s; that is 130 ms after the fuel cell power and current reached the lowest local point, which is in agreement with

the time constant of the response of the valves. It can be noticed from Fig. 5.4, Fig. 5.5 and Fig. 5.6 that the pressure of hydrogen usually drops when the consumption of hydrogen decreases, and the quicker the rate of decrease in consumption the more the drop is in hydrogen pressure. However, for oxygen, and product water, the situation is reversed because of the mixture of gases at the cathode and the large difference in molecular weight between hydrogen on one hand and oxygen and water on the other hand. When the power output and current increase, the rate of oxygen consumption increases and the rate of water production increases, and although the total pressure of the cathode tracks the pressure of the anode, a significantly larger variation in the partial pressures of oxygen and water takes place. That can be noticed in Fig. 5.5 from the scale of the y-axis of hydrogen compared to the combined y-axis of oxygen and water.

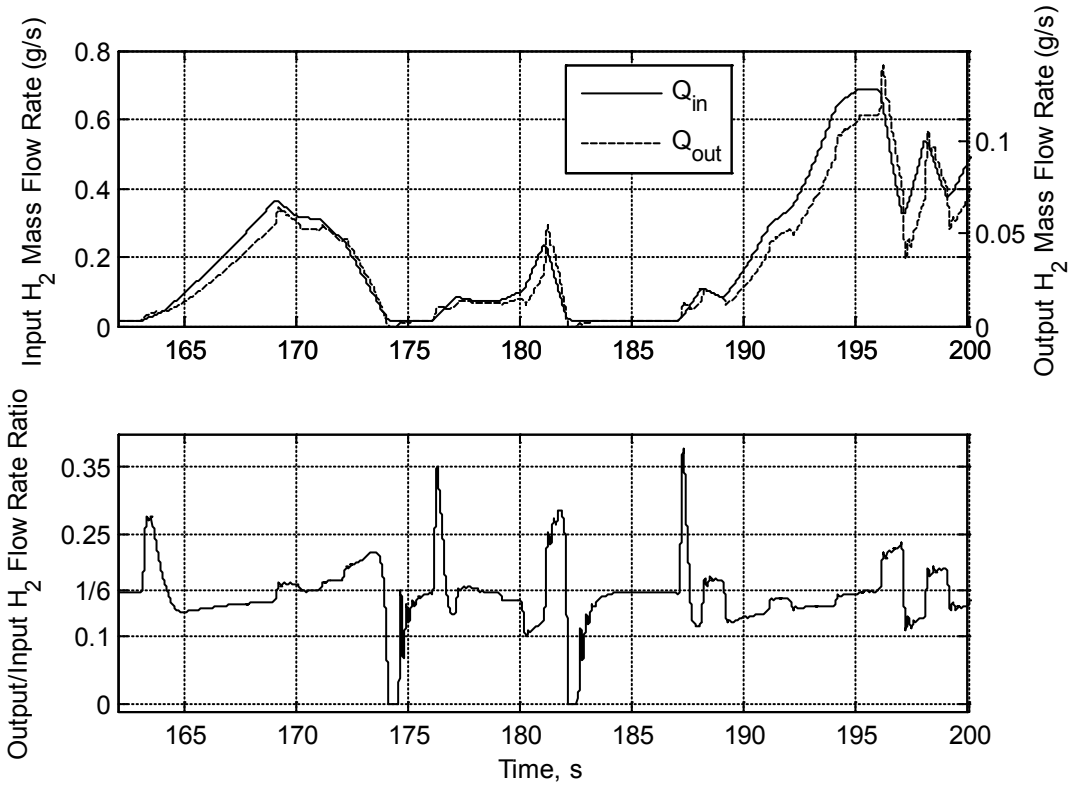

Fig. 5.6. Inlet and outlet mass flow rates of hydrogen, and their ratio for case study 1.

In Fig. 5.6, the ratio of outlet to inlet mass flow rate of hydrogen is plotted. One of the aims of the reactant flow design is to supply 20 % excess hydrogen, which results in an outlet to inlet flow ratio of 1/6. This is met by the inlet valve, but the fluctuations

around the 1/6 target line are due to the outlet valve which is controlled by a feedback loop with the pressure objective as a reference. It can be seen that with this strategy, the pressure of hydrogen is well regulated within 0.1 % for rates of change in power demand between –20 kW/s and 15 kW/s.

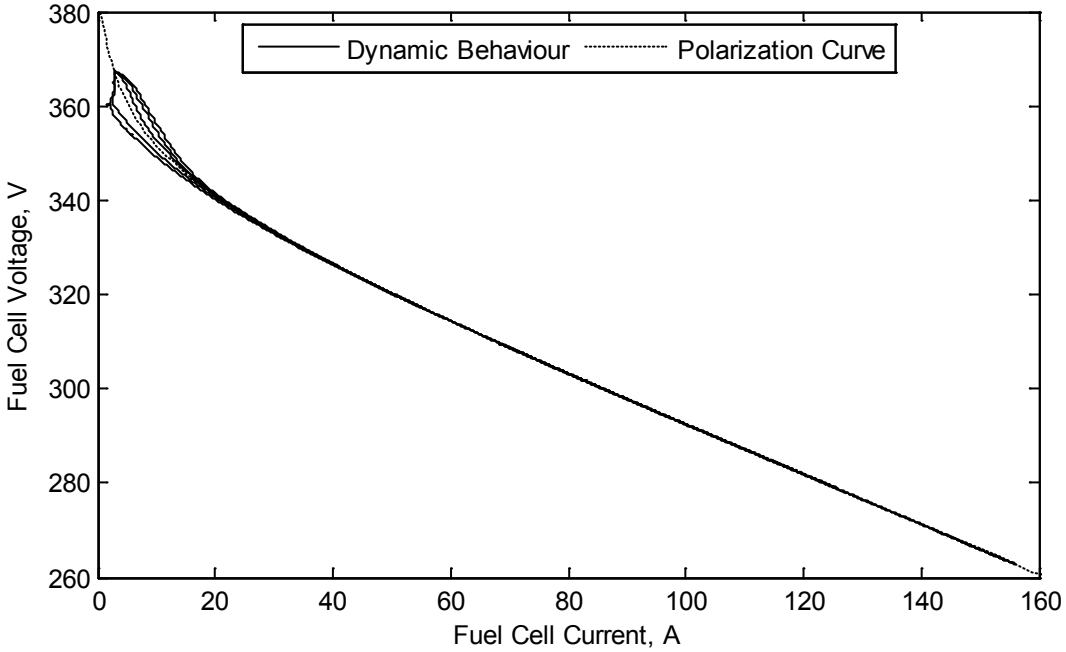

Fig. 5.7. Fuel cell polarization curve and the dynamic behaviour for case study 1.

The polarization curve of the fuel cell showing the steady state operating points (voltage versus current) and the dynamic path of the instantaneous operating points are shown in Fig. 5.7. Most of the fuel cell operation in the ohmic overvoltage region is slowly varying as it can be seen that the dynamic path is almost overlapping the steady state polarization curve. Closer to the activation overvoltage region, settling times increase, due to the large equivalent resistance of the fuel cell connected load. In addition, from Fig. 5.4 it can be seen that the equivalent resistance of the fuel cell load varies considerably faster at higher resistance values than at lower resistance values.

From an automotive driving point of view, the shortage of power has a minimal influence on the driving experience. The maximum shortage in power is nearly 160 W at a power consumption of 17400 W or at another instance 34700 W, which in both

cases is less than 1 %. Excess power, however, need to be dissipated and preferably in an electrical storage device, such as in a battery, to avoid losses.

Power demand for vehicle acceleration from zero velocity (standstill) is well met by the fuel cell system, as it can be seen from Fig. 5.2 at timestamp 163 s, where the shortage of power is less than 75 W.

5.1.2 Case Study 2: Maximum Power Shortage, and Maximum Rate of Change of Power Demand

In this case study between timestamps 260 s and 275 s, the rate of change of power demand reaches its maximum values for the UDDS driving schedule (15.6 kW/s) at timestamp 265 s, as shown in Fig. 5.8. The shortage of output power starts to build up, but 100 ms after the initial increase in power demand, the shortage of power dips shortly before continuing to increase. Since the error in the output voltage reflects as the difference between the power output and the demand, the dip in the shortage of power can be clarified by explaining the behaviour of the output voltage at this instant of time. At the start of the change in power demand rate, the resistance value drops from a relatively large value of 180 Ω at a large rate to 90 Ω in about 90 ms (Fig. 5.9). At this rate, the current through the output inductance of the converter varies slower than the change in the resistance. Hence, the same current that was passing through the larger resistance would now pass through the smaller resistance producing less voltage. The feedback control on the voltage as the resistance suddenly decreases causes some oscillations that appear as a dip in voltage 100 ms after the change. These oscillations disappear after this point and cannot be seen at this scale.

Although the error in voltage is decreasing, the error in power is increasing, because the rate of change of power demand portrayed as load resistance is increasing at a larger influential rate. At the end of one-second length of the maximum rate of demand, the shortage of power reaches its maximum value of 245 W for the whole UDDS schedule.

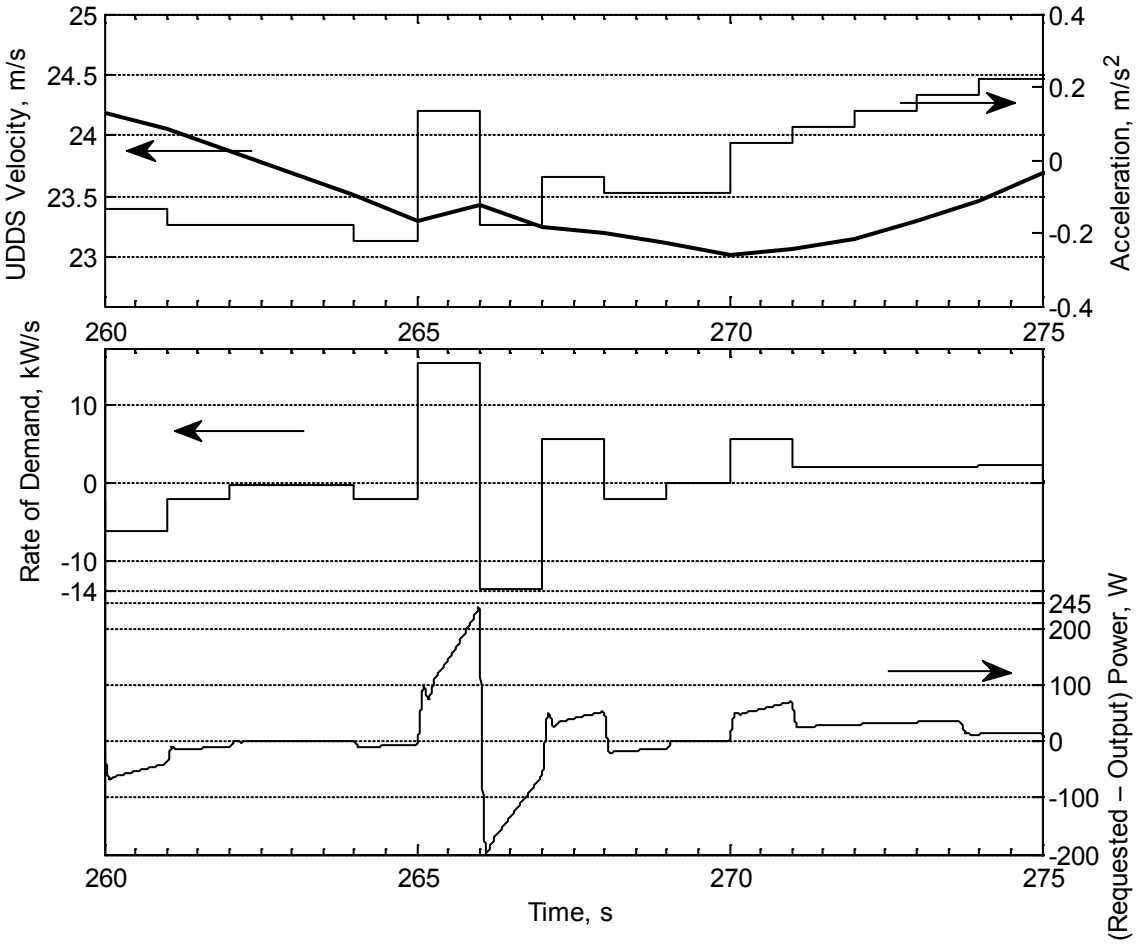

Fig. 5.8. Velocity, acceleration, rate of change of power demand and the difference of output power for case study 2.

After the maximum rate of change of power demand, a comparatively large negative rate in power demand follows. However, it is noted that only the rate of change of power demand and the initial level of output power determine the initial amount of excess power.

The output voltage, Fig. 5.9, drops to its minimum value of 492 V (nearly 2 % of the reference voltage) over the whole UDDS schedule at timestamp 265 s coinciding with the maximum rate of change of power demand. However, as mentioned earlier, this minimum value lasts for a brief amount of time then gains upon the reference point. The short durations of changes in power demand intervals make it difficult to conclude the ultimate result of such an event. It should be noted however, that at a rate of change in power demand of 15.6 kW/s, the power demand level would reach its maximum value

within 2.5 seconds, assuming the initial level of power demand is 1 kW. Such voltage undershoots may influence the performance of the electrical systems of the vehicle if they exceed the specifications limits of such devices. However, as with most electrical equipment, they are designed to withstand a variation of voltage within a certain range.

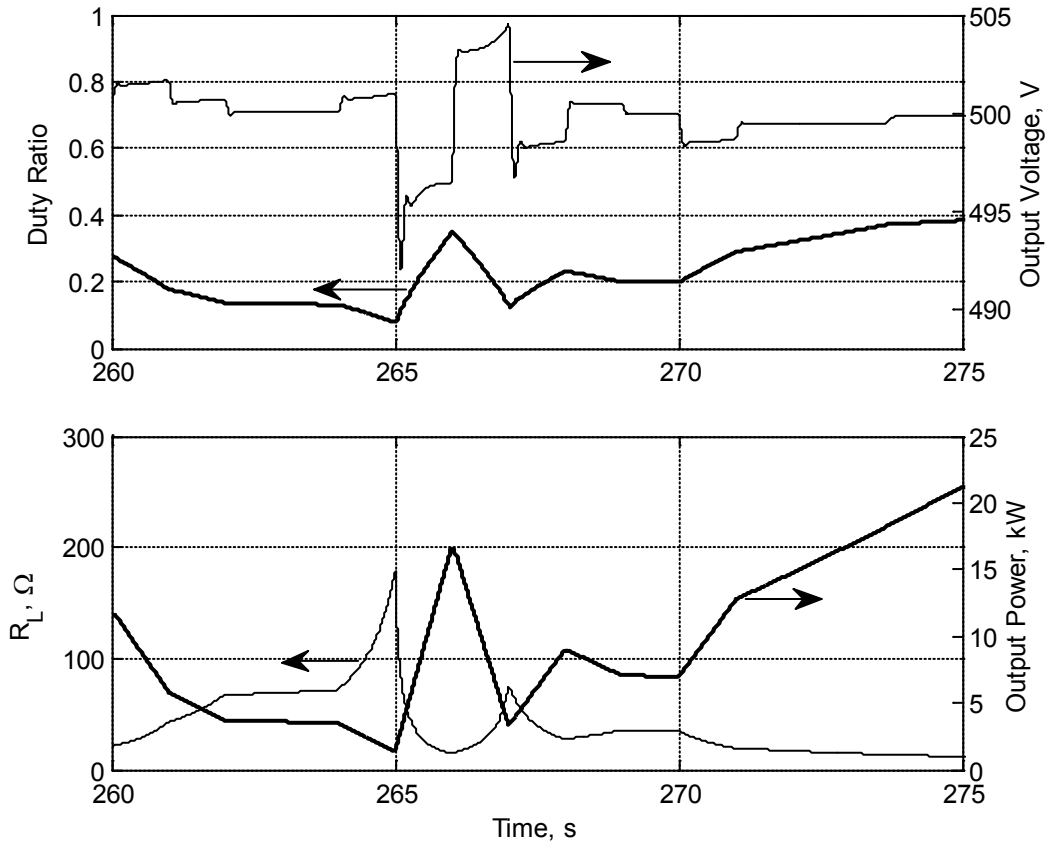

Fig. 5.9. Duty ratio, output voltage and power, and the load for case study 2.

In this case study, Fig. 5.10 shows that the fuel cell operates at low power outputs near the activation region and follows the unsteady nonlinear behaviour, as discussed in case study 1. Nonetheless, the control of power and voltage are within acceptable measures.

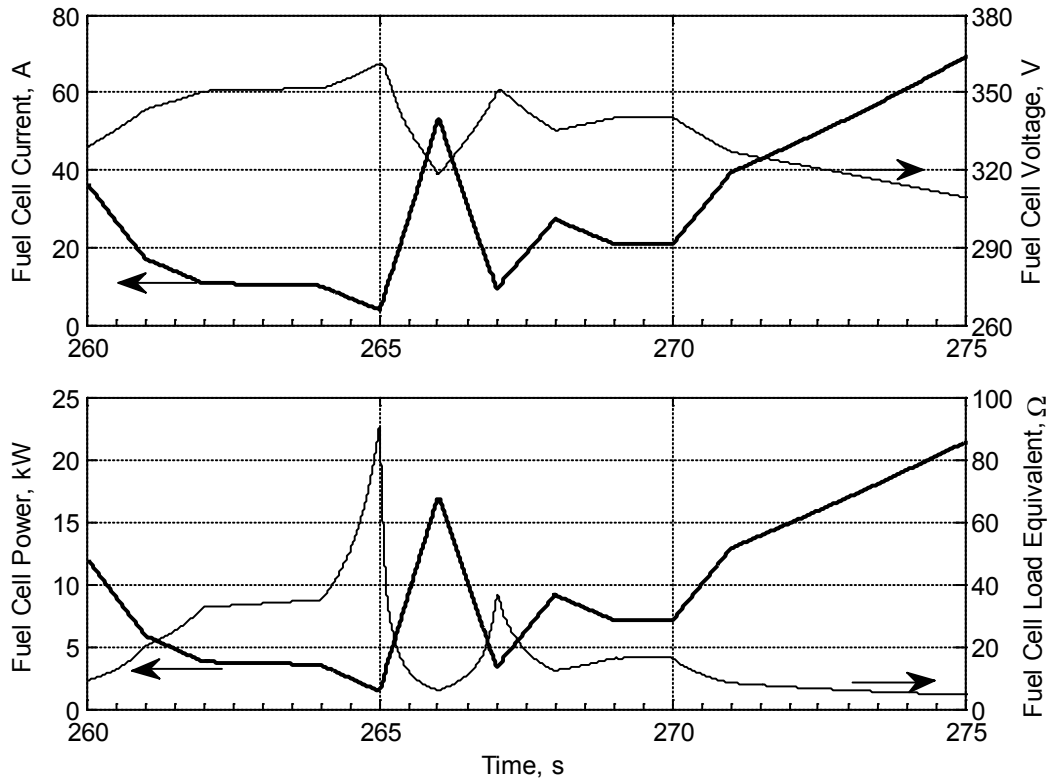

Fig. 5.10. Current, voltage, power & equivalent resistance of the FC for case study 2.

At timestamp 266 s, the pressure of hydrogen (Fig. 5.11) increases when the rate of change of power demand varies from a large positive value to a large negative value. This might seem to contradict with what was concluded in the previous case study at timestamp 171 s, however, the two situations are different. This is explained by studying Fig. 5.10 and Fig. 5.12; at timestamp 266 s, the fuel cell current reaches a sharp peak value. By the time the inlet flow valve catches up with the mass flow rate required by this peak value of current, the consumption rate has already decreased. Thus, due to the 100 ms delay of the inlet valve, excess hydrogen builds-up the pressure until both inlet and outlet valves catch up with the reference variables.

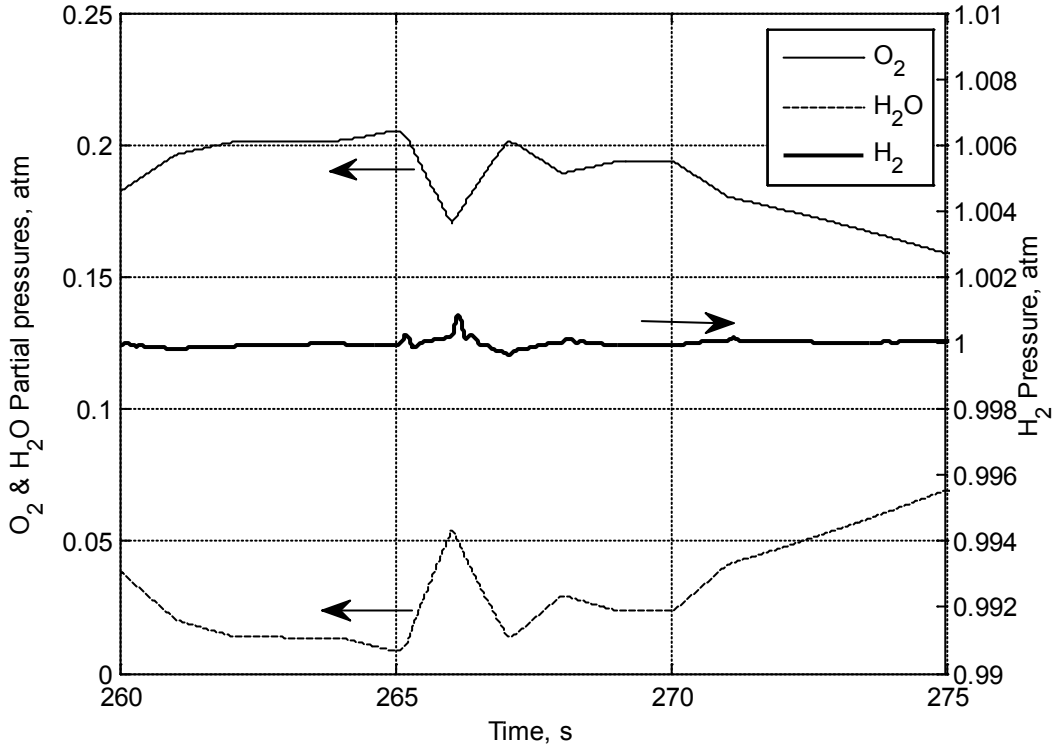

Fig. 5.11. Hydrogen, oxygen, and water partial pressures for case study 2.

Overall, Fig. 5.11 shows that hydrogen pressure is well regulated in this case study. At maximum rate of change of power demand the pressure fluctuates within 0.03 % of the reference point, and after the immediate drop in power demand, the pressure fluctuates within 0.09 % of the reference point.

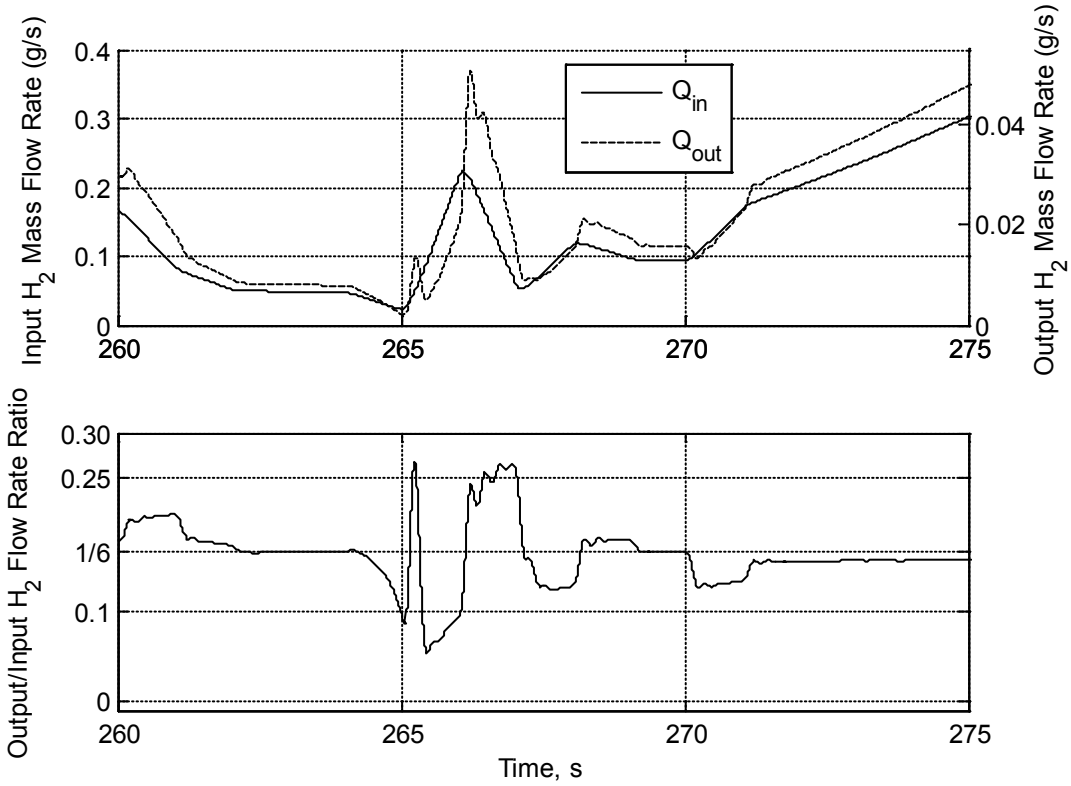

Fig. 5.12. Inlet and outlet mass flow rates of hydrogen and their ratio for case study 2.

5.1.3 Case Study 3: Maximum Acceleration

In this case study, shown in Fig. 5.13 to Fig. 5.17, the power required fluctuates greatly compared to the previous case studies, and a maximum value of acceleration over a relatively long duration between timestamp 447 s and 455 s is investigated. During this case study, the velocity is increasing from zero to 11.8 m/s, or 42.5 km/hr, in 8 seconds.

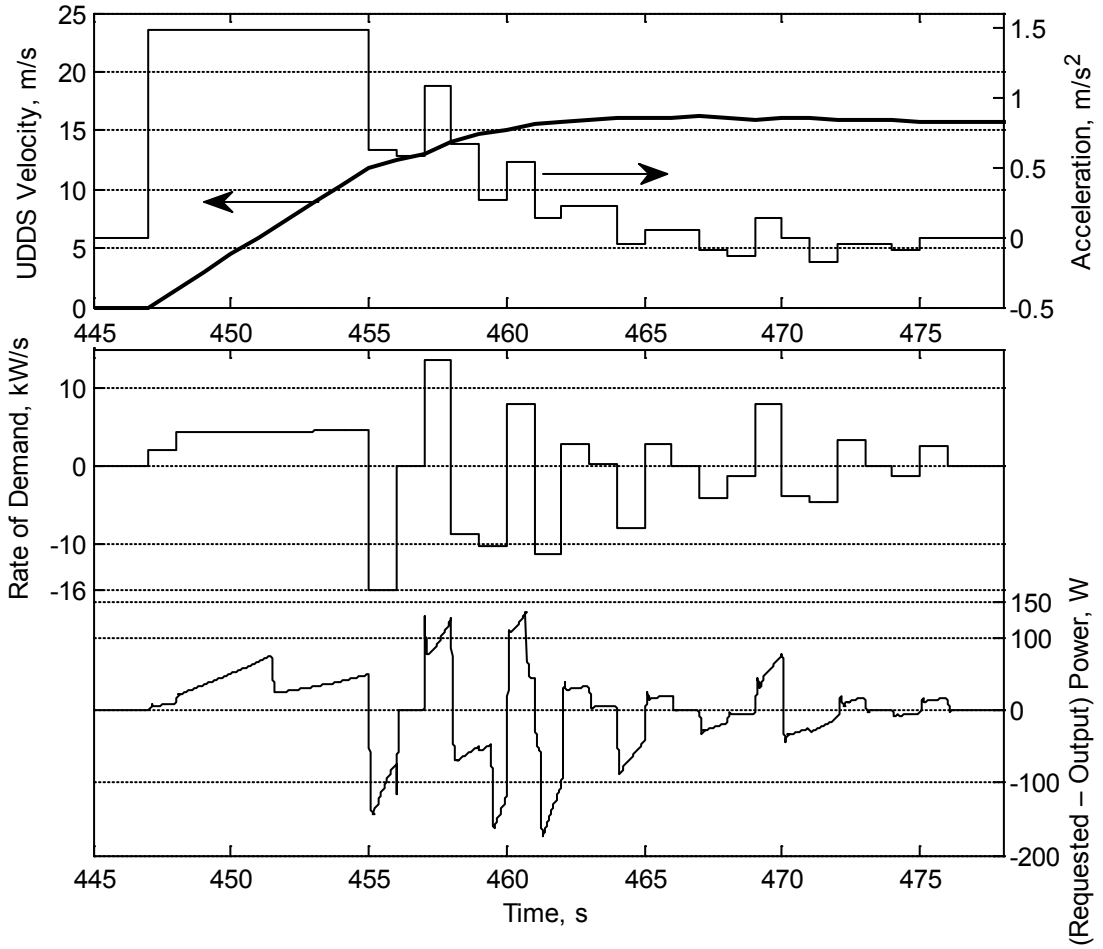

Fig. 5.13. Velocity, acceleration, rate of change of power demand and the difference of output power for case study 3.

At timestamps 451.5 s, 459.5 s, 460.7 s, and 461.2 s, the output voltage (Fig. 5.14) changes, although the rates of change in power demand are not varying. This behaviour is attributed to the discontinuous current mode of operation of the converter, where the amount of power transferred to the load is small, such that the current of inductor L_3 (Fig. 3.25) reaches zero while the switching device is still turned off, as opposed to the inductor current being greater than zero in continuous current mode. This problem has been well documented in electrical and electronics engineering literature, for example references [60, 61], and is known to cause nonlinearities, hence, difficulty in controlling the output voltage [62]. A lot of work focuses on controlling the nonlinearities of converters such as [63]. This work, although very important and interesting, was not considered to be relevant to the present research. In the continuous

current mode described in Chapter 3, the relationship governing the input (V_{fc}) and output (V_L) voltage ratio, and the duty ratio is shown in Eq.5.1. However, in discontinuous current mode, this relationship does not apply. The actual relationship is more complicated, and is not relevant to this study. Only the influence of this mode on the control of the fuel cell system is investigated.

$$D_{calculated} = 1 - \frac{V_{fc}}{V_L} \tag{5.1}$$

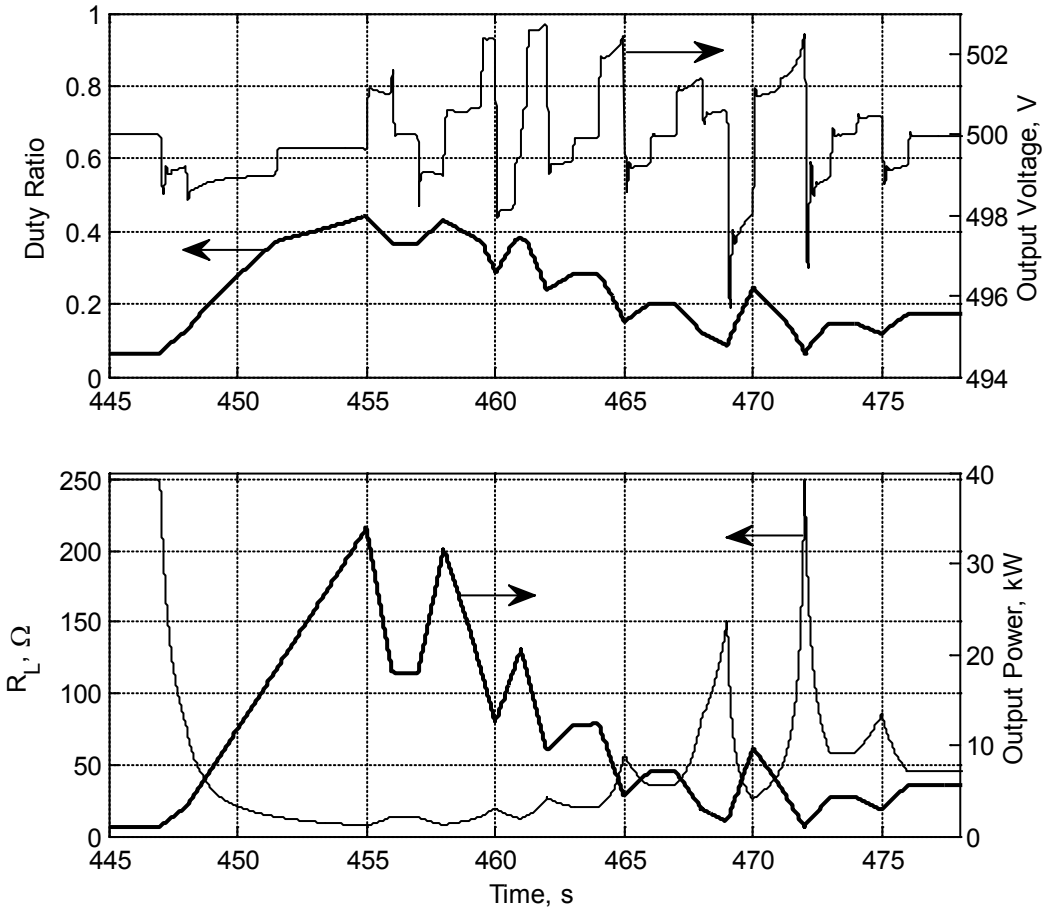

Fig. 5.14. Duty ratio of the converter, output voltage and power, and load resistance for case study 3.

In order to verify the above explanation, a closer look at the calculated duty ratio from Eq.5.1, along with the actual duty ratio of the converter and the output voltage are shown in Fig. 5.15. It can be observed that a transition in the output voltage level occurs when the calculated duty ratio converges or diverges with the actual duty ratio at a value

of 0.37, at timestamps 451.5 s, 459.5 s, 460.7 s, and 461.2 s. The transition in voltage is observed to move closer to the reference voltage when the calculated duty ratio converges with the actual duty ratio line, and deviates from the reference voltage when the duty ratios diverge.

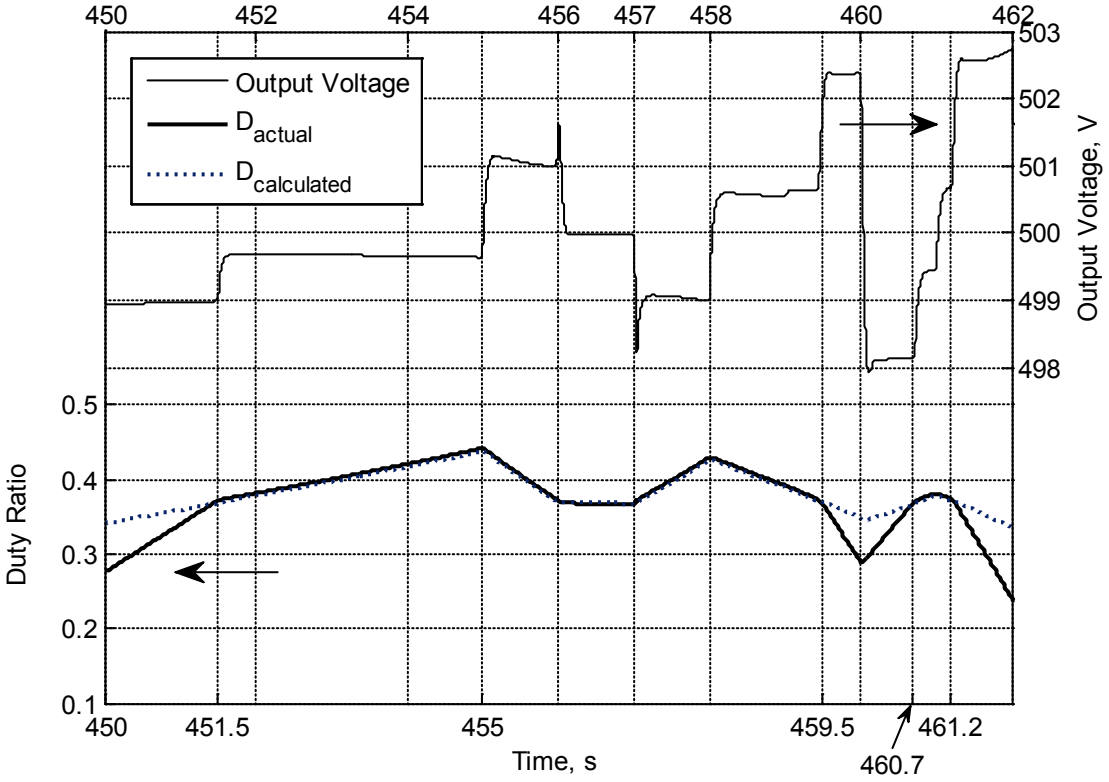

Fig. 5.15. The actual and calculated duty ratio, and the output voltage for case study 3.

The current of inductor L_3 is plotted in Fig. 5.16 showing additional timestamps, 456 s and 457.1 s, where the current drops to zero. However, these additional timestamps do not seem to cause an influence on the output voltage because they coincide with load changes occurring at nearly the same timestamps. In addition, between timestamps 456 s and 457.1 s, the converter is running at the boundary between the continuous and discontinuous current modes, as shown in Fig. 5.15. It should be noted that the reason why the current through L_3 appears as shown is the scale used in the axis; the current is a sawtooth waveform with a frequency of 1 kHz.

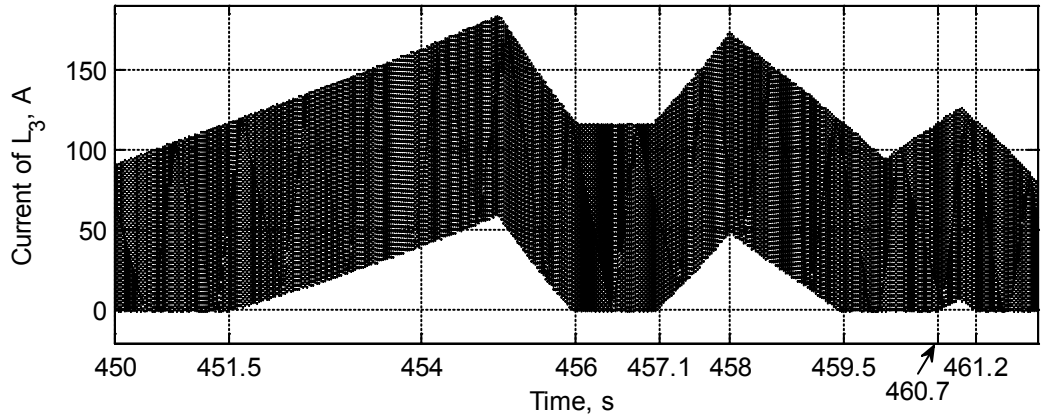

Fig. 5.16. The current of the inductor L_3 in the converter, showing the discontinuous current mode of operation.

The nonlinearity due to the discontinuous current mode of the converter seems to have insignificant influence on the fuel cell voltage and current, as shown in Fig. 5.17. At the timestamps that define the boundary of the discontinuous current mode, it is noted that the fuel cell operating points are nearly equal. This agrees with the description of this mode, that is when the power transferred to the load is smaller than a certain value, which in this case is nearly 18 kW. It should be noted that the value of power at which the discontinuous current mode occurs is large. This can be reduced by using a larger inductor L_3 and/or by increasing the frequency of the switching device in the converter.

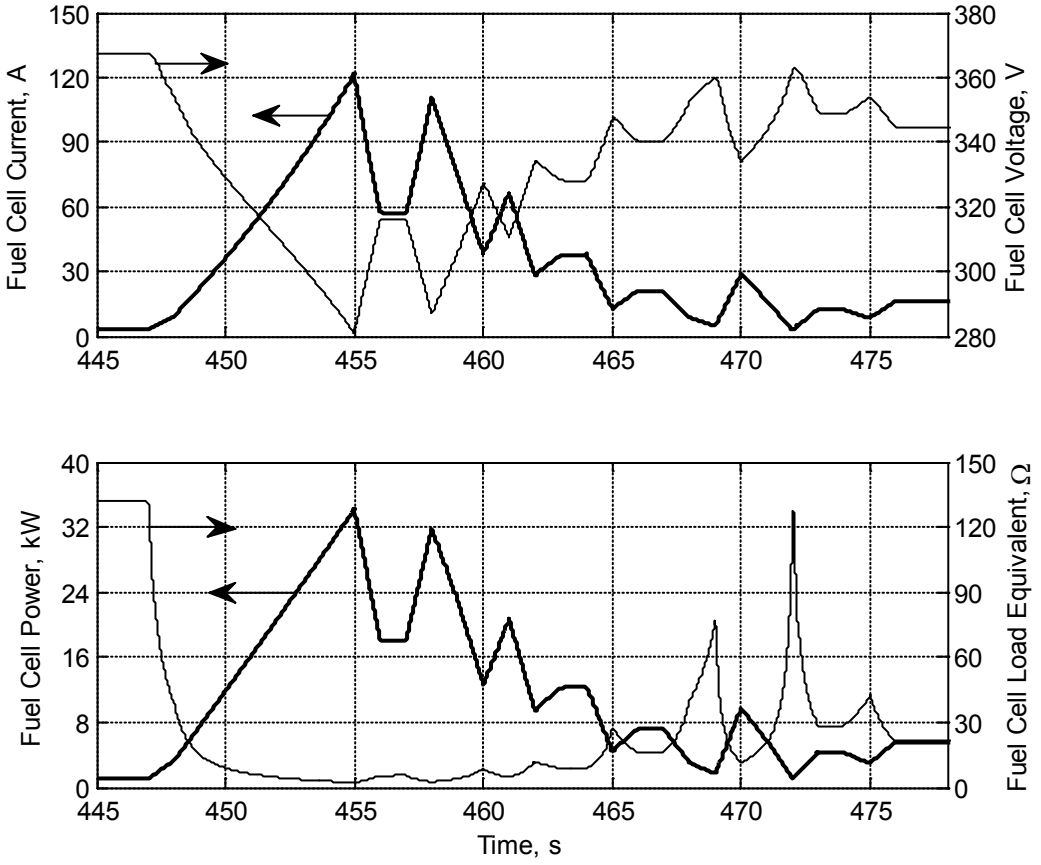

Fig. 5.17. Current, voltage, power & equivalent resistance of the FC for case study 3.

5.2 Highway Fuel Economy Driving Schedule

The Highway Fuel Economy Test driving schedule (HWFET) is used to represent the driving of a light duty vehicle on motorways. The velocity profile, shown in Fig. 5.18, is obtained from the US Environment Protection Agency, EPA. The acceleration, power demand, and rate of change of power demand are calculated as detailed in Chapter 3. The maximum and minimum rates of change of power demand are 12.1 kW/s and -13.7 kW/s, respectively. As expected from a highway driving schedule, the rate of change of power demand is less than that of UDDS driving schedule. Similarly, simulation results show the maximum shortage and excess power are smaller than UDDS with values equal to 201 W and 196 W, respectively.

The fuel cell system is simulated under the power demand requirements of the HWFET driving schedule, as described earlier in the methodology chapter. The main variables of the fuel cell system are recorded for a general analysis of the performance of the full driving schedule, and a few case studies are investigated showing in detail the different events during the driving schedule. Table 5.2 shows a summary of the entire driving schedule.

Table 5.2 : HWFET analysis

Maximum velocity	26.8 m/s (96.4 km/hr)
Maximum acceleration	1.43 m/s^2 (1.85 x 10^4 km/hr^2)
Maximum deceleration	1.48 m/s^2 (1.92 x 10^4 km/hr^2)
Maximum Power demand	33.661 kW
Standard deviation of power difference	28.12 W
Mean of power difference	2.06 W
Maximum power shortage	201.4 W
Maximum excess power	196.2 W
Maximum rate of change of power demand	12.1 kW/s
Minimum rate of change of power demand	–13.7 kW/s

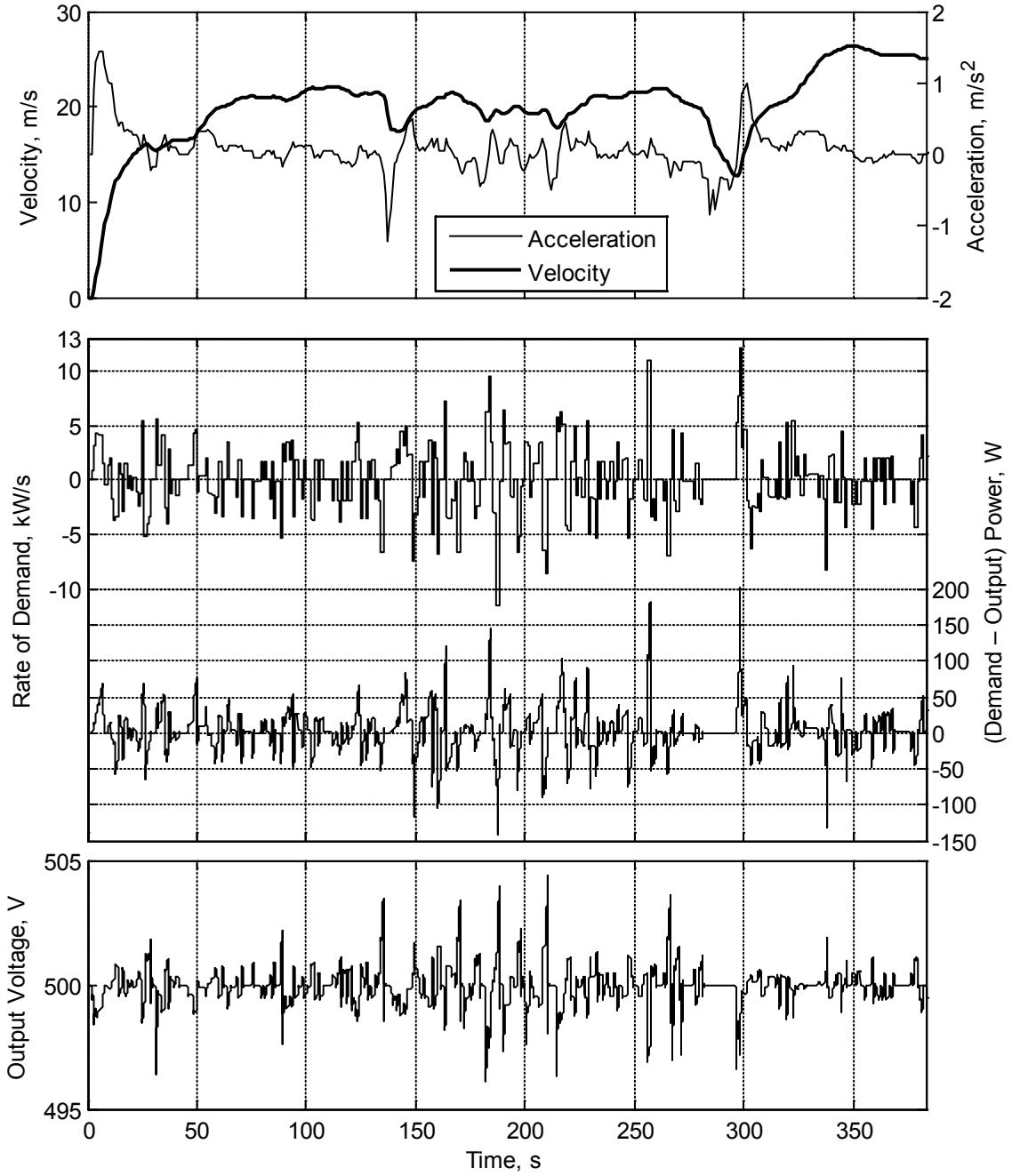

Fig. 5.18.(A) HWFET velocity, acceleration, rate of change of power demand, difference in power and the output voltage for duration From 0 s to 383 s.

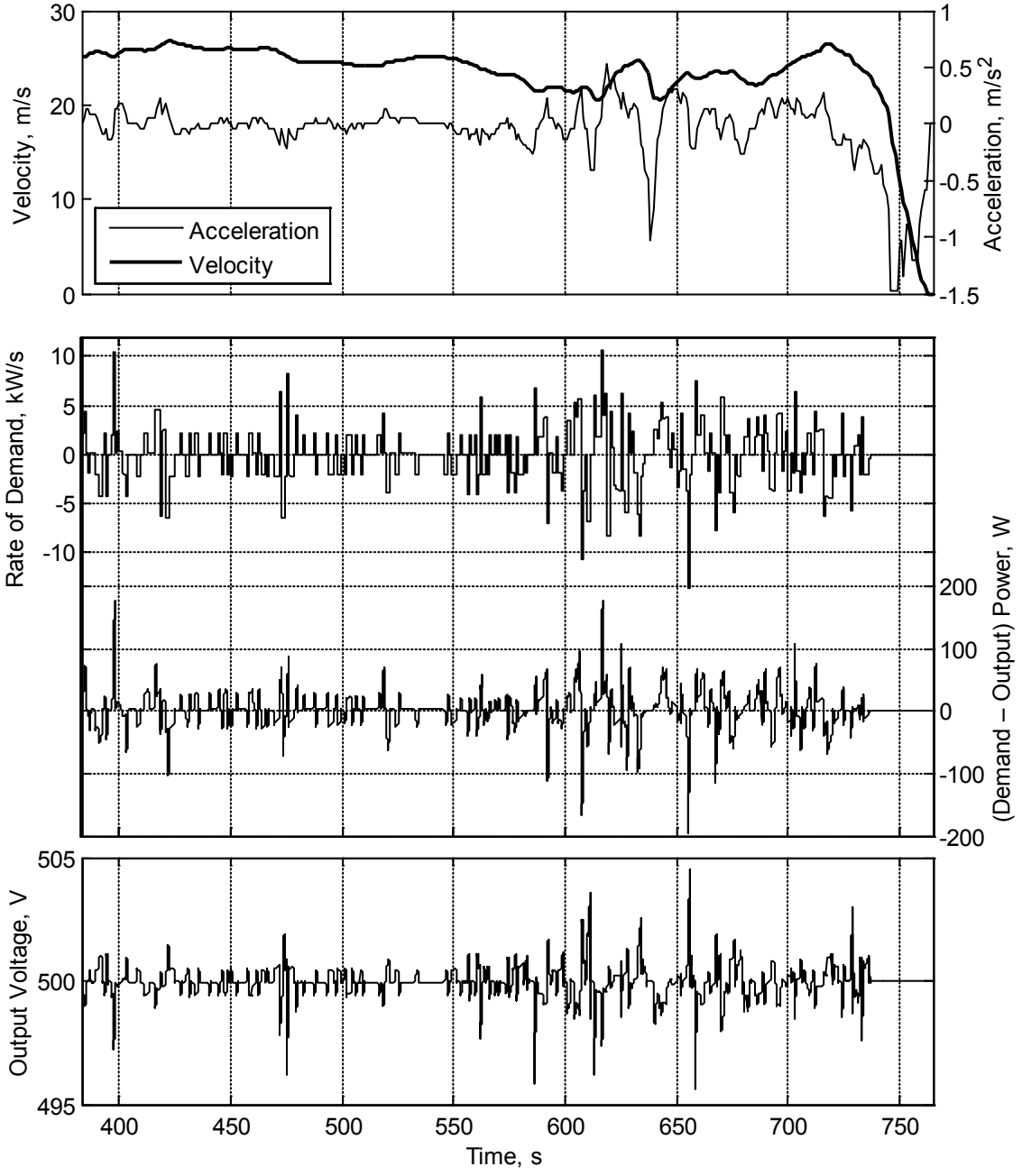

Fig. 5.18.(B) HWFET velocity, acceleration, rate of change of power demand, difference in power and the output voltage for duration 383 s to 765 s.

5.2.1 Case Study 1: Maximum Acceleration

This case study is the beginning of the HWFET driving schedule, where the velocity starts from zero to 6.48 m/s at timestamp 7 s. The maximum acceleration value

is 1.43 m/s^2 between timestamps 4 s and 7 s, as shown in Fig. 5.19. Prior to vehicle movement, the output voltage is maintained at 500 V and the power demand for auxiliary vehicular equipment is 1 kW. As soon as power is drawn to initiate vehicle movement, the power demand increases at a rate of 0.85 kW/s, resulting in a voltage undershoot of nearly 0.6 V, as shown in Fig. 5.20. However, the voltage rapidly gains up to converge to the reference voltage. At the end of the maximum acceleration period, the shortage in power is nearly 69 W, which compared to the equivalent case study in UDDS, is less by 40 W. This is an expected behaviour, since the maximum acceleration value for HWFET is less than that for UDDS, and the velocity and power output attained at the end of the maximum acceleration period is greater in UDDS than that of HWFET.

In terms of power output, it is noticed that the shortage of power (Fig. 5.19) keeps increasing as the rate of change of power demand persists. At timestamp 7 s, the rate of change in power demand drops to 1.5 kW/s, and the shortage in power becomes nearly constant at 27.5 W. This continues until the power output reaches 18 kW at timestamp 7.5 s (Fig. 5.20), where the converter enters the continuous current mode, and the controller is able to reduce the shortage of power to a nearly constant level of 10 W. The fraction of shortage in power to the power demand is negligible (0.4 %) and would have a minor, if any, noticeable effect on the performance of the driving experience.

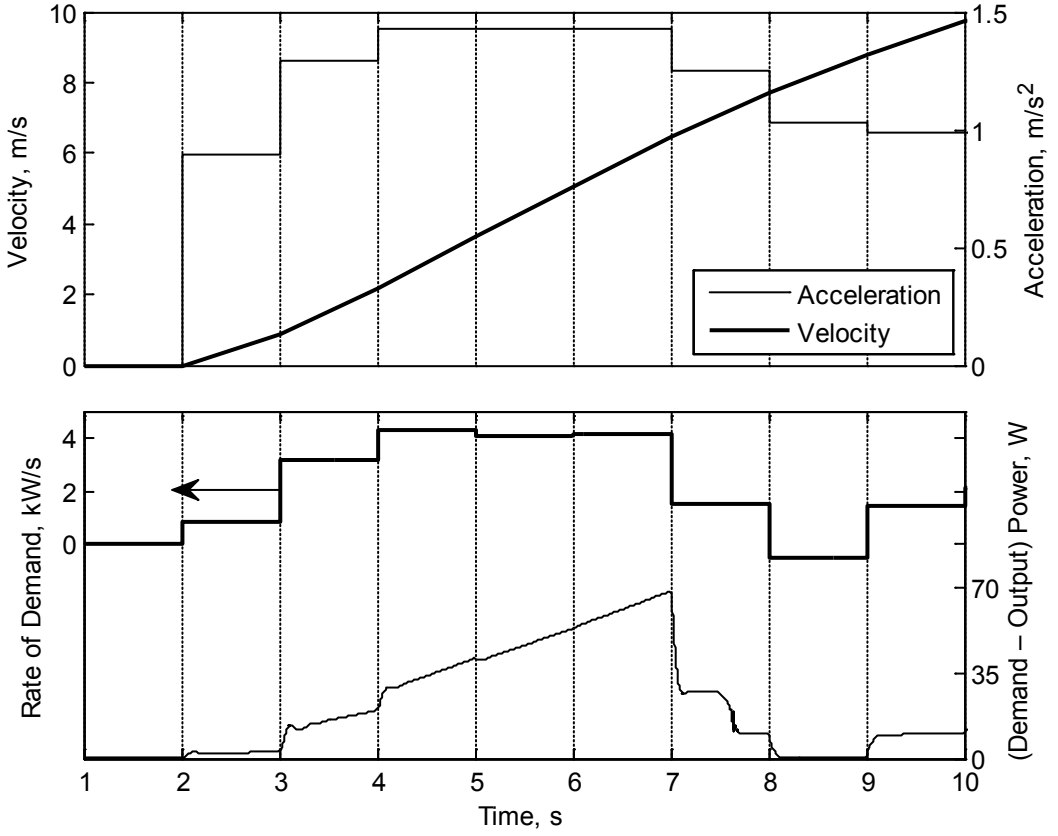

Fig. 5.19. Velocity, acceleration, rate of change of power demand and the difference of output power for case study 1.

At timestamp 8 s, the rate of change of power demand drops to (–0.5 kW/s) reducing the output power to 18.5 kW, and resulting in an output voltage nearly matching the reference voltage. The voltage variations in this case study are within acceptable tolerances of less than 0.4 %.

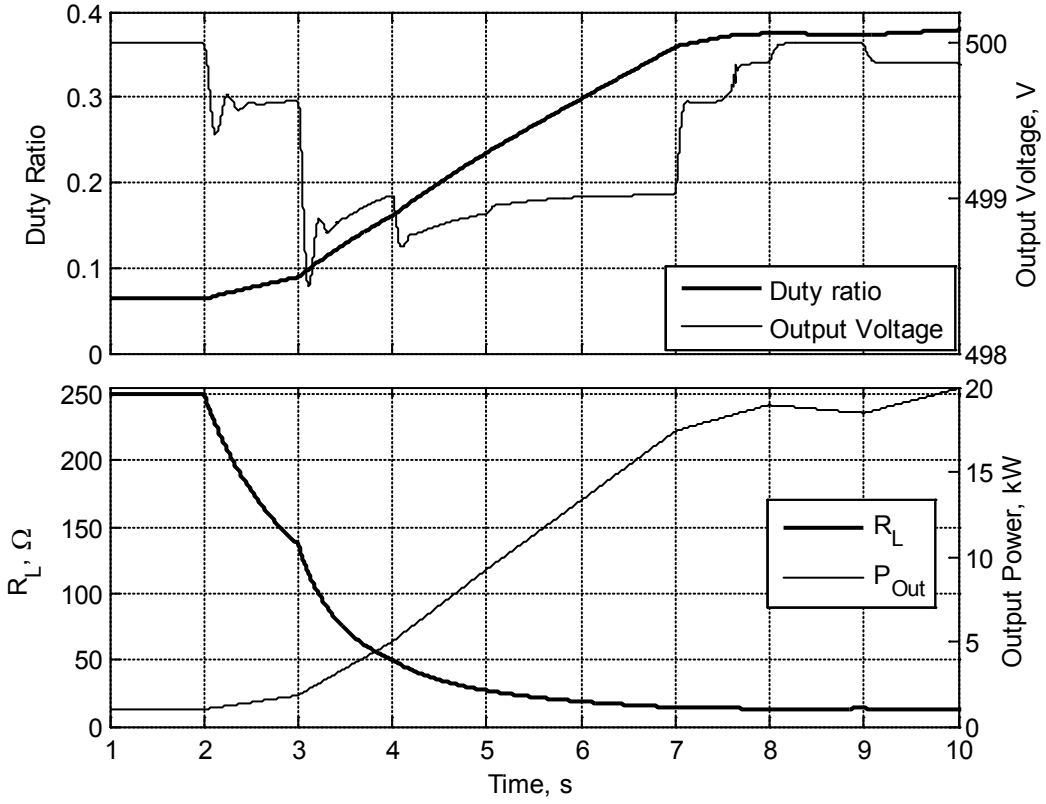

Fig. 5.20. Duty ratio of the converter, output voltage & power, and load resistance for case study 1.

It is noticed that when the converter is in the discontinuous current mode of operation, the regulation of the output voltage is inferiorly governed by the controller compared to the continuous current mode. Nonetheless, the controller is maintaining an acceptable error in voltage within 1.5 V.

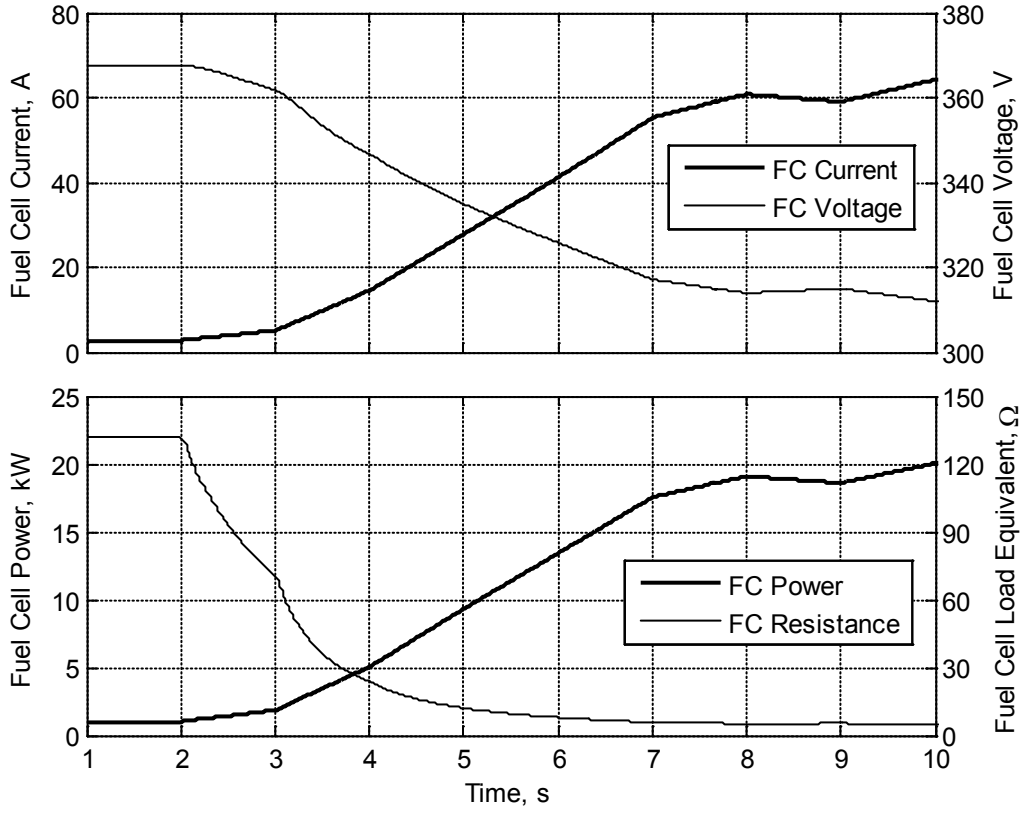

Fig. 5.21. Current, voltage, power & equivalent resistance of the FC for case study 1.

After the start-up maximum acceleration period, there are almost no high accelerations for the remainder of the HWFET driving schedule, and this is expected on a smoothly running traffic on motorways. However, a decrease in velocity at timestamp 270 s followed by an increase in velocity at timestamp 296 s, demands a relatively high acceleration of 1 m/s^2, but in this situation, a maximum rate of change of power is required over the entire driving cycle. This is discussed in the following case study.

5.2.2 Case Study 2: Maximum rate of demand, and maximum shortage in power

In this case study, maximum rate of change of power demand (12.1 kW/s) and maximum shortage of output power (201.4 W) are investigated. Not surprisingly, these two events occur at the same instance at timestamp 298.4 s, as shown in Fig. 5.22. Three step changes in the rate of change of power demand occur prior to reaching the maximum rate of 12.1 kW/s. Although the maximum undershoot in output voltage is at

the first step occurring at timestamp 296 s (Fig. 5.23) this is not reflected on the shortage in output power, because in addition to the output voltage, the output power is a function of the load resistance. At low power loads with high resistance values, variations in the output power are less sensitive to variations in the output voltage but more sensitive to variations in the load resistance, and vice versa at low resistance values, such as at timestamp 298 s.

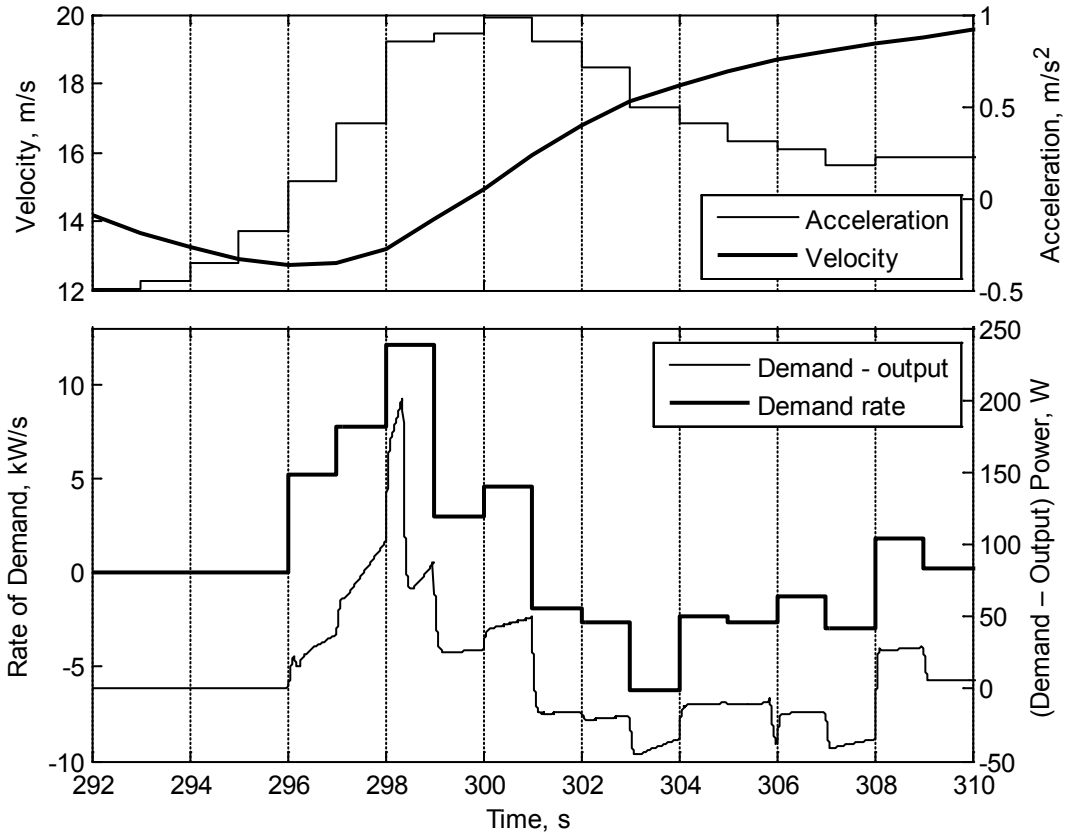

Fig. 5.22. Velocity, acceleration, rate of change of power demand and the difference of output power for case study 2.

At timestamp 298 s, the rate of change of power demand reaches its maximum value of 12.1 kW/s, causing the maximum shortage in power output. However, at timestamp 298.4 s, the actual output power crosses the 18 kW boundary of the discontinuous current mode of the converter. This results in a drop in the shortage of power and a drop in the output voltage error. An increase in excess power is noticed at

timestamp 305.85 s when the output power drops below 18 kW. The voltage variations in this case study are also within acceptable tolerances of less than 0.6 %.

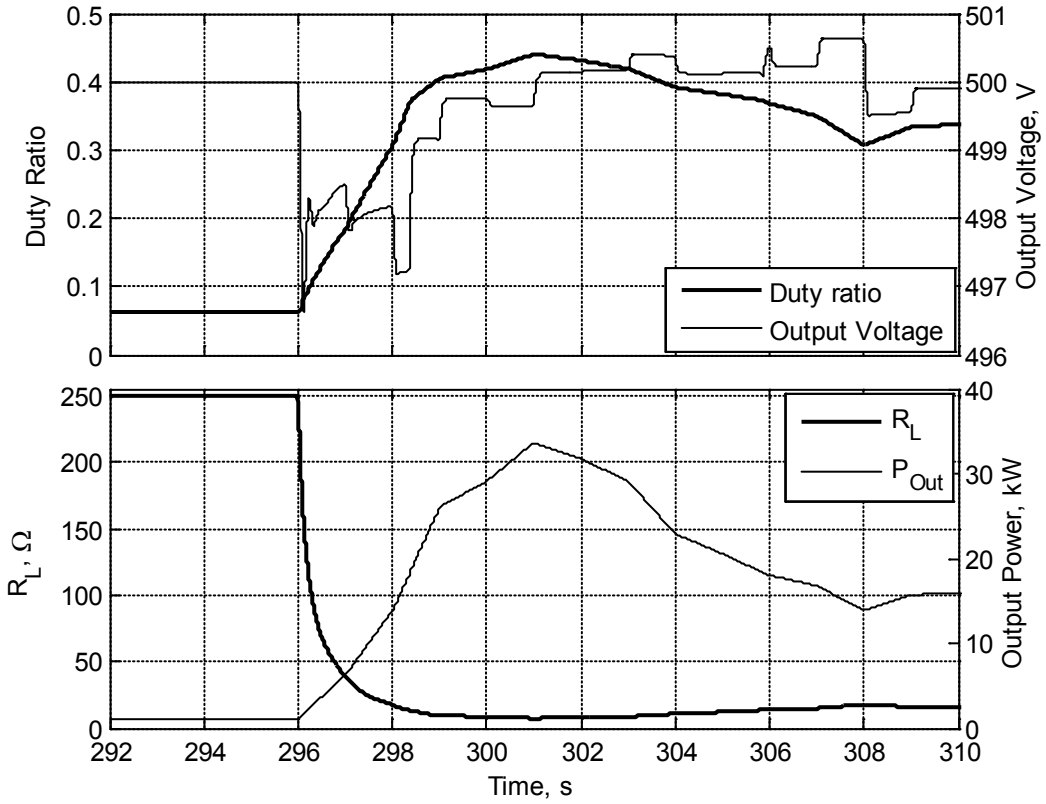

Fig. 5.23. Duty ratio of the converter, output voltage & power, and load resistance for case study 2.

5.2.3 Case Study 3: Minimum rate of demand, maximum excess power, and maximum and minimum voltage drop

In the HWFET driving schedule, the minimum rate of change in power demand (–13.7 kW/s) occurs at timestamp 655 s (Fig. 5.24) when the acceleration drops from 0.13 m/s^2 to –0.18 m/s^2. Although the deceleration drops to lower values than that, as at timestamp 637 s, the rate of change of power demand is not changing, because during deceleration, when the driver disengages the accelerator pedal and whether or not the brakes are used, once the output power drops to the minimum value (1 kW), no further drop may occur. At timestamp 655 s, the converter is operating in the discontinuous current mode, where output voltage regulation is inferior. Hence, all these combined

factors cause a maximum excess in power, and a large voltage overshoot (Fig. 5.25). The output voltage continues to increase as the power demand drops, until the rate of change in power demand increases at timestamp 656 s. At this timestamp, the rate of change of power demand increases to –2 kW/s, where the system has enough time to settle down to dissipate the energy at a rate that results in a smaller error in voltage, and less excess power.

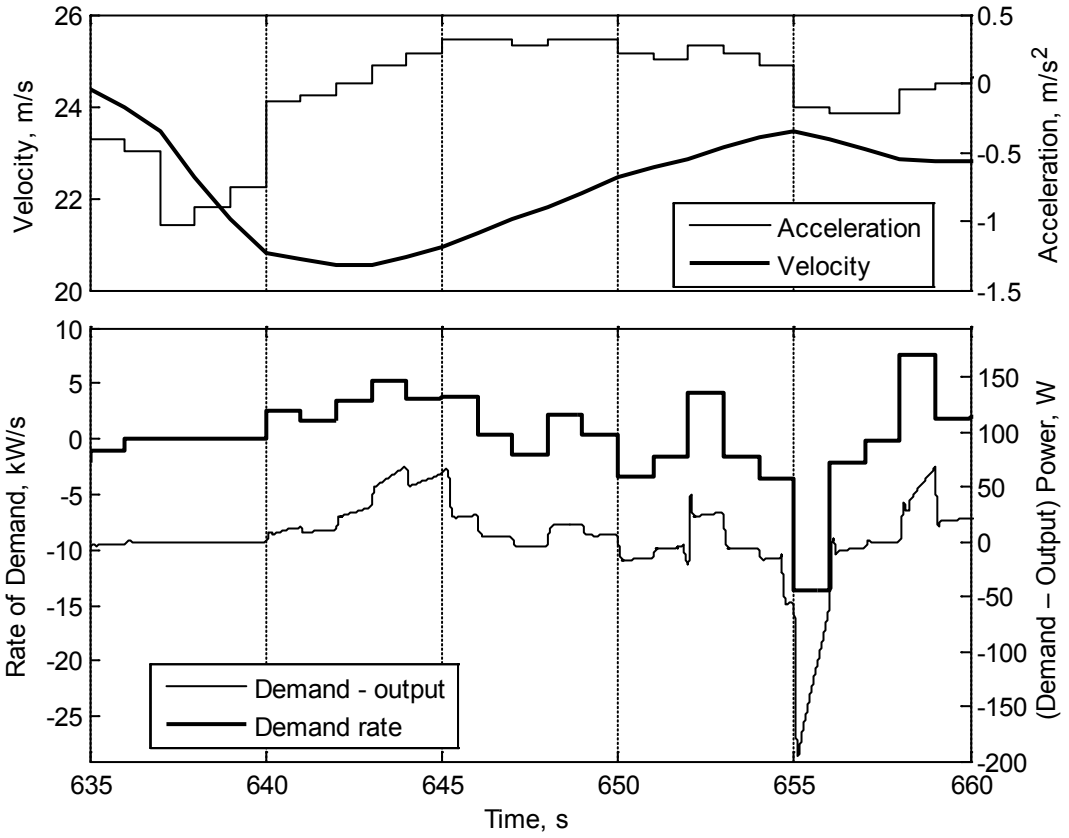

Fig. 5.24. Velocity, acceleration, rate of change of power demand and the difference of output power for case study 3.

The maximum output voltage undershoot (495.6 V) is observed at timestamp 658 s, where the vehicle stops decelerating and requires a constant velocity of 23 m/s. the voltage overshoot is due to an increase in the rate of change in power demand from −0.1 kW/s to 7.5 kW/s. The shortage of power is about 30 W, and increases to 68 W then drops to 20 W at timestamp 659 s, as the rate of change in power demand drops to

2 kW/s. The voltage variations in this case study are within acceptable tolerances of less than 1 %.

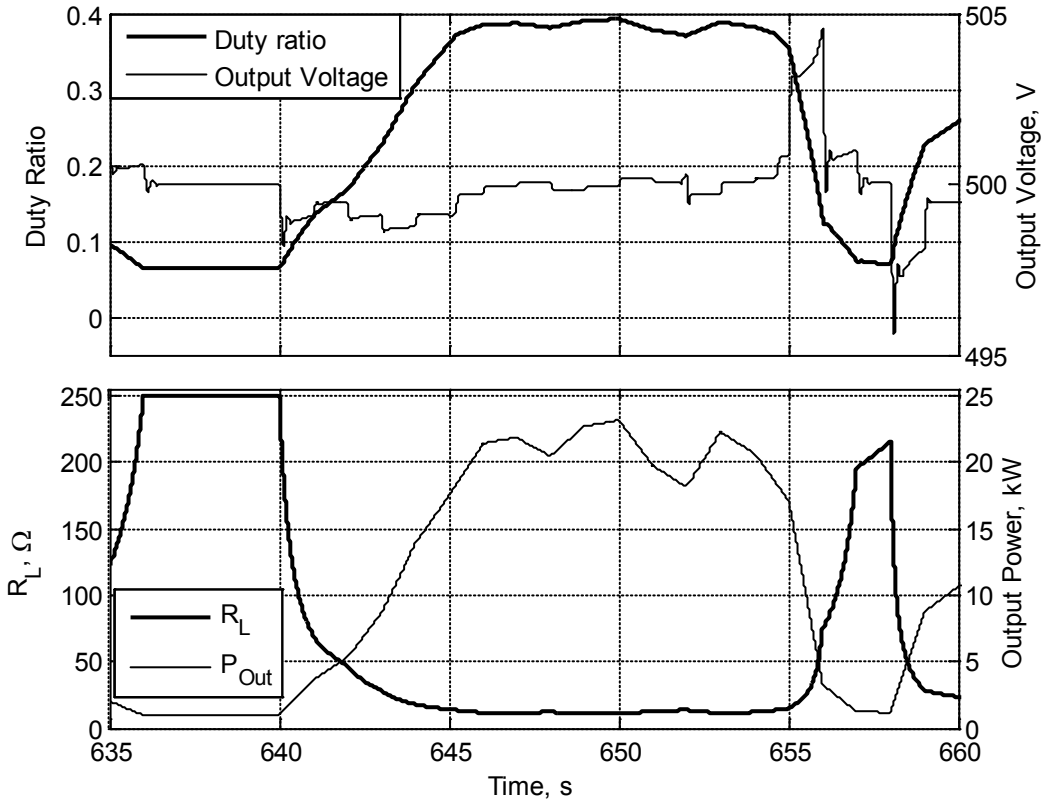

Fig. 5.25. Duty ratio of the converter, output voltage & power, and load resistance for case study 3.

With the HWFET being less aggressive than UDDS in terms of driving fluctuations, better performance of power devliery is noticed in the HWFET and less voltage fluctuations are observed.

5.3 Hydrogen Flow Analysis

The aim of the Hydrogen flow control is to supply 20 % excess hydrogen to improve the dynamic behaviour of the fuel cell voltage during transients. The problem with finding out the value for the 20 % excess hydrogen lies with the inability to measure the actual consumption rate of hydrogen, because the reaction current is not

measurable, and only the external current is accessible. The relationship between the external and reaction currents is presented here again in the following equation:

$$i_r = i + i_c \tag{5.2}$$

Equation 5.2 states that the reaction current (i_r) equals summation of the external current (i) and the cross over current (i_c). However, this relationship is only valid under steady state operation, and the actual value of the reaction current during transients depends on other aspects as detailed in Chapter 3. Real-time calculations of the dynamic reaction current using a built-in processor subroutine attached with the mass flow controller may be possible. However, this is a very expensive option, in terms of processing time and processing power. In addition, the calculations are going to suffer anyway from some inaccuracies. Hence, in this study, the excess amount of hydrogen is calculated based on the external current, as it is the closest approximation, but not the actual one. The effect of using the external current instead of the reaction current, which is rarely seen in the literature, is discussed in this section.

5.3.1 UDDS

Over the whole UDDS driving schedule, the amount of consumed hydrogen was 87.5 grams, and the supplied hydrogen was 105 grams, while the outlet hydrogen was 17.5 grams. It is worth pointing out that the amount of hydrogen consumption rate is calculated using the reaction current, which for simulation and analysis purposes is available, like any other variable in the model, but in real life applications, it is not measurable. The instantaneous ratio of the supplied to the consumed hydrogen ranges between 96 % and 157 % (Fig. 5.26), while the total excess ratio over the entire period is found to be equal to 20 %. However, during the whole cycle, hydrogen pressure was regulated between a minimum value of 0.9986 atm and a maximum of 1.001 atm, which is nearly 0.1 % of the reference point, as shown in Fig. 5.27. Hence, using the external current to calculate the amount of hydrogen supply gives an excellent average value for the excess ratio.

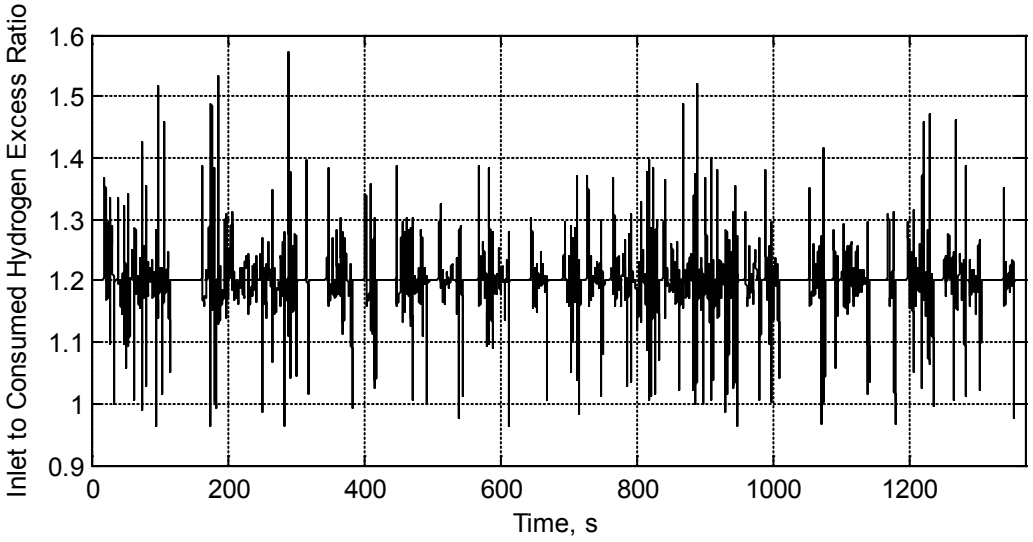

Fig. 5.26. Instantaneous Hydrogen inlet to consumed excess ratio over UDDS.

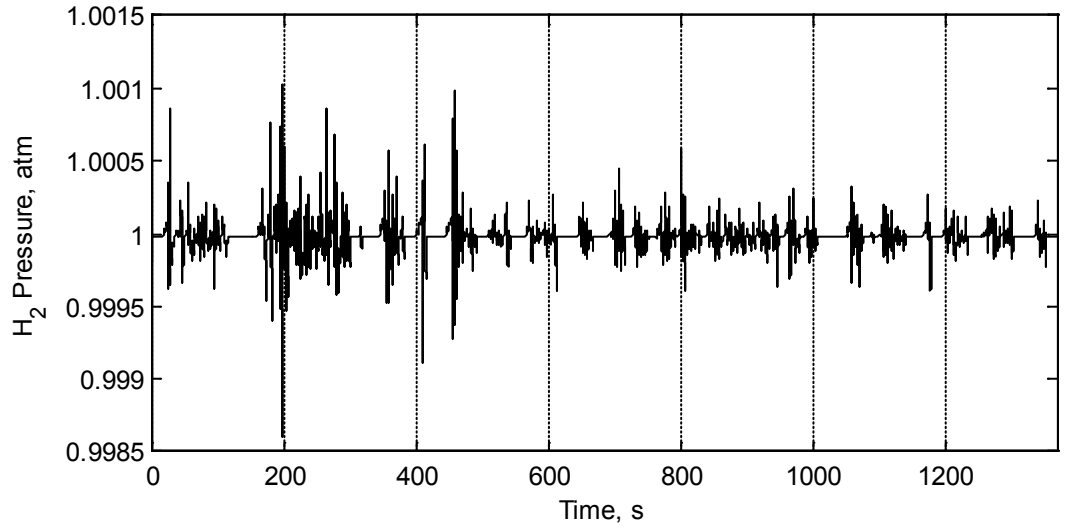

Fig. 5.27. Hydrogen pressure during UDDS driving schedule.

5.3.2 HWFET

Over the entire HWFET driving schedule, the amount of consumed hydrogen was 99.4 grams, and the supplied hydrogen was 119.3 grams, while the outlet hydrogen was 19.9 grams. The instantaneous ratio of hydrogen supply rate to hydrogen consumption rate ranges between 85.3 % and 226.6 % (Fig. 5.28). Over the entire

period, the amount of excess hydrogen supplied is equal to 20 % of the total amount of hydrogen consumed by the fuel cell reaction. During the whole cycle, hydrogen's pressure was regulated between a minimum value of 0.9995 atm and a maximum of 1.0006 atm, which is nearly 0.05 % of the reference point, as shown in Fig. 5.29.

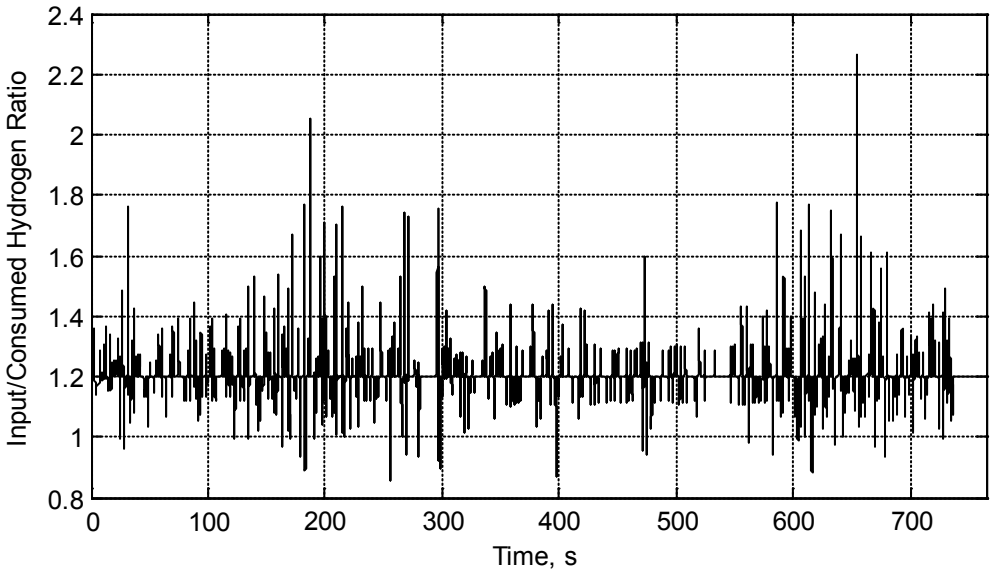

Fig. 5.28. Inlet to consumed Hydrogen flow rate ratio during HWFET.

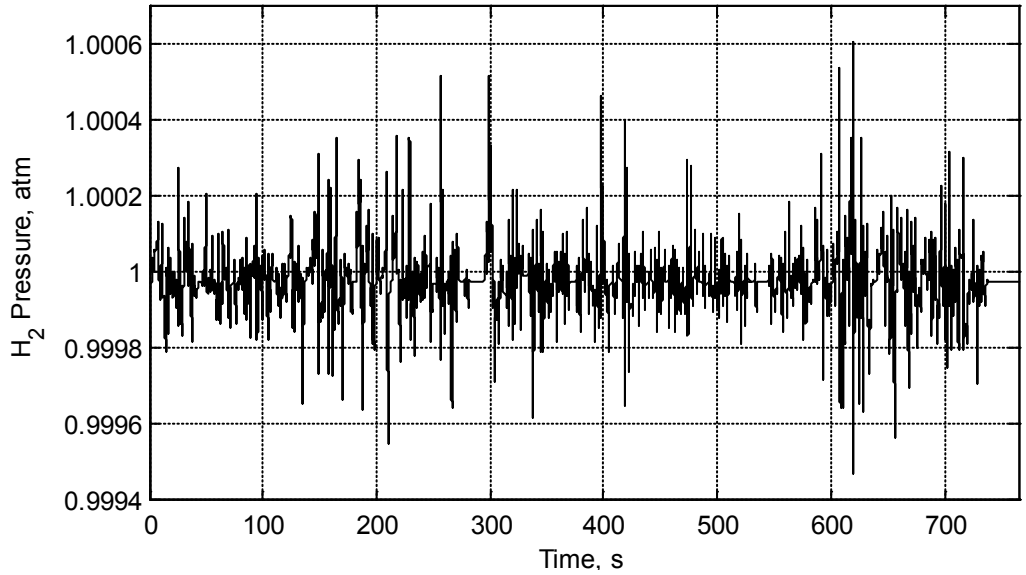

Fig. 5.29. Hydrogen pressure during HWFET driving schedule.

5.4 Energy Analysis

5.4.1 UDDS

For the entire UDDS driving schedule, the total amount of excess energy is 8.90 kJ, and the total energy shortage is 10.29 kJ. The net in energy excess and shortage is calculated by performing a cumulative integration on the difference of power, and is found to be equal to –1.39 kJ at the end of the driving schedule, with a minimum value for the net of energy difference reaching –1.49 kJ. The net energy shortage not met by the fuel cell is not considerable taking into account that the total energy demand during the entire cycle is 7.486 MJ. However, an energy buffer could be used along side the fuel cell system to meet these shortages of power at an appropriate discharge rate, and to utilise the excess energy. The minimum value of the cumulative net energy is one factor needed for determining the capacity of the energy buffer. From the above calculations, the energy storage device should have a capacity of 1.49 kJ.

5.4.2 HWFET

Over the HWFET driving schedule, the total amount of excess energy is 6.13 kJ, and the total energy shortage is 7.71 kJ. The net in energy excess and shortage is calculated by performing a cumulative integration on the difference of power, and is

found to be equal to –1.58 kJ at the end of the driving schedule, with a minimum value for the net of energy difference reaching –1.78 kJ. The net energy shortage not met by the fuel cell is not considerable taking into account that the total energy consumed during the whole cycle is 8.542 MJ. However, an energy storage device could be used along side the fuel cell system to meet these shortages of power at an appropriate discharge rate, and to utilize the excess energy.

5.5 Summary

The fuel cell system was investigated under two driving schedules that proved to perform well without the use of an energy storage device. Voltage variations in the UDDS driving schedule were within ±8 V, or 1.6 % of the reference voltage (500 V), which is well within voltage tolerances of electrical machines. The mean and standard deviation of the error in voltage were 499.98 V and 0.773, respectively. However, an energy storage device would improve the efficiency of an electric vehicle that stores braking energy and utilises it during increases in power demand. This would further reduce the variation in output voltage and shortages in power demand.

Uzunoglu and Alam [21] carried out a similar study tested on UDDS power profile using energy storage devices, but neglected the dynamic behaviour of the fuel cell voltage. They obtained results for the output voltage variations that varied between –5 mV and 20 mV around a reference voltage of 188 V.

Although the results are based on numerical models and simulations, the overall approach in the proposed control strategy is expected to be valid for an actual fuel cell vehicle.

Chapter 6

DOMESTIC APPLICATION

6.1 Introduction

The use of fuel cells in domestic applications is an important aim for being independent of fossil fuels. Therefore, it is necessary to investigate the use of fuel cell systems for domestic load within the scope of this thesis. Most domestic appliances and electrical devices are designed to operate on AC voltage that varies from one country to another. For example, the mains electricity supply voltage in the USA is 110 V at 60 Hz while in the UK it is 230 V at 50 Hz. Newer devices that operate on DC power, e.g. computers and mobile phones, have adapters that convert the AC power over an input voltage ranging between 100 V to 240 V at 50 Hz or 60 Hz.

There are many options available in the literature to convert the DC power directly into AC power, or to convert the DC power to another DC power but with voltage regulation. In addition, some applications may require isolating the electrical circuit of the fuel cell from the load to protect against propagating electrical faults from one circuit to another. This is commonly accomplished using transformers in power converters, where energy is transferred from one side to another through the magnetic field, and the voltage may be further stepped up by increasing the turns ratio of the transformer.

In this thesis, the domestic load is considered as the load power profile at a constant DC voltage of 500 V, similar to the work done on the automotive application. The reference voltage of 500 V is chosen for convenience, to reduce resistive losses in the fuel cell power system. In addition, 500 V is within recommended voltage range for converting DC power to AC, as discussed in Chapter 3.

The fuel cell power system was originally designed to output 50 kW, however, typical household power profiles are less than 10 kW. The power profile adopted in this

thesis has a maximum power demand of 7.2 kW. Therefore, the fuel cell maximum power output is reduced to 8 kW. In a practical situation, the number of cells and the area are considered for changing the rated output power of the fuel cell. However, in order to be able to use the same PI controller parameters of the DC/DC converter, with minimum changes on the fuel cell system, only the fuel cell area is reduced to change the maximum output power. Changing the number of fuel cells, changes the range of the input voltage to the DC-to-DC converter, thus affecting the PI parameters of the controller, and makes it more difficult to compare the results of the domestic application with the automotive application. As mentioned earlier in the methodology chapter, the fuel cell area is reduced from 225 cm^2 to 36 cm^2 to change the fuel cell power rating from 50 kW to 8 kW.

6.2 Typical Household Case Study

Typical household power demand profiles are widely available in the literature, however, detailed power profiles have not been found. The maximum resolution found in the literature was on a 1-minute scale, and this is only the scale at which the work was done. However, the results were given at the 100-minute scale, as shown in Fig. 6.1. The domestic power demand profile includes electrical and heating usage in a typical household.

Manual graph digitization was carried out and some adjustments on the resultant data were performed to take into account the acceptable output voltage tolerances, as shown in Fig. 6.2. In the methodology chapter, it was found that a maximum load transient less than 35 kW/s results in an output voltage within acceptable tolerances. In a practical system, a current rate-limiting device could be used to limit the maximum rate of power demand. However, the power profile data were adjusted to incorporate the maximum limitation in power demand rate.

Due to the large amount of time needed to simulate the entire domestic power demand profile, as indicated in Chapter 3, the main portions of interest were simulated as shown in Fig. 6.3 (A) and (B). The first portion of simulated data shown in Fig. 6.3.(A) is between timestamp 07:00 and 10:00. While the second portion of

simulation shown in Fig. 6.3.(B) runs in intervals between timestamps 14:26 and 19:00, with dotted lines representing un-simulated intervals. In Fig. 6.3 (A) and (B), the load power demand is shown as well as the rate of change of power demand and the difference between the power demand and the actual output power. The rates of change of power demand are within ±35 kW/s and both the rates of change of power demand and the difference in demand and output power appear as single lines due to the large time scale. Therefore, a few case studies of the simulation are investigated at higher resolution over short intervals, to show the performance and behaviour of the fuel cell power system under domestic power profile. These case studies are indicated in Fig. 6.3 as 2 kW, P_{min}, V_{min}, V_{max}, and P_{small} showing extreme conditions of the load and its influence on the main variables in the system. A description of each case study is presented in relevant sections.

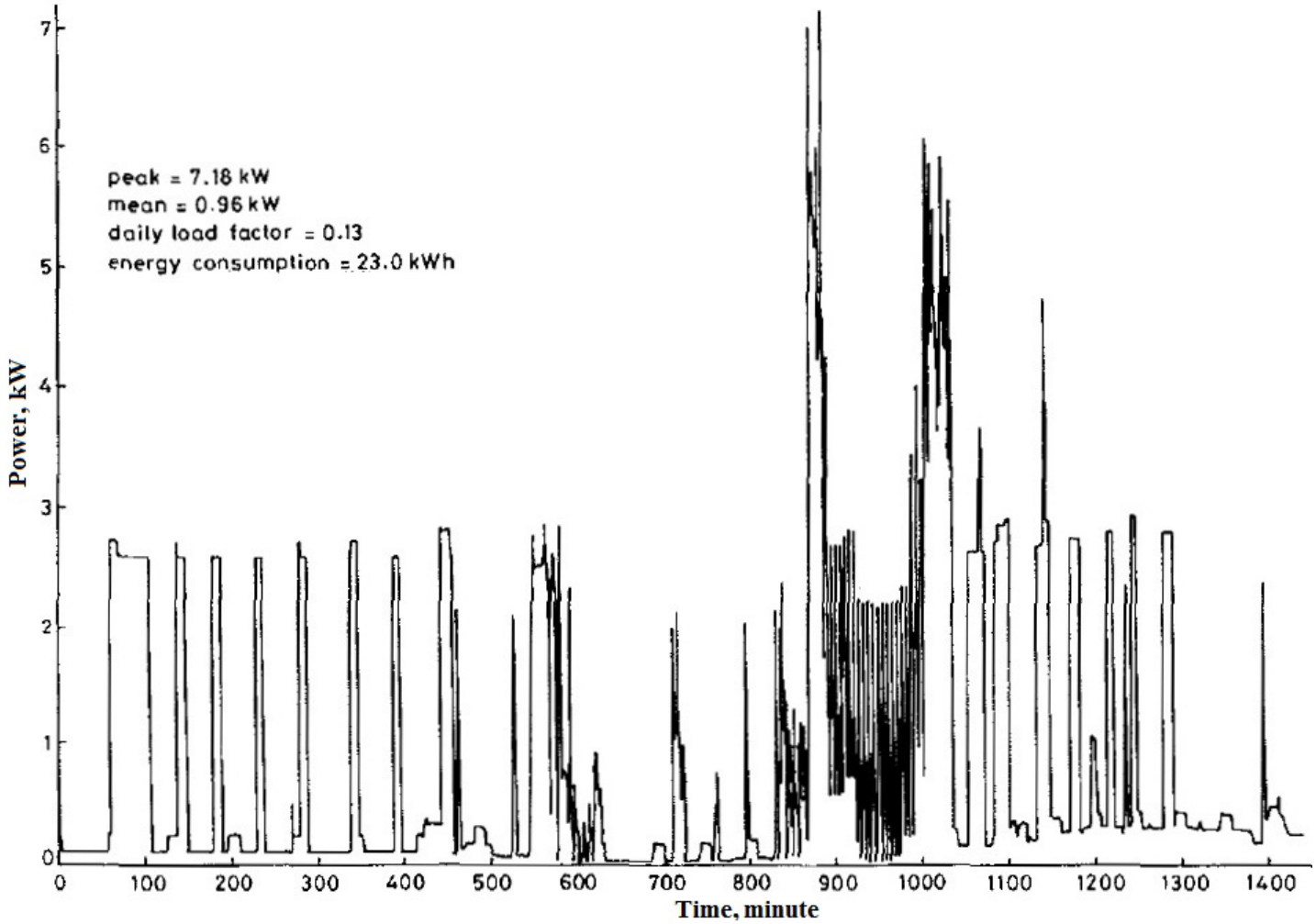

Fig. 6.1. Household daily load profile with a conventional electric cooker and immersion heater [64].

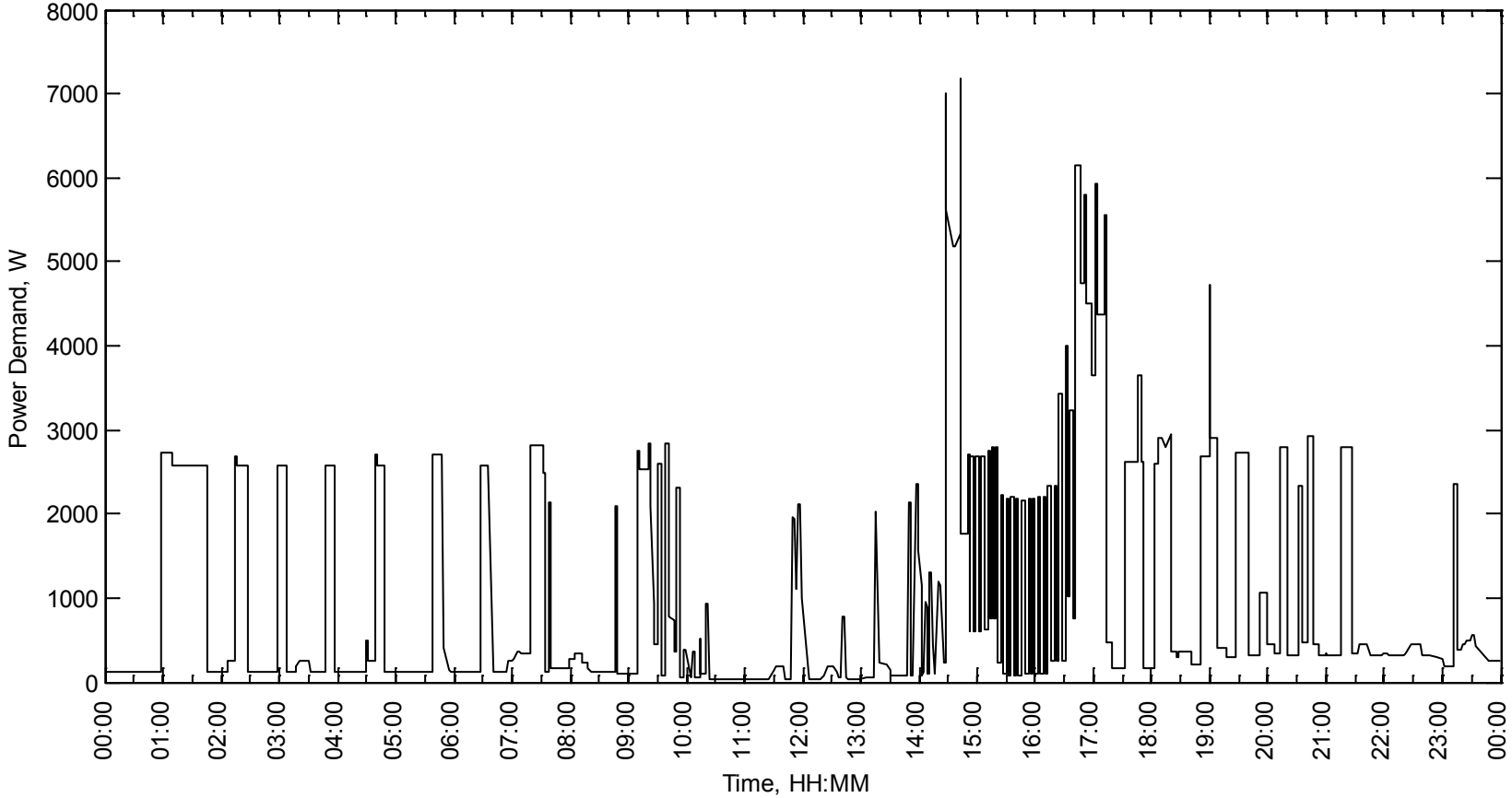

Fig. 6.2. Digitized Household daily load profile

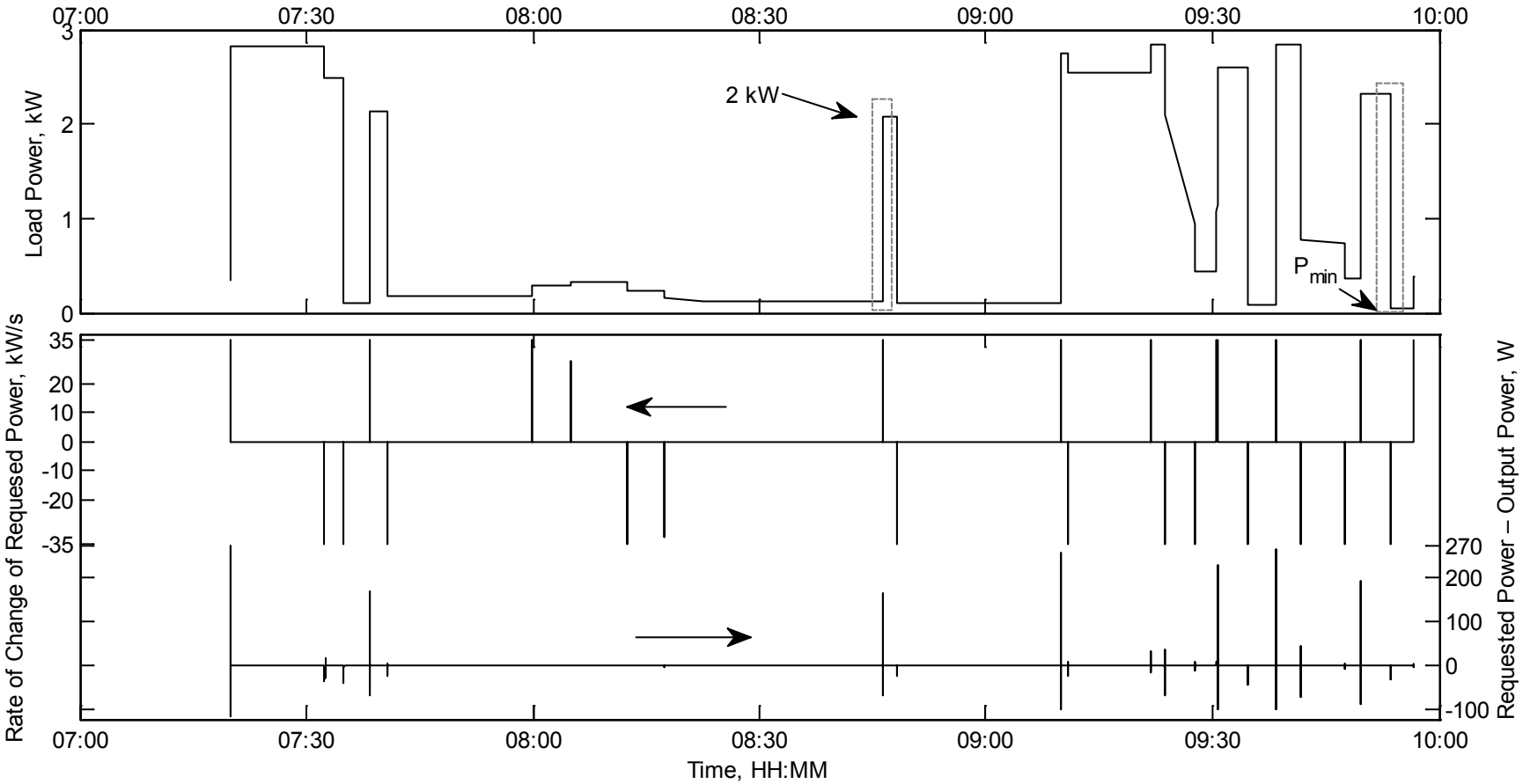

Fig. 6.3.(A) The domestic load power, rate of change of power and results of difference between requested and output power from 07:19 to 09:57

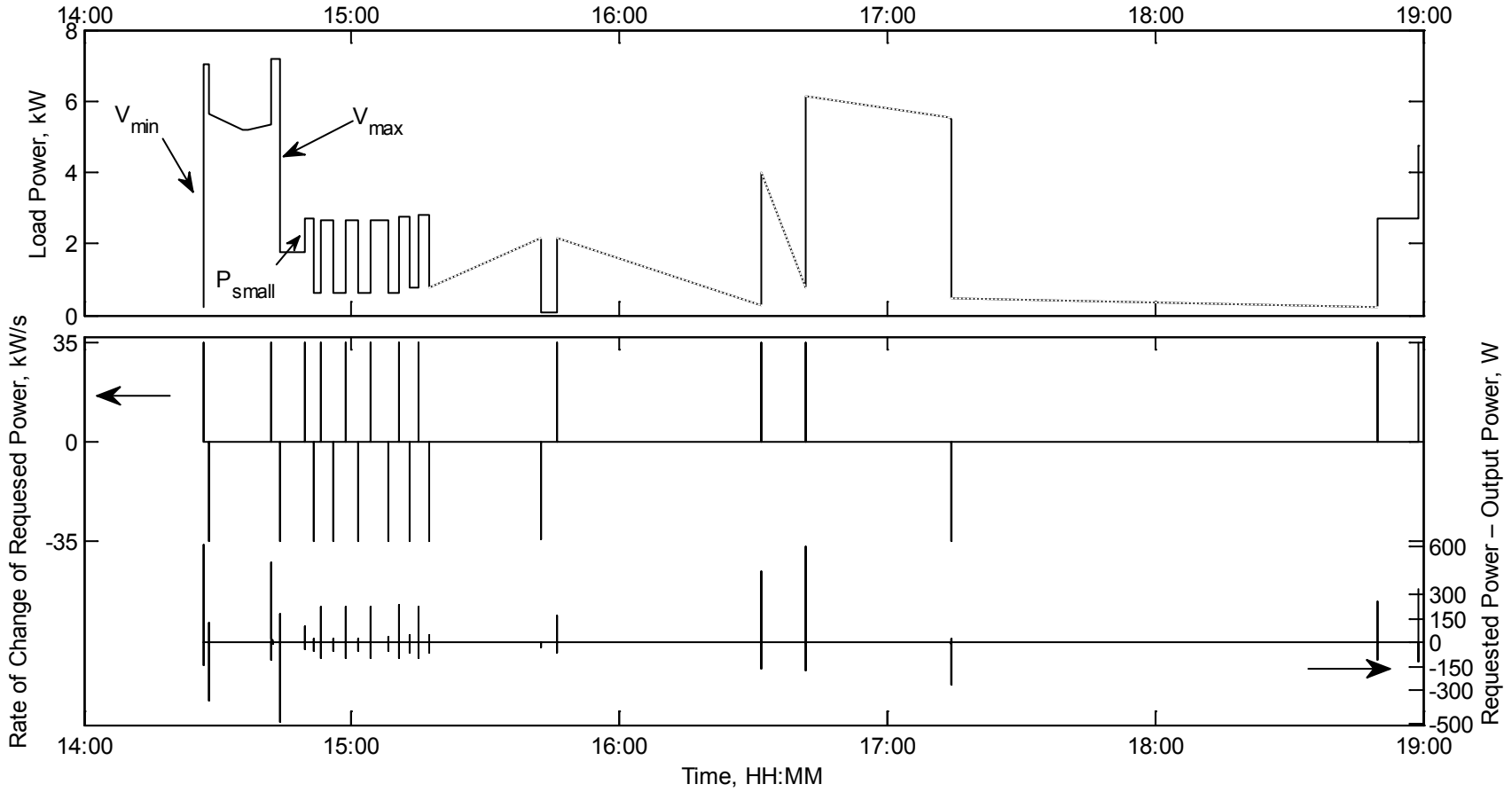

Fig. 6.3.(B). The domestic load power, rate of change of power and results of difference between requested and output power from 14:26 to 19:00. Dotted lines indicate non-simulated portions.

6.2.1 Case Study 1: 2 kW Power Demand

The first case study investigates the response of the fuel cell power system to a power demand by a 2 kW toaster at timestamp 08:46:20. Fig. 6.4 shows the response of the output voltage and power, and the duty ratio for a change in the load resistance from 1923 Ω to 120 Ω. The power demand is varying from 130 W to 2084 W in 55.8 ms at a rate of change in power demand of 35 kW/s. The initial response of the output voltage is a sharp undershoot reaching 480 V, 100 ms after the increase in power demand, followed by a few oscillations. The behaviour of the output voltage response is mainly due to the behaviour of the DC-to-DC converter and its controller, as can be seen from the duty ratio. The sinusoidal converging output voltage is a typical response of a PI controller [65].

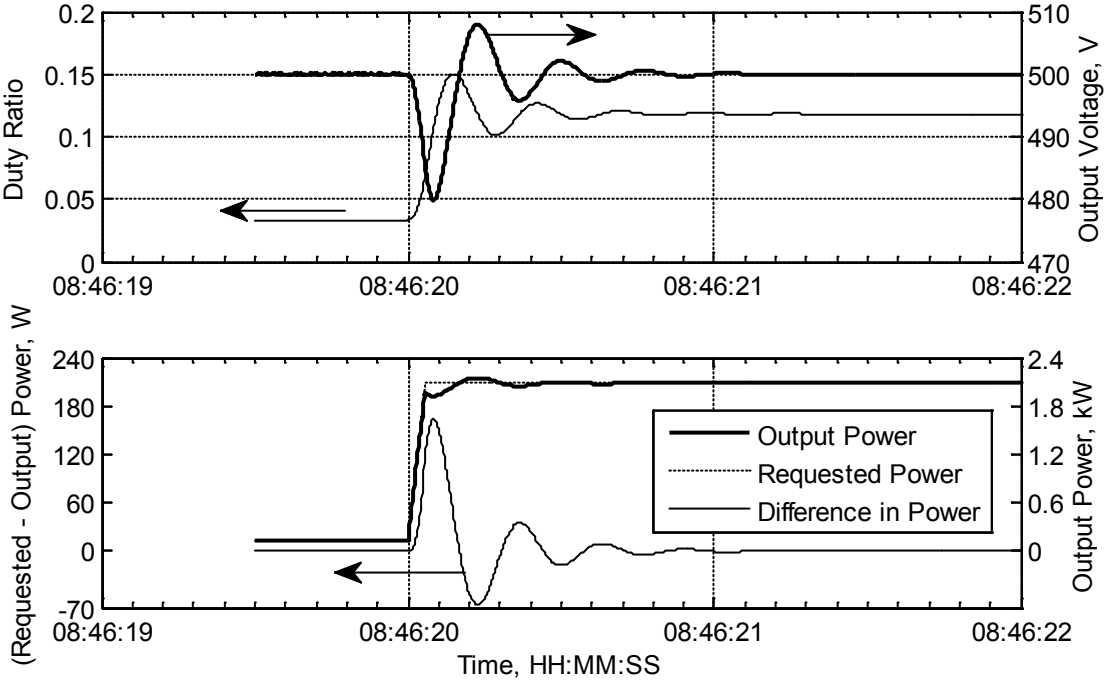

Fig. 6.4. Duty ratio, output voltage, requested and output power, and difference between them for case study 1.

The output power reaches 92 % of the power requested by the toaster 30 ms after the power demand had reached its final value, and within a settling time of nearly 200 ms the output power remains within a 2 % error band of the final value of power

demand. As mentioned earlier, another phase of power conversion is needed to obtain the standard electric mains supply, with performance similar to that presented here with one conversion phase. The overall response of the voltage and the output power have minimum, if any noticeable, influence on the current operation of the toaster, taking into account that a single use of the toaster lasts for about 115 seconds.

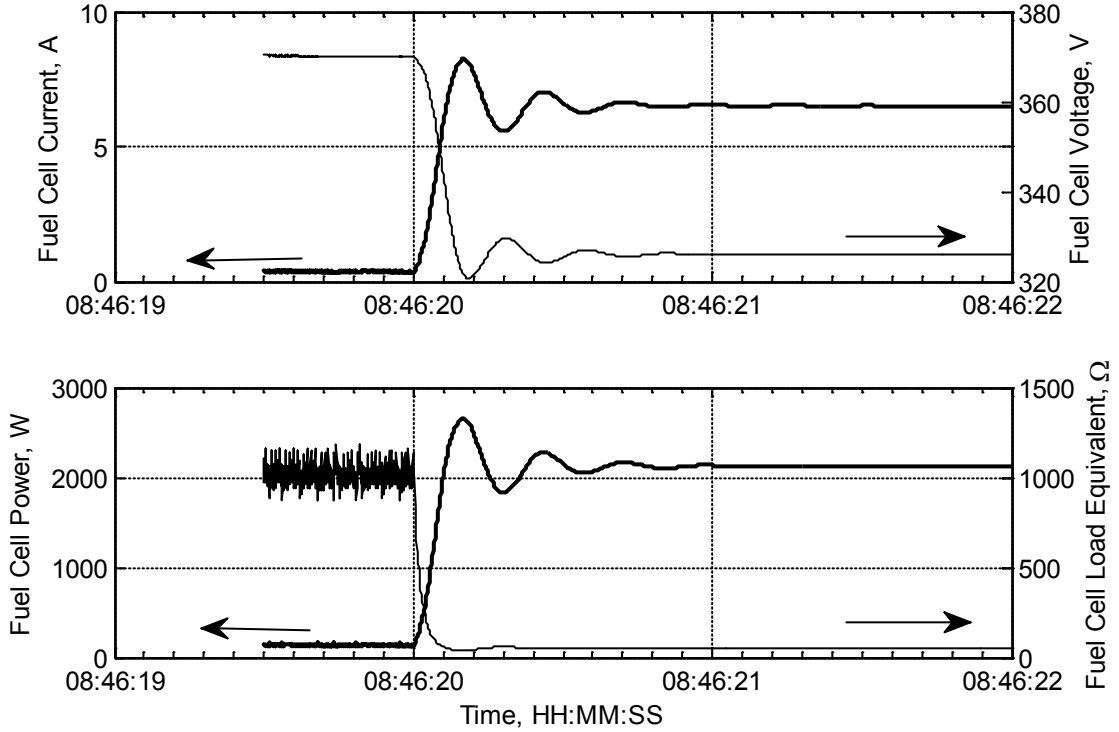

Fig. 6.5. Fuel cell current, voltage, power and equivalent resistance in case study 1.

In terms of the fuel cell response (Fig. 6.5), the equivalent load variations at the fuel cell terminals are relatively fast. This can also be verified by the transient path shown in Fig. 6.6, where the actual operating points of the fuel cell do not lie on the steady state polarization curve. However, the change in the equivalent load seen by the fuel cell is slightly slower than a step change because the transient path follows a curved line instead of a straight line. It has been indicated earlier in the methodology chapter that a step change in the load connected at the fuel cell terminals follows straight lines. The spirally shaped response near the final steady state operating point is due to the oscillatory decaying response of the controller of the DC-to-DC converter, which is faster than the fuel cell response time.

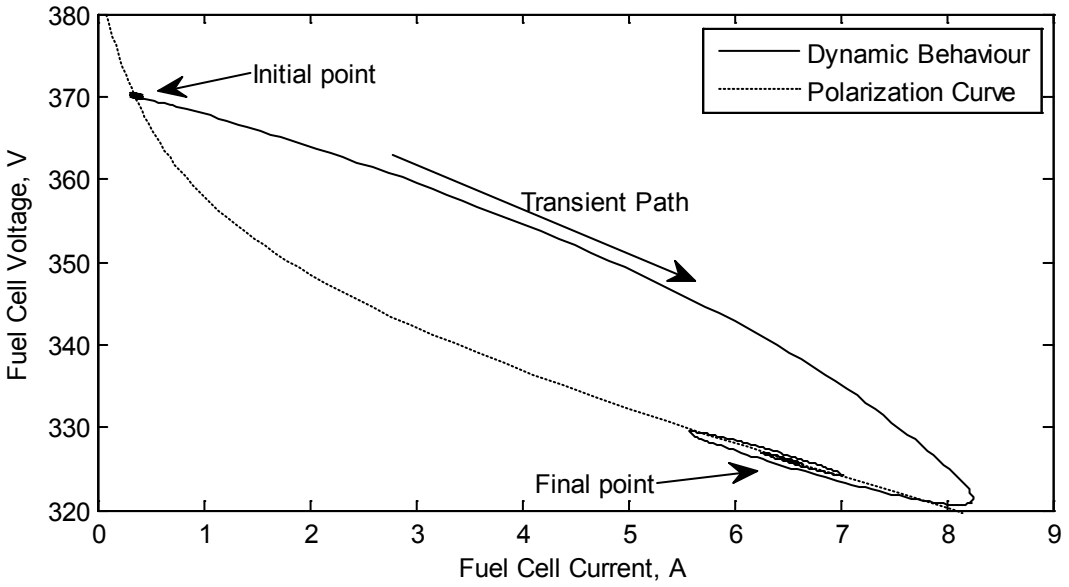

Fig. 6.6. The dynamic operating points of the fuel cell compared to the polarization curve for case study 1.

With relation to the reactant pressures, Fig. 6.7 shows that hydrogen's pressure was approaching the reference point prior to the power demand by the toaster, due to an earlier condition. However, oxygen and water partial pressures seem to be at a steady state, and the reason hydrogen shows unsteady state is merely due to the scale of the axes, where hydrogen is only 0.001 atm deviating from the reference point. The response of the reactants' pressure is not different from the response explained in the automotive application Chapter 5.

Concerning hydrogen flow, shown in Fig. 6.8, the outlet valve was closed prior to the change in power demand, since hydrogen pressure is below the reference point. The current starts to increase in response to the power demand at timestamp 08:46:20, and the inlet flow rate builds-up proportionally to the current according to the feedforward controller and the delay of the valve. On the other hand, the response of the outlet valve oscillates for nearly one second due to the feedback control loop. The reason for these oscillations is that the parameters of the PI controller were set to handle larger flow rates needed for power outputs up to 50 kW at slower rates of change, as shown in the vehicle application results.

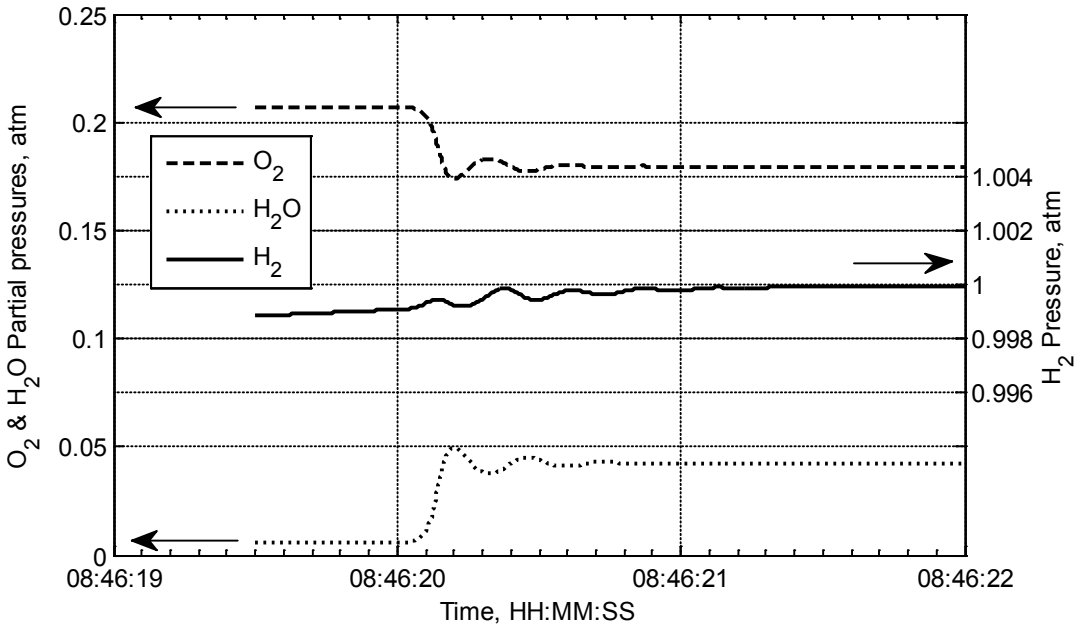

Fig. 6.7. The response of the partial pressures of H_2, O_2, and H_2O in case study 1.

These oscillations do not have a considerable influence on the pressure, as it can be observed from Fig. 6.7 and Fig. 6.8 that the variations in hydrogen pressure are concurrent with the variations in the inlet mass flow rate. However, the oscillations in the outlet valve, which are also known as ringing, have a deteriorating effect on the lifetime of the control-valve, and it would be vital to improve the performance of the outlet valve controller.

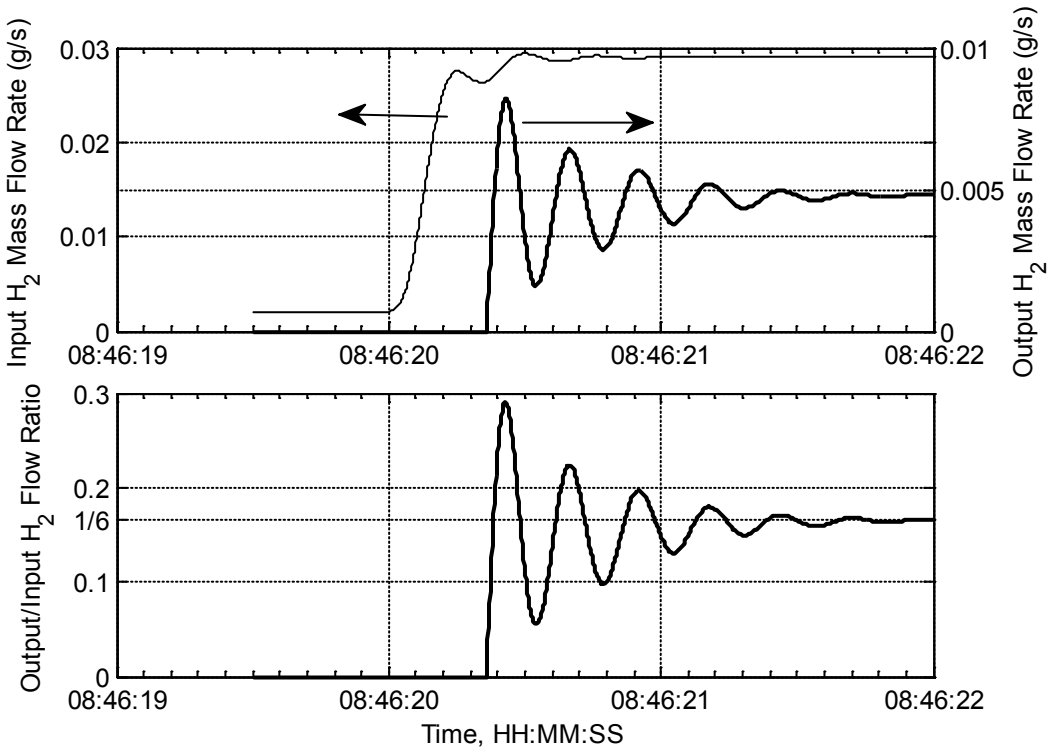

Fig. 6.8. Inlet and outlet mass flow rates, and the ratio between them in case study 1.

6.2.2 Case Study 2: Minimum Power Demand

The case study investigated here, which is part of the washing machine cycle, is for a change in demand from 2318 W to 55 W at timestamp 09:53:38, as shown in Fig. 6.9. The rate of power demand change is –34.998 kW/s taking place within 64.66 ms. A drop in power demand causes the output voltage to overshoot in proportion to the amount and rate of power demand drop. The duration of the overshoot is inversely proportional to the final value of power demand after the drop; a drop to a smaller power demand level results in an overshoot with a longer settling time. This is due to the time it takes to consume the energy stored in the capacitive and inductive components of the DC/DC converter. With all these factors combined in this case study, the overshoot in the output voltage (Fig. 6.10) results in the longest duration over the entire cycle.

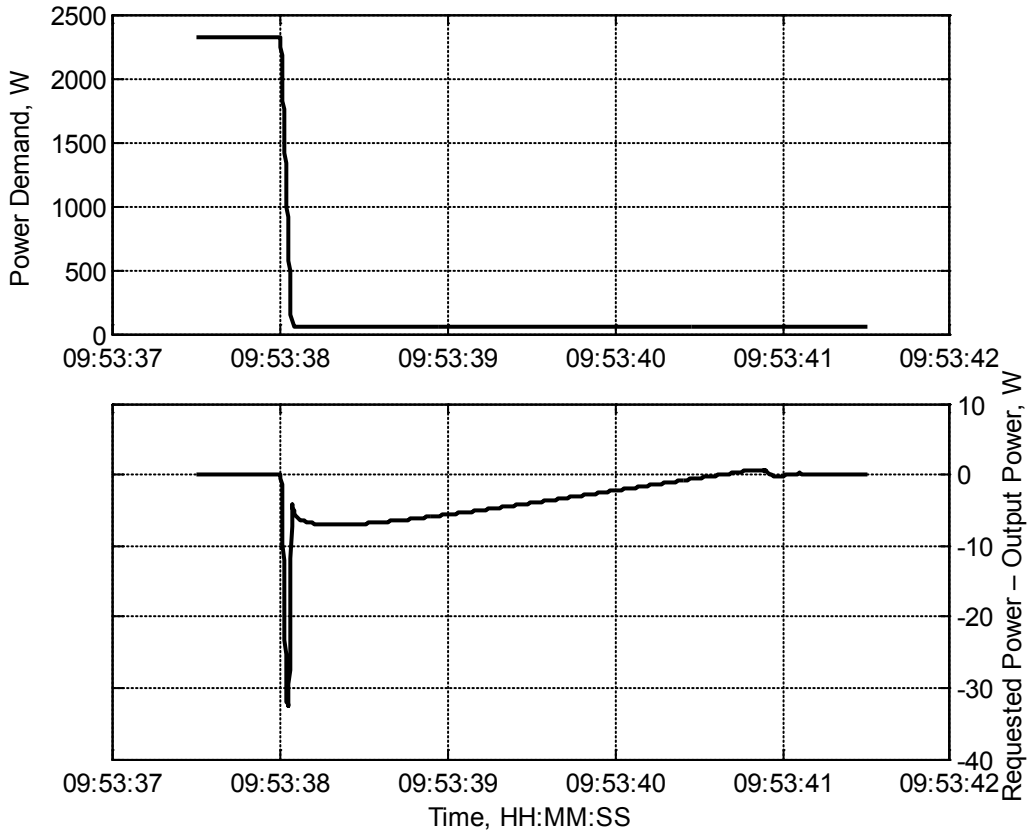

Fig. 6.9. Power demand and the excess power in case study 2.

The peak of excess power (32.6 W) occurs 42 ms after the onset of the change in power demand at timestamp 09:53:38.42 and this consists of nearly 4 % of the power demand at this timestamp, and 14 ms later the excess power drops to 4 W. If the washing machine, for example, were completing a spinning cycle or a water heating cycle, the excess power would cause a delay of up to 3 seconds until the washing machine reaches its desired operating point, however, taking into account the amount of excess power, this would not cause a significant influence on the performance of the washing machine.

The overshoot and persistence of the error in output voltage drives the PI controller of the DC-to-DC converter to reducing the duty ratio until it reaches the minimum possible limit of zero. For a stand-alone PI controller, the integral function would saturate causing deterioration on the performance of the controller. It can be seen

from Fig. 6.10 that as soon as the output voltage reaches its reference point of 500 V (i.e. the error drops to zero), the duty ratio increases, which proves that the anti-windup mechanism is operating effectively.

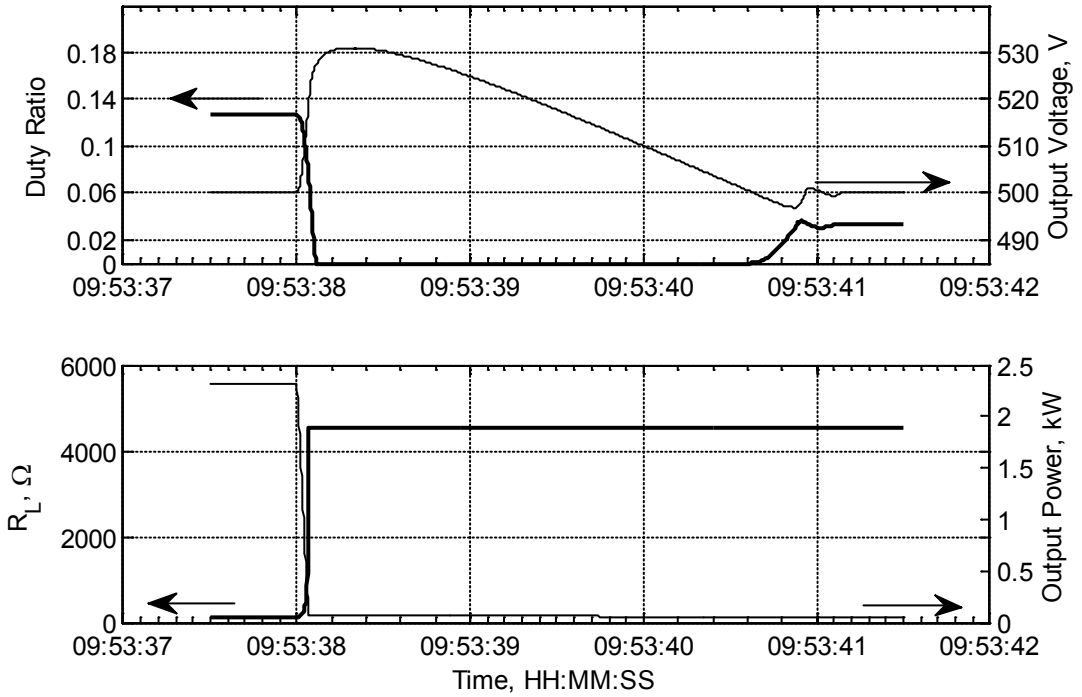

Fig. 6.10. The duty ratio, load resistance, output voltage and power in case study 2.

At a power demand of 55 W, the energy is transferred through the converter from the fuel cell to the load in a duration smaller than the switching period of the converter. In this case, the converter is said to be in the discontinuous current mode of operation, and the output to the input voltage ratio is not equal to $(1–D)^{-1}$. In this mode, it is noticed that the controller is less effective in maintaining a good grip of the output voltage, although the observed error in voltage is not greater than 2 volts. The reason for the deterioration in the controller's performance may be attributed to the non-linearity of the converter's response in the discontinuous mode of operation, as described in Chapter 5.

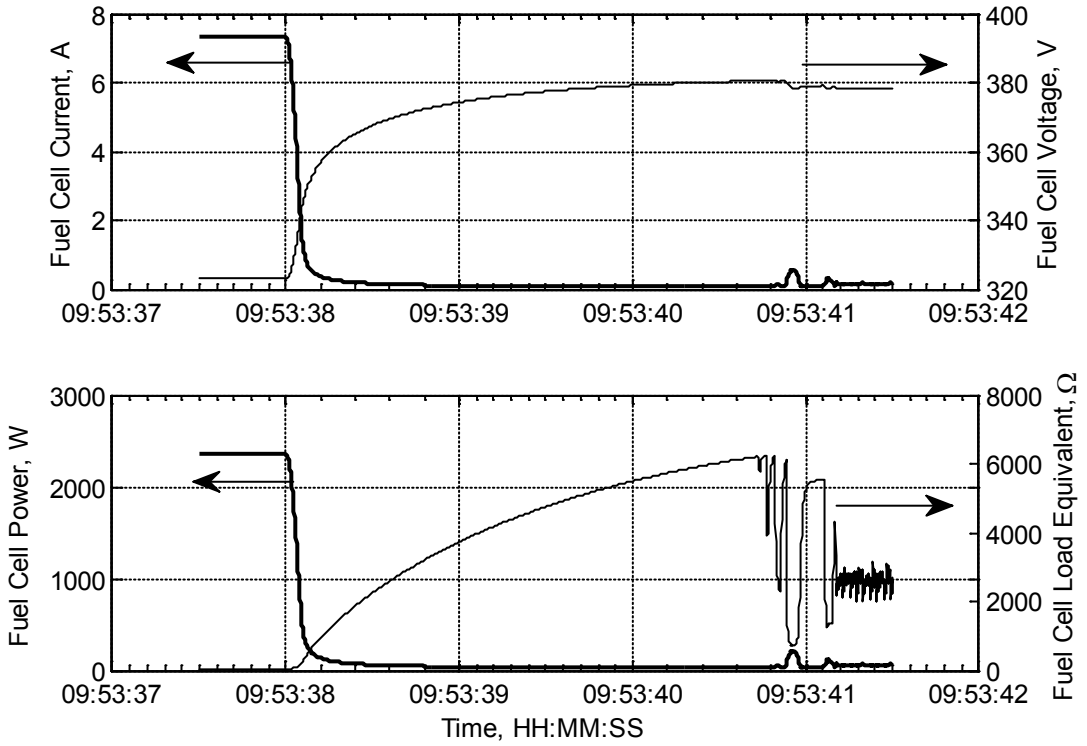

Fig. 6.11. Fuel cell current, voltage, power and equivalent resistance in case study 2.

The onset of the rapid fluctuations in the fuel cell equivalent load resistance seen in Fig. 6.11 coincides with the point where the output voltage reaches its reference point and the duty ratio increases above its minimum limit value. At this point, the fuel cell is near the open circuit operating point, and the small variations in the duty ratio result in large variations in the equivalent resistance of the fuel cell. As mentioned earlier, the converter is operating in the discontinuous mode of operation, which results in reduced performance of the controller that contributes to the fluctuations in the equivalent resistance seen by the fuel cell. Nonetheless, these fluctuations are not influential on the fuel cell performance as they are met by relatively small variations in the fuel cell voltage and current, as seen in Fig. 6.11 and Fig. 6.12.

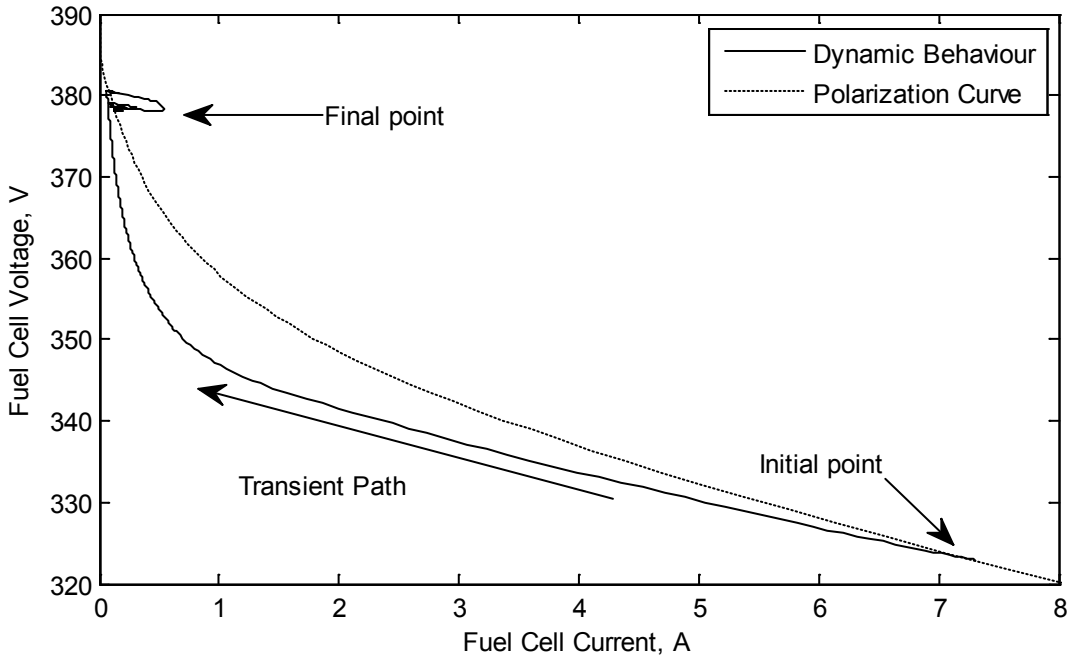

Fig. 6.12. The dynamic operating points of the fuel cell compared to the polarization curve for case study 2.

Transient behaviour of the fuel cell during this change in power demand takes a relatively long time to settle down as seen from Fig. 6.11. This is due to the small fuel cell current that reflects on the discharge rate of the double layer capacitance of the fuel cell.

The partial pressure of hydrogen tends to increase (Fig. 6.13) after the power demand drops due to the time delay of the inlet valve. This increase in the pressure causes the outlet valve controller to increase the outlet mass flow rate (Fig. 6.14). However, after the delay of the input valve passes, the input mass flow rate drops to its expected low value causing a drop in the pressure. As a response to the drop in pressure, the outlet valve is closed. However, due to the small inlet mass flow rate; the pressure builds up gradually within 3 seconds.

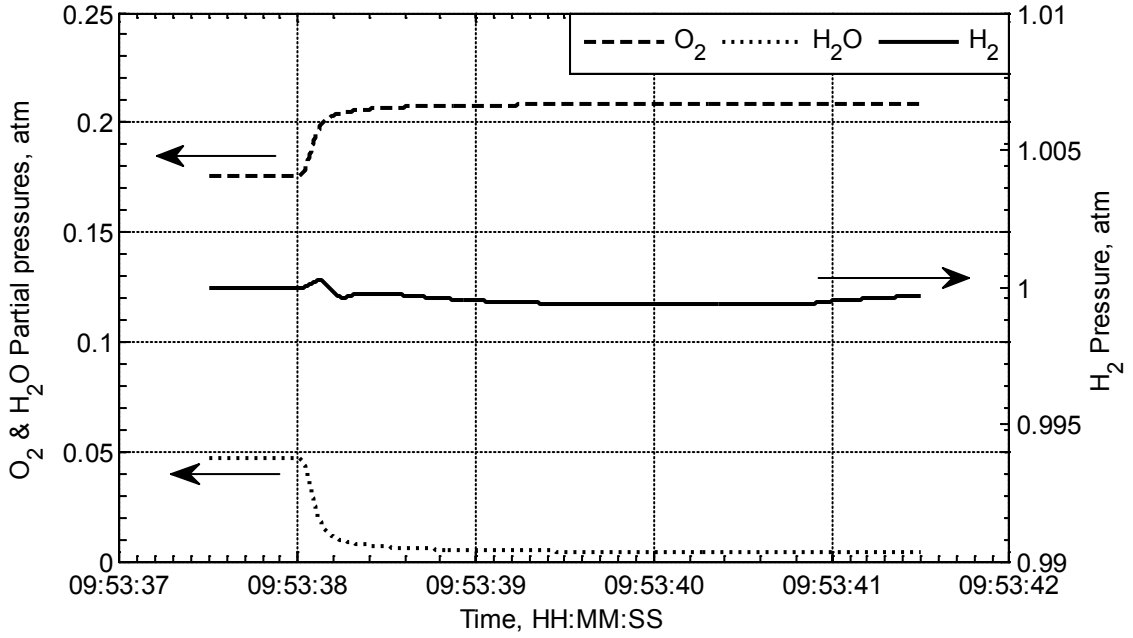

Fig. 6.13. The response of the partial pressures of H_2, O_2, and H_2O in case study 2.

The variations of the pressures of oxygen and water are more significant than hydrogen pressure because the aim of the controller is to maintain minimum differential pressure across the membrane. Hence, only the total pressure of the cathode is controlled by varying the flow rate of the inlet and outlet airflow rates. Since the consumption of oxygen is met by the production of water, the partial pressures of oxygen and water are proportional to the fuel cell current.

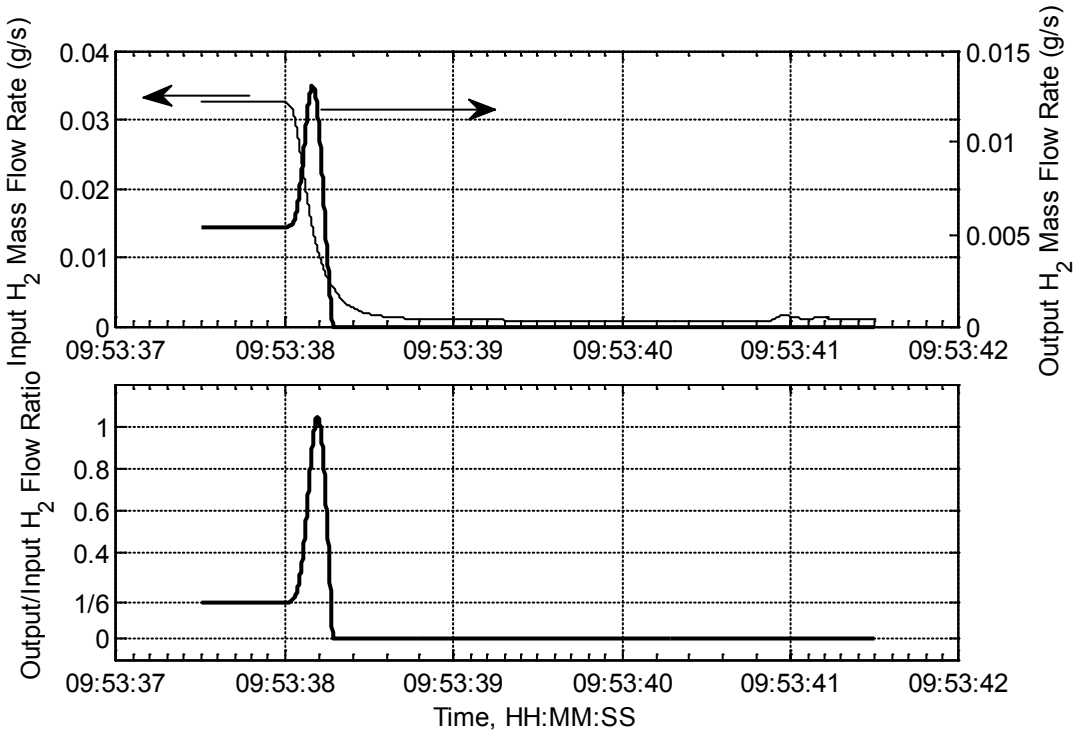

Fig. 6.14. Inlet and outlet mass flow rates, and the ratio between them in case study 2.

6.2.3 Case Study 3: Minimum Voltage Undershoot

The case study investigated here involves a power demand of an electric oven in its preheating phase. An increase in power demand occurs at timestamp 14:26:40 from an initial value of 230 W at a rate of change of 34.998 kW/s to a maximum value of 7.01 kW. This level of power demand is maintained for 89 seconds, and only a 2-second portion including the settling time is shown in Fig. 6.15 to Fig. 6.20. In this case study, the output voltage drops to its minimum value of 471.1 V (Fig. 6.15) over the entire load profile. The reason behind this is that the rate of change in power demand is persistent for the longest period of 193.8 ms compared to any other increase in power demand in the household profile. It can be seen from Fig. 6.16 that the shortage in power continuously increases until the rate of change of power demand drops to zero.

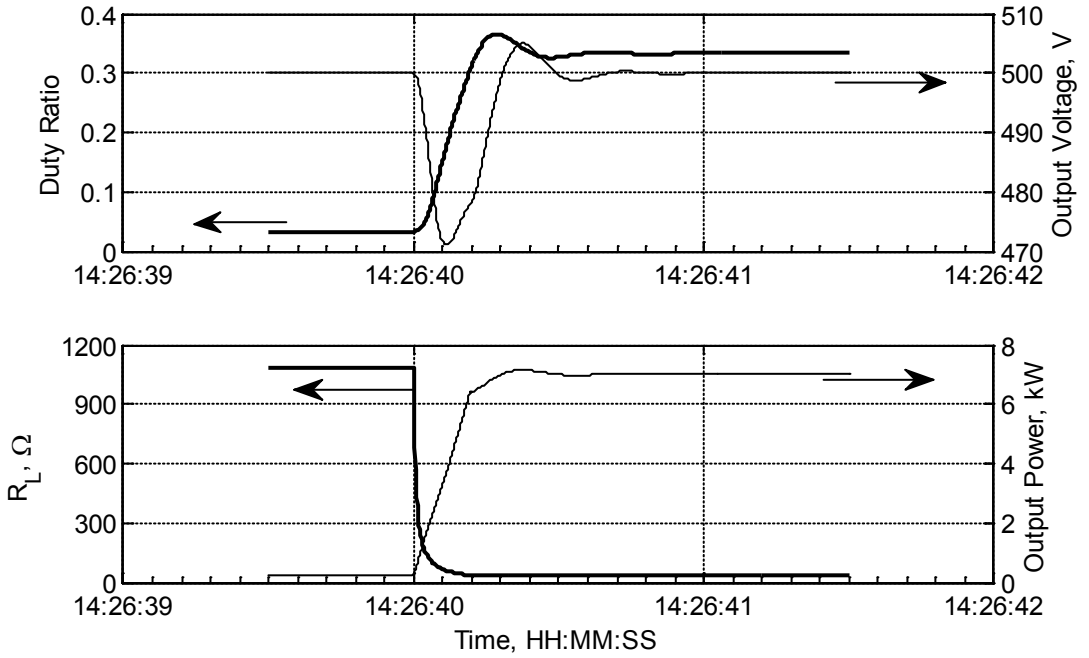

Fig. 6.15. The duty ratio, load resistance, output voltage and power in case study 3.

In nearly 500 ms, the output power matches the power requested by the oven. In terms of oven operation, the delay in output power delivery, which is roughly equivalent to a shortage of energy of 90 J, does not create a significant loss to the total generated heat of 620 kJ needed to raise the temperature of the oven over a period of 89 seconds. The overall response of the output power and voltage do not have a significant influence on the operation of the electric oven. However, the output voltage shown in Fig. 6.15 represents the mains supply voltage for the entire household that all other appliances and devices are connected to. Therefore, voltage undershoot caused by switching on the electric oven will have a significant influence to other sensitive devices. The degree of influence depends on the application and the human interactions with the device or appliance, and the electrical protection against damage, such as that needed for computer electronic components. For example, light bulbs would emit lower light intensity during voltage undershoot, and may cause some inconvenience to the residents.

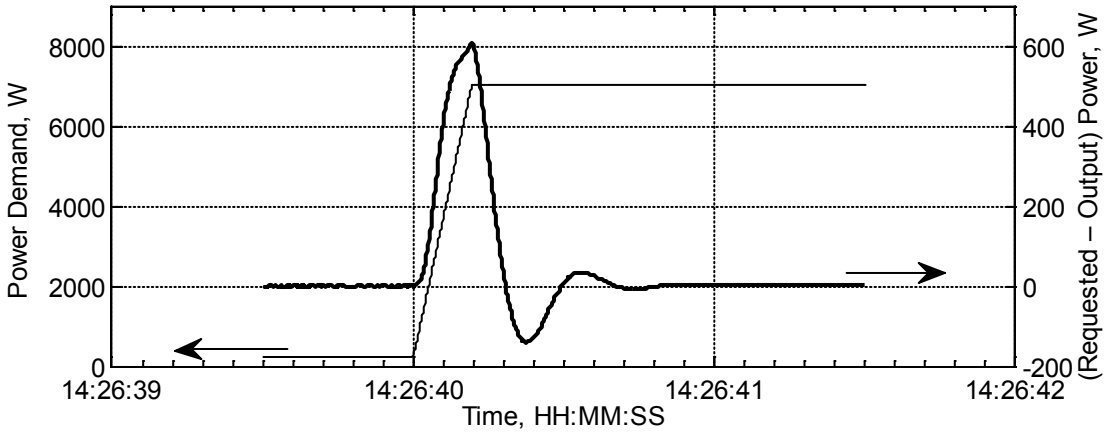

Fig. 6.16. Power demand and the difference in power in case study 3.

In terms of fuel cell response in this case study, it is noticed in Fig. 6.17 that the fuel cell equivalent resistance prior to the change in power demand fluctuates around a high resistance value. The reason for this is that at low output power (230 W) the fuel cell voltage is close to the open circuit state and the current is small. This makes the quotient $R = V/I$ very sensitive to the smallest variations in the current. Regarding the transition in the operating point due to the power request of the oven, the fuel cell instantaneous operating points (Fig. 6.18) follow a path that is further from the steady state polarization curve near the initial point of transition than that closer to the final point. This indicates that the fuel cell time constant is larger in the activation overvoltage region than the ohmic overvoltage region. In general, transitions from low power demands to higher power demands have faster response times.

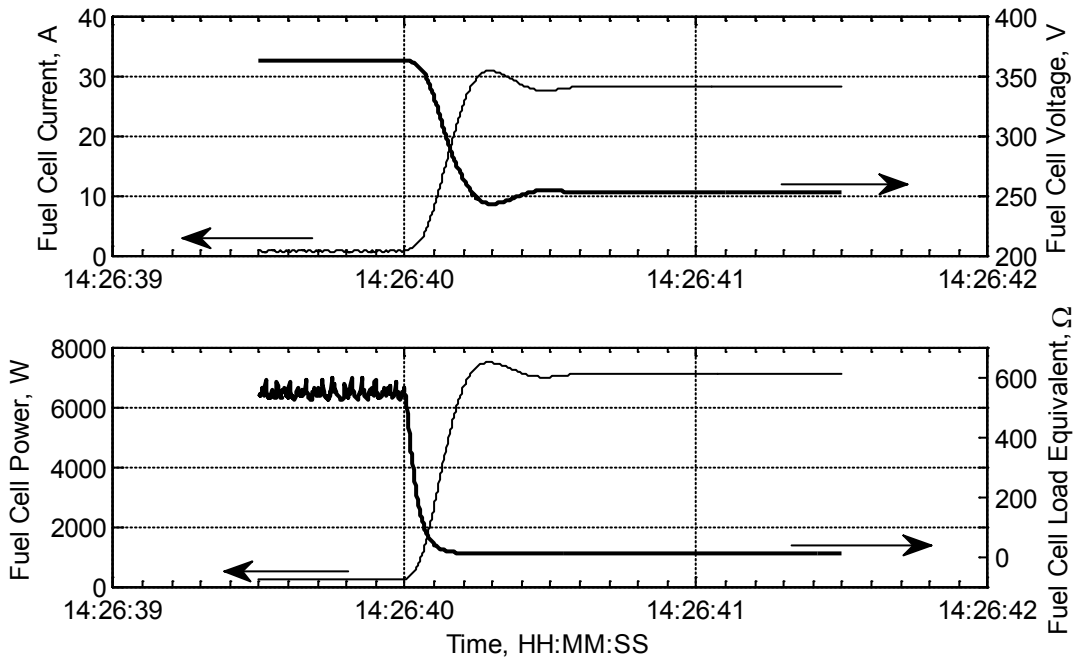

Fig. 6.17. Fuel cell current, voltage, power and equivalent resistance in case study 3.

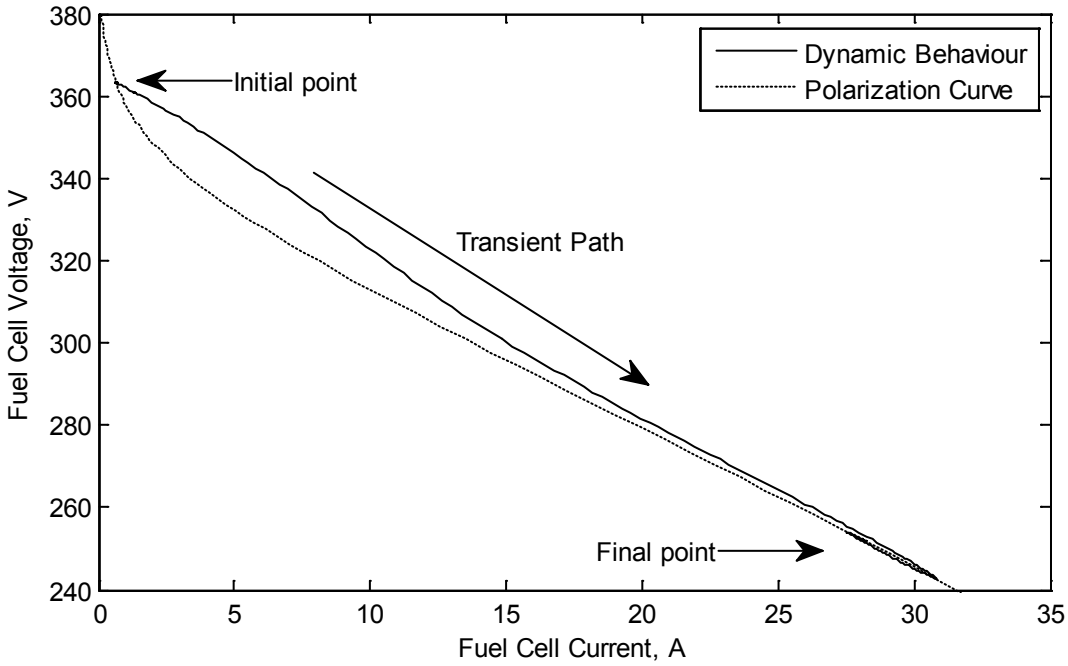

Fig. 6.18. The dynamic operating points of the fuel cell compared to the polarization curve for case study 3.

In terms of the reactants response, it was noticed in the previous case studies that hydrogen pressure rises when the demand increases due to the feedforward effect of the inlet valve. However, in this case study where the demand increases to the highest power level for the entire household profile, hydrogen's pressure initially raises for a relatively small amount, as it can be noticed by the increase in the flow rate of outlet valve (Fig. 6.19).

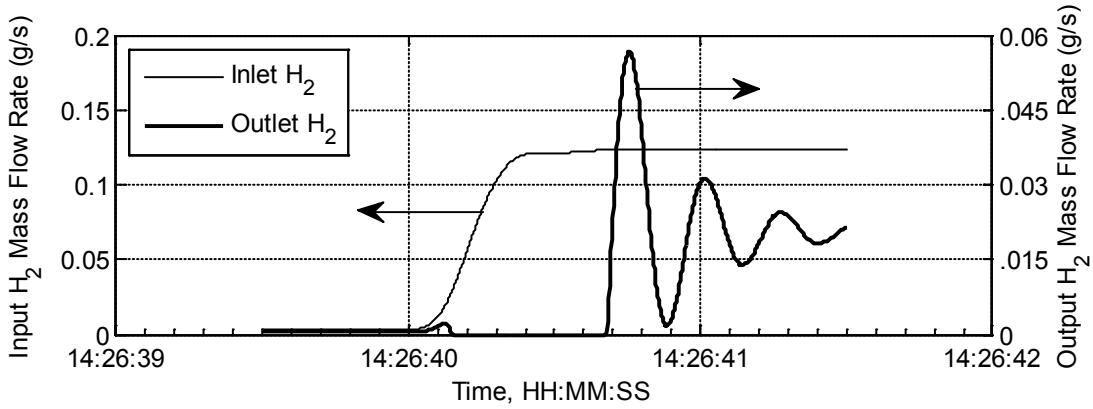

Fig. 6.19. Inlet and outlet mass flow rates in case study 3.

After nearly 110 ms, hydrogen pressure drops sharply and the outlet valve shuts off as the rate of consumption of hydrogen exceeds its inlet flow rate due to the delay of the valve. This is because the transition is taking place over a relatively longer time span than previously studied cases.

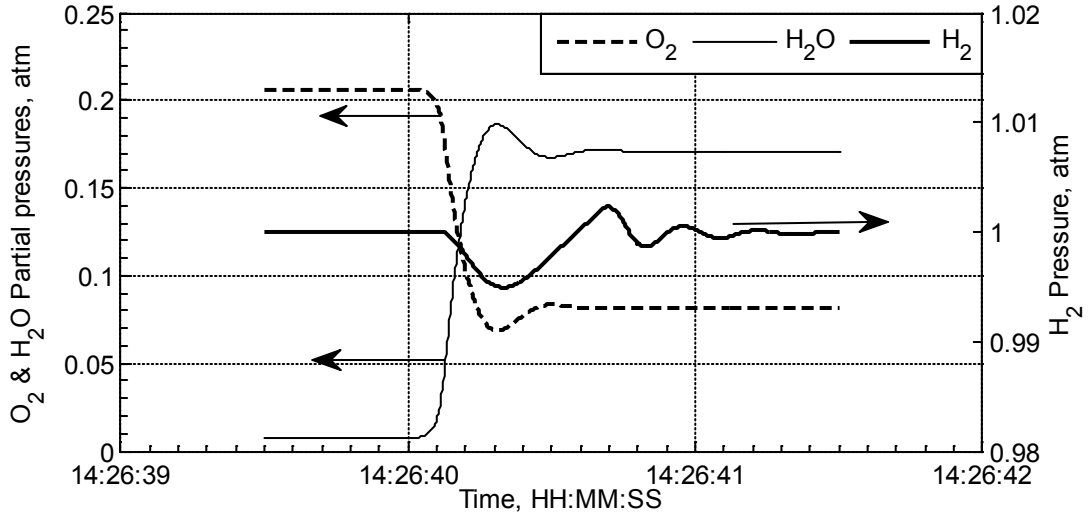

Fig. 6.20. The response of the partial pressures of H_2, O_2, and H_2O in case study 3.

6.2.4 Case Study 4: Maximum voltage overshoot

In this case study, the maximum voltage overshoot over the entire household profile occurs when the power demand drops at the end of the oven preheating phase (Fig. 6.21). The power demand drops at timestamp 14:43:47 from 7.18 kW to 1.78 kW at a rate of −35 kW/s (Fig. 6.22). The voltage overshoot reaches 540 V, which is still within the tolerance specified in the methodology chapter to 550 V.

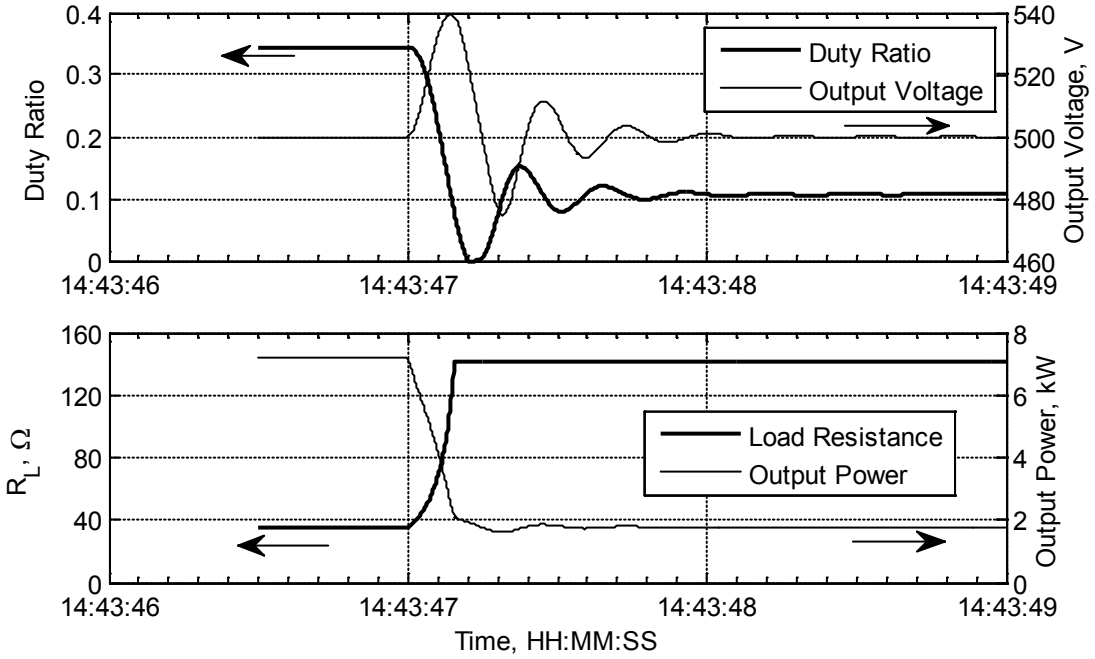

Fig. 6.21. The duty ratio, load resistance, output voltage and power in case study 4.

Although the drop in power demand in this case study is much higher than that discussed earlier in case study 2 of the washing machine cycle (Fig. 6.9), the time it takes for the voltage to settle down (nearly 1 second) is much smaller than that of case study 2 (nearly 3 seconds). Two reasons cause the difference in the settling times; the first is that, the final level of power demand in this case study is higher, which helps consume the energy stored in the elements of DC-to-DC converter at a faster rate. Secondly, since in both case studies the rate of change in power demand is equal, the duration of the transition between the initial and final power demand levels is larger (154 ms) for this case study, compared to 65 ms of case study 2. In other words, not only the rate of change of power demand determines the size of the voltage overshoot, but also the duration of the transition and the final level of power demand.

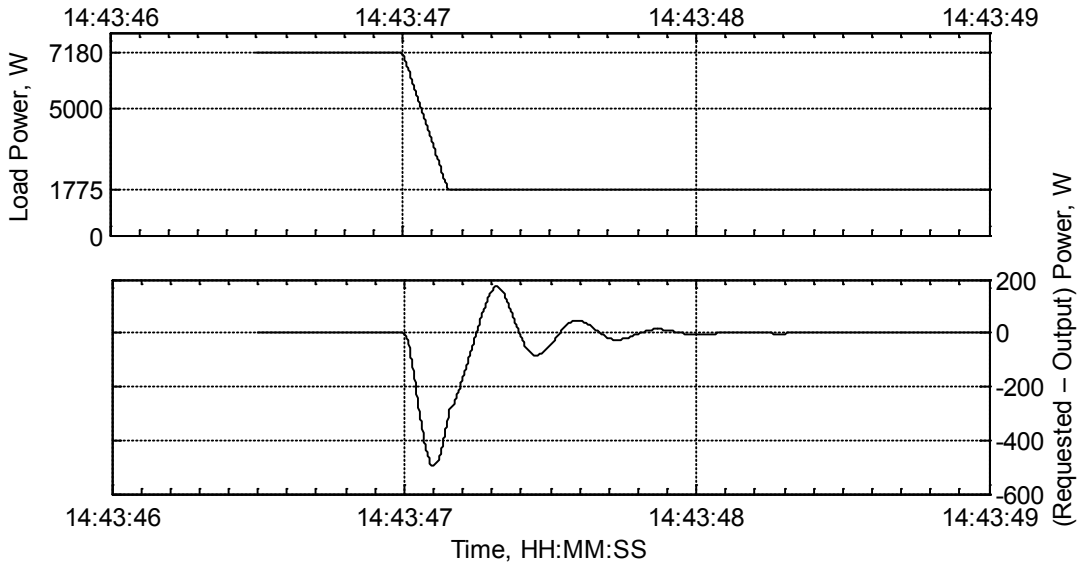

Fig. 6.22. Power demand and the difference in power in case study 4.

It should be pointed out that during a drop in power demand the voltage overshoot is the main issue. However, it is noticed in this case study that the first oscillation of the output voltage drops to a minimum value of 474.7 V, which is very close to the lower threshold of electrical supply tolerance (470 V). These oscillations in the voltage are due to the dynamic interactions between the PI controller of the DC/DC converter, the capacitive element of the fuel cell and the load. Because at low power demand, the fuel cell operates near the activation region, which is nonlinear and the settling times are slower compared to the operation at higher power demands, as shown in Fig. 6.23 and Fig. 6.24.

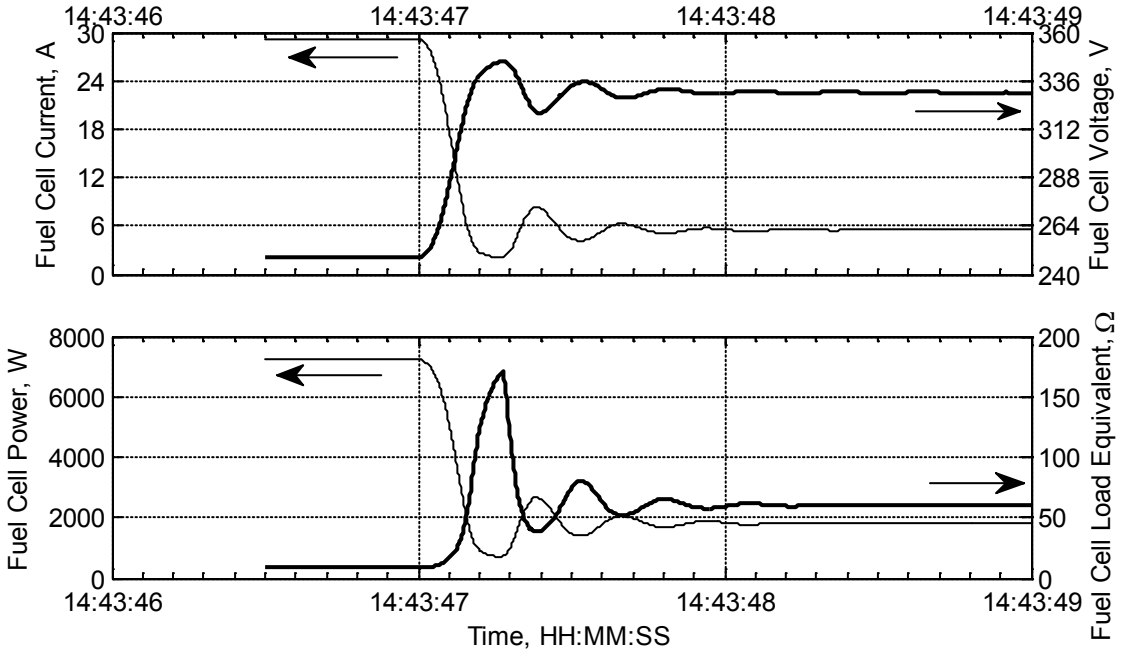

Fig. 6.23. Fuel cell current, voltage, power and equivalent resistance in case study 4.

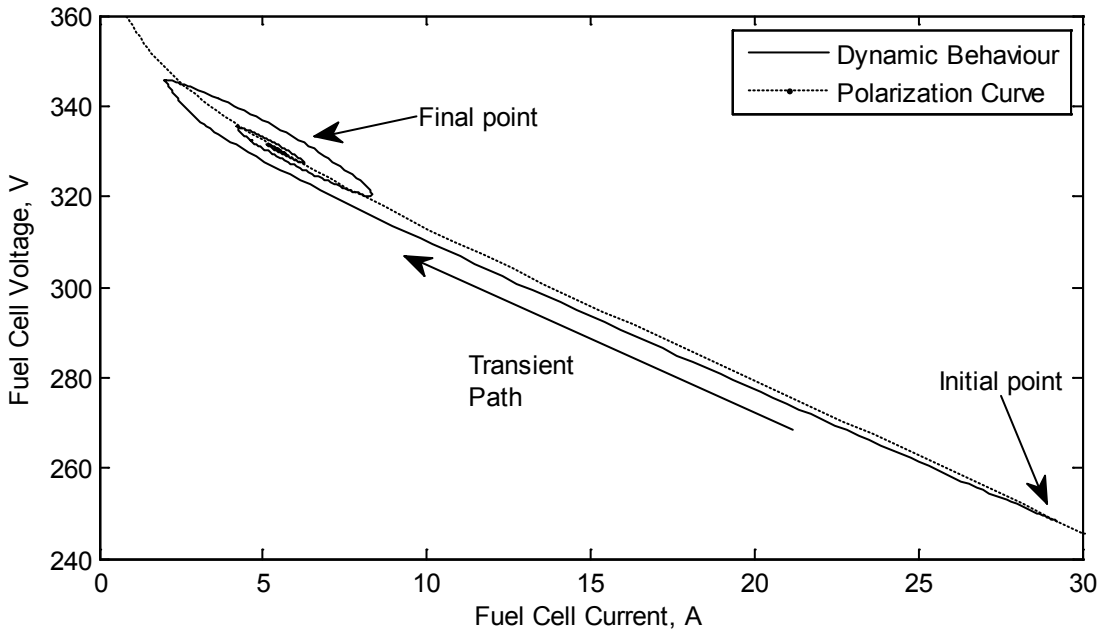

Fig. 6.24. The dynamic operating points of the fuel cell compared to the polarization curve for case study 4.

6.3 Energy and Reactant Flow Analyses

The aim of the energy analysis is to determine the amount of energy shortage of the fuel cell system in household applications. The household profile covers a 24-hour period. Due to the constraints of processing time, selected periods were investigated, out of which only two were continuous in time. The remaining periods were sampled for 3−6 second durations. Therefore, for the energy and reactant flow analyses only the two continuous periods may be considered. Table 6.1 summarises the analysed periods and the corresponding energy results.

Surpluses and shortages in energy occur during changes in power demand. From the previous results, it is observed that the amount of excess/shortage energy depends mainly on the size of the change in power demand.

Table 6.1 : Energy analysis of domestic application

	Period 1	Period 2
Range	07:19:58−08:17:25	08:46:15−10:14:50
Duration	57 min 27 s	1 hr 28 min 35 s
Energy Demand	3332230 J (925.62 W.hr)	5266715.5 J (1.46298 kWh)
Energy Output	3332097 J (925.58 W.hr)	5266654.1 J (1.46296 kWh)
Total Excess Energy	81 J	222.0 J
Total Energy Shortage	214 J	283.4 J

For the first period, it is found that the total shortages in energy equal 214 J, while the excess energy generated is 81 J. This indicates that if an energy storage device (ESD) is used to recover the excess 81 J, the overall energy balance is in shortage of 133 J. Similarly, for the second period, the overall energy balance is found to be in shortage of 61.4 J.

Without an energy storage device, the excess energy cannot be considered as an advantage to the fuel cell system or its efficiency. Although for some devices in certain circumstances, such as heaters in the ON state, excess energy will aid in raising the temperature of the system being heated, however, in most cases, excess energy may cause damage or may not be useful to the load, such as TV and light fittings. Hence, excess energy is considered as lost energy reducing the overall efficiency of the system.

Regarding shortage of energy, this does not count in the efficiency reduction in terms of output to input energy, since all the output energy is considered to be consumed and utilised to its optimum value. However, the shortage of energy will have influence on the performance of the appliances.

In order to utilise excess energy and improve the efficiency, an energy storage device should have the capacity to absorb and store the excess energy for later use when the fuel cell system cannot meet the power demand. Energy analysis is an important step in designing the energy storage device, in terms of capacity. In order to determine the capacity of the required ESD, average values may not be appropriate to use, since the maximum and minimum of energy differences are needed. A maximum increase in power demand at timestamp 14:26:40 occurring outside the two periods defined in Table 6.1 , results in the maximum energy shortage of 101 J. While a maximum drop in power demand at timestamp 14:43:47, results in a maximum excess energy of 64 J. Since the studied power profile is based on a fixed sequence of expected use of energy, the actual power demand for another household might be different. Hence, the ESD should always maintain energy level that meets the maximum shortage of energy, that is 101 J, and at the same time, it should be capable of absorbing the maximum excess in energy, that is 64 J. Consequently, the capacity of the ESD should be the summation of 64 J and 101 J, which is 165 J. It should be noted that this conclusion is only valid for the 1-day profile presented in this thesis. Therefore, a rigorous study needs to take into account the various possibilities of load profiles that can occur during a year. However, this study is out of the scope of this thesis.

For reactant flow analysis, Table 6.2 summarises the results obtained from the two periods mentioned earlier.

Table 6.2 : Hydrogen flow analysis of domestic application

	Period 1	Period 2
Range	07:19:58−08:17:25	08:46:15−10:14:50
Duration	57 min 27 s	1 hr 28 min 35 s
Supplied Hydrogen (g)	47.563	74.778
Consumed Hydrogen (g)	39.635	62.312
Excess Hydrogen(g)	7.927	12.465

The amount of excess to consumed hydrogen ratio in period 1 is 20 % and in period 2 is 20.004 %. Although the excess amount of hydrogen was set to 20 % based on the external current, the average value is equal to what is anticipated. Excess hydrogen must be reused to avoid a significant drop in the fuel cell efficiency.

The aim of supplying excess hydrogen was to improve the dynamic performance of the fuel cell power system, and this has been accomplished very well, as noticed in the results earlier. A smaller excess ratio would result in poorer dynamic performance especially for large changes in power demand. However, as mentioned in Chapter 4, the amount of excess ratio could be varying such that it decreases as the steady state operating output power of the fuel cell increases.

6.4 Summary

Although it may seem that automotive applications have faster changes in power demand, domestic applications impose greater requirements on transients particularly when appliances are switched on or off. The shortage and excess power values varied within ±600 W during changes in power demand, compared to ±250 W in automotive applications. However, in domestic applications, the number of changes is far less than that in a driving schedule. In addition, shortages in power during transients are more tolerable for most household appliances, such as heating (space, water, etc), electric ovens.

The results presented of a fuel cell system under domestic load profile show that the control of the fuel cell system performs well in matching the power demand and maintaining acceptable voltage tolerances during steady and varying load conditions. Hydrogen pressure and flow control performs well during transients. However, using air on the cathode causes large variations in the partial pressure of oxygen that limit the output power of the fuel cell. Pure oxygen use would improve the performance considerably, but the storage of oxygen would add more complications.

Chapter 7
CONCLUSIONS AND SCOPE FOR FURTHER WORK

7.1 Conclusions

A dynamic fuel cell model was developed and integrated with the external circuit in what is believed to be a new approach to reproduce and analyse actual fuel cell-load interactions. Upon this, a control strategy was developed in this study to match the demand and regulate the output voltage for varying power demand. The strategy is based on using DC-to-DC converters and regulating the flow of the reactants. Unlike most numerical and experimental studies, the overall nonlinear fuel cell system model was elaborately tested for the entire operating region. Consequently, the behaviour of the system was observed in the discontinuous current mode of the converter, which caused small errors in the output voltage. In addition, the fuel cell was operated near and beyond the concentration losses region that showed irrecoverable control of the output voltage, which would short-circuit and damage the fuel cell. A strategy was put forward to prevent this common control problem by modifying the PI controller of the DC-to-DC converter.

In order to generalise the control problem of matching the fuel cell output to the requirements of the load, the design of the fuel cell output is kept at an earlier stage of power delivery, before the final delivery point of power, which connects to the load. In this study, the aim was to deliver a constant DC voltage of 500 V.

The response of the fuel cell system to changes in power demand is very close to, but less than, that of existing energy conversion devices. Although the deficiency in meeting the power demand may be acceptable for most applications, an additional quick-discharge energy storage device may be used to compensate for the shortage in power not met by the fuel cell. In addition, using an energy storage device is preferable,

where the system's excess power may be recovered for later use. This would also reduce the time needed for the voltage to settle down, when the power demand suddenly decreases.

The main conclusions drawn from the work of this study are:

1. A fuel cell system model was successfully developed reproducing the dynamic behaviour of a fuel cell-load required for building control strategy. The model showed comparable behaviour to experimental data. The modularity approach followed in developing the model makes it flexible to changes in design and applications studied.
2. Although maintaining optimum operating temperature and moisture in the membrane is important for efficient operation of the fuel cell, their slow response to changes makes their influence on the control strategy for varying power demands negligible.
3. The flow rates of the reactants have the major influence on the fuel cell dynamic performance. Two control valves were necessary to regulate the flow rates successfully by supplying excess amounts of the reactants. One valve is solely used to regulate the inlet mass flow rates including the excess amount, by feedforward control based on measureable variables; the external fuel cell current. The second valve regulates the amount of outlet flow rates, which are controlled by a PI controller with the pressure of the reactants as a reference. Under steady state operation, this ensures the excess amounts of supplied reactants are outlet, while during transients it ensures that the amounts of the reactants do not increase or drop.
4. The excess ratio of reactants flow rates can be controlled such that its value decreases as the power demand or flow rates increase.
5. In order to improve the efficiency of the fuel cell, hydrogen recirculation is necessary.
6. A DC-to-DC converter with PI control is used to match the power demand with the power output from the fuel cell. It is believed that it is the first time the entire electrical system model (fuel cell and converter) was implemented and simulated without linearization techniques followed in most studies. This enabled studying the entire operating range of the power conversion processes. As a result, a few control

problems, which were not approached before, were observed and resolved. The nonlinearity in the fuel cell near the concentration region is a major problem that damages the fuel cell and leaves the system uncontrollable. This problem was mentioned in some studies, but only a complete shutdown of the system was offered as a solution. A careful investigation led to solving this problem by modifying the PI controller of the converter to limit its duty ratio. Operating the converter in the nonlinear discontinuous current mode was observed in Chapters 5 and 6, which gave results within acceptable tolerances. In addition, a suitable anti-windup mechanism for the PI controller was implemented that addressed the ringing behaviour near boundary conditions of operation. The overall control strategy of the converter is expected to have addressed real problems of an actual implementation.

7. The results of using fuel cells in automotive applications showed promising performance of a vehicle powered solely by a fuel cell. As with existing combustion engine vehicles, an auxiliary energy storage device is needed for starting up the energy conversion system. In fuel cell systems, the energy storage device can be further utilised with a slightly increased capacity to utilise braking energy and bolster the fuel cell power output to meet or even exceed the typical driving schedules.
8. In the domestic sector, results also showed promising performance. The domestic power profile was limited to transients of ±35 kW/s in order to meet the standard voltage regulations and requirements. Step changes that occur in domestic applications have transients that exceed the automotive applications. However, these large transients are due to the short duration (Δt) of the changes taking place, not the change in power demand levels. Maximum power demand, in other words maximum ΔP, in domestic applications is less than 7 kW. Hence, a much smaller energy storage device than that required for automotive applications may be used in domestic power applications to perfect the use of fuel cell in this sector.

7.2 Scope for Further Work

In the control of DC-to-DC converters, further study could be undertaken to investigate the effects of fuel cell aging and/or catalyst poisoning on the performance of the fuel cell, and consequently on the maximum output power of the fuel cell. The controller would require further rules and conditions to prevent operation in concentration losses.

The excess ratio of the supplied reactants could be investigated where a variable ratio may be implemented. As the power output increases, the amount of sudden changes in power demand decreases, as it is limited by the ratings of the load and/or the fuel cell.

Cold start up is an important control problem for fuel cells. Further work could be performed to raise the temperature of the fuel cell to the optimum operating point.

For automotive applications, the control of electric motors is achieved by various methods depending on the type of motor used. Using the modelling of the fuel cell system, and taking into account the control issues in this thesis, further study could be performed to develop power conditioning units specifically for controlling electric motors.

Energy sharing between fuel cells and an energy storage device should be investigated, taking into consideration the probabilities of the change in power demand. For an increase in power demand, the energy storage device should have sufficient energy stored to meet a sudden increase in power demand. In addition, the ESD should have enough capacity to absorb and store the energy during a sudden drop in power demand.

LIST OF REFERENCES

1. *International Energy Outlook*. 2009, Energy Information Administration.

2. Winterbone, D.E., *Advanced Thermodynamics for Engineers*. 1997, John Wiley & Sons Inc. p. 346-347.

3. Grove, W.R., *On a gaseous voltaic battery*, in *Philosophical Magazine Series 3*. 1842. p. 417-420. Available online from: http://www.archive.org/stream/londonedinburghp21lond#page/418/mode/2up.

4. National Energy Technology Laboratory, *Fuel Cell Hand Book*. 2002. p. 3-5.

5. Larminie, J. and A. Dicks, *Fuel Cell Systems Explained*. 2003, Chichester, West Sussex :: J. Wiley.

6. U.S. Department of Energy. *Types of Fuel Cells*. December 2008; Available from: http://www1.eere.energy.gov/hydrogenandfuelcells/fuelcells/fc_types.html.

7. Berning, T. and N. Djilali, *Three-dimensional computational analysis of transport phenomena in a PEM fuel cell - a parametric study.* Journal of Power Sources, 2003. **124**(2): p. 440-452.

8. Hou, Y.P., M.X. Zhuang, and G. Wan, *A transient semi-empirical voltage model of a fuel cell stack.* International Journal of Hydrogen Energy, 2007. **32**(7): p. 857-862.

9. Wang, Y. and C.Y. Wang, *Transient analysis of polymer electrolyte fuel cells.* Electrochimica Acta, 2005. **50**(6): p. 1307-1315.

10. Lee, J.H., T.R. Lalk, and A.J. Appleby, *Modeling electrochemical performance in large scale proton exchange membrane fuel cell stacks.* Journal of Power Sources, 1998. **70**(2): p. 258-268.

11. Berning, T., D.M. Lu, and N. Djilali, *Three-dimensional computational analysis of transport phenomena in a PEM fuel cell.* Journal of Power Sources, 2002. **106**(1-2): p. 284-294.

12. Sivertsen, B.R. and N. Djilali, *CFD-based modelling of proton exchange membrane fuel cells.* Journal of Power Sources, 2005. **141**(1): p. 65-78.

13. Um, S., C.Y. Wang, and K.S. Chen, *Computational fluid dynamics modeling of proton exchange membrane fuel cells.* Journal of the Electrochemical Society, 2000. **147**(12): p. 4485-4493.

14. Fuller, T.F. and J. Newman, *Water and Thermal Management in Solid-Polymer-Electrolyte Fuel Cells.* Journal of the Electrochemical Society, 1993. **140**(5): p. 1218-1225.

15. Wu, H., X.G. Li, and P. Berg, *Numerical analysis of dynamic processes in fully humidified PEM fuel cells.* International Journal of Hydrogen Energy, 2007. **32**(12): p. 2022-2031.

16. Weydahl, H., et al., *Transient response of a proton exchange membrane fuel cell.* Journal of Power Sources, 2007. **171**(2): p. 321-330.

17. Zenith, F., et al., *Control-oriented modelling and experimental study of the transient response of a high-temperature polymer fuel cell.* Journal of Power Sources, 2006. **162**(1): p. 215-227.

18. Benziger, J.B., et al., *The power performance curve for engineering analysis of fuel cells.* Journal of Power Sources, 2006. **155**(2): p. 272-285.

19. Ceraolo, M., C. Miulli, and A. Pozio, *Modelling static and dynamic behaviour of proton exchange membrane fuel cells on the basis of electro-chemical description.* Journal of Power Sources, 2003. **113**(1): p. 131-144.

20. Correa, J.M., et al., *An electrochemical-based fuel-cell model suitable for electrical engineering automation approach.* IEEE Transactions on Industrial Electronics, 2004. **51**(5): p. 1103-1112.

21. Uzunoglu, M. and M.S. Alam, *Dynamic modeling, design and simulation of PEM fuel cell/ultra-capacitor hybrid system for vehicular applications.* Energy Conversion and Management, 2007. **48**(5): p. 1544-1553.

22. Meiler, M., et al., *Dynamic fuel cell stack model for real-time simulation based on system identification.* Journal of Power Sources, 2008. **176**(2): p. 523-528.

23. Woo, C.H. and J.B. Benziger, *PEM fuel cell current regulation by fuel feed control.* Chemical Engineering Science, 2007. **62**(4): p. 957-968.

24. Thounthong, P., S. Rael, and B. Davat, *Control strategy of fuel cell/supercapacitors hybrid power sources for electric vehicle.* Journal of Power Sources, 2006. **158**(1): p. 806-814.

25. Zenith, F. and S. Skogestad, *Control of fuel cell power output.* Journal of Process Control, 2007. **17**(4): p. 333-347.

26. Rodatz, P., G. Paganelli, and L. Guzzella, *Optimizing air supply control of a PEM fuel cell system*, in *Proceedings of the 2003 American Control Conference, Vols 1-6*. 2003, IEEE: New York. p. 2043-2048.

27. Pischinger, S., C. Schonfelder, and H. Ogrzewalla, *Analysis of dynamic requirements for fuel cell systems for vehicle applications.* Journal of Power Sources, 2006. **154**(2): p. 420-427.

28. Jiang, Z.H. and R.A. Dougal, *A compact digitally controlled fuel cell/battery hybrid power source.* IEEE Transactions on Industrial Electronics, 2006. **53**(4): p. 1094-1104.

29. Drolia, A., P. Jose, and N. Mohan, *An approach to connect ultracapacitor to fuel cell powered electric vehicle and emulating fuel cell electrical characteristics using switched mode converter*, in *IECON'03: The 29th Annual Conference of the IEEE Industrial Electronics Society, Vols 1 - 3, Proceedings*. 2003. p. 897-901.

30. Rodatz, P., et al. *Performance and Operational Characteristics of a Hybrid Vehicle Powered by Fuel Cells and Supercapacitors*. in *Fuel cell power for transportation 2003*. 2003. Detroit, MI: SAE.

31. Rodatz, P., et al., *Optimal power management of an experimental fuel cell/supercapacitor-powered hybrid vehicle.* Control Engineering Practice, 2005. **13**(1): p. 41-53.

32. Caux, S., et al., *Modelling and control of a FuelCell System and Storage Elements in transport applications.* Journal of Process Control, 2005. **15**(4): p. 481-491.

33. Choe, S.Y., et al., *Integrated modeling and control of a PEM fuel cell power system with a PWM DC/DC converter.* Journal of Power Sources, 2007. **164**(2): p. 614-623.

34. Williams, K.A., et al., *Experimental investigation of fuel cell dynamic response and control.* Journal of Power Sources, 2007. **163**(2): p. 971-985.

35. Fontes, G., et al., *Interactions between fuel cells and power converters: Influence of current harmonics on a fuel cell stack.* IEEE Transactions on Power Electronics, 2007. **22**(2): p. 670-678.

36. Liu, C.R., A. Ridenour, and J.S. Lai, *Modeling and control of a novel six-leg three-phase high-power converter for low voltage fuel cell applications.* IEEE Transactions on Power Electronics, 2006. **21**(5): p. 1292-1300.

37. Chiu, H.J. and L.W. Lin, *A bidirectional dc-dc converter for fuel cell electric vehicle driving system.* IEEE Transactions on Power Electronics, 2006. **21**(4): p. 950-958.

38. Marshall, J. and M. Kazerani. *Design of an efficient fuel cell vehicle drivetrain, featuring a novel boost converter*. in *Industrial Electronics Society, 2005. IECON 2005. 31st Annual Conference of IEEE*. 2005.

39. *Documentation for MathWorks Products, R2008A*, The MathWorks, Inc.

40. Khan, M.J. and M.T. Iqbal, *Modelling and analysis of electrochemical, thermal, and reactant flow dynamics for a PEM fuel cell system.* Fuel Cells, 2005. **5**(4): p. 463-475.

41. Zhang, J., et al., *PEM fuel cell open circuit voltage (OCV) in the temperature range of 23 °C to 120 °C.* Journal of Power Sources, 2006. **163**(1): p. 532-537.

42. Winterbone, D.E., *Advanced Thermodynamics for Engineers*. 1997, John Wiley & Sons Inc. p. 279.

43. Noren, D.A. and M.A. Hoffman, *Clarifying the Butler-Volmer equation and related approximations for calculating activation losses in solid oxide fuel cell models.* Journal of Power Sources, 2005. **152**(1): p. 175-181.

44. Springer, T.E., et al., *Characterization of Polymer Electrolyte Fuel Cells Using AC Impedance Spectroscopy.* Journal of the Electrochemical Society, 1996. **143**(2): p. 587-599.

45. Bird, R.B., W.E. Stewart, and E.N. Lightfoot, *Transport Phenomena*. 1960, New York: Wiley.

46. Shimpalee, S., et al., *Predicting the transient response of a serpentine flow-field PEMFC I. Excess to normal fuel and air.* Journal of Power Sources, 2006. **156**(2): p. 355-368.

47. Salas, V. and E. Olías, *Overview of the state of technique for PV inverters used in low voltage grid-connected PV systems: Inverters below 10 kW.* Renewable and Sustainable Energy Reviews. **13**(6-7): p. 1541-1550.

48. Chan, W.C.Y. and C.K. Tse, *Study of bifurcations in current-programmed DC/DC boost converters: from quasiperiodicity to period-doubling.* Circuits and Systems I: Fundamental Theory and Applications, IEEE Transactions on, 1997. **44**(12): p. 1129-1142.

49. Mazumder, S., et al. *A theoretical and experimental investigation of the nonlinear dynamics of DC-DC converters*. in *Power Electronics Specialists Conference, 2000. PESC 00. 2000 IEEE 31st Annual*. 2000.

50. Toribio, E., et al., *Numerical and experimental study of the region of period-one operation of a PWM boost converter.* Power Electronics, IEEE Transactions on, 2000. **15**(6): p. 1163-1171.

51. Visioli, A., *Modified anti-windup scheme for PID controllers.* IEE Proceedings - Control Theory & Applications, 2003. **150**(1): p. 49.

52. *Testing and Measuring Emissions: Dynamometer Drive Schedules*. [cited 15/02/2010; Available from: http://www.epa.gov/nvfel/testing/dynamometer.htm.

53. Guzzella, L. and A. Sciarretta, *Vehicle propulsion systems: introduction to modeling and optimization*. 2nd ed. 2007, Berlin: Springer.

54. Ehlers, K., H.-D. Hartmann, and E. Meissner, *42 V – an indication for changing requirements on the vehicle electrical system.* Journal of Power Sources, 2001. **95**(1-2): p. 43-57.

55. Wang, Y. and X. Cai, *DC link voltage optimized control for efficient residential fuel cell converter.* International Journal of Electrical Power & Energy Systems, 2010. **32**(9): p. 1031-1036.

56. *Nominal voltages for low voltage public electricity supply systems.* British Standards Institution, 1993. **BS 7697:1993**.

57. Song, C.J., et al., *PEM fuel cell reaction kinetics in the temperature range of 23-120 °C.* Electrochimica Acta, 2007. **52**(7): p. 2552-2561.

58. Xue, X.D., K.W.E. Cheng, and D. Sutanto, *Unified mathematical modelling of steady-state and dynamic voltage-current characteristics for PEM fuel cells.* Electrochimica Acta, 2006. **52**(3): p. 1135-1144.

59. Andrea, E., et al. *A simplified electrical model of small PEM fuel cell*. in *International Conference on Renewable Energy and Power Quality ICREPQ'06*. 2006. Palma de Mallorca, Spain.

60. di Bernardo, M. and F. Vasca, *Discrete-time maps for the analysis of bifurcations and chaos in DC/DC converters.* Circuits and Systems I: Fundamental Theory and Applications, IEEE Transactions on, 2000. **47**(2): p. 130-143.

61. Mazumder, S.K., A.H. Nayfeh, and D. Boroyevich, *Theoretical and experimental investigation of the fast- and slow-scale instabilities of a DC-DC converter.* Power Electronics, IEEE Transactions on, 2001. **16**(2): p. 201-216.

62. Hamill, D.C., *Power electronics: a field rich in nonlinear dynamics*, in *Workshop on Nonlinear Dynamics of Electronic Systems*. July 1995: Dublin. p. 164-179.

63. Mazumder, S.K., A.H. Nayfeh, and A. Borojevic, *Robust control of parallel DC-DC buck converters by combining integral-variable-structure and multiple-*

sliding-surface control schemes. Power Electronics, IEEE Transactions on, 2002. **17**(3): p. 428-437.

64. Newborough, M. and P. Augood, *Demand-side management opportunities for the UK domestic sector*. IEE Proceedings: Generation, Transmission and Distribution, 1999. **146**(3): p. 283-293.

65. Åström, K.J. and T. Hagglund, *PID Controllers: Theory, Design, and Tuning*. 2nd ed. 1995: Instrument Society of America. 343.